NOVEL DESIGN AND ANALYSIS OF AN ORAL CANNABIDIOL (CBD) THERAPEUTIC DELIVERY SYSTEM FOR PAIN MANAGEMENT

Faryal Khan-Flear

A research report submitted to the Faculty of Health Sciences, University of the Witwatersrand, in partial fulfilment of the requirement for the degree of Master of Science in Medicine in the field of Pharmaceutical Affairs

Supervisors:
Professor Pierre P. D. Kondiah,
Professor Yahya E. Choonara,
Doctor Samson A. Adeyemi

University of the Witwatersrand; Department of Pharmacy and Pharmacology; Johannesburg; South Africa

2023

DECLARATION

I, Faryal Khan-Flear, declare that this dissertation is my own work. It is being submitted for the degree of Master of Science in Medicine in the field of Pharmaceutical Affairs in the Faculty of Health Sciences as a research component at the University of the Witwatersrand, Johannesburg. It has not been submitted before for any degree or examination at this or any other University.

_____

Signature of Candidate

On this 23rd day of November 2023

ACKNOWLEDGEMENTS

I am grateful to God, my mother, my father, and my spouse for their constant support and my children for inspiring me. Doctors Samson Adeyemi and Phil Ubanako, thank you for your guidance, leadership, and mentorship. Thank you, Professor Kondiah, Department of Pharmacy and colleagues, for your patience and assistance, which made the endeavour more enjoyable. Thank you, Motshidiso Grace Papala, for maintaining my home while I was away. A special thanks to the Gauteng Department of Agriculture and Rural Development (GDARD) and South Africa's National Research Foundation (NRF), under Professor Kondiah's grantsmanship, for providing all running costs and expenditures in line with this project's completion.

ABSTRACT

Cannabidiol (CBD) is a non-psychoactive cannabinoid used for its antinociceptive, analgesic and anti-inflammatory properties in chronic pain. The endocannabinoid system (ECS) influences CBD: receptor binding to generate or regulate antinociceptive responses, producing centrally acting analgesia predominantly through Cannabinoid receptor 1 (CB1) abundant in the brain and spinal cord. In contrast, Cannabinoid receptor 2 (CB2) modulates inflammatory responses in immune system cells and tissues.

Most oral medications can have inefficient absorption ability and insufficient therapeutic bioavailability due to the solubility of active ingredients and dosage form dissolution. Although the high lipophilicity of CBD enables it to cross the blood-brain barrier (BBB), which prevents the entry of most systematically administered drugs, the oil-soluble CBD is poorly soluble in water, resulting in erratic, incomplete absorption and poor drug bioavailability, preventing therapeutic doses from reaching specific receptors and regions in the brain. Directly ingested CBD also undergoes hepatic and intestinal metabolism, further contributing to therapeutic insufficiencies.

Lipid-Based Drug Delivery Systems (LBDDS) can circumvent the drug's physicochemical properties and the body's protective biological barriers to enhance drug-receptor interaction and elicit a biological response. Lipid combinations in self-emulsifying lipid formulations (SELF) create liposome nanocarriers that entrap and release CBD, providing a non-invasive, transitory, regionally selective delivery method. Nanoliposomes restrict therapeutic delivery to targeted areas, minimizing systemic toxicity and improving drug bioavailability. Manipulating the physical, chemical, and mechanical aspects of nano-liposomes and the material properties of their constituents concerning human anatomy and physiology can help or hinder therapeutic efficiency, drug safety, and delivery.

Most therapeutic nanoliposome designs fall within 50–100 nm, facilitating passive transport across the BBB enabling drug receptor binding at brain and spinal cord receptor sites. Modulator uptake and interactions with host cells, enhanced uptake by target cells, and limits accumulation in specific tissues. Nanoliposomes smaller than 100 nm also extend blood circulation by evading renal, hepatic, and immunogenic sequestration and clearance by the mononuclear phagocyte system (MPS), the reticuloendothelial system (RES), opsonization, modulator uptake and interactions with host cells, limited accumulation in specific tissues, low uptake by target cells.

This experiment used established system predictors such as HLB and LogP values, Poulton's Lipid Classification System (LCS), Biopharmaceutics Classification System (BCS), Lipinski's Rule of 5 (Ro5), FBDD Rule of 3 (Ro3), Biopharmaceutics Drug Disposition Classification System (BDDCS) to evaluate the critical quality attributes of two optimized formulations able to deliver CBD to the brain and spinal cord. Both formulations consisted of a phospholipid (soy lecithin), unmodified vegetable oils (coconut, olive/castor oil), surfactants (Span 80 and Tween 20), and a cosolvent (ethyl acetate) in the same ratios with the same ingredients, except that the olive oil in one formulation replaced castor oil in the other. These formulations molecularly dispersed CBD in the polymeric matrix of an unstable amorphous solid dispersion (ASD), improving drug solubility and bioavailability compared to crystalline forms. Thermodynamically unstable ASD must be assessed for quality, stability, and resilience to design helpful dosage forms. Both optimized validation batches successfully encapsulated CBD in liposomes in the eutectic ASD mixtures, as reflected in Fourier transform infrared spectroscopy (FTIR) spectrograms and the Differential scanning calorimetry (DSC).

The olive oil-containing formulation produced self-micro-emulsifying drug delivery system (SMEDDS). At the same time, the castor oil preparation formed a self-nano-emulsifying drug delivery system (SNEDDS), accounting for the differences in particle size, size distribution, zeta potential, rheology, morphology, drug release and cell culture analysis. The differences arose due to the oils' unique fatty acid composition and chemistry. Drug release test results of each formulation loaded in hydroxypropyl methylcellulose (HPMC) capsules showed good timing for capsule dissolution and a burst release preceding sustained release over 48 hours. Drug release test results established cell viability in culture studies. The positive cell proliferation indicated that the CBD concentrations released by both formulations were non-toxic to mouse embryonic fibroblasts (NIH/3T3) and human embryonic kidney epithelial cell (HEK 293) cultures. Although both formulations yielded favourable results, the analysis indicated that the castor oil formulation was more robust and, therefore, suitable as a nanocarrier for CBD.

ETHICAL DECLARATION

This study project does not include any danger to humans or animals because none of them were involved in any of the experiments or activities described in this research report; hence, neither an ethics application nor a waiver is needed.

TABLE OF CONTENTS

LIST OF FIGURES

LIST OF TABLES

LIST OF EQUATIONS

LIST OF ABBREVIATIONS

ABC	Adenosine triphosphate-binding cassette
ABN-CBD	Anandamide/Abnormal-Cannabidiol
ADME	Absorption, distribution, metabolism and excretion
AFM	Atomic force microscopy
API	Active pharmaceutical ingredient
ASD	Amorphous solid dispersion
AUC	The area under the curve
BA	Bioavailability
BBB	Blood-Brain Barrier
Bcrp	Breast cancer resistance proteins
BCS	Biopharmaceutical classification system
BDDCS	Biopharmaceutical Drug Disposition Classification System
BE	Bioequivalence
BS	Back Scattering
BSE	Bovine spongiform encephalopathy
C	Carbon
CB1	Cannabinoid Receptor 1
CB2	Cannabinoid Receptor 2
CBC	Cannabichromene
CBD	Cannabidiol
CBG	Cannabigerol
CBT	Cognitive behavioural therapy
CCK	Cholecystokinin
CH	Cholesterol
CL	Plasma clearance
C_{max}	Maximum serum concentration
CMC	Critical micelle concentration
CME	Clathrin-mediated endocytosis
CO	Castor oil

CNS	Central Nervous System
CO2	Carbon dioxide
CoA	Co-enzyme A
CoS	Co-solvent
COX	Cyclo-oxygenase enzymes
CPP	Critical Packing Parameter
CQA	Critical Quality Attributes
CRSS	Critical resolved shear stress
CTA	Cell transformation assay
CvME	Caveolae-mediated endocytosis
DLPC	Dilauroylphosphatidylcholine
DLS	Dynamic light scattering
DMEM	Dulbecco's Modified Eagle Media
DMPC	Dimyristoylphosphocholine
DMSO	Dimethyl Sulfoxide
DOF	Degrees of Freedom
DOPC	Dioleoylphosphatidylcholine
DPPC	Dipalmitoylphosphatidylcholine
DSC	Differential Scanning Calorimetry
DSPC	Distearoylphosphatidylcholine
ECS	Endocannabinoid system
EE%	Encapsulation efficiency
EMA/EMEA	European Medicine Agency
EOS	Endogenous Opioid System
EPC	Ethyl phosphocholine
EV	Extracellular vesicles
FA	Fatty acids
FAAH	Fatty acid amide hydrolase
FBS	Foetal bovine serum
FTIR	Fourier Transformation Infrared Spectroscopy
g	Gram

GABA	Gamma-aminobutyric acid
GIT	Gastrointestinal tract
GPCR	G protein-coupled receptors
GRAS	Generally recognised as safe
h	Hours
H	Hydrogen
HCl	Hydrochloric Acid
HCO	Hydrogenated castor oil
HDL	High-density lipoprotein
HEK293	Human Embryonic Kidney
HLB	Hydrophilic/Lipophilic balance
HMOG	High molecular weight organogels
HPLC	High-pressure liquid chromatography
HPMC	Hydroxypropyl methylcellulose
HSPC	Hydrogenated soy phosphatidylcholine
IASP	International Association for the Study of Pain
ICAM-1	Intercellular adhesion molecule-1
ICH	International Council for Harmonisation
IL	Interleukin
INL	Interferon
i.t	Intrathecal
i.p.	intraperitoneal
i.v.	intravenous
K_{el}	Elimination rate
kg	Kilogram
L	Litre
LBDDS	Lipid-based drug delivery systems
LC%	Loading capacity
LC	Liquid crystalline & Lamellar crystals
LCS	Lipid Classification system
LCFA	Long-chain unsaturated fatty acids

LCS	Lipid class system
LCT	Long-chain triglycerides
LDL	Low-density lipoprotein
LLC	Lyotropic liquid crystal
LMOG	Low moleculer weight organogels
LMW	Low moleculer weight
LNC	Lipid nano-capsules
LogP	Partition coefficient
LPS	Lipopolysaccharide
mg	Milligram
ml	Millilitre
MAP	Mitogen-activated protein
MAPK	Mitogen-activated protein kinase
MCT	Medium-chain triglycerides
MeOH	Methanol
min	Minutes
MPP	Molecular Packing Parameter
MPS	Mononuclear phagocyte system
MTT	3-(4,5-dimethylthiazole-2-yl)-2,5-diphenyltetrazolium bromide dye
MUFA	Monounsaturated fatty acids
MWD	Molecular weight distribution
N	Nitrogen
NaOH	Sodium hydroxide
NAPE	N-acylphosphatidylethanolamine
ng	Nanogram
NGF	Nerve Growth Factor
NIH/3T3	Mouse Embryonic Fibroblasts
nm	Nonometer
NME	New molecular entities
NO	Nitric oxide
NP	Nanoparticle

NRU	Neutral red uptake
NSAID	Non-steroidal Anti-inflammatory drug
O	Oxygen
OO	Olive oil
P	Phosphorus
PAG	Periaqueductal gray
PBS	Phosphate Buffer Solution
PC	Phosphatidylcholine
Pdi	Polydispersity index
PE	Phosphatidylethanolamine
PEG	Polyethylene Glycol
PG	Phosphatidylglycerol
PGE2	Prostaglandin E2
P-gp	P-glycoprotein
PK	Pharmacokinetic
PLO	Pluronic lecithin organogels
PNL	Pro-nano-liposphere
PNS	Peripheral Nervous System
PPAR	Peroxisome proliferator-activated receptors
PrLO	Premium lecithin organogels
PSA	Polar surface area
PUFA	Polyunsaturated fatty acids
RA	Ricinoleic acid
RES	Reticuloendothelial system
SAL	Sterility assurance levels
SCS	Spinal cord stimulation
s.c.	Subcutaneous
RVM	Rostral ventral medulla
SCT	Short-chain triglyceride
s	Seconds
S	Surfactant

$ScCO_2$	Super critical carbon dioxide
SEDDS	Self-emulsifying drug delivery systems
SELF	Self-emulsifying lipid formulations
SEM	Scanning Electron Microscopy
SGF	Simulated gastric fluid
SIF	Simulated intestinal fluid
SFA	Saturated fatty acids—one double bond), and
SLM	Solid lipid microparticles
SLN	Solid lipid nanoparticles
SMEDDS	Self-micro-emulsifying Drug Delivery System
spp.	Species
SNEDDS	Self-nano-emulsifying Drug Delivery System
SSL	Steroid-stabilised Liposome
$t_{1/2}$	Half-life
T_c	Crystallization temperature
td	Solvent diffusion time
TCA	Tricyclic antidepressants
TEM	Transition electron microscope
TENS	Percutaneous nerve electrostimulation
T_g	Glass transition temperature
THC	Tetrahydrocannabinol
TLC	Thermotropic crystals
T_p	Phase transition temperature
T_m	Melting temperature
T_{max}	Time to peak drug concentration
TPSA	Topological surface area
TRP	Transient receptor potential
tr	Polymer relaxation time
TSC	Thermally stimulated current
TSE	Transmissible spongiform encephalopathy
TXA2	Thromboxane

USFDA	The U.S. Food and Drug Administration
USP	U.S Pharmacopeia
VO	Vegetable oil
VCO	Virgin coconut oil
WHO	World Health Organization
XRD	X-ray diffraction

CHAPTER 1
INTRODUCTION TO PAIN AND THE RATIONALE FOR DELIVERING CANNABIDIOL AS AN ORAL NANOFORMULATION

1.1 Introduction to Pain

Injuries, infections, and genetic changes can damage tissues, organs, and the nervous system, producing sensory, emotional, or psychogenic pain (1–3). The type of cell damage determines nociceptive, inflammatory, neuropathic, or psychogenic pain (Section 2.2), further classified as acute, chronic, malignant, and non-malignant pain by "WHO criteria" (4,5,10,11,12). Pharmaceutical, physical rehabilitation, neuromodulation, psychological, and invasive pain treatments exist (Table 2.1) (1) Pharmacotherapy with modern analgesics and proper diagnosis is the primary pain management strategy (21, 22). Medications stop pain by changing pain signals and chemicals before, during, or after pain transmission (15, 18–20). After inflammation, opioid therapies assist pain by up-regulating opioid receptors. The WHO Scheme three-stage analgesic ladder advocates starting with non-opioids, then moderate opioids, then potent opioids until the patient is pain-free (1,3,5,6).

Opioids, anticonvulsants, and antidepressants relieve severe, persistent pain. Any opioid can safely treat cancer-related pain in adults and adolescents, the dose depending on clinical evaluation and pain intensity (3). Opioids combined with adjuvant analgesics can treat pain and psychological disorders such as anxiety, depression, and sleeplessness. Instead of "on-demand," drugs should be given “on the clock” every 3–6 hours to relieve pain. Acute nociceptive pain can be treated like neuropathic pain to prevent central sensitization (1,3,6). Rapid-acting opioids, such as morphine, should treat breakthrough pain instead of slow-acting opioids (1–5). On treating the root cause of the pain, opioids can be reduced or discontinued (3,10). Wean the patient off the opioid dosage gradually to avoid withdrawal symptoms if an opioid dependency forms during pain treatment (3,7).

Cancer patients with inadequately controlled pain may respond negatively to increasing opioid dosages before obtaining analgesia (3). Opioids, a potent analgesic for treating moderate to severe pain, can produce appetite loss, drowsiness, nausea, constipation, respiratory

depression, opioid-induced hyperalgesia, drug tolerance, and dependency, which discourage their usage; however, opioid switching may improve the balance between analgesia and side effects (12,13).

Cannabinoids antagonize several side effects of opioids and provide efficient antinociception and analgesia for various neuropathies and chronic diseases, presenting an alternative or adjunct to existing analgesics, used as rescue drugs or as opioid-sparing agents when opioid analgesia fails (1–3). Cannabinoids and opioids control severe neuropathic and cancer pain through synergistic G-protein-coupled antinociception (13,14).

1.2 Rationale and Motivation for an Oral CBD Delivery System

Orally ingested cannabis or cannabis-based products such as Tetrahydrocannabinol (THC), Cannabidiol (CBD), and their analogues are favoured by patients and drug developers and recommended by the globally accepted WHO best practice guidelines for pain (2,4). Scientific research suggests that CBD is easy and safe to take and avoids the parenteral administration's discomfort, challenges, and expense (3).

Pharmacokinetic studies comparing intraperitoneal, intravenous, inhalational, oral, and subcutaneous administration routes have shown that orally administered CBD yields the highest levels in the brain. However, directly ingesting the highly lipophilic, poorly soluble CBD (soluble in oils but not water) causes irregular absorption, substantial first-pass metabolism, and low bioavailability. Water solubility restricts oral CBD absorption and bioavailability. Furthermore, the BBB prevents systemically circulating medicines from entering the CNS (13,15). Although CBD's lipophilicity allows it to cross through the BBB from the central circulation and bind to brain endothelial receptors following oral delivery, orally consumed CBD is inefficient if it cannot reach and bind to specific brain receptors at therapeutic amounts (16,17).

CBD-loaded Lipid-Based Drug Delivery Systems (LBDDS) provide fast, non-invasive, receptor-specific delivery to specified brain locations, avoiding harmful systemic distribution, enhancing drug absorption, and overcoming BBB impermeability while treating pain and CNS illnesses. Modifying formulations and administration modalities can adjust CBD-loaded LBDDS' pharmacokinetic properties for therapeutic application (17). CBD formulations include oils or

alcohols, soft and hard gel capsules, oral, sublingual, oromucosal spray, or food items (16). As Nabiximols (Sativex® from G.W. Pharmaceuticals) is the only currently available oromucosal spray containing a 1:1 ratio of THC and CBD, used as an adjunctive treatment for cancer and neuropathic pain conditions, there is a need to develop a safe and efficacious oral drug delivery method for CBD to treat pain (11).

Under the heading "Designing the SELF" (See section 2.10), the predictors used to design the CBD-loaded LBDDS in this article are covered, and Chapter 3 covers the characterisation of the concept formulations. This article also discusses the development of liposomes (see section 2.8 and Figure 2.3) and SELF (2.7.3.4).

Delta-9-tetrahydrocannabinol (THC), the most potent psychotropic cannabinoid, induces opioid-like analgesia. CBD's pharmacologic profile differs from THC's but has the same analgesic and anti-inflammatory properties (14). Whether administered chronically (0.7 g/day for six weeks) or at very high doses (up to 1,5 g/day), clinical investigations show oral CBD is safe and well-tolerated in humans as it is non-toxic in healthy cells and retains its antinociceptive and anti-inflammatory properties at high doses without CNS effects (16–18). Cannabigerol, cannabichromene, and CBD are not psychoactive.

CBD does not affect psychological, psychomotor or physiological (body temperature, blood pressure, heart rate and dry mouth) functions, nor does it induce catalepsy or interfere with food consumption or gastrointestinal transit (5). Therefore, CBD isolates and synthetic analogues are good candidates for developing analgesic and anti-inflammatory drugs (10,11).

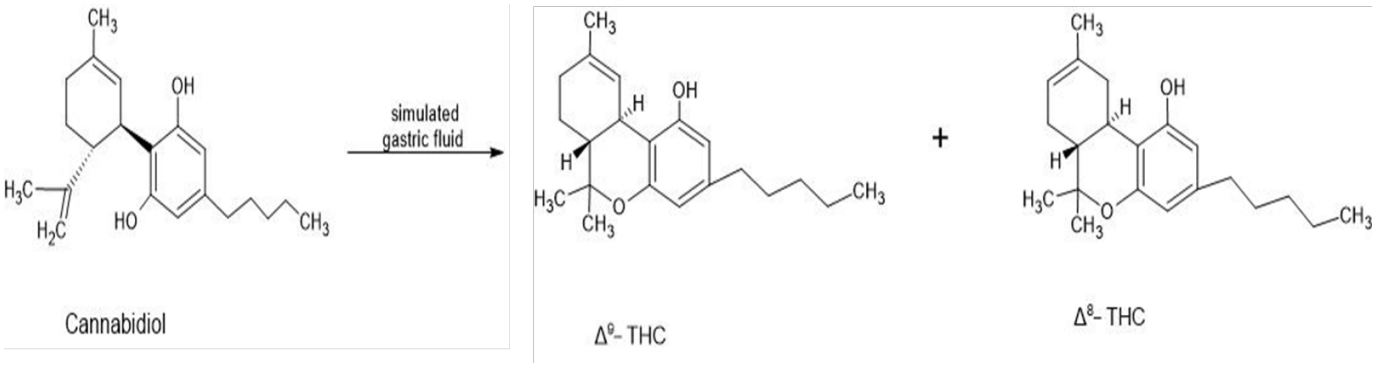

Figure 1.1: Acid Instability of CBD (8)

CBD molecules can convert to delta-9-THC and other cannabinoids in simulated gastric fluid (SGF). Unlike the oral route, CBD administered via parenteral, inhaled, rectal and transdermal routes do not convert. However, SGF protocols differ from the stomach's physiological environment, and the body does not contain biosynthetic enzymes or pathways that can bioconvert CBD to THC or metabolites, making studies on CBD metabolism to hazardous components unclear. Furthermore, reported adverse effects result from Drug-Drug interactions between the CBD. Hence, CBD ingestion is considered safe (27)(29).

1.3 Aims and Objectives of Formulating an Oral Nano delivery system

This study aimed to formulate a suitable oral nanocarrier to deliver Cannabidiol (CBD) to pain receptors in the CNS. The following objectives were undertaken and fulfilled:

Objective 1: To formulate a nanocarrier to transport CBD to its effective site

Objective 2: To characterize the formulation by analysing its critical quality attributes (CQA):

- Determining the particle size, particle size distribution (Pdi) and electric charge (zeta potential) of the emulsion using Dynamic Light Scattering (DLS) analysis
- Identifying molecular functional groups, chemical bonds and water content using Fourier Transform Infrared (FTIR) spectroscopy
- Assessing the thermal behaviour of the LBDDS using Differential Scanning Calorimetry (DSC)
- Determining the crystallinity of the LBDDS using X-Ray Diffraction (XRD)
- Examining the morphology of nanocarrier by Scanning Electron Microscopy (SEM)
- Analysing the rheology of the formulation for yield stress and viscosity with a viscometer

Objective 3: To assess the suitability of filling the formulation into a hard HPMC size 00 vegan capsule for oral administration. To determine if the HPMC capsule could host the formulation and release its contents under simulated gastric and intestinal pH within a given time frame.

Objective 4: To conduct drug release studies by dissolving the HPMC capsule loaded with the test formulation in pH-adjusted phosphate buffer solution (PBS), removing aliquots of the supernatant under sink conditions and analysing the amount of drug released using high-pressure liquid chromatography (HPLC)

Objective 5: To conduct cell studies on NIH/3T3 and HEK 293 cell lines to determine whether the cumulative drug concentrations released in the dissolution study promote cell proliferation or cell death.

1.4 Overview of this Dissertation

Chapter 1: Acquaints the reader with the concept of pain and rationalizes the oral route for CBD administration.

Chapter 2: Describes the mechanism of action of different types of pain and profiles CBD as a candidate for pain treatment. This chapter also presents a comprehensive literature review on the technique used to prepare LBDDS to improve drug bioavailability and targeting to the brain.

Chapter 3: Describes the materials, formulation, and preparation method of the LBDDS. Descriptions of analytical tests run to characterize CQA and parameters of the formulations presented along with the results include DLS (particle size, distribution, and Zeta Potential valuation), FTIR Spectroscopy, DSC, SEM; XRD; Rheological Analysis; Drug Release Studies and Cell Proliferation Tests.

Chapter 4: Discusses the release of CBD from the capsule and formulation and its implication in cell proliferation/viability. Cellular viability studies showed minimal toxicity to physiological tissue below 0,0625 µg/ml.

Chapter 5: Provides a conclusion and future recommendations to enhance the study. The CBD LBDDS showed positive results from the physicochemical characterization, dissolution analysis, and ex-vivo studies

CHAPTER 2
A LITERATURE REVIEW OF THE PHARMACOLOGY AND PHARMACOKINETICS OF CBD AS AN ANALGESIC IN LIGHT OF ITS PHYSICOCHEMICAL CHARACTERISTICS AND FORMULATION STRATEGY

2.1 Introduction

Non-psychoactive CBD from *Cannabis Sativa* L*. spp*. has antinociceptive, analgesic, and anti-inflammatory effects in chronic and neuropathic pain states. CBD can be used as an alternative, an adjunct, a rescue drug, or an opioid-sparing agent when opioids fail to treat acute, chronic, malignant, and chronic non-malignant pain.

Endocannabinoids and exogenous cannabinoids (THC, CBD, and analogues) interact synergistically with the same opioid and ECS receptors and enzymes (Table 2.2). Through G-protein coupled pathways, opioids and cannabinoids synergistically generate antinociception. CBD isolates and synthetic analogues are ideal for analgesic and anti-inflammatory medications because they retain their antinociceptive and anti-inflammatory characteristics at high dosages without CNS effects.

This chapter explores vital scientific principles for designing an oral CBD-LBDDS formulation that delivers therapeutic amounts to pain receptors to induce analgesia for chronic pain and inflammation.

2.2 Mechanisms of Pain

2.2.1. Nociceptive Pain

Nociceptors convey pain sensations to the dorsal horn neurons in the substantia gelatinosa of the spinal cord, where they synapse before accessing the brain (7,16). The thalamus registers the initial pain sensation before continuing to the limbic system (emotional centre), cerebral cortex, pain perception and interpretation sites.

Pain has two phases, caused by two fibres: fast-conducting A fibres and slower C fibres (7,16). Large, myelinated, opioid receptor-free Aδ fibres give a sharp "first pain" when a blow, cut, or electrical shock triggers nerve fibres. The action potential travels towards the CNS so fast that the body reflexes quicker than the pain stimulus to retract the affected body before perceiving the pain. Smaller, thinner, branching C fibres form a "net" over a vast region. Lacking myelin, they process pain slowly, creating dull, burning, or agonizing sensations called the "second pain" stimulated by mechanical, thermal, and chemical stimuli. Opioid and cannabinoid receptors at C fibre ends transmit and modulate pain more than other receptors (9).
Opioid receptors anchored in the cell membrane are Gi/o - protein-coupled receptors. Endogenous and exogenous opioids activate cannabinoid receptors, causing the sensation of pain. DOR (δ), MOR(μ), and KOR (κ) are the primary opioid receptors in the brain (CNS), spine (PNS), and non-neuronal tissues, respectively. MOR affects pain perception and sensorimotor integration, and KOR affects feeding, neuroendocrine function, and pain. DOR affects cognition, olfaction, and muscle.

The Endogenous Opioid System (EOS) has three opioid peptide families: dynorphins, endorphins, and enkephalins. Opioid peptides and receptors modulate spinal, supraspinal, and peripheral analgesia, pain-reward systems (including food and drug addictions), and emotional and stress responses. Opioid receptor activation in projection neurons reduces opioid receptor expression, pre- and postsynaptic responses, and subtype-specific localization. Resident inhibitory interneurons enhance opioid-induced behaviour (9,10).

The immune and neurological systems raise the pain threshold synergistically (2). Inflammatory cells release cytokines, prostaglandins, and other mediators that enter the injured perineurium and attach to dormant "sleeping" receptors, activating C-fibre opioid receptors. Non-steroidal Anti-inflammatory drugs (NSAIDs) and corticosteroids diminish fibre nerve sensitivity by inhibiting prostaglandin production and inflammation.

Cannabinoids interact with CB1, CB2, WIN, and ABN-CBD (anandamide/abnormal-cannabidiol) receptors. Cannabinoid receptor agonists modify neuronal activity and nociceptive thresholds by

binding to CB1 and CB2 receptors at the spinal (peripheral) and supraspinal (central) levels, suppressing peripheral and inflammatory responses (7,8).

Mast cells, peripheral nerves, the spinal cord, and the brain containing CB1 receptors inhibit synaptic transmissions, contribute to anti-inflammatory responses, and induce ataxia and cataleptic seizures.

CB2 receptors in the inflammatory and immunocompetent cells of the immune system are responsible for the peripheral effects of cannabis. CB2 receptors modulate immunological responses by inhibiting neutrophil accumulation and Nerve Growth Factor (NGF)-induced mast cell degranulation, indirectly stimulating opioid receptors in primary afferent pathways, and inducing hyperalgesia without causing CNS side effects like short-term memory loss, disruptive psychomotor behaviour, intoxication, appetite stimulation, and antiemesis.

Non-neuronal cells near nociceptive nerve terminals suppress pro-inflammatory factor release, causing antinociception in inflammatory hyperalgesia and neuropathic pain.

2.2.2. Neuropathic Pain

Neuropathic pain is caused by nerve damage, whereas central pain originates from the spinal cord. Hypersensitive CNS or PNS neurons may emit persistent, abnormal ectopic impulses that cause chronic pain. Injury-sensitized peripheral nociceptors become hyperexcitable as lower firing thresholds increase ectopic discharge in response to benign stimuli.

Phenotypic changes to non-neuronal cells, Schwann cells, and glia in nerve-nourishing axons alter growth factors, degrade myelin sheaths, and impair axonal function. Instead of restoring neural tissues, cut or injured C or A fibres develop neuromas (swelling) surrounding the re-joined axon. Damage alters sodium channel distribution, expression, and gating, causing dorsal root ganglia neuromata to discharge electrical impulses spontaneously. Uninjured axons spread into the injury site, spreading pain to those areas and causing 'mirror' pain. Physical, metabolic, and chemical cues near neighbouring axons also synergize ectopic firing.

2.2.3. Inflammatory Pain

Injured cells release inflammatory chemicals into the periphery after tissue destruction or nociceptive CNS neuron stimulation, causing inflammation and pain. Systemic alterations in co-morbidities such as sympathetic nervous system activation, cachexia, depression, dyslipidemia, tiredness, and insulin resistance result from chronic inflammation. Metabolic transitions initiated by changes in sympathetic activity maintain inflammation and increase cardiovascular risk.

Prostaglandins, chemical mediators of pain, inflammation, and fever, modify capillary permeability, vasodilation, and vasoconstriction at the injury site. Histamine, acetylcholine, bradykinin, leukotrienes, substance P, and prostaglandins initiate pain. Cyclooxygenase (COX) enzymes produce prostaglandins (pro-inflammatory chemicals; PGE2, PGI2, PGF2a) from arachidonic acid (omega-6 polyunsaturated fatty acid). NSAIDs limit prostaglandin synthesis by inhibiting COX-1 and COX-2 enzymes and their half-lives and affecting Thromboxane (TXA2), a potent hypertensive agent that stimulates platelet aggregation. NSAIDs diminish spinal cord and neurogenic brain inflammation peripherally.

2.2.4. Psychogenic Pain

Psychogenic pain has no biological cause since severe pain or social or occupational impairment exceeds physical findings.

2.2.5. Cancer Pain

Patients with cancer frequently feel persistent pain from the tumour or therapy side effects. Pain significantly impacts cancer patients' physical, functional, and emotional quality of life; consequently, effective pain management measures are crucial.

Opioid analgesics are the current standard treatment for persistent or chronic neuropathic pain in end-stage and terminal cancer; nevertheless, variances in patient response or opioid side effects are troublesome for specific patients and limit compliance. Independent of the opioid route, THC and CBD can control and relieve pain, inflammation, and immunological activity via the ECS. CBD may have medicinal benefits as an alternative to opiate therapy for treating cancer pain (31).

Cholesterol, the principal sterol synthesized in the body from acetyl-CoA via the isoprenoid pathway, originates from the diet or lipid formulations and forms a structural component of cell membranes. Cancerous cells synthesize cell membranes rapidly by feeding on large amounts of cholesterol and fats.

Liposomes carrying anti-cancer medications, regarded as a potential source of nourishment by cancer cells, absorb into cancer cells, destroying them (29).

Cholesterol, a precursor to bile acids, steroid hormones, and vitamin D, causes several cancers. Lipoprotein complexes carry cholesterol from the gut to the liver, enhancing lipogenesis and generating cancer cell membrane components such as phospholipids and cholesterol.

Malignant cells and tissues have high LDL receptor activity and cholesterol needs due to rapid proliferation and cell change. The overexpression and high-affinity receptor-mediated absorption of LDL particles raises cholesterol demand. Thus, CBD-drug targeting can use pro-drugs containing cholesterol and LDL.

There is an association between low cholesterol blood levels and lung, cervical, breast, colon, and leukaemia cancers, and high cholesterol (lipid-rich) serum levels to brain and prostate cancers. Cholesterol, an oestrogen precursor, increases breast cancer risk.

Table 2.1: Current Treatments of Pain

Treatment	Examples
Pharmacotherapy	Non-opioids (paracetamol, NSAIDs), potent opioids (hydromorphine, morphine, oxycodone, fentanyl, methadone), weak opioids (codeine), adjuvants (anticonvulsants, antidepressants, bisphosphonates), and steroids (4)
Physical Rehabilitation	Cryotherapy (cold), electrotherapy, kinesitherapy, laser therapy, manual techniques, medicinal extracts, and thermotherapy (heat) (10) Stretching, exercise/ reconditioning, Gait and posture training, Immobilization, SCS, I.C., Massage, Acupuncture
Neuromodulation	Neuromodulation activates pain-inhibitory mechanisms that stimulate pain systems, like PNS (peripheral nerve stimulation), TENS (percutaneous nerve electrostimulation), vibration and acupuncture (10).

Psychogenic /Psychological methods	Medication Benzodiazepines, Tricyclic antidepressants (TCA's), significant tranquillizers Psychological: Cognitive behavioural therapy (CBT), Biofeedback (relaxation with imagery), Hypnotherapy, Psychotherapy, Group psychotherapy, Family therapy, Supportive psychotherapy, Patient education, Contingency management, Cognitive restructuring, coping skills training, Distraction. Psychotherapy includes cognitive therapy and relaxation techniques (10).
Invasive techniques	Neurosurgical intervention may provide pain relief if drugs or alternative treatment methods are ineffective, such as individual nerves blocked by intrathecal drug administration (e.g., epidural anaesthesia during childbirth) or neurodestractive methods(e.g. neurolysis, thermolesion) or surgery (10).

2.3 The Endocannabinoid System (ECS)

Endogenous cannabinoids (endocannabinoids), cannabinoid receptors and the enzymes that synthesize and degrade them compose the Endocannabinoid System (ECS), a facet of the pain pathway (Table 2.2) (11). The ECS regulates nociceptive thresholds by prolonging or producing hyperalgesia in chronic pain (17). Targeting and activating endocannabinoid receptors induces antinociception that alleviates neuropathic and inflammatory pain without conventional treatment and avoids opioid overuse (11).

Table 2.2: Composition of the Endocannabinoid System

Category	Type
Endocannabinoids (E.C.):	Arachidonyl ethanolamine (anandamide, AEA)
	2-arachidonylglycerol (2-AG)
Exogenous Cannabinoids	THC, CBD, and their Analogues
Endocannabinoid receptors:	Cannabinoid receptors I (CB1) – Central
	Cannabinoid receptors 2 (CB2) - peripheral
	Vanilloid 1 (TRPV1)
	GPR55, GPR18
	PPAR
Endocannabinoid enzymes:	Fatty acid amid hydrolase (FAAH):
	Endocannabinoid degrading enzyme.

2.3.1. Endogenous cannabinoids

WIN55 (cannabinoid receptor agonist), anandamide (endogenous cannabinoid), glycine, and gamma-aminobutyric acid (GABA) models influence pain. The endocannabinoid's mediation and the host's response to inflammation influence immune-cell migration and cytokine production.

2.3.2. Exogenous cannabinoids-

Cannabinoid-receptor binding induces antinociception when THC, CBD, and analogues interact with ion channels, receptors, transporters, transcription factors and enzymes (13,22). CBD-receptor interactions occur 50-fold less than THC and thus lack the psycho-activity of THC, even at high dosing (12). Prominent therapeutic targets for CBD include serotonin receptor 5-HT1A, 7-transmembrane G-protein coupled receptors (α1A, δ-OPR, μ-OPR, GPR18, GPR55, CB2, CB1); ligand-gated ion channels (GABAA, NaV, GlyR, nAch), nuclear receptors (PPARγ), opioid receptors, transient receptor potential channels (TRPV2, TRPV1, TRPM8, TRPA1) and enzymes (CYP450 and FAAH) (Figures 2.6 and 2.7; Table 2.3) (8,13,14).

CBD is a partial CB2 agonist and CB1 antagonist. CBD is a weak CB1/CB2 receptor antagonist and a negative allosteric modulator at CB1 (32)(29). Although CBD's affinity for receptors is low, it still benefits antinociception and brain disorders by interacting with neuromodulatory receptors CB1 and CB2 in the brain and the immune system, reducing prostaglandin E mediators, chronic inflammatory pain states, cell activation, apoptosis, and immune cell proliferation. CBD modulates proinflammatory cytokine production, brain-derived neurotrophic factor expression and immune suppression. In addition, it prevents oxidative stress-dependent cell death by preserving cellular redox potential and acting as an endoplasmic reticulum stress attenuator (13).

Ingested CBD yields the highest CBD levels in the brain because its high lipophilicity enables it to traverse the BBB; however, at the same time, the BBB prevents therapeutic concentrations from reaching brain regions. Taking unmodified CBD can cause drug-mediated toxicity, hence the need for a non-invasive, transient, site-selective CBD delivery method to restrict delivery to target areas and minimize the toxic, systemic distribution of therapeutic molecules (13).

2.3.3. Cannabinoid Receptors

Cannabinoids activate cannabinoid receptors to relieve chronic inflammatory pain in disorders including cancer, fibromyalgia, multiple sclerosis, and osteoarthritis (34). Cannabinoid receptors include CB1, CB2, TRP and PPAR. CB1 and CB2 receptors signal mostly via Gi and Go GPCR and occasionally via Gs and Gq/11. Depending on the cell type, inhibitory G protein activation stimulates CB1 receptors, which, in turn, inhibits adenylyl cyclase, specific voltage-gated calcium channels, mitogen-activated protein (MAP) kinases, and G protein-linked inwardly rectifying potassium channels (4, 29).

Co-administered opioid agonists mitigate the risk of using opioid painkillers. Morphine with CB2 agonists like CBD synergistically reduces inflammatory pain with minimal adverse effects in a dose-time contingency.

Active pain signalling suppresses neuronal excitability and neurotransmission when endocannabinoids stimulate CB1 receptor signalling pathways on presynaptic terminals. CBD inhibits opioid receptors 5-HT2C, KOR, MOR, DOR, H3, α2C, α2b, and D1 (17). CBD inhibits GPR55 and TRPM8 at nanomolar to micromolar concentrations, activating 5-HT1a, α1, α3, and TRPA1 channels.

CBD's potent antioxidant properties are attributable to its polyphenolic nature (25). CBD increases intracellular calcium in normal physiological circumstances but reduces it under high excitability conditions. At higher concentrations, CBD activates PPAR-γ, TRPV1, and TRPV2 channels. Moreover, CBD inhibits cellular uptake and fatty acid amide hydrolase–catalyzed degradation of N-arachidonoyl-ethanolamide.

2.3.3.1. CB1 Receptors

Activating or inhibiting CB1 receptors with cannabinoids modulates peripheral and central neurotransmitter release, increasing or decreasing neuronal excitability (15). CB1 receptor agonism regulates ion channels, TRPs, adrenergic signalling, bone resorption, cytokine and ghrelin secretion, heart rate, and lipolysis by raising the action potential threshold on presynaptic nerve terminals.

Activated CB1 receptors desensitize nociceptors by modulating neurotransmitter release and blunting membrane depolarization and exocytosis by modifying potassium and calcium channels. CBD inhibits voltage-activated calcium (Ca^{2+}) channels and adenylyl cyclase in nerve cell mitochondria, lowering Ca^{2+} conductance and cAMP generation and boosting potassium and mitogen-activated protein kinase (MAPK) activity.

CB2 receptor activation inhibits adenylyl cyclase without affecting ion conductance (13). CBD's high lipophilicity ruptures membranes and affects bilayer flexibility through its non-discriminating ion channel-modulating activities (18).

CNS CB1 receptors adversely affect psychotomimetic and addictive (cannabinomimetic) behaviour, even though selective CB1 agonists have analgesic properties (16). CB1 receptors predominate in CNS areas that modulate pain, like the spinal (spinal cord) and supraspinal (brain) regions. CB1 receptors occur most abundantly in the spinal regions of the dorsal horn, dorsolateral funiculus, dorsal root ganglia and substantia gelatinosa, consolidating nociceptive and sensory afferent information in pathways ascending to cortical structures.

Significant CB1 concentrations occur mainly in brain regions that produce psychoactive effects by cannabinoids like D9-THC. Lower concentrations occur in regions less responsive to cannabinoids, such as the brainstem nuclei, spine, peripheral nerve terminals, extra-neural sites, and respiratory centres of the medulla glutamatergic terminals.

Superior concentrations of CB1 receptors occur in the supraspinal regions such as the amygdala, higher cortical brain regions such as the dorsalraphe nucleus, dorsolateral PAG, submedius and posterior-lateral regions of the thalamus noradrenergic A5 region, rostral ventral medulla (RVM), periaqueductal gray (PAG), and superior colliculus. Similarly, CB1 receptors prevail in the cortex, hippocampus, cerebellum, and basal ganglia. In the cortex and hippocampus, CB1 receptors flourish in cholecystokinin-containing basket cells (CCK positive basket cells), interneurons (low threshold spiking interneurons), and dwindle in glutamatergic and medium spiny neurons of the dorsal and ventral striatum.

In addition, axon and preterminal axonal segments, GABAergic interneuron subsets, direct pathway axons entering the globus pallidus en route to the substantia nigra, cerebellar climbing and parallel fibres, basket cells and peripheral sensory nerve ending have CB1 receptors in plenitudes.

Both CB1 and CB2 receptors in non-neuronal cells proximate to primary afferent nerve terminals participate in immune and inflammatory processes. CB1 receptors are prolific on the terminal axon segment and axons but less prevalent on proximal neurones, dendrites, and the cell body. A tiny fraction of CB1 receptors occur in C-fibres, while the majority occur on the more giant myelinated A-fibre neurons, a distribution consistent with their modulating pain perception at both (spinal and supraspinal levels. CB1 receptors in peripheral tissues (fat adipocytes, liver, pancreas, and skeletal muscle) participate in the metabolic consequences of CB1 receptor blockade (11,17–19).

2.3.3.2. CB2 Receptors

Nerve/tissue injury or inflammation induces CB2 receptors to increase their expression 100-fold (23,25). CB2 receptors proliferate less in the CNS than CB1 receptors and predominate outside the CNS in immune system cells and tissues, such as inflammatory and immune/immunocompetent cells (e.g., macrophages, microglia, osteoclasts, osteoblasts, vascular elements, and specific neurons). Increased CB2 receptors in the CNS result from the increased expression of innate CNS CB2 cells or the passage of peripheral immune cells (e.g., CB2-expressing monocytes) into the CNS.

Cannabinoids control neuropathy and inflammation. CBD neuromodulates the immune system and brain CB1 and CB2 receptors, causing analgesia. Analgesia from intra-cerebroventricular and systemic cannabinoid receptor agonists implies central-acting antinociception control (14).
The opioid and endocannabinoid systems regulate pain similarly. CB2 receptor activation modulates inflammation and nociception by indirectly exciting primary afferent opioid receptors, counteracting the CNS adverse effects of CB1 receptor activation.
Cytokines (inflammatory mediators that potentiate pain signals) influence peripheral tissue inflammation and immune system activity via CB2 receptors. Interferon (INF)- activated CB2

receptors release interleukins IL-10 and IL-12 and macrophages to stimulate the immune system. Non-neuronal cells near nociceptive neuron terminals limit proinflammatory release, lowering cytokines, inflammatory hypersensitivity, and promoting antinociception.

CB2 also has a direct anti-inflammatory action in target cells, inducing apoptosis, modulating adhesion and migration, and reducing matrix metalloproteinase production (27). CB2 receptors and CB2-selective agonists reduce inflammation and pain by inhibiting inflammatory hypersensitivity without unwanted behavioural or CNS side effects (15).

2.3.3.3. Cannabinoid enzymes

Enzymatic degradation controls the number of cannabinoids circulating in the body. Fatty acid amide hydrolase (FAAH) enzymes link to cannabinoid receptors, digesting fatty acid amides and alleviating chronic inflammatory pain. By desensitizing TRPV1, FAAH decreases peripheral inflammatory pain (26,27).

2.4 Targeting with CBD

Passive targeting prevents many CNS drugs from crossing the BBB. Nanoparticles targeting brain tissue activate transcytosis by interacting with brain endothelial cell transporter molecules, allowing drugs to cross the BBB. Small cannabinoid-decorated lipid nanocapsules (LNC) improve brain-targeting capacity, presenting a novel approach to designing and developing new therapies for CNS diseases.

On the luminal surface of the BBB, astrocytes, microglial cells, and pericytes express CB1. CB1 interacts with astrocyte-produced anandamide to produce IL-6, which modulates autoimmune processes.

Cannabinoids interact with CB1 receptors on presynaptic axons, inhibiting neurotransmitter release and producing protective effects. CB1-cannabinoid interaction also opens potassium channels, which reduces neuronal firing, closes voltage-gated calcium channels, and inhibits calcium influx into the cell.

CB2 receptors and agonists reduce neuroinflammation at the blood-brain barrier (BBB). Neurodegenerative diseases increase the expression of CB2 receptors in brain tissue. CB2

agonists increase trans-endothelial electrical resistance and decrease leukocyte adhesion to the brain's vasculature, hence inhibiting the LPS-induced breakdown of the BBB. CB2 agonists reduce proinflammatory mediator-induced surface expression of ICAM-1 and VCAM-1 on endothelial cells in the brain, suggesting that CB2 agonists can protect the BBB against neuroinflammation.

Formulations targeting cannabinoid receptors must consider pharmacological drug interactions, as functional selectivity and partial or inverse agonism can induce receptor-ligand interactions (4). Targeting CB2 receptors with CB2-selective agonists reduces hypersensitivity to inflammatory and neuropathic without the unwanted behavioural and CNS side effects of cannabis.

WIN-55,212-2, a high-affinity cannabinoid agonist, suppresses allodynia, mechanical and thermal hyperalgesia, neuropathic pain, and peripheral inflammation via CB1 receptor-mediated pathways. Repeated treatment with WIN-55,212-2 sensitizes peripheral sensory nerve terminals and reduces the effects of inflammatory mediators, including NO and PGE2, without inducing tolerance. Only peripheral (s.c.) and not central (intrathecal, i.t.) administration of the CB1 receptor antagonist/inverse agonist SR141716A counteracts its effects.

Table 2.3: CBD Receptor-Mediated Analgesic Mechanisms and Cell Targets (20)

RECEPTOR CLASS	RECEPTORS	FUNCTION
CANNABINOID SYSTEM	CB1	Negative Allo Modulator
	CB2	Weak Antagonist
	FAAH	Weak Inhibitor
	FABP	Inhibitor
ATYPICAL CANNABINOID RECEPTORS	GPR18	Antagonist
	GPR55	Antagonist
SEROTONIN RECEPTORS	5-HT1A	Full Agonist
	5-HT2A	Weak Partial Agonist
	5-HT3A	Negative Allo Modulator
DOPAMINE RECEPTORS	D2High	Partial Agonist
OPIOID RECEPTORS	μOR	Negative Allo Modulator
	δOR	Negative Allo Modulator

ADENOSINE SYSTEM	ENT1	Inhibitor
GLYCINE RECEPTORS	GlyR	Positive Allo Modulator
GABA RECEPTORS	GABA-A	Positive Allo Modulator
ACETYLCHOLINE RECEPTORS	α-7-AChR	Negative Allo Modulator
TRP CHANNELS		Agonist
	TRPV1	
	TRPV2	Agonist
	TRPV3	Agonist
	TRPV4	Agonist
	TRPA1	Agonist
	TRPVM8	Antagonist
NUCLEAR RECEPTORS	PPARY	Agonist

2.5 Cannabinoid Physiology

2.5.1. The Blood Brain Barrier

The Blood Brain Barrier (BBB) forms a functional interface that separates the CNS from the blood circulation, shielding the CNS parenchyma from potential toxins and dangerous elements in the blood. Studies report that the BBB blocks 95% of intravenous drugs, and just 1% enter the brain. The impermeable BBB prevents several drugs from crossing, resulting in low drug concentrations in brain tissue and therapeutic failure of brain and CNS agents (18,24). Linking polar drug ends to lipid groups or coating lipid nanocarriers with lipophilic CBD molecules increases BBB permeability by enabling binding to various brain endothelium receptors. However, linking drug molecules to lipid carriers promotes hydrophobicity and allows brain-wide dispersion rather than site-specific targeting. Ligands in therapeutic drug-specific endothelial transporters trigger receptor-mediated transcytosis at BBB endothelium (18).

The BBB prevents transcellular movement of oxygen, CO_2, water, ions, glucose, and other essential components for brain cell metabolism, creating a homeostatic environment for neurovascular units' neuronal and glial cells. Endothelial cells, myocytes, pericytes, and extracellular matrix components cause vascular changes, vasoconstriction, and vasodilation, while microvessel-attached neurons and astrocytes control blood flow. Peripheral capillaries contain widely spaced fenestrations of up to 50 nm, while brain capillaries have vital intercellular

junctions and zonulae occludent (31). (22). BBB tight junctions connect capillary basement membranes, pericytes, and astrocyte endfeet (29). Tight junctions restrict paracellular hydrophilic solute transport, preventing pathogens, toxins, or chemicals from entering the brain via circulation (22).

The microglia and BBB provide the first line of defence of the CNS. Cerebrovascular inflammation weakens the ability of the BBB to protect the brain, leading to brain dysfunction. Inflammatory BBB disorders caused by chronic systemic inflammation alter ion homeostasis, dysregulate regulatory proteinases and disrupt BBB's integrity and tight junction architecture. During CNS inflammation, peripheral and central immune cells such as leukocytes pass from the systemic blood circulation through the BBB, activating local immune cells that damage the neurons. Intraperitoneal administration of CBD post-infection limits leukocyte crossing from the systemic circulation by attenuating microglial activation and down-regulating chemokine expression, indicating reduced inflammation. Activation of the ECS prevents immune and endothelial cell interactions by maintaining tight junctions. The cognitive system positively responds to the preservative effects of cannabinoids that protect the structure and function of the BBB, thus offering neuroprotection (14).

Encephalitis induced by Lipopolysaccharide (LPS) breaks down the BBB architecture because cytokines disrupt the tight endothelial junctions. CBD preserves BBB integrity by inhibiting vasodilation, LPS-induced leukocyte margination and damage through vessel diameter and permeability changes. Increased BBB permeability causes lesions aggravated by septic shock. With its potent anti-inflammatory and immunosuppressive activity, CBD endows protective effects on the BBB by preserving the function and reducing the architectural alteration of the BBB, preventing endothelial cell inflammation, and stimulating the expression of proteins that compose tight junctions.

Diabetes type 2 patients risk dementia as chronic inflammation and oxidative stress disrupt the BBB preceding cognitive decline. High glucose levels damage the endothelial function of the BBB. CBD can improve cognitive system deficits by preventing cellular margination and reducing

adhesion molecule expression and chemotaxis, implying that CBD molecules can target and protect the BBB to avoid diabetes-related dementia (14).

Efflux pump proteins like Adenosine triphosphate-binding cassette (ABC) transporters carry substances across cellular membranes and barriers like the BBB to remove them.
Endothelial and astrocyte transporters in brain vessels express breast cancer resistance proteins (Bcrp or Abcg2) and P-glycoproteins (P-GP or Abcb1). Chemical substrates attracted to ABC transporter proteins make poor therapeutic agents because they are deported from the brain into the blood, hindering their accumulation in the brain.

CBD, a THC isomer, is neither a P-gp nor Bcrp substrate. Therefore, as P-gp or Bcrp do not impede CBDs' entry into the brain, CBD may prevent drug resistance when interacting with ABC transporters by reducing P-gp and Bcrp transport through upregulations (24). Moreover, drug-P-gp or drug-Bcrp binding precludes import across the BBB to target sites, resulting in drug resistance. Drug-P-gp or drug-Bcrp binding induces drug resistance, inhibiting BBB transport to target sites (23). CBD, a THC isomer, is neither a P-gp nor Bcrp substrate and enters the brain unimpeded by P-gp or Bcrp. Thus, CBD may reduce P-gp and Bcrp trafficking and upregulate ABC transporters to avoid drug resistance (24).

2.5.2. Physiological factors affecting *in-vivo* solubility of CBD

2.5.2.1 Absorption in the gastro intestinal tract (GIT)

Oral bioavailability, the quantity of drug absorbed into the systemic circulation following drug ingestion, can be affected negatively by several physicochemical and physiological mechanisms, impacting the rate and extent of a drug's oral absorption. Absorption into the systemic circulation requires the drug to pass through the GI wall. A drug unable to dissolve in the GIT hinders its passage through the gut wall and into the systemic or lymphatic circulation, making it ineffective. Despite its good pharmacologic activity, a drug with unfavourable physicochemical properties compromises bioavailability, leading to poor therapeutic performance. A drug like CBD with poor aqueous solubility and a corresponding low dissolution rate, a Log P ≤ 1 or ≥ 3 to 5, indicates poor permeability through the luminal wall, and a drug

molecule with a chemical structure prone to degradation via acid catalysed and enzymatic reactions in the gastrointestinal mucosa and bloodstream.

LBDDS offers intrinsic sustained release features and overcomes bioavailability barriers by improving the drug's solubilisation, permeation, and stability before and after digestion.
LBDDS, like liposomes, fully or partially solubilize the drug before it reaches the digestive system, maintaining it in solution by spontaneously forming micelles in emulsions that protect the sensitive drug molecules from water-soluble reactants and degradation mechanisms in aqueous body fluids (21).
A drug must permeate the GIT wall for absorption. Increasing the oral absorption of liposomes and their payloads involves improving liposome instability and integrity in the aqueous milieu of the GIT, prolonging gastrointestinal residence time, and penetrating the mucus layer (22).

2.5.2.2 The gastrointestinal environment:

Gastric fluid: is physiologically complex, containing inorganic substances such as potassium, sodium, and calcium and several digestive proteins like gastricsin, pepsin, trypsin (1 and 2), gastric lipase, gastric amylase, gelatinase, and mucin-glycoproteins. Bile salt micelle solubilization increases intestinal drug absorption, although gastric transit takes 2.5-3 hours to empty 50% of stomach content.
The stomach (pH 1.4-2.1) becomes more acidic after a meal; however, under fasting conditions, pH becomes more basic, moving along the GI Tract to the duodenum (pH 4.9-6.4) and jejunum (pH 4.4-6.6), eventually reaching the ileum (pH 6.5-7.4) within about 85 minutes. By this time, drug product dissolution is usually complete, meeting the rapid dissolution criterion (≥85% dissolved within 30 minutes) (5,23).

Acidic drugs with low solubility and pH absorb poorly in the stomach and better in the distal intestine. Gut wall and cytochrome P450 3A4 isozyme metabolism significantly reduce from the jejunum to the ileum, although absorption does not always reduce between the ileum and colon. Modified-release products leave the stomach within an hour and reach the colon about 3 hours later. Small intestinal transit time in the fasted state is longer than the gastric residence time (3 h), making drug dissolution more reliable for poorly soluble drugs at the gastric pH as the drug

has sufficient time to dissolve. A minimum fluid volume of about 250 ml, swallowed with the oral dosage form, should be present in the stomach for solubilization and dissolution. Under fasting conditions, dissolution failure in the stomach will expose it to the variable physiological fluid volumes of the small intestine (50-1100 ml with a 500 ml average) on gastric emptying (23).

Bile salts, a type of surfactant secreted by hepatocytes, are required for lipid absorption and the oral bioavailability of hydrophilic and lipophilic drugs; however, they strongly bind to phospholipids to form bilosomes that disrupt lipid bilayers and hydrolyze phospholipids, thereby compromising liposome integrity. Bile salts effectively damage liposomes containing phospholipids with phase transition temperatures (T_p) below 37°C, but to a lesser extent, those in the GIT with higher T_p. Bile salts paradoxically stabilize liposomes when incorporated into lipid bilayers during liposome production, lowering membrane degeneration, preserving liposome integrity, and boosting stability, mucoadhesion, and intestinal permeability. Like cholesterol, bile salts may be easily incorporated into liposomal membranes, making them the polymer of choice for oral delivery of drugs.

2.5.2.3 Digestion of LBDDS

The digestion of LBDDS produces colloidal rug dispersions that attract to the protective aqueous monolayer (or unstirred water layer) lining the lumen, improving drug permeability and the opening of the tight epithelial junctions. Intestinal permeability also depends on drug supersaturation, efflux inhibition, and membrane fluidity.

Initially, API supersaturation (an increase in free drug fraction) decreases the solubilization capacity of the LBDDS following dispersion in the gastric and intestinal fluids in the small intestine, creating a pressure gradient for drug absorption. The imbalance created between the solubilized drug's initial concentration in the GI fluids and its solubility in the colloidal species generated post-dispersion and post-digestion fuels the drug's supersaturation even further. In the meantime, as the lipid metabolites are absorbed, the ability of the remaining colloidal phases to dissolve during digestion declines, causing supersaturation to continue (24).

An LBDDS's triglycerides break down by lipolysis in the GI tract to create fatty acids and monoglycerides. Fatty acid absorption via the hepatic or lymphatic routes depends on the hydrocarbon chain length. Albumin binds to fatty acids with hydrocarbon chains longer than 12 carbons, rendering them water soluble and enabling them to passively permeate through the epithelial cells lining the intestine into the bloodstream and onto the liver via the portal vein. Hydrophobic fatty acids with a chain length ≥14C act as substrates that carry proteins into cells, where they are reassembled into lipoproteins (chylomicrons) and taken up by the lymphatic system for absorption. Long-chain unsaturated fatty acids (LCFA) decrease the first-pass hepatic drug metabolism, which boosts lymphatic absorption and stimulates chylomicron secretion. As a result, adding LCFAs to LBDDS can enhance the absorption of highly lipophilic drugs (LogP > 5), very soluble in triglycerides (Cs > 50 mg/mL), and are excellent candidates for lymphatic absorption (24).

2.5.2.4 Improving the survival rate of the liposome and its drug payload:

Liposome drug carriers have outstanding entrapment, biocompatibility, and safety, but physical instability, physiological obstacles, and gastrointestinal bio-membranes hinder their bioavailability. Conventional liposomes, comprised of phospholipids and cholesterols, are destabilized by stomach acid, bile salts, and pancreatic enzymes, decreasing the concentration of intact liposomes and drug payload leakage. Liposomes, in transit from the stomach to the small intestine, gradually degrade, releasing drug payloads directly into the gastrointestinal lumen or transferring them to secondary carriers, such as mixed micelles, which interact with the intestinal epithelia to facilitate absorption. Only liposomes that survive the gastrointestinal environment and penetrate the mucus layers can reach the intestinal epithelia and be absorbed with their payloads.

2.5.2.5 Formulation strategies:

Optimising lipid composition during formulation development can improve liposome stability. Adding polymers or ligands improves stability and permeability. Liposome instability in aqueous dispersions necessitates solid dosage formulations with good reconstitution capacities, traditionally achieved through freeze-drying or spray-drying methods. Modulation, surface coating, and interior thickening can also stabilize liposomes.

Modulation: Drug release can occur in the GIT lumen, or poorly water-soluble drugs can form mixed micelles from the remnants of liposomes and re-encapsulate drugs for absorption by the intestinal epithelia. Modulating lipid bilayer compositions by adding polymers or ligands reduces the drug release by improving liposome stability and permeability.

Surface coating: Liposomal membranes are protected from gastric acid, bile salts, and pancreatic lipases by exterior coatings such as chitosan, PEG, pectin, and Silicone. Coating liposomes with mucoadhesive polysaccharide polymers or modulating surface charges enhance liposome cohesion, resistance to enzyme destruction, oral absorption, and bioavailability. Mucoadhesive polymers prolonged GIT residence and liposome contact with intestinal epithelia. Chitosan is the ideal coating material for liposomes. Positively charged Chitosan interacts with negatively charged liposome surfaces to generate a protective coating for drug-loaded liposomes, insulating them from gastrointestinal attack. Chitosan is mucoadhesive, with low-molecular-weight chitosan exhibiting the most vigorous adherence. Upon contact with mucin, Chitosan-coated liposomes release their drug payloads. The drug molecules adhere to the mucus layers, enhancing translocation and increasing intestinal epithelial cell penetration and absorption. Chitosan polymers and oral derivatives allow hydrophilic macromolecules to cross the paracellular membrane.

Absorption enhancers improve permeation across enteric epithelia through carrier-mediated transmembrane absorption, penetration through intercellular regions, interfering with cellular lipid bilayer structure, opening tight junctions, and forming lipophilic ion-pair complexes with organic cations.

Interior thickening: Thickening the internal aqueous phases of lipid bilayers increases the physical stability of liposomes. Interior gelling boosts lipid bilayer stability by protecting the liposome against destabilizers, increasing stiffness, and sustaining payload release (22).

2.5.2.6 Strategies to overcome physiological barriers

Physiological mechanisms that decrease the bioavailability of orally administered drugs include pre-systemic elimination by digestive enzymes, P-glycoprotein-mediated efflux transport of

drugs back into the gastrointestinal tract lumen, and hepatic first-pass metabolism. Strategies to overcome physiological barriers include phospholipids with higher Tp, bile salt incorporation, and intact vesicles for bilosomes to withstand gastrointestinal destabilizing factors.

Alternative routes for absorbing orally administered liposomes:

Degradation of liposomes may result in payload leakage, inactivation of labile medicines, and precipitation of lipophilic components, hence reducing oral absorption. Liposomes that survive the stomach-intestine process absorb as integral vesicles through the M cell-to-lymph route. Stable liposomes are more likely to survive GIT conditions, allowing intestinal epithelia to absorb and increase their bioavailability. Enzyme inhibitors stabilize proteins released from liposomes. *Uptake by M cells:* Biomacromolecule absorption improves through limited liposome uptake by M cells in Peyer's patches, while gastrointestinal mucus secretion and shedding restrict oral liposome absorption. M cells in Peyer's patches are specialized epithelial cells that transfer particles from the intestinal lumen to lymphoid tissues. M cells are more accessible to liposomes as they are less shielded by mucus. Liposome absorption via the M cell route depends on their surface charge and through adsorptive endocytosis, fluid-phase endocytosis, and phagocytosis. The longer residence time in the gut milieu by polymer-coated liposomes enhances liposome absorption and mucus layer penetration, which improves M cells transfer.

Clathrin-dependent endocytosis, caveolae-dependent endocytosis, macrocytosis, or fusion: Inhibition of P-gp, a multidrug transporter responsible for the efflux of various drug substrates, is a potential mechanism for enhancing oral absorption of liposomal payloads.

Ligand-mediated endocytosis targets receptors in enteric epithelia with nutritional ligands, enhancing liposome uptake and transport through pinocytosis and phagocytosis, while antibodies improve gastrointestinal permeability.

Ligand-receptor interaction facilitates receptor-mediated transport, adherence, accumulation, and release of liposomes at absorption sites. Receptor-mediated pinocytosis occurs generally by clathrin-mediated endocytosis (CME) or caveolae-mediated endocytosis (CvME), depending

on liposome size. Liposomes processed by CvME are helpful for the oral delivery of enzyme-sensitive drugs.

Receptor-mediated endocytosis is highly efficient in drug substrate efflux and inhibition, enhancing the oral absorption of liposomal payloads. Ligand-mediated endocytosis involves receptor-mediated transport, targeting specific receptors in the enteric epithelia, enhancing cellular uptake and trans-epithelial transport at absorption sites. Liposomes exploiting CvME may be advantageous for the oral delivery of enzyme-sensitive drugs.

Mucoadhesion of liposomes to intestinal epithelia prolongs exposure and improves oral absorption, but mucus trapping capacity and turnover time inhibit liposome transit and permeability. The intestinal mucin turnover period is between 50 and 270 minutes, and mucoadhesive liposomes do not stick to mucus for more than 4–5 hours, a factor that limits their absorption efficiency.

Pegylation of DPPC and PC liposomes, or coating with mucin or silica, inhibits enzymatic degradation, improves the stability of encapsulated drugs, and extends their residence in the GIT via mucin interweaving and deep penetration of mucus layers, thereby enhancing M cell uptake and oral immunization efficacy.

Ionic interactions between mucus layers and liposomes coated with polymers (such as Pluronic F127), polysaccharides, PEGs, and carbopols promote mucoadhesion, which gives liposomes a longer elimination half-life by facilitating direct contact with epithelia, prolonging drug residence time, and increasing passive intestinal permeability and caveolae- or clathrin-mediated endocytosis (22).

2.6 Cannabidiol (CBD) Profile

2.6.1. Molecular Chemistry of CBD

CBD's IUPAC name is: 2-[(1R,6R)-3-methyl-6-prop-1-en-2-ylcyclohex-2-en-1-yl]-5-pentylbenzene-1,3-diol (PUBCHEM). CBD's molecular properties explain its medicinal,

biochemical, and physiological actions (Table 2.4). Modifying the CBD molecule and creating suitable formulations can improve oral bioavailability, solubility, and physicochemical stability.

The chemical structure of CBD (Figure 2.1) is 2-[1R-3-methyl-6R-(1-methylethenyl)-2-cyclohexen-1-yl]-5-pentyl-1,3-benzenediol. CBD, a 21-carbon terpenophenol, has a cyclohexene (terpenic) ring perpendicular to a phenolic (aromatic) ring and a pentyl side chain. In addition, CBD has four absolute trans configuration side-chain homologs in positions 1R and 6R: methyl, n-butyl, n-pentyl and n-propyl. CBD's chemical action comes from the phenolic ring's hydroxyl groups (C-2′ and C-6′), the cyclohexane ring's methyl group (C-3′), and the pentyl chain's phenolic ring (C-4′). The phenolic ring's hydroxyl groups (C-2′ and C-6′) may hydrogen link CBD to amino acids. The open CBD ring (C-6) is dormant (25).

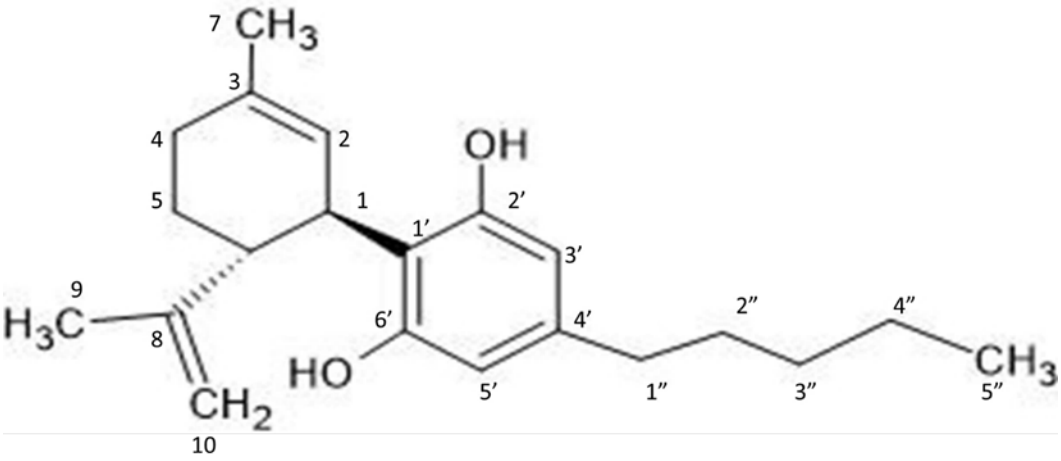

Figure 2.1: The Cannabidiol Molecule **(25)**

Table 2.4: Molecular Chemistry of CBD (26)

Chemical Property	Specification	Chemical Property	Specification
CAS Registry number	13956-29-1	Hydrogen Bond Donor Count	2
Molecular Formula	C21H30O2	Hydrogen Bond Acceptor Count	2
Molecular weight:	314,5	Rotatable Bond Count	6
Exact Mass	314.224580195	Heavy Atom Count	23
Monoisotopic Mess	314.224580195	Isotope Atom Count	0
Boiling Point	188.5 °C	Defined Atom Stereocenter Count	2

Melting Point	67,0 °C	Undefined Atom Stereocenter Count	0
XlogP3- A.A.:	6,5	Covalently-Bonded Unit Count	1
Topological Polar Surface Area	40.5 Å²	Canonicalized Compound	Yes
Formal Charge	0	Complexity	414

2.6.2. Physicochemical Properties of CBD

Oral CBD is safe at chronic and high dosages and contains no persistent, bioaccumulative, or toxic components. CBD has demonstrated analgesic, anti-inflammatory, neuroprotective, anticonvulsant, muscle relaxant, anxiolytic, and antipsychotic activity. Humans tolerate up to 1500 mg/d of CBD well (34).

CBD's poor bioavailability, water solubility, and lipophilicity make absorption problematic (11). Changing CBD formulations can improve oral bioavailability, solubility, and physicochemical stability (11,35). CBD is a light yellow or white crystalline powder that forms a clear light yellow to a colourless solution. CBD is soluble in 10 mg/ml MeOH and partially soluble in water at 20°C. Identification and assay: >98 % pure (HPLC). CBD degrades in temperature, light, and auto-oxidation to form D9-THC and D8-THC contaminants; hence, it must be kept between 2-8°C in sealed containers in dry settings (14,18). CBD is also incompatible with oxidizing agents. Oxidation causes rancidity, deterioration of fats and decreased concentrations of cannabinoids and terpenes. CBD solubilized in MCTs is less prone to oxidative degradation (27).

The o/w partition coefficient (LogP) describes the lipophilicity/hydrophobicity and the preference of a drug to exist in a solution's water or oil phase. The highly lipophilic CBD molecule with a LogP of 6.3 distributes to a greater extent into the oily portion of the solution (27).

CBD has at least two polymorphic, crystalline forms that affect drug absorption and bioavailability. Polymorphs are chemically equivalent yet have distinct crystalline forms formed by variable crystallization speeds and circumstances, resulting in diverse molecular conformations. In solution, chemically identical polymorphic compounds behave the same. Polymorphism screening during pharmaceutical drug development is vital. Polymorphism can alter drug qualities like kinetic, thermodynamic, mechanical, and surface properties, affecting quality, safety, effectiveness, and performance. APIs modelled on a single polymorph are safer

and more effective (36). CBD molecules display stereoisomerism. The (-) enantiomer of CBD occurs naturally, while the (+) enantiomer is synthetic and has a modest affinity for CB1 and CB2 receptors (8,25,28).

2.6.3. Pharmacokinetics of CBD

CBD pharmacokinetics depends on the administration route, dosage schedule (single, multiple-dose), formulation type and diet (fasted vs. fed).

2.6.3.1. Administration routes

Administration routes affect plasma and brain CBD concentrations. CBD's half-life ($t_{1/2}$) is 1.4–10.9 hours (h) after oromucosal spray, 2–5 days after chronic oral dosing, 24 h after intravenous (i.v.), and 31 h after smoking (37). CBD plasma bioavailability after cannabis inhalation is 31% (range 11–45%). CBD plasma bioavailability after cannabis inhalation is 31% (range 11–45%). Brain CBD levels rapidly peak 15 minutes after inhalation before progressively dropping. CBD nasal absorption takes 30s (seconds) and reaches peak drug concentration ($T_{max)}$ in 10 minutes (min).

Cyclodextrins momentarily open tight connections in nasal epithelial membranes, enhancing brain CBD permeability (14). THC and CBD (1mg/kg) delivered intravenously to rats produced greater brain concentrations of unaltered CBD than THC. In rats, intraperitoneal (i.p.) CBD treatment produced considerably greater brain and plasma concentrations than oral, with a T_{max} of 1-2 h and an AUC at 0–6 h of 1229 µg/g min. In contrast, orally administered CBD levels peaked faster with a T_{max} of 1 hour in the plasma and 6 hours in the brain, and AUC at 0–6 h of 319 µg/g min. Brain/plasma ratios for CBD with AUC at 0–6 h were 0.84 and 0.51, demonstrating that i.p. and oral delivery enter the brain similarly. No drugs were detected 24 h after administration (14).

A 40 mg oral dose of CBD over six hours gives an equivalent plasma course to a 20 mg oral dose of THC. A comparative study gave rats single dose THC, CBD, and THC/CBD combos at 10 mg/kg via different routes of administration. THC/CBD administration revealed that subcutaneous (s.c.) dosing produced CBD brain concentrations that were two times lower and

four times higher than individually administered CBD and THC. In contrast, the inhaled THC/CBD combination performed similarly to CBD or THC alone.

Orally administered THC/CBD levels peaked two hours after administration, whereas brain concentrations of THC or CBD given individually remained high for two hours. Although oral and inhaled dose serum peaks were similar, brain levels were 3-6 times higher for four hours, indicating a build-up of THC and CBD in brain tissue, explaining the protracted effects of oral cannabis intake. Thus, cannabinoid brain and serum concentrations peak swiftly and dip gradually on inhalation, while s.c. and oral administration retain long-lasting effects, with oral intake producing the highest level in the brain (14).

2.6.3.2. Absorption:

Unformulated highly lipophilic CBD in an oil base taken via oral, oromucosal or sublingual routes yields similar low bioavailability values of approximately 6% because of poor solubility, incomplete, variable absorption, and significant first-pass metabolism. Furthermore, the precipitation of CBD in oil in the GIT slows absorption and increases elimination rates (29).
A comparative bioavailability study of MCT-CBD (CBD in oil) and LBDDS-CBD (i.e., SEDDS, SMEDDS, and SNEDDS) showed that SEDDS-CBD increased AUC and C_{max} compared to MCT-CBD. CBD's oral bioavailability improves by solubilization in aqueous gastric fluids. SEDDS-CBD spontaneously forms tiny droplets that solubilize the co-administered lipophilic CBD upon contact with the gastric or intestinal fluid. The droplets diffuse across the aqueous lumen of GI-tract to the enterocyte, where single CBD molecules dissociate from the droplets and transfer to the enterocyte membrane (flip-flop) and then further to the blood vessels (2).

Food Effect: Plasma concentrations of CBD increase with increased dose and are higher in the fed vs. fasted state; therefore, taking CBD orally with food promotes optimal absorption. The highly lipophilic CBD molecule dissolves in high-fat/high-calorie meals, increasing micelle and chylomicron formation, solubility, gastric transit time and absorption. Moreover, biliary secretion and drug efflux transporter activity on the apical membrane of enterocytes reduces, and AUC, C_{max} and lymphatic drug transportation increase bioavailability (12,35).

Oral CBD is still subject to first-pass metabolism despite bypassing the liver into the systemic circulation via lymphatic transport. Naturally found in black pepper, piperine added to CBD formulations increases CBD's AUC and C_{max} by inhibiting first-pass metabolism mechanisms such as Cytochrome P450 family enzymes and P-glycoprotein efflux pumps, increasing CBD and THC, solubility and bioavailability (2,8,30).

CBD's oral bioavailability varies between men and women. The metabolic rate of cytochrome P450 (CYP) enzymes and relevant transport networks create gender disparities. During the absorption, distribution, metabolism, and excretion phases in females, physiological factors such as hormonal status, slower stomach motility, a higher proportion of body fat, a lower glomerular filtration rate, and changes in distribution volume are present. MCT-CBD absorbs at a higher rate in women than in men; however, gender differences were less apparent with SEDDS-CBD than with MCT-CBD due to the improved delivery of cannabidiol (12).

2.6.3.3. Distribution:

CBD penetrates tissues at 32 litre per kilogram (L/kg) (between 26 000 and 31 000 L). CBD accumulates in fatty tissue for weeks before progressively dispersing into the blood and liver due to its high lipophilicity (20,25).

CBD concentrations in brain tissues are lower than plasma concentrations despite the absence of significant obstacles to CBD entry into the human brain (23). CBD plasma concentrations range from 5.9 to 11.2 nanogram per millilitre (ng/ml) (0.019 to 0.036 m) after six weeks of repeated oral CBD (700 mg/day) and average 1.5 ng/ml (0.0048 m) one week after therapy. Thus, oral CBD removal takes 2–3 weeks (38).

The Free Drug Principle asserts that only circulating free or unbound compounds may generate a pharmacological effect. 90% of CBD binds to plasma proteins and blood cells (5). Strong plasma protein binding protects CBD against chemical transformation but cannot predict in vivo levels (16,20).

2.6.3.4. Metabolism:

Nanocarriers must overcome obstacles such as instability during systemic circulation, limited renal clearance, tissue-specific accumulation, and insufficient uptake by target cells. Cannabis has low oral bioavailability due to physicochemical factors, including surface charge, dimensions, deformability, uptake control, host-cell interaction, and the consequence of poor absorption. CBD also undergoes hepatic Phase I metabolism ("first-pass action") and gastrointestinal Phase II metabolism.

Phase I metabolism is a result of Phase I metabolic enzymes such as CYP3A4 and CYP2C metabolisms of CBD to 7-hydroxy CBD (44), which then metabolizes in the liver by pooled human liver microsomes (HLMs) to eight mono-hydroxylated metabolites (of which 6α-OH-, 6β-OH-, 7-OH-, and 4”-OH-CBDs were the major ones). The seven recombinants of human CYP enzymes metabolising CBD are CYP1A1, CYP1A2, CYP3A4, CYP3A5, CYP2C9, CYP2C19, and CYP2D6. The two main isoforms responsible for 6α-, 6β-, 7-, and 4″- hydroxylation of CBD in HLMs are CYP3A4 and CYP2C19 (28) (11,45,46).

Phase II metabolism involves intestinal enzyme conjugation, sulphation, and glucuronidation (11). Intra-enterocytes phase II metabolic enzymes (e.g., N-acetyltransferases, sulfotransferases, UDP-N-glucuronosyltransferases, methyltransferases, and glutathione-S-transferases) efflux from the enterocytes back to the gastrointestinal lumen by efflux pumps that export lipophilic and amphiphilic drugs that impede their intracellular absorption) such as P-GP (extensively distributed and expressed in the intestinal epithelium) (11).

2.6.3.5. Elimination and Excretion of CBD

Although subject to the hepatic first-pass effect, CBD and THC are excreted unchanged, more in the faeces and less in the urine, suggesting a significant unabsorbed proportion that matches findings of low bioavailability. The kidneys eliminate over 25% of oxidised and glucuronidated metabolites unaltered. Depending on the administration route, CBD’s $t_{1/2}$ is 18–32 h with a clearance of 57.6–93.6 L/hour. Oral delivery (oil, oromucosal spray, or nebulizer/aerosol) has $t_{1/2}$ = 2 h, smoking 24-31 h, and chronic oral administration 2-5 days (20,25). (16,23).

Plasma clearance (CL): CBD clearance fluctuates in the fed vs. fasted state. Oromucosal spray (5-20 mg): In the fasted state, CL ranges from 2500 to 4700 L/h; in the fed state, CL decreases to 533 L/h. In contrast, CBD's mean elimination rate (K_{el}) remains relatively constant irrespective of feeding and fasting states but varies according to the administration route. Oromucosal spray administration has 0.12-0.17 K_{el} (1/h), a nebulizer 0.98 K_{el} (1/h), and an aerosol 0.4 K_{el} (1/h) (8).

2.6.3.6. The enhanced permeability and retention (EPR) effect

Hepatic uptake and accumulation, diffusion, extravasation, distribution, excretion (hepatic and renal), clearance, serum protein binding, and activation in target tissues depend significantly on nano-lipid carriers' size and size distribution. Particle size is a critical parameter that passively targets therapeutic agents to tumours. Tumour vasculature is denser, widespread, heterogeneously dispersed, permeable, and leaky than normal tissues. Vascular mediators and high-molecular-weight therapies concentrate in locations with poor lymphatic drainage and malignancies with leaky blood arteries due to the enhanced permeability and retention (EPR) effect. EPR passively directs nanocarriers under 150-200 nm to the tumour via the cancer vasculature, increasing liposomal drug delivery.

2.6.3.6.1. Reticuloendothelial System (RES)

Monocyte-derived RES cells phagocytose foreign debris and particles, destroy tumour cells, and modulate the immune system (39). Liposomes are immediately phagocytosed and removed from the systemic circulation by RES cells. Despite macrophage absorption without serum proteins, the RES clears liposomes after plasma protein opsonisation (39). Bone marrow, kidneys, liver, lungs, spleen, and lymph nodes store liposomes. The liver stores 90% of the RES, whereas the spleen gathers ten times more liposomes.

2.6.3.6.2. The Mononuclear phagocyte system (MPS)

Physiological obstacles to liposomes include RES, opsonization and immunogenic MPS. Pinocytosis and phagocytosis, the principal mechanisms of endocytic action, use the cell's phospholipid bilayer and ATP for energy to engulf small molecules/particles. Pinocytosis engulfs extracellular fluids and dissolves solutes into the cells.

Macrophages, neutrophils, and dendritic cells absorb particles more significantly than one μm. Pdi and particle size affect endocytosis-dependent cellular absorption of nanocarrier systems. In mice, decreasing nanoliposome size to 50 nm significantly decreased MPS-mediated clearance with a plasma half-life similar to long-circulating (PEGylated) vesicles 100–150 nm. PEG polymer coating on lipid carrier surfaces reduces phagocytic cell uptake and lengthens blood circulation. Saturating the blood with API-encapsulated or empty nanoliposomes to block phagocytic activity reduces MPS uptake. Destroying MPS phagocytic activities may make these therapies clinically ineffective (a natural protective mechanism against pathogenic invasions).

2.6.3.6.3. The Opsonins

In the bloodstream, opsonins, LDLs and HDLs interact with and destabilize circulating liposomes. Opsonins (e.g., fibronectin and immunoglobulins) assist in RES recognising and eliminating liposomes. Capillary pores size and interstitial tissue spaces affect lipid nanocarrier retention. Liposomes amass in the liver and spleen in concentrations sufficiently significant to treat pathogenic diseases or delay the removal of lipophilic anticancer drugs. The body eliminates most phagocytes that accumulate in the liver and spleen.

After plasma protein opsonization, the RES clears liposomes, although macrophage uptake can proceed without serum proteins. Small liposomes cannot support opsonic activity, so opsonization diminishes between 800-200 nanometer (nm). PEG sterically stabilises liposomes to limit RES elimination, improving circulation time. PEG provides a local surface concentration of highly hydrated groups, which sterically hinders electrostatic and hydrophobic interactions with serum proteins or cells, decreasing cell absorption of the RES (39).

Table 2.5: Physiological significance of nanocarrier sizes (31)

Nanocarrier Size	Physiological Significance
≤ 10 nm	This nanocarrier size undergoes renal filtration without reabsorption
10-15 nm	Size of kidney glomerulus and pancreas' islet tissue pores
≤ 35 nm	Size of pulmonary capillary barrier pore size
20–100 nm	This nanocarrier size circulates to the spleen, liver, bone marrow sinusoids, and leaves via leaky capillaries.

≤ 50-80 nm	This nanocarrier size undergoes a reduction in MPS-dependent clearance
50-100 nm,	This nanocarrier size avoids MPS uptake and prolongs blood circulation; hence, most therapeutic nanoliposome designs fit this size range.
100-150 nm	This nanocarrier size does not leave the tissue capillaries and undergoes decreased hepatic and MPS uptake and decreased plasma protein binding.
≥100-150 nm	This nanocarrier size remains in bone marrow, liver, spleen, and lung tissues for an extended time, consumable by phagocytes.
≤ 150 nm	This nanocarrier size enters/exits fenestrated capillaries of the liver endothelium or tumour microenvironment.
50-200 nm	This nanocarrier size cannot escape from tissues and blood capillaries.

Table 2.6: Estimated particle sizes versus route of administration (31)

Nanocarrier Size	Administration route
10 to 50 nm	Lymphatic (RES).
50 to 200 nm	Long circulating carriers
10 to 600 nm	Transdermal
200 to 2000 nm	Intravenous/intramuscular
100 to 3000 nm	Ocular
1 to 10 μm	Aerosol
8 to 20 μm	Nasal

2.6.3.7. Toxicology

CBD taken in modest dosages (≤100 mg) in various ways is safe (20).

2.7 Lipid-Based Drug Delivery Systems (LBDDS)

2.7.1. The rationale for using LBDDS

Lipid-based drug delivery system (LBDDS) is an umbrella term for formulations that contain a drug dissolved or suspended in lipidic excipients. LBDDS features a low-risk profile because they are cost-effective, biocompatible, non-toxic, non-allergenic, non-irritating, biodegradable, and simple to scale up, sterilize and validate. LBDDS demonstrates high drug encapsulation efficiency and manipulation of lipid excipients and formulations, enables control of drug release, and targets specific disease sites. Compared to polymeric/surfactant-based carriers, LBDDS

formulated with water-based technologies eliminates organic solvents, reducing formulation toxicity (31).

There are different types of LBDDS (see section 2.7.2). The versatility and flexibility of LBDDS derive from the multitude of lipid excipients available, while the chemical composition and combination of lipid excipients determine their functionality (see section 2.9) (29)(30).
LBDDS oral dosage formulations incorporating lipid excipients can range from solutions, suspensions, emulsions, and simple drug-in-oil mixtures to more complex self-emulsifying lipid formulations (SELF) that spontaneously emulsify on contact with aqueous media. Spontaneous emulsification generates mixed micelles from detergent-lipid mixtures, disc-like lipid bilayer structures that shield lipid and drug molecules from surface water (32).
LBDDS can assume liquid or semi-solid dosage forms filled in hard or soft capsules or formulated as solid dosage such as dry emulsions; self-emulsifying: capsules beads; suppositories; implants, solid dispersions; self-emulsifying controlled/sustained release tablets; pellets; micro/nanospheres and particles (47).

LBDDS, stable systems that carry a significant drug content of lipophilic and hydrophilic drugs, can be manipulated for controlled drug release and disease targeting (42). Highly lipophilic drugs (e.g., CBD) are oil-soluble. Only oily liquids dissolve highly lipophilic drugs. LBDDS efficiently transport oral lipophilic drugs, provided the drug is sufficiently soluble in the oil system. CBD formulations are thus oily liquids, solutions, suspensions, emulsions, self-emulsifying lipid formulations (SELFs) and SLN delivery systems. Lipids are fatty acid esters and lipophilic hydrocarbon chains connected to a hydrophilic group such as glycerol, polyglycerol, or polyalcohol. The length and degree of unsaturation of the fatty acid chain determine the melting range, solubilization capacity, and miscibility of the excipient. Hydrophilic Lipophilic Balance (HLB) measures the dispersibility of excipients in aqueous media and characterizes the amphiphilicity or dual polar and non-polar nature of lipids.

Depending on the drug's method of administration and the patient's physiology, CBD's physicochemical qualities (dissolution, stability, solubility, metabolism, and permeability) might affect bioavailability and PK parameters, resulting in therapeutic inefficacy. Although these

LBDDS enable drug delivery via different routes, such as dermal/transdermal, intranasal, ocular, parenteral or vaginal, the preferred route by patients and formulators is oral. LBDDS are predominantly oral formulations that increase the oral bioavailability of lipophilic drugs by incorporating the drug into inert lipid vehicles. Moreover, the oral route is non-invasive, less expensive, less prone to side effects, and the most expedient method of delivering chronic drug therapies (42).

Enhancement of Intestinal Permeability: Passage through the GI wall is necessary for drug absorption into the systemic circulation. The resulting colloidal dispersions brought about by digestion of the LBDDS improve the drug affinity for the protective aqueous monolayer (or unstirred water layer) lining the lumen and facilitate the conditions for API permeability, opening the epithelial tight junctions.

Supersaturation of the drug in the GI lumen is the leading mechanism for enhancing permeability. Drug supersaturation increases free drug fraction by decreasing solubilization capacity. The imbalance between the initial solubilized drug concentration in the gastric and intestinal fluids and drug solubility in the colloidal species formed post-dispersion and digestion creates pressure for drug absorption. In addition, absorption of the lipid metabolites further reduces the solubilization capacity of the remaining colloidal dispersion phase during digestion, thus promoting ongoing supersaturation.

In the GI tract, lipolysis breaks down the triglycerides in LBDDS to produce monoglycerides and fatty acids. The hepatic and lymphatic routes absorb fatty acids depending on the hydrocarbon chain length. Fatty acids with hydrocarbon chains below 12C bind to albumin, making them water soluble and able to passively diffuse through the epithelial cells lining the intestine, into the bloodstream through the portal vein and onto the liver.

Fatty acids with a chain length of 14C or longer are hydrophobic and act as substrates for transporting proteins into the cells, where they can be resynthesized into lipoproteins (known as chylomicrons) for uptake by the lymphatic route.

The unsaturated long-chain fatty acids (LCFA) stimulate chylomicron secretion and increase lymphatic uptake, bypassing the liver. Therefore, LBDDS formulated with LCFAs offer a promising strategy for drug molecules like CBD that are highly lipophilic (LogP > 5), highly soluble in triglycerides (Cs > 50 mg/mL), and extensively metabolized in the liver.

2.7.2. Types of Lipid-Based Drug Delivery Systems (LBDDS)

2.7.2.1 Vesicular systems

Vesicles include archaesomes, colloidosomes, ethosomes, herbosomes, liposomes, niosomes, pharmacosomes, phytosomes, transferosomes, and vesosomes (41). Extracellular vesicles (EV) are nano to micro-sized vesicles secreted into extracellular spaces by cells. Liposomes, microscopic synthetic self-assembled vesicles made of amphiphilic phospholipids, form spherical bilayers like cell membranes and EVs when hydrated. Hydrophobic and amphiphilic medicines solubilize and disseminate in the liposome's fatty acid layer, whereas hydrophilic compounds embed into the inner watery core/s. Liposomes boost lipophilic medication bioavailability (45).

2.7.2.2 Lipid particulate systems

Lipid particulate systems include nanostructured lipid carriers, solid lipid microparticles (SLM), solid lipid nanoparticles (SLN), lipid drug conjugates, and lipospheres (41). SLN forms spherical particles (10–1,000 nm) capable of solubilising lipophilic molecules in a surfactant-stabilised solid lipid core matrix. Lipids used in SNL are di-glycerides, monoglycerides, triglycerides, waxes, steroids (e.g., cholesterol), and fatty acids.

2.7.2.3 Emulsions

Emulsions include microemulsions, nanoemulsions, Pickering emulsions, and self-emulsifying lipid formulations (SELFs). Emulsions consist of at least two immiscible fluids; one disperses as microscopic globules in the other (32).

Table 2.7: Grading Behaviour of o/w Emulsions

Grade	Behaviour

A:	Swift emulsion formation, transparent/bluish appearance
B:	Swift emulsion formation, opaque-bluish appearance
C:	The emulsion has a refined, milky appearance
D:	Slow emulsion formation; dull, greyish-white, oily appearance
E:	Poor emulsification: big oil droplets on the surface

Multiple emulsions form drops containing droplets of a different phase, divide into water-in-oil-in-water (W/O/W) or oil-in-water-in-oil (o/w/o) droplets, stabilized with surfactants soluble in both water and oil (Figure 2.2) (50). Significantly water-soluble surfactants/emulsifying agents stabilize oil in water (o/w) nanoemulsions that disperse oil beads in a continuous water phase. In contrast, significantly oil-soluble surfactants/emulsifying agents stabilize water in oil (w/o) nanoemulsions with water beads dispersed in the continuous oil phase. Colloidal vesicular systems are liposomes containing solubilized and encapsulated drugs (45).

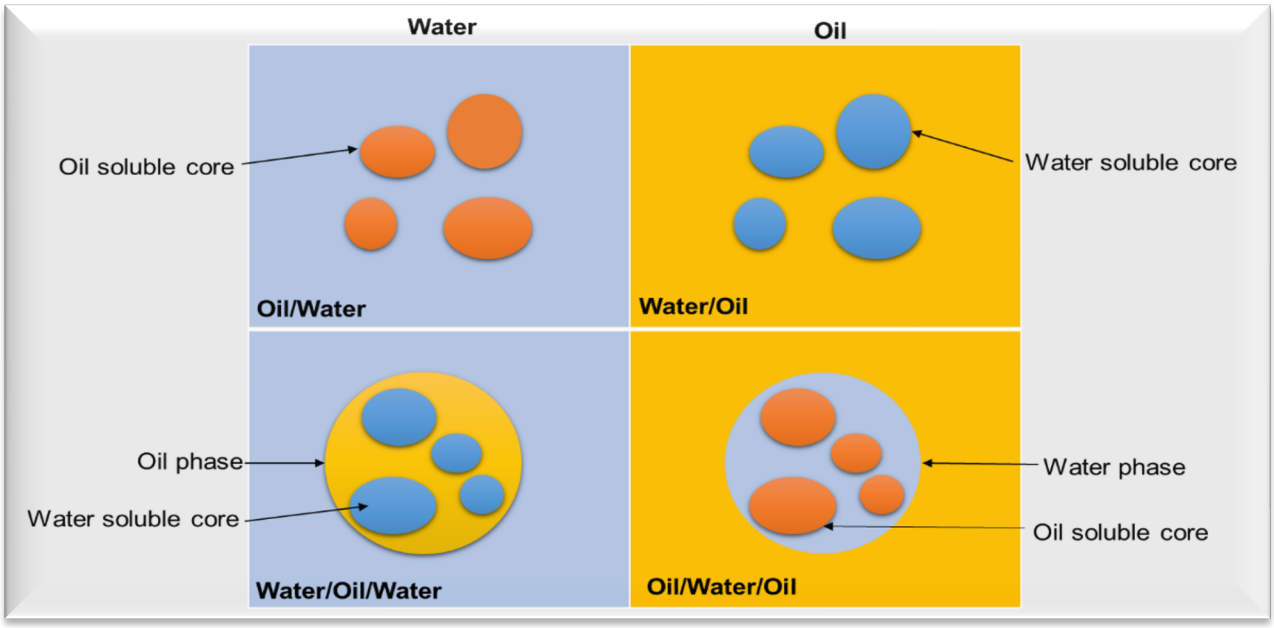

Figure 2.2: Types of Emulsions

2.7.3. Self-Emulsifying Drug Formulations (SELFs)

SELFs are thermodynamic or kinetically stable o/w emulsions. Pro-nano-liposphere (PNL) pre-concentrates are isotropic mixtures of a drug, lipids, co-solvent (CoS), and surfactants (S).

Table 2.8: Distinctive features of SEDDS, SMEDDS, SNEDDS (33)

PROPERTY	SEDDS	SMEDDS	SNEDDS
Size	> 300 nm	< 250 nm	< 100 nm
Appearance	Turbid	Clear	Clear
HLB Value of surfactant	<12	>12	>12
Lipid formulation class	Type II	Type IIIB	Type IIIB
Oil concentration	40% - 80%	>20%	> 20%
Surfactant concentration	30% - 40%	40% - 80%	40% - 80%

SELF pills or tablets promote patient compliance. Lipophilic drugs with a high LogP value, like CBD, solubilise in the oily phase and are then dispersed by surfactant action in gastric fluids and GIT motility. Surfactants/surfactant blends added to the oily phase emulsify the SELF. SELFs have three aspects that promote medication delivery and performance: SEDDS>SMEDDS>SNEDDS (Table 2.8) (45).

2.7.3.1 Self-emulsifying drug delivery systems (SEDDS)

Self-Emulsifying Drug Delivery Systems (SEDDS) are macro emulsions that combine with hydrophobic, non-ionic surfactants (HLB <12) and occasionally co-solvents to generate minute globules (>300 nm) that disperse in opaque o/w emulsions upon gentle peristaltic agitation (33,34). SEDDS improves oral bioavailability, therapeutic efficacy, and drug-loading capacity and reduces drug dose and dose-related adverse effects of poorly soluble hydrophobic molecules like CBD by solubilization. In aqueous gastric/intestinal fluids, SEDDS-CBD pro-nanoliposomes (PNLs) quickly disperse into tiny droplets containing solubilized CBD. Solubilized CBD drops reach enterocytes through the watery GI lumen. CBD molecules dissociate and flip-flop from droplets to the enterocyte membrane, circumventing the hepatic first-pass action by conveyance via lymphatic routes to blood arteries (12).

2.7.3.2 Self-micro-emulsifying drug delivery systems (SMEDDS)

SMEDDS improve the solubility of Class II and IV hydrophobic drugs and transport poorly permeable Class III and IV drugs (BCS). SMEDDS employs hydrophilic surfactants (HLB >12) and co-solvents (CoS) to generate translucent o/w emulsions with nanoparticulate globules (100–250 nm) when slightly agitated in aqueous stomach contents (44)(42). When a water-

soluble surfactant mixes with an oil-soluble co-surfactant, interfacial tension reduces sufficiently to form thermodynamically stable SMEDDS. Microemulsions require co-surfactants to reduce interfacial tension to a minimum. SMEDDS are vulnerable to changes in temperature and dilutions (33).

2.7.3.3 Self-nano-emulsifying drug delivery systems (SNEDDS)

SNEDDS have identical constitutions to SMEDDS but differ in surfactant and co-surfactant concentrations (33). Although SNEDDS needs substantial quantities of surfactants, which can cause gastric irritation, minuscule oil droplets spread rapidly and distribute extensively throughout the GIT, minimising gut wall irritation caused by prolonged drug interaction. SNEDDS improve hydrophobic and lipophilic drug solubility, bioavailability, therapeutic effectiveness, drug-loading capacity, and dose-related adverse effects (47).

SNEDDS solubilizes API based on oily phase drug solubility. LBDDS drug precipitation depends on surfactant/co-surfactant solubilization. SNEDDS are thermodynamically unstable but kinetically stable systems that destabilize slowly (over months) even under stressful fluctuations in temperature and dilutions (42). SNEDDS have more surface area and free energy than SMEDDS. SNEDDS are unsuitable for poorly water-soluble drugs at high doses, and lipids are the hardest to administer. SNEDDS functionality depends on phase behaviour, nano-emulsion droplet sizes, ionizable groups, log P value, molecular structure, pKa, amount, and weight.

Lipophilic medicines with LogP values ≥ 5 are better candidates for SNEDDS than high melting point medications with LogP values of approximately 2. SNEDDS prolong drug release, focus the medication to a specific GIT absorption window, and protect sensitive drugs (e.g., peptides) against degradation and enzymatic hydrolysis in the hostile gut environment. SNEDDS lowers dietary impacts and unpredictability without affecting lipid digestion. The long-term preservation of SNEDDS as solid dosage forms improves when filled in gelatine capsules or converted into SNL systems.

2.7.3.4 Mechanism of SELF's Formation

Reversible chemical reactions affect Gibb's "free" energy (ΔG) in thermodynamic systems under constant pressure and temperature. Gibb's "free" energy (ΔG) is the energy available to accomplish the most work in a chemical process. Reducing Gibb's free energy is needed for a spontaneous reaction at constant pressure and temperature. A positive ΔG means adding energy to make ΔG smaller than the non-pressure-volume (non-PV) work for the reaction to occur. For reactions to occur, ΔG must be negative because ΔG must be smaller than the non-PV work (equal to zero). When a thermodynamically closed system (one that can exchange heat/work with its surroundings but no matter can enter/exit) moves reversibly from an initial to a final state, the drop in ΔG is equal to the system's work minus pressure forces.

Therefore, the energy needed to establish a new surface/interface between the oil/water phases in an emulsion increases the dispersion's surface area (44,47). Emulsification needs the interfacial areas of vesicles to compress, without shear resistance, to disintegrate with low energy (35). Folding bilayers into concentric vesicles reduces unfavourable hydrophobic-hydrophilic interactions. Giant vesicles diminish hydrophobic-hydrophilic free energy differences. Energy derived from entropy changes increases self-emulsification in emulsions when dispersion energy needs exceed surface area energy.
In emulsions, free energy (ΔG) is described by

Equation 2.1: The Gibbs Free Energy Equation

$$\Delta G = \Sigma N \pi r^2 \sigma$$

ΔG = free energy linked to the process

N = droplet number

r = droplet radius

σ= interfacial energy

Entropy is a measurable physical property in a thermodynamic system that measures the "molecular disorder" and the” wasted energy” in a system as energy transforms from one state or form. Entropy changes the mix/spread of each constituent of a system's total energy over its quantized energy. Dispersal (spreading out) of energy or matter accompanies spontaneous changes at a specific temperature.

In the second law of thermodynamics, the summed entropies of interacting thermodynamic systems never decrease until they enhance another system's entropy. Heat flow from colder to warmer materials/bodies cannot occur without applying work (heat energy) to the colder mass. Therefore, in an isolated system, the entropy of that system will not diminish spontaneously with time because internal domains with differing temperatures will thermodynamically equilibrate to the single uniform temperature of the highest entropy.

Phase separation of the emulsion lowers the interfacial energy and, consequently, the system's free energy over time. Spontaneous emulsion formation (SELFs) requires low or negative free energy (44). Emulsifiers stabilise emulsions. A liquid crystalline (LC) phase monolayer encompasses the oil droplets. Water disrupts and penetrates the interface in aqueous cores, solubilising the oil phase until the solubilization limit is almost the same as the interfaces (47). LC interfaces minimise interfacial energy and prevent coalescence, providing stable emulsions (48). Gentle peristaltic agitation by the GIT and dilution by physiological fluids keep the hydrophobic drug solubilized (36).

2.8 Liposomes

2.8.1. Mechanism of liposome formation

Amphiphilic phospholipids in liposomes feature a hydrophobic tail of two fatty acid chains (10-24 carbon atoms with 0-6 double bonds per chain) and a hydrophilic head of phosphoric acid that binds to water-soluble molecules. In watery media, phospholipids spontaneously form lamellar sheets (Figure 2.3A), with the polar head group facing the aqueous region, shielding the non-polar fatty acid tails facing each other (Figure 2.3B). Lamellar sheets exposed to an aqueous medium and an energy source like heating, homogenization, shaking, and sonication (Figure 2.3C) form bilayers of closed concentric spherical vesicles (Figure 2.3D) due to unfavourable hydrophobic/hydrophilic / interactions between lipid-water and lipid-lipid molecules (50). Aqueous domains separate the bilayers (37). The aqueous-lipid system reaches thermodynamic equilibrium by reducing the system's substantial, unfavourable free energy differences by forming spheres with low surface tension and high stability (50).

The constituent molecules of the two-dimensional fluid/liquid lipid bilayer have free lateral movement in their confined monolayer. A lipid bilayer has self-sealing and self-healing properties promoted by the same forces that create bilayers from phospholipids. Hydrophilic heads facing the water shield hydrophobic tails to create energetically favourable bilayers (45). Free edges in lipid bilayers are energetically unfavourable; thus, any rip or opening exposing hydrophobic tails to water will spontaneously rearrange lipids to close in on themselves to eliminate the free edges and create a structurally stable, sealed compartment (47). At the freezing point, liposomes change from a rigid crystalline (gel) to a liquid crystalline (sol) state (48).

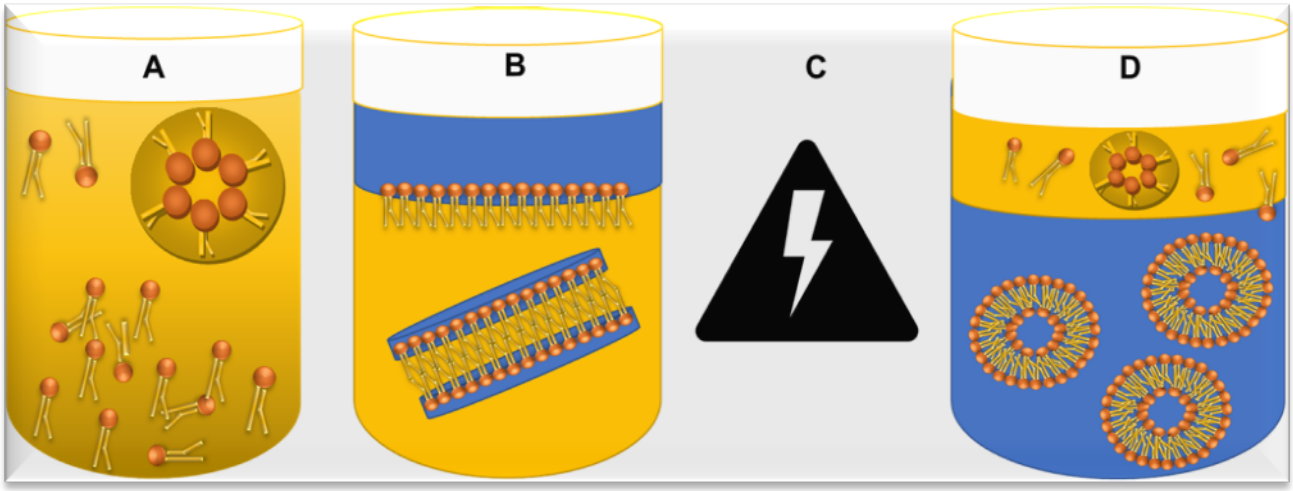

Figure 2.3: Mechanism of liposome formation A) Lipid molecules and inverse micelles in oil; B) Lamellar sheets and lamellar bilayers; C) Addition of energy source, D) Liposome and nanoliposomes formation (49)

The phase transition temperature in lipid bilayers with short hydrocarbon tails and double bonds is lower because short hydrocarbon chains interact less, and cis-double bonds kink the hydrocarbon chains, making them more difficult to pack together, making the lipid bilayer more difficult to freeze. The membrane thus remains fluid at lower temperatures (36). The transition temperatures of natural lipids like lecithin are broad. Liposome production is optimal between 41.4°C and 58°C, the temperatures at which pure lipids transition and lecithin's Krafft point exist, respectively. Liposome formation only occurs above the transition temperature, while drug release occurs during crystalline phases (50).

Table 2.9: Three generations of liposomes (38):

Generation	Type	Action
First-generation	Conventional liposomes	long-circulating transport vehicles
Second generation	Stealth liposomes	Improves circulation time by decorating the surface with PEG chains
Third-generation	Target specific liposomes	contains targeting ligands that trigger stimuli-sensitive drug release

2.8.2. Liposome drug delivery to biological cells

Liposome-cell interaction at the target site is a prerequisite to the drug's therapeutic efficacy. Liposomes must sustain drug release and plasma concentration at therapeutic levels at the target location for maximum therapeutic effectiveness. Lipid exchange happens when the cell membrane's lipid transfer proteins recognise liposomes. Liposomes integrate into cells through fusion, diffusion, pore formation, and the release of soluble content. The liposomes' lipid bilayer adsorbs to, fuses with, and assimilates into the cell membrane when lipids diffuse laterally. Endocytosis directly deposits liposomal contents in the cytoplasm. Liposomal content release depends on the target cell, its activation state, or the liposome's physical features (e.g., pH, charge, size, steric stabilisation).

At low pH, liposomes disintegrate or merge with endosomal or lysosomal membranes. In the cell interior, endocytic or phagocytotic pathways actively consume released cargo. Clathrin-coated pits swallow tiny particles (<150 nm) attached to cell surface receptors, coating the vesicles in receptor-mediated endocytosis. After internalisation, eliminating the clathrin covering allows vesicle fusion with lysosomes, lipid breakdown, and content release. Macrophages or cells with adequate ligands phagocytose big particles (>150 nm). Cell junctions (paracellular), pores, specialised receptors and shuttling vesicles allow macromolecules to penetrate the endothelium barrier (39).

Phosphatidylcholine liposomes mono-directionally transfer lipids to high-density lipoproteins in the bloodstream, destabilising their lipid bilayer and leaking cargo. Liposome distribution in organs other than the liver and spleen depends on the clearance rate. DMPC liposomes clear the plasma 8-fold less than DPPC and 20-fold less than DSPS liposomes because DSPC-serum

protein binding occurs much more than DPPC liposomes, followed by DMPC liposomes. Hence, DMPC liposomes have a limited oral applications but promising systemic applications (40). Increased phospholipid protein binding decreases its circulation half-life; conversely, decreased phospholipid-protein binding increases circulation half-life.

2.8.3. Lamellar Classification of Liposomes

Size and lamellarity classify liposomes (Table 10). Lamellarity affects encapsulation, cargo release, and drug fate following cellular absorption (45,50).

Table 2.10: Classification of Liposomes (39–41)

Class	Abbrev.	Size	Lamellae	Method
Small Unilamellar	SUV	20-100 nm	a single outer lipid bilayer	Freeze-thaw MLV
Medium Unilamellar	MUV	-	a single outer lipid bilayer	Extrusion
Large Unilamellar	LUV	100-1000 nm	a single outer lipid bilayer	Fusion
Multilamellar	MLV	0.5 μm	5-20 consecutive concentric lipid bilayers	Reverse phase evaporation
Oligolamellar	OV	0.1 – 1 μm	5 consecutive concentric lipid bilayers	Reverse phase evaporation
Giant vesicular	GV	>1000 nm		French press
Multivesicular	MMV	>1μm	A multi-compartmental structure. Separate, smaller vesicles exist within a single outer lipid bilayer.	Dehydration-rehydration

However, water-insoluble organic compounds consisting of fats, waxes, oils, sterols, and triglycerides are soluble in nonpolar organic solvents.

Liposomes are artificial, colloidal, spherical vesicles composed of lipids and phospholipids, forming spontaneously upon water dispersion. A liposome's basic structure comprises amphiphilic lipid/phospholipid molecules, but constituents can include non-toxic cholesterol

surfactants, sphingolipids, glycolipids, and medium or long-chain fatty acids, membrane proteins, and drugs in the vesicular system. Liposomes increase poorly soluble drugs' bioavailability by integrating hydrophilic and lipophilic molecules, proteins, peptides, and nucleic acids without activity loss. The liposome's amphiphilic lipid/phospholipid molecules entrap and release lipid-soluble, water-soluble, and amphiphilic materials to designated cells or tissues. Drug location in liposomes depends on the lipids' physiochemical characteristics and composition. Including additives such as polypeptides (antigens), sterols (cholesterol), polymers (chitosan or poly-ethylene-glycol), and antioxidants (α-tocopherol) in their structure improves the shelf-life and stability of the product.

Drugs lacking delivery systems circulate briefly and need regular administration. Steady drug levels extend circulation time. Liposomes improve pharmacokinetics, pharmacodynamics, therapeutic efficacy, and drug-target selectivity. In vitro and in vivo, liposomes protect pharmaceuticals from enzymatic, chemical, and immunological destruction. However, charged lipids become toxic at higher concentrations, and encapsulation effectiveness, sterilisation, stability, and short shelf-life are problematic.

Key physical attributes determining liposomes' quality, safety, efficacy, and stability in vitro and in vivo are size distribution, particle size and charge uniformity. These are fundamental parameters used for quality control assays (39).

2.8.4. Liposomes and size

Nanoliposomes, like liposomes, are colloidal nanostructures composed of lipid/phospholipid bilayers that share physical, chemical, and thermodynamic properties imparted to them by their ingredients and the suspension media. The optimal vesicle size depends on phospholipid concentration, the vesicle’s purpose and administration route and the vesicle’s purpose. Vesicle diameter determines the route of administration, but vesicle size controls clearance. More giant liposomes clear faster from circulation and release less content than smaller vesicles. Giant liposomes, however, cause severe medical pathologies, e.g., embolisms.

Encapsulation efficiency is related to liposome size, as increased encapsulation efficiency enables higher drug concentrations in biological systems. Liposome encapsulation reduces GI irritation by avoiding direct contact with the drug in the intestinal environment (39). More giant liposomes increase encapsulation efficiency and deliver higher drug concentrations to biological systems, although they can cause pathology such as embolisms. The saturation of lipid constituents increases liposome stability. DSPC, DPPC, and DMPC, fully saturated lipids, are more stable than unsaturated lipid egg phosphatidylcholine. Stable liposomes (100-200 nm) retain drugs more than giant liposomes of the same composition; however, excessive stability (e.g., DSPC) holds cargo without leakage, disabling the encapsulated drug from reaching the target (42).

2.8.5. Liposomes and charge

Lipids impart anionic (negative), cationic (positive), or zwitterionic (neutral) charges to lipid head groups, which impacts stability, a controllable property in practical liposomal drug design.
Liposomes have a nearly neutral surface charge and readily circulate, eluding the immune system. The encapsulation effectiveness of neutral liposomes is greater than that of anionic or cationic vesicles, and they interact less with serum proteins that regulate liposome dispersion and bilayer integrity.

Increased residence time in the body improves the opportunity for vesicles to associate with other tissues. Negatively charged liposomes transfer polar compounds more efficiently than positively charged ones; however, negatively charged unilamellar liposomes clear faster from the bloodstream than neutral or positively charged vesicles because they are consumed by scavenging endothelial cells and macrophages in the blood.

Cationic liposomes induce non-specific endothelial cell adsorption and their identification by scavenging endothelial cells and macrophages. Positively charged liposomes remain in circulation longer than vesicles with a near-neutral and negative surface charge because they clear from circulation more slowly and interact more with tumour tissue (45).

2.8.6. Liposome stability

Lipid formulation is critical to developing stable liposomes with good drug retention and release profiles, which are crucial for LBDDS efficacy.

2.8.6.1 Liposome stability and acyl chain length

Liposome stability relies on lipid acyl chain type and phase transition temperature. Longer acyl chains increase T_c and liposome stability regardless of cholesterol level. Liposome membranes with short hydrocarbon chains have greater encapsulation efficiencies (e.g., DSPC <DPPC <DMPC). Lengthening the fatty acyl chain of phospholipids reduces liposome leakage. DMPC liposomes release more content than DPPC or DSPC liposomes; however, DSPC liposomes are so stable that they release minimal material, preventing the encapsulated drug from reaching its target. Unsaturated phosphatidylcholines from egg or soybean create porous, less stable bilayers, whereas saturated phospholipids with long acyl chains (DDPC) make rigid, impenetrable bilayers (57, 50).

2.8.6.2 Liposome stability and temperature

LBDDS dosage forms must be physically, chemically, and microbiologically stable for 18–24 months throughout production, storage, delivery, and marketing. Stable liposomes shield drug molecules from endogenous enzyme breakdown until they reach their therapeutic target (50). Freeze drying after manufacture extends shelf life but physically degrades liposomes; hence, reconstitution cryoprotectants.

Physical deterioration alters the structure of liposomes, which impairs the therapeutic effectiveness of the drug molecule. Incubating the liposomes at temperatures near the phase transition temperature until the lipids re-arrange and merge into an equilibrated state corrects the packing density discrepancies of the lipids in the bilayer structure that cause physical deterioration (50).

Chemical degradation through oxidation and hydrolysis can be mitigated by only using high-quality fresh and new reagents, avoiding techniques involving high temperatures, manufacturing and storing liposomes in de-oxygenated, inert atmospheres and aqueous solutions, adding an antioxidant such as α-tocopherol (40).

Phospholipid hydrolysis is affected by chemical degradation, temperature, and pH during storage. The type, concentration, and phase transition temperatures of the phospholipids, lipids, and cholesterol utilised in the formulation influence the stability and release of liposomes and can avoid the loss of entrapped pharmaceuticals.

Liposomes composed of different lipid/phospholipid components at different concentrations have different phase transition temperatures (T_c), a crucial factor controlling liposomal stability. Temperatures above 25°C increase the physical instability of liposomes; therefore, refrigerating freeze-dried liposomes at 4°C with no light exposure improves shelf life (42).

Lipid compositions leak or increase drug release in the pre-transition temperature range because lipid membrane barrier effectiveness drops rapidly around phase change temperatures. Incorporating lipids with various transitioning temperatures can change liposome states at physiological temperatures. Thermosensitive liposomes release drugs at high temperatures. DMPC has poorer encapsulation efficiency than DSPC and DPPC, which have higher Tcs (52).

DSPC = 54.5°C, DMPC = 23°C, and DPPC = 41.5°C are the transition temperatures of typical liposomes. Phospholipid gels and liposomes constructed from saturated lipids with T_c values exceeding body temperature show superior drug retention and stability compared to those with lower Tcs. Gel phase lipids exhibit decreased liposomal permeability in plasma at 37°C when Tcs is above body temperature, lowering the liposome leakage rate (52).

2.8.6.3 Liposome stability and molecular structure

Colloidal systems stabilize electrostatically, sterically, or electro-sterically; however, neutral liposomal formulations do not consider electrostatic effects. The steric effect of larger headgroups (e.g., DPPC) increases liposome stability as it hydrolyses slower than smaller headgroups (e.g., DMPC has the littlest head) (42).

Liposome diversity, flexibility, and versatility derive from phospholipids, oils, emulsifiers, and cholesterol compositions with specific chain lengths, chain saturations, head groups, lamellarity,

shapes, sizes, and production methods. Unique lipid properties can improve encapsulation efficiency, vesicle stability, membrane fluidity and mechanics and manipulate the physical and pharmacokinetics of liposomes. Moreover, rigidity, fluidity, lamellarity, size and composition of liposomes are mechanical properties and parameters manipulated to control the degree of cellular uptake and pharmacokinetics (47).

Vesicles are soft fluid-filled container systems enclosed by a 3–4 nm thick lipid bilayer membrane suspended in a liquid medium. Vesicles at equilibrium have fluid membrane properties that impact changes in cell shape. Spherical and quasi-spherical shapes are affected by membrane fluidity, incompressibility, and resistance to bending (47) (69).

2.8.6.4 Liposome stability and cholesterol

Adding cholesterol to lipid mixtures can reduce the fusion between liposomes by raising the transition temperature and configuring the bilayer in a defined liquid-ordered phase. The cholesterol in the bilayers broadens or eliminates the T_m and causes the liquid phase to assume the physical characteristics of a solid-ordered gel phase (56).

Bilayer rigidity, fluidity, and charge depend on bilayer composition, making liposomes tuneable to target selected tumour cells. Vesicle stiffness increases with lamellarity (Table 2.10). Fluidic membranes help liposome-encapsulated medicines leak. Increased liposomal fluidity reduces cellular absorption, although rigid particles cross the cell membrane more easily. Fluid liposomes typically interact with tumour cells, while rigid liposomes converge more on the non-malignant cells. Fluid liposomes clear from circulation and decay swiftly in target cells, unlike solid liposomes that break down slowly and release intracellularly.

Membranes fluidise at high temperatures, decreasing hydrocarbon chain interaction, membrane stiffness, and liposome-coated drug stability through pore and disc bilayer formation. Cholesterol decreases lipid bilayer fluidity, hydrocarbon chain aggregation, crystallisation, and phase transition. Cholesterol concentrations, chain lengths, and saturations affect fluidity (83). Cholesterol incorporated into phosphatidylcholine liposomes to fill gaps increases their integrity, physical stability, rigidity, and strength, decreasing bending modulus and vesicle deformation (Figure 6A). Cholesterol fractions stabilise and protect the drug in the liposome by reducing

content leakage and regulating its release, circulation time and uptake in RES-rich organs and cancer cells. Cholesterol reduces phospholipid-lipid interaction with red blood cells and lipoproteins and replaces lipids' high phase transition temperature with less physiologically stable components (44).

Cholesterol has a 4-membered cyclopentanophenanthrene ring, hydroxyl group, and short hydrophobic tail. Cholesterol's hydroxyl groups are near the bilayer's polar phospholipid head groups. Their stiff, platelike steroid rings immobilise hydrocarbon chains at the bilayer polar head groups, limiting bilayer deformation and permeability to microscopic, water-soluble compounds (51).

Hydrophobicity causes membranes/vesicle assembly in the aqueous medium, leaving behind a tiny proportion of 'free' lipid molecule remnants. A limited number of lipid molecules create the bilayer/ vesicle area and adjust to a constant optimal value at a stable temperature. The slow interchange of lipid molecules between monolayers (flip-flop) facilitates membrane stability by forming an activation barrier as the polar phospholipid head group drags through the hydrocarbon chains. This flip-flop rate between monolayers increases with the addition of cholesterol. The presence and concentration of cholesterol in lipid bilayers significantly affect liposome stability.

Cholesterol concentration cannot exceed 50% of the liposome structure. Lipid formulations tempered with fixed proportions of cholesterol produce different liposome release profiles. Studies show the optimal cholesterol level as 30% of the LBDDS; however, 21% is sufficient to increase packing density, modulate rigidity and bilayer permeability, induce the conformational ordering of lipid chains, and serum-induced instability in vesicle structure. Large quantities of cholesterol reduce bilayer permeability by forming a barrier, but low concentrations (5–8%) form defects in the bilayer's ripple structure, decreasing vesicle stability and increasing membrane leakage. Therefore, cholesterol concentrations cannot be too low or high, or drug release will not initiate. Cholesterol improves the encapsulation efficiency of a liposome, enabling the transport of a more significant drug quantity to the target site. Lower cholesterol concentrations reduce liposome stability and encapsulation efficiencies (42).

2.8.7. The minimal model of energy

The minimal energy model describes the local curvature energy of fluid membranes in vesicles consisting of a symmetrical bilayer in which lipid molecules rapidly flip-flop between the two monolayers. Mixtures of two or more lipid components add degrees of freedom to the bilayer, enabling curvature, whereas single-component systems cannot form bilayers. Pure cholesterol and lipid molecules with polar head groups adjoined by hydrocarbon chains do not form bilayers following the minimal energy model.

2.8.8. Degrees of freedom and molecular motion

In three-dimensional space, gas molecules have unrestricted movement in any direction. Degrees of freedom (DOF) describe molecular movement and orientation in a three-dimensional space. A molecule's number of atoms and geometry determines the number and type of degrees of freedom it will have. DOF can be translational, rotational, or vibrational; molecules (mono-, di-, or tri-atomic) can be linear or non-linear.

Translational DOF is moving a particle's centre of mass from its original position to another along a Cartesian coordinate system's x, y, and z-axis. Monoatomic molecules have no rotational, only translational DOF, as the centre of mass sits directly on the atom, making changes impossible. The vibrational DOF is the movement of atoms within a molecule that creates minor changes in the internuclear distances between the atoms relative to one another, e.g., bond stretches or bends.

Table 2.11: Degrees of Freedom in Molecular Motion

Degree of freedom	**Monatomic**	**Diatomic**	**Triatomic**	
Type	**Monatomic**	**Diatomic**	**Linear molecules**	**Non-linear molecules**
Translational	3	3	3	3
Rotational	0	2	2	3
Vibrational low temperatures	0	0	3N – 5	3N – 6
Vibrational high temperature		1		3
Total	3	6	3N	3N

Rotational DOF changes a molecule's orientation as it rotates about its centre of mass in space. Diatoms rotate about any axis at right angles to its axis. Diatoms have no vibrational DOF at room and one at high temperatures; therefore, diatoms have six degrees of freedom at high temperatures and five at room temperature because the vibrational motion does not contribute.

Non-linear molecules have three rotational degrees of freedom, whereas linear molecules have two. Nonlinear triatomic molecules possess six DOF at ambient temperatures, three translational, three rotational, and nine at high temperatures. Polyatomic molecules with N atoms have 3N degrees of freedom after subtracting rotational and translational DOF from the total.

2.9 Components of the LBDDS

2.9.1. Lipids

Lipids are freely soluble in non-polar solvents like ether but not in polar solvents like water. Homolipids (simple lipids) only consist of carbon (C), hydrogen (H), and oxygen (O) and are esters of fatty acids with alcohols. Examples include glycerides (fats and oils), cerides (waxes), and sterides (esters of cholesterol with fatty acids/fatty alcohols).

In LBDDS, homolipids matrices can protect the incorporated bioactive from chemical and physical degradation and modify the drug release profile. Heterolipids (compound lipids) consist of nitrogen (N) and phosphorus (P) atoms in addition to C, H and O, e.g., glycolipids, sulfolipids, and phospholipids. Oral delivery vehicles are medium and long-chain fatty acids attached to a glycerol molecule known as triacylglycerol (Figure 2.3B) (37).

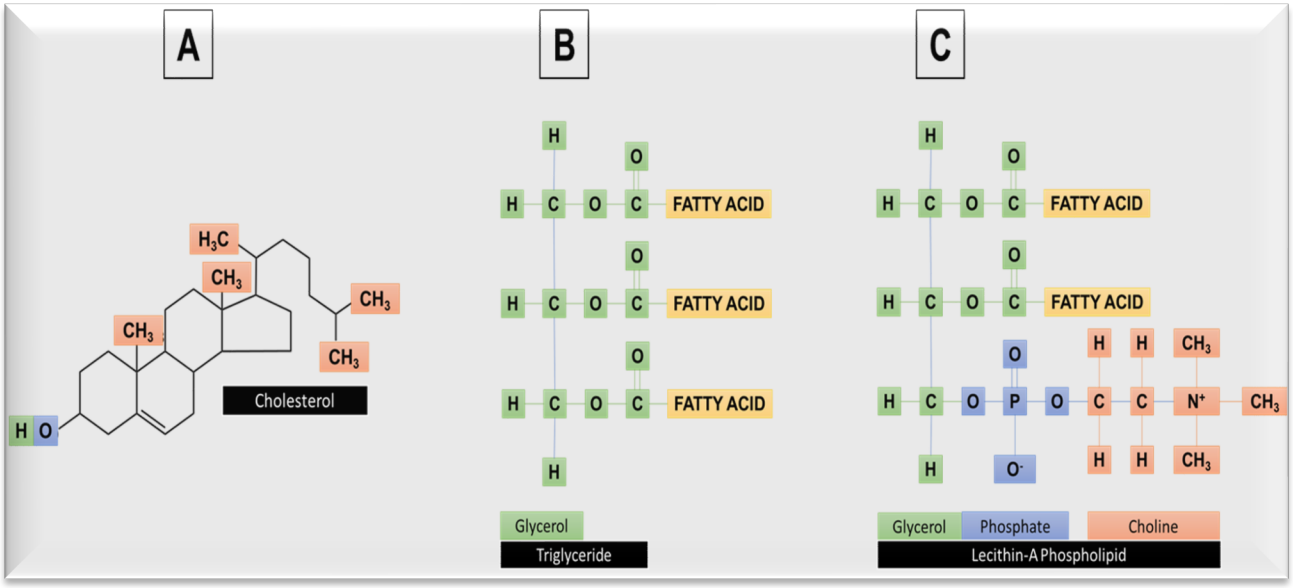

Figure 2.3: Three types of lipids: A) Cholesterol, B) Triglycerides, C) Phospholipids

The emulsification and solubilization of lipophilic drugs with biological lipids, surfactants, oils, co-surfactants, and co-solvents are quantity-specific. Increasing the lipophilic drug volume transported via the intestinal lymphatic system increases absorption. Biodegradable hydrogenated oils are cost-effective, efficient excipients for the sustained release of LBDDS.

2.9.2. Phospholipids

Phospholipids are surface-active, amphiphilic molecules with emulsifying, solubilizing, wetting, and building functions used in drug design and targeting, emulsion stabilization and drug coating to provide hydrophilicity to hydrophobic drugs. All phosphorus-containing lipids are phospholipids, comprised of a glycerol backbone esterified with fatty acids in positions 1 and 2 and phosphate in 3 (Figure 2.3). The carbon atom at position sn-2 of glycerophospholipids is a chiral centre. Phospholipids self-assemble into different types of liposomes and micelles. Depending on the polar region's structure and the medium's pH, Phosphatidyl Ethanolamine (PE) and Phosphatidyl Choline (PC) are zwitterionic, neutrally charged at about pH 7, whereas Phosphatidyl glycerol (PG) has a negative charge (43).

2.9.2.1. Types of Phospholipids

Natural or synthetic phospholipids can form liposomes. Natural phospholipids isolated from natural sources like eggs and soybeans in enantiomerically pure form take precedence over synthetic phospholipids as excipients in formulations. Eco-friendly renewable resources contain fewer chemicals and solvents and produce higher yields, allowing large-scale manufacture at relatively lower costs than synthetic phospholipids. Synthetic phospholipids (e.g., DSPC, DPPC, and DMPC) have saturated lipid constituents that increase liposome stability, whereas saturated lipid egg phosphatidylcholine liposomes are comparatively less stable.

Lecithin's primary ingredient, phosphatidylcholine, is a natural, effective alternative to synthetic emulsifiers such as sucrose fatty acid esters, polysorbates, and polyoxyethylene castor oil derivatives. Synthetic phospholipids are utilised explicitly for parenteral/injectable administration, although the administration of natural ones can use any method (43).

2.9.2.2. Phospholipid properties

Phospholipid properties vary because of differences in aliphatic chains, alcohols, and sources. Liposome stability is affected by transition temperatures (T_c), at which 50% of the material is liquid and 50% is solid or gel. Manipulating lipid acyl and hydrocarbon chains can control drug release rate, liposome stability, and encapsulation efficiency.

The barrier efficiency of lipid membranes decreases abruptly near the phase transition temperatures; however, combining lipids with different Tc in liposomes can temper this. Lipid saturation stabilises liposomes. Liquid crystalline phospholipids at ambient and body temperature form flexible structures upon hydration (42). Unsaturated fatty acids in natural phospholipids form a gel below 0°C.

Gel phase lipids that transition above body temperature have decreased plasma liposome permeability at 37°C, reducing leakage (54). Short or unsaturated hydrocarbon chain gel matrices are less stable than phospholipid organogel structures with Tc exceeding body temperature.

Phospholipids with saturated fatty acids, produced by hydrogenating natural phospholipids with unsaturated fatty acids, have higher phase transition temperatures that enhance liposomes' stability in body fluids. Hydrocarbon chains contain covalently bonded carbon and hydrogen atoms linked in a chain, while acyl chains contain a double-bonded oxygen atom and an alkyl group (R-C=O).

2.9.2.3. Phospholipid curvature

Curvature is a consequence of the collective behaviour of several molecules that form entities that fluctuate with changing entropies, time, and transient interactions between the membrane and other cellular components, such as solutes, proteins, vesicles and membranes (44). Intrinsic lipid curvature arises from the packing of the lipid molecules controlled by intermolecular interactions.

The critical packing parameter (CPP) explains structural transitions founded on the spatial stacking of amphiphilic molecules to predict system structure. Theoretically, the CPP provides a framework for predicting the type of surfactant aggregation, e.g., flexible or fixed bilayers, spherical or cylindrical micelles or vesicles. CPP hypothesises that different phases correspond to different CPP values.

The molecular self-assembly of surfactants is a function of the volume and length of the surfactant tail and the surface area of the aggregate's hydrophobic core (area per molecule). The molecular packing parameter (P) estimates the structure of the lipid aggregate and the stability of specific molecules in aggregates. Molecular packing parameter values geometrically relate to the shape and size of the aggregate (45). The molecular packing parameter describes intrinsic membrane curvature in terms of a chain packing parameter defined relative to the equilibrium area per lipid molecule at the polar-apolar interface, the size derived from thermodynamic considerations (44).

Aggregate structure influences the properties of surfactant solutions, such as solubilization capacity for hydrophobic substances or their viscous and viscoelastic properties, and consequently, the performance of surfactants in various applications. The molecular packing

parameter predicts molecular self-assembly in surfactant solutions. Specific values of the molecular packing parameter translate via simple geometrical relations into the specific shape and size of aggregates at equilibrium.

The MPP assumes that the tail's volume-to-length ratio (vo/lo) is constant and independent of the tail length for typical surfactants, making the surfactant headgroup determinant of the surface area per molecule of equilibrium in aggregates, negating the role of the surfactant tail in estimating the size and shape of equilibrium aggregates. If the radius of the sphere, cylinder, or half-bilayer thickness (R) cannot exceed length (lo), the molecular packing parameter relates to the aggregate shape as follows: (P= 1/3) for spherical micelle. If the micelle core compacts with surfactant tails without leaving any space, then the radius of the micelle R cannot extend beyond the length lo of the tail.

Equation 2.2: "Israelachvili–Mitchell–Ninham packing parameter" **(44,46)**
Equation 2.3: The geometric packing parameter

Equation 2.2	**Equation 2.3:**
P = v/al	RO = V/al,
Where:	Where:
P = Molecular packing parameter	RO = The geometric packing parameter
V = molecular volume	V = volume of the entire lipid molecule
a = cross-sectional area of the headgroup	A = lipid headgroup area at the lipid-water interface
l – length of the molecule	l – molecular length
P ≤1/3 for spherical micelle	V/Al = 1: lamellar structure; Planar structures with zero curvature
P ≤1/2 for cylinder	V/Al: <1 normal (oil-in-water); Negative for normal structures
P= 1 for bilayer	V/Al: >1, inverted (water-in-oil); Positive for inverted structures
1/3 ≤ P≤1/2 (cylindrical aggregates).	
1/2 ≤ P≤1 (planar aggregates)	

Elastic curvature-free energies determine thermodynamic properties, while the geometric packing parameter relates directly to structural data from x-ray diffraction. Although analogous to the packing parameter, the geometric packing parameter is purely geometric and includes the whole lipid molecule instead of only lipid chains and thermodynamically deduced interfacial area. Based on lipid packing configurations and volume-to-surface area ratio, the geometric model predicts the inherent curvature of a single lipid monolayer.

2.9.2.4. The shape of lipid molecules

Each lipid species curves according to its chemical makeup, structure, and form. Based on variations in their acyl chains or heads, lipids have three categories: type 0, type I, and type II. Lipid monolayer curvature can be positive, zero or negative according to the conicity of the lipid molecule. Multiple lipid types in a membrane conform to the domains of curvature that they prefer (Figure 2.4) (47). The tail length must be at last l Rsphere, or P = v/la, to prevent a gap from forming within the micelle.

The MPP provides information regarding the amphiphile's aspect ratio. Conical amphiphiles with a "big head and short tail" destabilise lamellar bilayers, form spheres, and have a moderate packing parameter. Amphiphiles with large packing parameter values pack into two-dimensional planar aggregates and seem cylindrical (62). Positive lateral pressure on the head group propagates negative tensile pressures to the interfacial zones and positive pressures in the acyl chains. Since lateral pressure equals normal pressure, self-assembled lipid bilayers contain no tension.

Table 2.12: Phospholipid structure and curvature

Phospholipid tail group	diameter of the head group	Ratio	Intrinsic Curvature
Two-tailed PC lipids	Large head group	~ 1	~ 0
Two-tailed PS lipids	Smaller head group		-ve (negative)
Two-tailed PE lipids	Smaller head group		-ve (negative)
One-tailed lysolipids	Smaller head group		+ ve (positive), spontaneous
If a lipid deviates significantly from zero intrinsic curvature, it will not form a bilayer.			

Lipid bilayers naturally bend unless the lipids composing them are firmly constrained. Bending causes intrinsic curvature stress, weakening and destabilising the lipid bilayer. "P" predicts lipid molecule curvatures based on their structures. Wedge-shaped lipid molecules create micelles, whereas cylinder-shaped phospholipid molecules form bilayers. Conical lipid molecules ($P \neq 1$) destabilise the lamellar lipid bilayer due to increased curvature stress from fatty acid chains, decreasing membrane permeability and increasing liposome content leakage. Curly disordered chains increase unsaturation in unsaturated lipids ($P > 1$) by shifting pressures toward the membrane–water interface. Cholesterol ($P < 1$) has a sizeable hydrophobic body and a tiny head that transfers pressure to the centre of the bilayer. Lysolipids ($P < 1$) release drugs because they are more water-soluble than fatty acids with the same acyl chain. The packing parameter is linearly related to HLB (44).

2.9.2.5. The Tail

Single-tail lipid molecules self-assemble into spherical micelles, whereas double-tail lipid molecules form bilayer vesicles. Double-tailed lipid molecules have double the packing parameter of single-tailed ones for the same equilibrium area. Nonionic surfactant aggregates have more molecules than ionic ones with the same tail length. Ionic repulsions reduce the headgroup interaction parameter R for nonionic surfactants compared to ionic ones. Thus, ae will be lower and Vo/alo greater for the nonionic than the ionic. By changing solution conditions that affect surfactant molecule headgroup repulsions, spherical micelles can shapeshift into rodlike and bilayer aggregates. A polar organic solvent in an aqueous surfactant solution converts bilayers into micelles, rods into spherical micelles, and spherical micelles into aggregates or small molecular clusters. Changing the solvent from water to a mixed aqueous-organic solution lowers the surfactant's interfacial tension, increasing the equilibrium area per molecule and decreasing MPP.

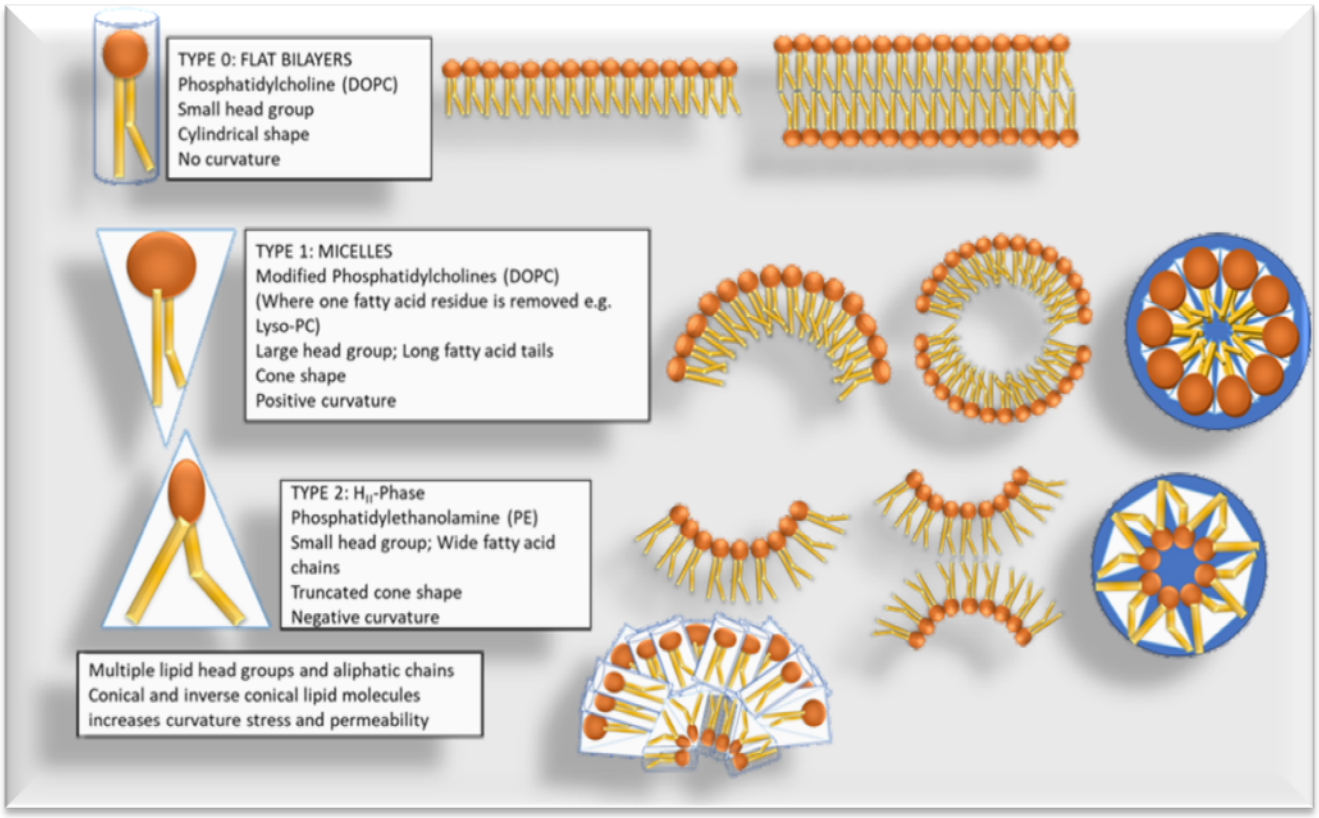

Figure 2.4 Spontaneous curvature of lipids (53,56)

2.9.2.6. The Head

The molecular packing parameter (MPP) describes intrinsic membrane curvature, a chain packing parameter related to the equilibrium area of each lipid molecule at the polar-apolar interface. The MPP employs the surfactant headgroup to estimate aggregate size and form, although the tail and ionic strength significantly impact micellar geometry by altering the equilibrium area, packing parameter, and aggregate size of spherical micelles, not cylindrical ones (rods). The tail affects the number of molecules in micellar rod endcaps and the volume of the aqueous cavity inside the bilayered vesicle, altering the sphere-to-rod transition parameter. MPP-predicted spherical bilayer vesicles and rodlike micelles cannot develop if the surfactant headgroups cannot fit in the aqueous cavity. The equilibrium aggregates' size and form depend on tail packing entropy. Thus, predictions of MPP-based equilibrium surfactant aggregate structure should include the tail and headgroup (56).

The thermal expansion coefficient depends on the lipid packing parameter. The geometric packing parameter specifies the intrinsic or spontaneous curvature (RO) radius of lipid monolayer assemblies for various geometries. Inverted hexagonal (H) phases and inverted cylindrical micelles are identical for R, describing a cylindrical shell of equal total lipid volume for the equivalent lipid length (l). Thermodynamics and extra hydrocarbons in the equivalent H phases determine size. Single monolayers spontaneously curve according to the lipid's molecular characteristics. For spontaneous nonzero intrinsic curvature of bilayers to occur, each asymmetrical monolayer must have a negative intrinsic curvature radius more significant than the lipid length at a specific temperature (48).

Normal micelles have hydrocarbon-filled micelle cores when V/Al = 1/2, corresponding to Ro = 1. The minimum packing parameter value is V/Al = 1/3, corresponding to R = 1, while the maximum value in inverted structures is the same as for cylindrical structures.

Without apolar components, amphiphilic lipids form inverted hexagonal (HI) phase structures that cannot bend spontaneously. The hexagonal lattice packing constraints violate the cylindrical symmetry of the hydrocarbon chain, causing curvature. The curvature elastic energy determines the lamellar-to-nonlamellar(HI) phase transition temperature (Eq. 11).

Temperature dependence of R.: Increasing temperature increases chain rotational isomerism, shortening lipid length. Planar bilayers show modest changes to intrinsic curvature and lipid packing because the headgroups rearrange themselves optimally as curvature changes. These compensatory molecular area modifications reduce bilayer lipid volume variability. Both methods are complementary and involve lateral pressure components. Therefore, as the complementary surface may lie deeper within the monolayer than the chain end, the bending modulus is a quarter or less than for a bilayer.

Lipid packing parameters and curvature elastic energy affect molecular geometry. The lipid molecular packing parameter represents lipid packing geometry, whereas V/Al describes amphiphilic lipid assembly intrinsic curvature. Lipid packing parameters for inverted hexagonal phases depend on the cylindrical lipid length.

A two-dimensional surface extending into a three-dimensional space portrays membrane curvature. "Total curvature" measures torsion and direction in 2D and 3D spaces, whereas "Gaussian curvature" measures the inherent "curvedness" of a membrane, which does not change unless the membrane is stretched or compressed. Curvature is positive or negative depending on the direction a curve faces relative to the membrane compartment or volume. Unlike negative curvature, positive curvature forms spheres (49).

Table 2.13: Phase and Forms of Critical Packing Parameter (CPP) (49)

CPP	Structure	Phase	Mesoform	Symbol
CPP< 1	The cross-sectional area of the hydrophilic head exceeds that of the hydrophobic tails	Normal phase	normal micelle	LI
			normal discontinuous cubic	II
			normal hexagonal	HI
			normal bicontinuous cubic	QI
CPP = 1	The area of the polar headgroup approximately equals the tail	lamellar phase		L
CPP > 1		reversed-phase	reversed bicontinuous cubic	QII
			reversed hexagonal	HII
			reversed discontinuous cubic	III
			reversed micelle	LII

Table 2.14: The model framework used by MMP is: CPP = Hydrophobic volume/(Hydrophobic length*area of the hydrophobic/hydrophilic interface) or CPP = V/(L*A) **(50)**

CPP	Aggregation form
< 0.35	spherical micelles
0.35-0.4	spherical or cylindrical micelles
0.4-0.55	cylindrical micelles
0.55-0.6	cylindrical micelles, vesicles, or flexible bilayers
0.6-0.85	flexible bilayers or vesicles
0.85-0.95	flexible bilayers
0.95-1.15	planar bilayers
>1.15	Inverted micelles or material is not a surfactant

The deformation of vesicles, drops, capsules, and cells depends on balancing interfacial forces such as interfacial stretching and fluid stresses. The interface between two simple fluids depends on the isotropic surface tension without surfactants or heating. The resting shape is a sphere because the surface tension minimises the interfacial area. A constrained fixed area gives two vesicle behaviour regimes, tank–treading and tumbling, subject to the contrast in viscosity between the interior and exterior fluid (52).

When the inner and suspending fluids are the same (no viscosity contrast), a stationary, tank–treading prolate ellipsoid forms with no transition to tumbling motion, and a critical viscosity contrast value separates the tank–treading and tumbling regimes. Tumbling increases with viscosity difference. The vesicle becomes a tank–treading ellipsoid below a crucial viscosity contrast.

The critical viscosity ratio decreases with the excess area (the difference in the areas of the vesicle and an equivalent sphere with the same volume). Area constraint leads to non-linear leading order evolution equations for the vesicle shape when only ellipsoidal deformation modes are independent of the membrane bending rigidity. Under shear flow, the drop initially deforms into an ellipsoid. As the flow strength increases, the drop area also increases. The drop breaks up if the flow strength and the moderate viscosity contrast are sufficiently high (52).

2.9.2.7. Bending and stretching of lipid membranes

A pure lipid membrane consists of two sheets of lipid molecules. The molecular thickness imparts bending resistance. Free movement of lipid molecules within the monolayer makes the lipid bilayer membrane fluid compared to solid-like polymerized membranes. Vesicle shapes can form by minimizing the membrane bending energy subject to constant area and enclosed volume constraints. The lipid bilayer contains a specific number of molecules with a fixed area per molecule (under moderate stresses), the membrane is incompressible, and the total area is constant. The enclosed volume is also constant at given osmotic conditions (52)

Hooke's law for membrane stretching states that stress is proportionate to strain, and the proportionality constant is the stretching modulus $K_{stretch}$. Shear stress relates to shear strain in

membranes, provided the membrane can support the shear strain in the first place. Lipid bilayers cannot support the shear strain because they are fluid, and like water, fluid lipid membranes do not have a shear modulus. Small elastic stresses in a three-dimensional chunk of material create small overall deformations. However, materials are not 3D if they form a thin plate in one direction or a rod in two directions. Plates and rods can bend in different directions away from the direction they extend, substantially changing the material's shape without excessive stress. Membranes are two-dimensional surfaces that can bend into the third dimension. When a material bends, the outer side stretches, the inner side compresses, and an unstrained region forms a neutral surface in the middle. Weak bending deformation costs less energy than stretching, and a high stretching modulus is more challenging to rupture by stretching rather than tearing. Bending energy depends on thickness, i.e., thinner membranes rapidly reduce bending energy.

Shear across the thickness of a bent elastic sheet allows stretching and compression to communicate between the outer and interior surfaces. Bending resistance is predictable. However, if the elastic sheet is sliced in half and stacked to slide past each other, no shear can be transmitted between them. Bending them is like bending two separate sheets of half the thickness (62). Bending rigidity computes the energy needed to alter membrane curvature. Faizi et al. have demonstrated that charged membranes increase the bending rigidity relative to the charge-free membranes and that the membrane bending rigidity correlates with zeta potential measurement.

In the bent bilayer of neutral membranes, the expansion and compression of the outer and inner lipid monolayers come with an energy cost directly related to bending rigidity. The surface charge stiffens the membrane because the repulsion between the charged lipids resists membrane bending. A higher proportion of charged lipids results in a more negative zeta potential value. Membrane bending rigidity increases rapidly with surface charge and, for the first time, demonstrates the theoretically predicted plateau above 20% surface charge (51).

Lipids are amphiphilic molecules and natural surfactants. The longer the fatty acid, the more hydrophobic the lipid and the thicker the membrane formed; the more double bonds, the more

disorderly the tails, increasing the transition temperature between the “fluid” and “gel” phase, increasing membrane fluidity. Phosphates hold a negative charge. A positive countercharge (e.g. choline but not serine) must attach to the phosphate to make neutral lipids (52).

2.9.2.8. Phospholipid–water interaction

Amphiphilic phospholipids serve emulsifying and wetting actions that stabilize emulsions, coat hydrophilic and hydrophobic drugs and facilitate drug targeting. Amphiphilic phospholipids comprising liposomes are polar lipids consisting of a hydrophilic polar head group and two hydrophobic hydrocarbon tails. Water's phospholipid solubility depends on the head-group type and the hydrocarbon chain length. The phosphoric acid head binds to a water-soluble molecule. The fatty acid tails have 10-24 carbon atoms and 0-6 double bonds in each chain.

Table 2.15: Effects of water concentration on the structure of phospholipids in vegetable oil **(54)**

Structural Group	Water concentration	Temperature	Structures
1.	Zero-low	24 °C	Tiny spherical/spheroidal reverse micelles form above the CMC at low water concentrations.
2.	Low-medium		Elongated cylinders with a wormlike appearance
	≥10-20 wt.-%	~2 to 225 °C	Lα phase Crystalline lecithin structures with liquidlike chains, i.e., cubic crystals (Qα), rhombohedral crystals, and hexagonal crystals(Hα)
	≥40-44 wt.-%		(Lβ)- phase Crystalline lecithin structures with stiff chains
	≤35 wt.-%	>220-232 °C	
3.	Medium-high	~40% water saturation	Phase separation of phospholipid in vegetable oil in water. Lamellar phospholipid precipitates in water

The phospholipid portion of lecithin gives form and function to lecithin (40,53). Water concentration, temperature and free fatty acid affect the shape and structure of phospholipids in

vegetable oil (Table 2.15), which differ depending on the water-to-phospholipid ratio (w/w), a factor used to control phospholipid self-aggregation in vegetable oil (54). External factors influencing phase transition include temperature, pressure, light, magnetic fields, and prescription factors, such as amphiphilic molecules, water content and additives. The water-to-phospholipid ratio (w/w) can control phospholipid aggregation and shape vegetable oil to form reverse, cylindrical lamellar structures, cubic liquid-crystalline phase spheroidal and rod-like reverse micelles. Phospholipids' properties and lipid bilayer morphology vary due to differences in aliphatic chains, alcohols, and sources. Phospholipid shapes include spherical and cylindrical reverse micelles, lamellar structures, reverse hexagonal phase, cubic liquid-crystalline phase, spheroidal reverse, and rodlike micelles.

The translational or rotational degrees of freedom of liquid water have a high entropy, enabling it to hydrogen bonds with itself, balancing energy and entropy. The insertion of other molecules disturbs this network, influencing water entropy. A molecule capable of hydrogen bonding (e.g., sucrose) will dissolve more readily than molecules that cannot do this (e.g., oil). Polar molecules with l; electrical dipole moments) amalgamate effortlessly into the hydrogen bond network. Around the non-polar surfaces of hydrocarbon chains, water molecules hydrogen bond with themselves as this region has fewer neighbouring molecules and less chance to bond, lowering the entropy in the water layer adjacent to a nonpolar surface and working against solubilization.

The phospholipid vegetable oil phase creates tiny spherical or spheroidal micelles at the critical micelle concentration. Micellar size increases with increasing phospholipid concentrations. Adding minute amounts of water to the two-phase system causes water to pool within the micelles, initiating swelling. Water molecules then hydrogen bond to the phospholipid phosphate groups of spherical reverse micelles, increasing the volume of the polar head group, reducing interface curvature, and elongating spherical or ellipsoidal reverse micelles into long, narrow reverse cylindrical micelles showing worm-like appearance. An energy balance controls the length and branching between the micelle endcaps and the branches. Both water concentration and temperature affect the L_α phase of lecithin. At higher temperatures, lecithin crystals melt into an isotropic liquid which coexists with excess water at elevated temperatures. Increased water concentration swells the phospholipid head, increasing its size and aggregating into insoluble

colloidal phospholipids. Small quantities of water morph phospholipid structures from the isotropic liquid phase (L2 phase) into lamellar structures that are insoluble in oil and that precipitate, causing phase separation of the reverse micelles. Small amounts of water-hydrated lecithin reverse cylindrical micelles into lamellar crystalline structures. Lecithin precipitation occurs with a small addition of water and the removal of solubilized lecithin aggregates.

Three types of water adsorb to phospholipid molecules: tightly bound water, intermediately bound water, and free water. Water absorption depends on the phospholipid's electrical charge, head group, and hydrophobic moieties. Increasing double bonds in the hydrocarbon chains and bound cholesterol increases water hydration. Hydration, or dehydration of water adsorbed to the polar head group, rearranges the lipid molecular organization (54). Water swells the phospholipid heads to form insoluble aggregates at the air-water interface. As water concentration increases, aggregate structures change from micelles to micellar networks at the oil phase-interface boundary to form a gel-like structure, encouraging the infiltration of more water molecules to form an organogel (53). Water absorption capacity ranges from 6.5 to 100 per phospholipid molecule, depending on the phospholipid type (54).

Table 2.16: Classes of Phospholipids according to their water solubility **(53,54)**

Class	Phospholipid Water-solubility.	Effect	Example
1.	water-insoluble	Do not absorb water	Waxes
2.	low water-solubility	Swell in water	long-chain phosphatidylcholine, phosphatidylethanolamine, sphingomyelin
3.	water-soluble Type 1	Form lyotropic liquid crystals at a low water content	lysolecithins
4.	water-soluble Type 2	Form micelles in water above (CMC) without crystallizing	saponins

Amphiphilic phospholipids can form solid or liquid thermotropic and lyotropic phase structures like 2-D lamellar crystals at different gel phases and 3-D lamellar crystals at low temperatures and hydration.

Temperature change induces solid-solid chain melting or fluid phase transition: phospholipid-hydrocarbon chain type and length influence critical chain-melting temperature. Longer phospholipid chains elevate phase transition temperatures. Hydrocarbon chains liquefy above the critical melting point, turning solids into liquids, while water-swollen phospholipids create bilayers.

2.9.2.9. Gels

Despite their disorderly molecular organisation and viscoelastic stress relaxation properties, gels are amorphous solids rather than fluids with finite shear viscosity. Gels are soft solids/semisolids formed from self-assembling solid components (gelator) that immobilise a liquid component (external apolar phase) within its spaces to form a three-dimensional network/mesh through physical interactions as electrostatic interactions, hydrogen bonding, hydrophobic and Van der Waals forces. Chemical cross-linking or physical entanglement" interactions localise the position of the molecules/particles in space, leading to "gelation" or "amorphous solidification". Molecular bond properties depend on the type of solute and solvent (natural oil) used and the agitation, cooling, ionic strength, pH, and temperature, which are adjustable to the formulation design.

Gels include organogels, hydrogels, bi-gels and xerogels. Depending on the nature of the liquid phase, water forms hydrogels and organic solvents organogels. Organogels are non-crystalline, non-glassy, thermoreversible (thermoplastic), viscoelastic, and semi-solid preparations.
Organogels' stable thermodynamics comes from the spontaneous formation of fibrous structures, which give organogels their low-energy state. Lipophilic solids and liquids mixed with low concentrations of organogelators, processed by heating, agitation, and cooling, dispersed in the oil phase and self-assembled into 3-D networks by trapping the structuring material in the liquid oil form organogels. Organogel types include eudragit, L-alanine derivatives, Lecithin, Limonene GP1 organogel, low molecular weight gelators, micro, nanoemulsion based, Pluronic lecithin organogels (PLO), polyethylene, Premium lecithin organogels (PrLO), sorbitan monostearate, supramolecular organogels.

The optical clarity of organogels, depending on the composition, may be transparent (Lecithin organogels) or opaque (sorbitan monostearate organogels). Isotropic organogels viewed under

polarized light appear as a dark matrix as they exhibit birefringence, i.e., polarized light cannot pass through the matrix. Lecithin only gels when no impurities are present and needs proper storage conditions to remain stable. Polymers immobilize the organic solvent through chemical cross-linkage or physical entanglement of chains stabilized by weak interchain interactions such as hydrogen bonding, van der Waals forces, and π-stacking, forming long overlapping aggregates that induce solvent gelation. The gel swells as it imbibes increasing volumes of liquid but naturally shrinks on standing as liquid oozes out by syneresis. The large or small inorganic particles/molecules interpenetrated with liquid" do not solubilise but dispersed throughout the continuous phase. The solid matrix prevents liquid flow via surface tension.

Hydrated phospholipid membranes reversibly transition between two extreme phases: the gel phase (solid order) and the fluid phase. The gel-liquid transitions occur above the phase transition temperature (T_m) of the lipid bilayer, typified by lateral order (different positions) and rotational order (different orientations). Above T_m, lipid chains change configuration (from all-trans to all-gauche) to less extended, compact structures (60). Different lipids have different T_m depending on the chemical structure (i.e., length and saturation degree of the acyl chains, nature of the polar heads, type, and ionic force of the dispersion medium. The higher the T_m of the phospholipid, the lower the difference between T_p and T_m (55). Longer hydrocarbon chains have a lower unsaturation (up to C22) than shorter acyl groups. Gel to the liquid phase transition precedes a gradual change in the distance between polar heads (pre-transition, T_p), occurring ~5–7 ◦C degrees before T_m (71). A simultaneous change in the phospholipid configuration and membrane curvature occurs above the T_p to form a ripple phase (periodic one-dimensional undulations in the bilayer surface) (71).

As different domains have different geometrical characteristics, alternating gel and liquid lipid domains in a single monolayer force lipids to arrange themselves on the surface, causing ripples (55). For mixed chains (i.e., EPC with a C18 component), T_p moves towards T_m and, in the presence of different metaphases, does not discriminate between the two T_m values (55). Saturated acyl chains (C10 - C13) do not pass through the ripple phase but undergo a natural gel-liquid transition (55). The tilt of hydrocarbon chains depends on their hydration level. Increased water content increases the tilt angle to form a thin bilayer (55). The type of

phospholipid polar head or the presence of cholesterol can influence the tilt of the chain (56). The hydrophobic steroidal cholesterol moiety promotes the all-trans configuration of acyl chains, decreasing the tilt angle in the gel phase (56). The gel-to-sol transition above room temperature needs an external energy supply to the organogels to disrupt the three-dimensional structure and transform the gel into the sol state.

Organogels can solubilise lipophilic, hydrophilic, and amphiphilic guest molecules, including enzymes. Thermodynamic stability and reversibility, insensitivity to moisture, resistance to microbial contamination, spontaneous formation and viscoelastic behaviour are valuable features of lecithin organogels. Thermodynamically stable organogels provide controlled drug release, longer shelf life and prolonged action, reduce drug dosing frequency, and diminish the diffusion rate of the drug because the drug is dissolved in polymer and transported between chains and hydrophobic and hydrophilic components. Organogels can only accommodate drugs with a good partition coefficient.

Low moleculer weight (LMW) organogels can consist of solid (or a firm) or fluid (weak) fibre networks depending on the molecule’s aggregating tendency; steric effects, rigidity, and polarity can counter the molecule's aggregating tendency. Organogels do not form semisolids on standing; macromolecules twist into matted strands by van der Waal forces to form crystalline, amorphous regions throughout the system. Organogels have low hydrations; the drug-dissolved polymer transports between the chains. Cross-linking increases the hydrophilicity of gels and diminishes the diffusion rate of drugs.

Lecithin dissolved in nonpolar media self-assembles into reverse spherical micelles that undergo massive uniaxial growth into tubular or cylindrical micellar aggregates (sphere-to-cylinder transformation), catalysed by the addition of critical quantities of polar additive. Lecithin dissolved in organic solvents gelate when a polar solvent is incorporated.

The polar solvent molecules bind stoichiometric ratios to the hydrophilic head portion of the lecithin molecules so that two adjacent lecithin molecules bridge with hydrogen bonds between

the polar and phosphate groups in linear formation, the 1-dimensional uniaxial growth of lecithin reverse micelles.

Further increases in polar additives form flexible, long tubular structures, which, on reaching critical length, overlap and entangle into a transient 3-dimensional network with increased viscosity and viscoelasticity to form a jelly-like phase instead of a low viscous solution. Organic solvents (external phase) provide a suitable environment for the inter-and intramolecular interaction between gelator and organic solvent molecules, influencing micellization during the gelling of lecithin monomers. Spaces between the entangled reverse micelles trap the external phase (~85% of the organic liquid). The hydrogen-bonding network built up by molecules of polar additive and phosphate groups stiffens phospholipid molecules in the region of the phosphate group and glycerol residue, stabilising the micellar aggregates. In the case of PLOs, the gelling mechanism and the structural network relate to the synergistic contribution of phospholipids and polymeric cosurfactant molecules in their respective hydrated states.

Hydrogen interaction between lecithin and polar solvent molecules forms a three-dimensional network of reverse cylindrical micelles in lecithin organogel.

Spherical lecithin micelles increase in the cross-sectional area of the lecithin polar region where the solvent infiltrates. The hydrated molecules are cylindrical, causing packing constraints in spherical micelles that diminish in cylindrical micelles with a smaller curvature. Lecithin and polar solvent molecules establish hydrogen bonds that create a three-dimensional network of reverse cylindrical micelles in lecithin organogel.

Organogel matrices consist of a surfactant (lecithin) as gelator molecules, a nonpolar organic solvent as the continuous external phase, and a polar agent, usually water. The jelly-like state only happens in nonaqueous solutions of naturally occurring unsaturated lecithin, like soybean and egg yolk derivatives. Lecithin organogels form by adding small amounts of water or polar substances to the non-aqueous lecithin solution. Lecithin organogel forms carriers for amphiphilic, hydrophilic, and hydrophobic drug molecules. Hydrophobic drugs dissolve in the oil

phase (lecithin + organic solvent), whereas hydrophilic molecules dissolved in water are added to an organic lecithin solution to induce gelation.

Span 40 and Span 60 gel organic solvents at low concentrations. Semi-solid Span 60 organogels form thermoreversible tubular microstructures dispersed in the continuous organic phase when the gelator/liquid mixture warms to 60°C in a water bath. The solvent and the gelator molecules self-assemble into tubules, forming an opaque, semisolid gel on cooling. Span 60 gels are more stable than Span 40 gels.

Sorbitan monostearate molecules form inverted bilayers within the tubules. Inverse toroidal vesicles, surfactant tubular precursors, grow in the organic phase until the gelation temperature and inverse toroidal vesicular structures grow in the organic phase.

Toroids are comparable to liposomes and niosomes, except their shapes are toroidal instead of spherical, and their orientation is inverse. Toroids are short-lived structures in the sol phase that form rod-shaped segments or tubules upon cooling in the organic medium. Microemulsions frequently form the thermodynamically stable transparent, single optically isotropic liquid system of water, oil, and surfactants in combination with suitable cosurfactants. Gel characteristics can vary by adjusting the proportion and concentration of the surfactant.

An organogel can remain in the sol phase at room temperature upon adding ethanol to a gelator/solvent solution because ethanol inhibits gelation by disrupting hydrogen bond formation (essential for gelator self-assembly into aggregates) between the gelator molecules; however, ethanol evaporation or diffusion away from the gel forms gelator-gelator hydrogen bonds and results in gel formation. Water loss by evaporation in organogels decreases viscosity, thus affecting gel stability.

Near-infrared spectroscopy studies the lecithin/IPP/water organogel system by measuring the water absorption in the NIR region (1800-2200 nm). In this region, water shows a firm absorption peak at 918nm. Structural elucidation characterises the physiochemical properties of the organogel. FTIR spectroscopy's analyses of the isotopic nature and optical clarity of the

organogel effectively establish hydrogen bonding as one of the major driving forces for the self-assembly of organogelator molecules in an organic solvent. Molecular packing within the organogel network uses SEM. TEM, DLS, and SANS analysis techniques.

Increasing the gelator concentration increases the viscosity and gel strength of viscoelastic organogels. Gels swell by absorbing increasing volumes of liquid. As the solvent penetrates the gel matrix, gel-solvent interaction replaces gel-gel interaction with H-O-H stretching overtones, easily detectable and quantifiable.

Charged polymers (polyanions) favour mucoadhesion over polycations. Charged polymer groups favour mucoadhesion. Mucoadhesive swell with moisture, increasing the mobility of polymer molecules at the interface, exposing more sites for bond formation, and changing entanglement and interaction after the polymer and mucins have interpenetrated.

The size of oil structuring molecules differentiates organogels into high molecular weight organogels (HMOGs) or low molecular weight organogels (LMOGs). HMOGs are polymers that form a supramolecular network by structuring an organic solvent with strands formed by physical or chemical interactions. MOGs physically organize within the oil phase and gel organic solvents in small amounts. The oil structuring method subdivides into three-dimensional networks of crystalline particles or a fibrillar network that fills space. The organogels solid fibrillar matrix improves the encapsulation rate of lipophilic or amphiphilic molecules by homogeneously distributing them within the particles' structural framework. High concentrations of LMW polymers provide sufficient viscosity for them to set. LMW gelators affect the growth and stability of solid-fibre networks. Chiral centres within the gelators help with compact molecular packing, which provides thermodynamic and kinetic stability to the organogels system.

A drug in the liquid state can be gelled directly as the main component of the formulation, with consistency dependent on the concentration of the organogelator. Physical organogels form by heating the solid and liquid components that form the organic solution/dispersion in the "first phase". Cooling the mixture fixes gel formation in the "second phase" as the solubility of the structural agent in the liquid phase decreases, and organogelator-solvent interactions reduce,

causing molecules of the structural agent to ooze out of the solution. If the temperature of the solubilised gel reduces, the degree of hydration reduces, and gelation occurs. Gel resulting from chemical cross-linking cannot liquefy by dilution or temperature changes.

Physical organogel synthesis involves solubilizing the organogelator (0.1% to 15%) in a heated solvent, depending on the nature of the structural agent. A decrease in temperature decreases organogelator and solvent molecule affinity, initiating their self-assembly into solid aggregates with increased intermolecular physical interaction. Increasing aggregate sizes entangle to form fluid-filled organogel matrices, trapping and immobilising the solvent due to surface tension into a three-dimensional network that emulates a solid fibre matrix. When gelators self-assemble, the total free energy of the organogel system decreases, making it a low-energy thermostable system, favourable when a longer shelf-life is desirable.

Organogels form transparent or opaque thermoreversible systems depending on the kinetic behaviour of these matrices. Solid matrices have a robust, permanent morphology, while fluid matrices are temporary structures in a constant state of flux. The temperature at which the organogelator dissolves in vegetable oil, solute-solvent interactions, and gelling concentration affect gelation. Organogelators melt between 40-90°C, depending on the melting point of the vegetable oil. Supersaturation during the initial stage of the gelling process, depending on the organogelator concentration and the gelling temperature, affects the gel network's topological and microstructure to various degrees. Organogels heated above their critical temperature lose their solid matrix-like structure and start flowing due to the disruption of physical interactions amongst the gelator molecules as thermal energy increases. However, as the heated organogels systems cool, the physical interaction amongst the organogelators causes the organogels to revert to more stable configurations.

High temperatures increase the solution's concentration as the organogelator molecules dissolve in an organic solvent at a high temperature, leading to a concentrated solution. Organogelators with high melting points affect oil quality as heating at high temperatures changes the triglyceride molecules' fatty acid constituents, altering the vegetable oil's physicochemical properties due to the change in chain length and degree and position of

unsaturation. The dissolution of organogelator molecules in organic solvents at high temperatures forms concentrated solutions that affect the oil quality since high-temperature heating changes the triglyceride molecules' fatty acid constituents. These alter the physicochemical properties of the vegetable oil due to the change in chain length, degree, and position of unsaturation. High temperatures elevate oil deterioration by losing essential fatty acids and oxidative rancidity.

The thermolabile actives in the molecular organogel network are susceptible to high temperatures; therefore, using structuring materials with high melting points (phytosterols, ceramides, fatty acids, fatty alcohols, long-chain monoglycerides and diglycerides, and waxes) are inconvenient.

Solvent quality can describe and predict solvent–gelling interactions using the theory of Hansen's solubility parameter (HSP) to quantify the quality of the solvent and subsequently adjust it to the optimal solubility of the gelling agent. Waxes affect critical gelation concentrations, organogel texture, oxidative stability, and physical properties of organogels and can act as pro-oxidants. Biocompatible, biodegradable, and non-immunogenic organogelators are safe for long-term application, enhance therapeutic efficacy and decrease fluctuation related to drug release. Simple lipids (fatty acids) efficiently hydrolyse two simpler constituents.

The polarities of vegetable oils and their constituents (triglyceride solvents) depend on the ratio of saturated/unsaturated fatty acids, fatty acid chain length, triglyceride chain conformation, and the presence of acids. Organogel synthesis using oils rich in long-chain monounsaturated fatty acids and polyunsaturated fatty acids promotes glycerol self-assembly. Waxes (long-chain alcohol esters) and glycerides (glycerin esters) are fatty acid esters. The degree of unsaturation, polarity, and fatty acid chain length influence the stability of these self-assembled lipids. Complex lipids (glycerophospholipids, glycosphingolipids, and glycoglycerolipids) hydrolyze poorly in acidic or basic aqueous solutions and yield three or more products. Amphipathic compounds affect the synthesis and characteristics of organogels.

Oil type impacts the physicochemical characteristics and texture of the organogel network due to its content of saturated, unsaturated, polyunsaturated materials and other minor constituents. Polar components in oils interact with organogelators, forming stiffer gels at lower concentrations, while higher concentrations negatively impact the gel's resistance because of saturation interactions with the organogelator. Polar components can come from emulsifiers, degradation products (oxidation, hydrolysis, thermal degradation), and natural compounds (tocopherols, phytosterols, water, free fatty acids, and mono-diglycerides). Modifying the oil's polarity mitigates the loss of elasticity and oil and can alter the structure and mechanical resistance of organogels. More polar oil forms a stiffer gel caused by the disorder of the lamellar structure at the nanometre scale. The solvent type affects the texture, viscosity, and crystal morphology. The appearance of firmer gels derives from oils rich in highly unsaturated fatty acids that impart a greater degree of freedom in lipid chain conformation. In fluid-filled matrices, organogels such as lecithin use a polar agent as a third component as a stabilizing and structure-forming agent.

The solvent's polarity and physicochemical properties strongly correlate to lecithin gelling. Several polar solvents thicken in hydrocarbon solutions and fatty acid esters of lecithin. Water, a polar solvent used for organogel formation, can be substituted with ethylene glycol, formamide, and glycerol to induce gelling. In organogels, the hydrogen bonds of solvent molecules bridge the phosphate groups of neighbouring lipid molecules, linking an extensive network of tubular aggregates. The organic solvent is critical in providing the desired action for the drug (hydrophobic) and lecithin in organogels. Natural oils provide useful organic solvents for preparing lecithin organogels. Polar solvent introduced into spherical lecithin micelles increases the cross-sectional area of the lecithin polar region, where the solvent assembles.

Gels and Rheology

Gels are amorphous solids whose constituent molecules or particles localize about their average positions in space due to constraints such as chemical cross-linking or direct physical associations like topological “entanglement” interactions between extended fibre or sheet structures in the fluid. These interactions lead to “gelation” or “amorphous solidification.

Gels are amorphous solids with a finite shear viscosity and disorderly molecular organization capable of viscoelastic stress relaxation. Gels are not fluids; their viscoelastic fluid, “jelly-like” consistency, forms as an intermediate between the ideal Newtonian fluid and Hookean elastic state instead of an elastic solid. The elastic stress response in gels is transient as the material relaxes after a long time. However, even crystalline solids will “flow” given enough time; therefore, lengthy stress relaxation periods in viscoelastic materials do not guarantee finite fluid viscosity.

Nematic gels involve topological interactions between particles/molecules localized by surrounding particles. “Weak gels” have infinite viscosity and a vanishing equilibrium shear modulus when transitioning between the fluid and solid states regions. At the same time, strong” physical gel materials have a finite shear modulus (84). The loss modulus (G″) and the storage modulus (G′) relate to shear relaxation, where a “strong gel” has the property, G′ > G″ (56).

The three-dimensional organogel structures follow the Maxwell model of viscoelasticity and exhibit plastic flow, behaving like a solid with elastic properties at low shear rates. Shear stress decreases the fibrous structures' physical connection until their breakdown causes plastic flow. Organogel phase behaviour (sol-gel or gel-sol) is temperature-dependent, and DSC gives an insight into the gelled microstructure. Organogels heated above critical temperature lose solidity and begin to flow because increased thermal energy disrupts the physical interactions amongst the gelator molecules; however, physical interaction resumes on cooling, and the organogels revert to a more stable configuration, endowing thermo-reversible properties on the organogel (57).

2.9.3. The Oil

Oil/oil blends must form nanoemulsions with the desired characteristics. Unmodified edible oils provide poor lipophilic drug dissolution and inefficient self-emulsification. Hydrolysed vegetable oils (VO) and semi-synthetic MCT oils with surfactant properties for solubilising and safety are preferred. VO-derived FA provides an environmentally friendly, non-toxic, biodegradable, renewable raw material source favourable for versatile, green, biomedical, and pharmaceutical nanochemistry, ensuring nanoparticles' dispersion in non-polar solvents. Vegetable oils (VO) are

nonpolar, lipophilic systems that belong to the biobased solvent class. VO can solubilise different molecules depending on the polarity of the target molecules: “Like dissolves like”. The solvent capacity of highly lipophilic triglycerides is a function of the effective concentration in ester groups. Solvent capacity for less hydrophobic drugs improves by blending triglycerides with mono- and diglycerides. Solubility determination can use predictor tools such as the COSMOthermX program. Triglycerides (Figure 2.3) are three fatty acid molecules esterified into one glycerol molecule and have complex and highly variable compositions. Fatty acids are classified as saturated, mono- and poly-unsaturated fatty acids of different configurations, resulting in different physical and chemical properties (58).

Table 2.17: Classification of fatty acids according to chain length (59)

Group	Chain length	Carbon atoms	Viscosity
I	Short	4 to 8	Viscous
II	Medium	8 to 12	More viscous
III	Long	12 to 22	Most viscous

Natural phospholipids include cis- or trans-unsaturated fatty acids. Natural unsaturated fatty acids are cis-configured, but modern processing like hydrogenation produces trans-configuration. Fatty acid saturation impacts lipid bilayer permeability to specific molecules (selective permeability). Unsaturated fatty acid-rich lipid bilayers have more gaps and, therefore, more permeability.

Table 2.18: Fatty acid composition of lipid excipients

			Water-soluble	Water Insoluble			Ref
				Long Chain triglycerides			
Carbon chain length	Fatty acid	Melting temp.	Soy PC Lecithin	Coconut oil	Castor Oil	Olive Oil	
C6:0	Caproic		-		-2 to -5 0 C		
C8:0	Caprylic acid	16.5	-	4.6-10.0	-	-	
C10:0	Capric acid	31.6	-	5.0-8.0	-	-	
C12:0	Lauric acid	44.8	-	45.1-53.2	-	-	

C14:0	Myristic acid	54.4	-	16.8-21.0	-	-	(60)
C16:0	Palmitic acid	62.9	13-18	7.5-10.2	0.70-1.4	7.5-20.0	(54,60–62)
C16:1n-7	Palmitoleic acid		-	-	-	0.3-3.5	(60,61)
C18:0	Stearic acid	70.1	3-6	2.0-4.0	0.51-1.2	0.5-5.0	(60,61)
C18:1n-9	Oleic acid	16.0	9-11	5.0-10.0	2.8-5.5	55.0-83.0	(60–62)
C18:1	Ricinoleic acid	6.0	-	-	84.2-90.2	-	(62)
C18:2n-6	Linoleic acid	-5.0	50-65	1.0-2.5	4.29-7.3	3.5-21.0	(60,61)
C18:3n-3	α-Linolenic acid	-11.0	6-9	-	0.2-1.12	≤1.0	(60,61)
C20:4n-6	Arachidonic acid	76.1	0	-	-	-	(60)
C22:0	Behenic acid	80.0	-	-	-		

The fatty acid composition of triglycerides in vegetable oils derived from plants and seeds varies according to their origin, agronomic and climatic conditions, production methods and quality (55). The presence or absence of double bonds classifies fatty acids (FAs) as saturated (SFAs—no double bonds or functional groups), monounsaturated (MUFAs—one double bond), and polyunsaturated fatty acids (PUFAs—two to six double bonds) and may have a cis or trans double bond configuration, indicated as n-3 or n-6. SFAs fully saturated with hydrogen atoms (C-H bonds) have more chemical energy than unsaturated fats with C=C bonds because these double bonds create spaces that enable molecules to pass through the tightly packed tails.

Short-chain triglycerides (SCT) (5 carbons or less)

Oxidation-resistant SCTs emulsify easily and have a high solvent capacity that depends on lipid ester concentration.

Medium-chain triglycerides (MCT) (6 to 12 carbon atoms)

LBDDS uses LCTs and MCTs or mixtures thereof under different degrees of saturation. MCTs have higher solvent capacities, oxidation resistance, and stability and are easier to emulsify than LCTs (33,63). MCTs balance drug loading capacities and promote micelles' solubilization, absorption, and transport through the unstirred water layer and enterocytes directly via the portal blood to the systemic circulation (49).

Long-chain triglycerides (LCT) (≥12 carbon atoms)

LCTs decrease unsaturation and oxidative degradation. Emulsifying and transporting LCTs through intestinal lymphatics is difficult. However, MCT with >12 carbon (C) atoms favours the lymphatic transport of digested products and endogenous lipoproteins (49). LCT forms larger globules than MCT in microemulsions; therefore, manipulating LCT and MCT combinations can create specific globule sizes that improve lymphatic uptake for drugs with a log P>5 and LCT solubility >50 mg/ml (33).

Mixed glycerides and polar oils

Medium-chain mixed glycerides (mono- and diglycerides) are non-oxidizing, solvent-rich amphiphiles with high emulsification potential. Mixed glycerides, produced by the partial hydrolysis of vegetable oil, have a chemical composition that varies with the starting materials and extent of hydrolysis (69). Non-oxidizing medium-chain mixed glycerides improve emulsification.

In the formulation, olive, coconut, and castor oil are water-insoluble. LCT and MCT phospholipids are water-soluble excipients, and span 80 and Tween 20 are the surfactants (48,49). Lipids metabolize into bioactive lipid molecules, composing cell membranes and mediating signalling pathways. Changes to lipid metabolism alter membrane composition and permeability, disrupt signalling networks, and cause pathologies such as cancer, cardiovascular, neurodegenerative, metabolic diseases, and inflammatory complications.

Table 2.19: Average values of oil parameters of castor, coconut and olive oil (59)

Oil	Viscosity	Diameter	Cloud point	Pour point	Saponification value	Acid Value	pH	Specific gravity
Castor oil	686,24	5,03	-18,2	-21,7	187,02	1,351	4,92	0,9598
Coconut oil	44,16	7,67	13,1	12,7	78,00	0,378	3,91	0,9138
Olive oil	63,61	7,4	-11,1	-14,2	130,32	1,361	4,6206	0,9185

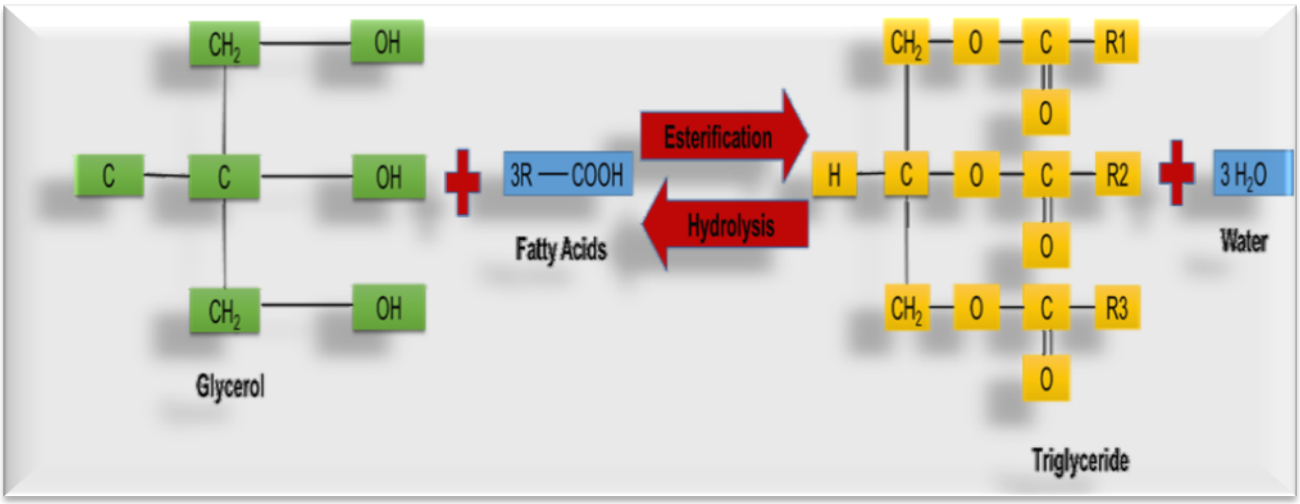

Figure 2.5: Esterification and hydrolysis of Fatty Acids

2.9.3.1. Coconut Oil

Virgin coconut oil (VCO), a triglyceride with (R1, R2 and R3) fatty acids, naturally comprises a 3:1 ratio of medium- and long-chain fatty acids. The significant proportion of saturated fats (C12:0, C14:0) limits oxidative rancidity, making coconut oil more stable when exposed to air than vegetable oils (VO); however, it also raises the pour point (64).

2.9.3.2. Castor Oil (Ricinus Oil)

Castor Oil (CO), a seed extract from the castor plant *Ricinus communis L.*, has a mild odour and distinctive taste and is a colourless to pale yellow viscous liquid at room temperature without solid fat formation at 8°C (65,66). CO, a non-toxic, biodegradable, renewable resource, consists of approximately 84–90% Ricinoleic acid (12-Hydroxyoleic Acid) and 10–16% other fatty acids such as Linoleic acid (4.2%), Oleic acid (3.0%), Stearic acid (1.0%), Palmitic acid (1.0%), Dihydroxy stearic acid (0.7%), Linolenic acid (0.3%), 675 acids (0.3%) (65,66).

Most CO triglycerides have three RA molecules linked to a glycerol moiety. The five primary triacylglycerides in CO are triricinolein (RRR) (84.1 %), diricinoleoystearoylglycerol (RRS) (8.2 %), di-ricino-leoyloleoylglycerol (RRO) (5.6 %), diricinoleoyllinoleoyl (RRL) (1.2 %), and RRP (0.9 %) (73,77).

Ricinoleic acid (RA), a multifunctional carboxylic acid, provides a suitable substitution for traditional, toxic, expensive carboxylic acids (like oleic and stearic acid) that function as solvents,

cosolvents, ligands, capping, coating and stabilizing agents in nanoparticle and polymer syntheses. RA has desirable physicochemical and mechanical properties to produce drug carriers. CO, an inedible VO and a natural source of polyols, is a rich RA source for chemical and biochemical reactions.

Nanoparticle surface functionalization ligands must be biomolecule-specific and minimally cytotoxic (73). A hydroxyl group, carboxylate and double bond, the three functional groups in RA, provide reaction sites and impart unique properties to castor oil when producing functional materials such as biopolymers and plasticisers (65)**.** These functional groups confer an approximately sevenfold higher viscosity on CO than other VOs. The **double bond** transforms CO through epoxidation, halogenation, hydrogenation, oxidation, polymerization, and sulfonation reactions (65,66).

Hydrogenated castor oil (HCO), although soluble in hot organic solvents like ether and chloroform, is insoluble in water and most organic solvents. This insolubility endows HCO with water resistance and lubricity (73). Hydrogenation occurs when hydrogen is added to an unsaturated fatty acid with a nickel or palladium catalyst, transforming liquid Ricinoleic acid into semi-solid saturated 12-hydroxystearic acid, increasing the melting point of CO and improving stability, taste, odour, and oxidative and thermal stability.

CO, the richest and only source of a monounsaturated 18-carbon hydroxylated fatty acid with a single, double bond (C9 and C10), is the absolute standard for viscosity because of its reliable, consistent, uniform physical properties and composition. CO has a relatively high viscosity (260.4 cSt at 40°C) and specific gravity (73). Molecular weight (MW) affects oil viscosity. CO has a higher MW and, thus, a more effective viscosity than Olive Oil (OO) (62). CO is a non-drying oil that does not harden on-air exposure because of the single, double bond (low iodine value) in each FA chain, imparting excellent emollient, lubricating, and wetting properties (55). The hydroxyl group beta to the double bond protects that double bond from peroxidation (70).

RA has a single, **double bond** and a hydroxyl group (at C12 in the C18 tail), making CO (and its derivatives) soluble in all alcohols with limited solubility; however, in aliphatic petroleum solvents.

Moreover, weakly bound dimers and trimers form from the original triglycerides, increasing the steric hindrance because hydrogen bonding between hydroxyl groups of hydroxylated triglycerides increases viscosity. Alkyl groups impose steric effects that control nanoparticles' growth, crystal structure, morphology, and surface characteristics (62).

Ester Linkages: Alcoholysis, Amidation, Esterification, Hydrolysis, reduction, saponification
RA presides over oleic acid for applications requiring more polar organic solvents. CO and RAs are compatible with highly polar organic solvents and possess antimicrobial properties. (66).

Hydroxyl Group: Alkoxylation, Caustic fusion, Dehydration, Esterification, Halogenation, Hydrolysis, distillation, Pyrolysis, Sulfation, and Urethane reactions (62,66)

The highly polar hydroxyl groups of CO affect the viscosity, pour point, melting point, heat of fusion, solubility, crystal structure, and polymorphism of CO (Table 2.18). The hydroxyl group on RA enables chemical modification and functionalization, tailoring the interaction of nanoparticles with target biomolecules. Nanoparticle surfaces are functionalised by joining the hydroxyl group attached to RA-capped nanoparticles with other groups to enhance their dispersion in different solvent media specific to a particular application. Moreover, specific applications include the compatibility and plasticization of natural and synthetic elastomers, polymers, resins, and waxes (74).

Alkoxylation, acetylation and dehydration of the hydroxyl group create new double bonds, increasing the unsaturation of CO to form conjugated acids, thereby improving flexibility, rapid drying, excellent colour retention, and water resistance for protective coatings.

An amorphous preparation formulated with HCO by the melt method achieved sustained drug release. It eliminates the burst release, two critical characteristics for the sustained release of a

drug from an ASD. The oil also increases friction to transport drugs into the intracellular compartment to increase the water solubility of the less water-soluble drugs. The Higuchi model is most suitable for modelling drug release from HCO granules, indicating diffusion-induced drug release (67).

2.9.3.3. Olive Oil

Oleic acid, an 18:1n – 9 MUFA, constitutes the principal bioactive portion of olive oil (~ 55% to 83%). Oleic acid can alter the structure and biophysical properties of the membrane. The 18-carbon fatty acid has a single cis-double bond located at the 9th carbon from the methyl extremity that bends at a ~ 120° angle in the middle of the carbon chain to form a boomerang-shaped structure, reducing the order within the lipid bilayer. In the lamellar phase, lipids are orientated perpendicular to the membrane surface; however, the fluid lamellar phase (L_α or liquid crystalline) can also shape into non-lamellar phases (L_ε frustrated membranes), e.g., cubic (micellar and bicontinuous), hexagonal (HI and HII), and rhombohedral phases. Oleic acid's molecular shape induces a negative curvature strain on the lipid bilayers, which organizes and stabilizes membranes into HII non-lamellar phases, drastically changing the temperature range of the stable single L_α phase, decreasing the lamellar to-hexagonal (L_α-to-HII) phase transition temperature in lipid membranes.

Comparative analysis of fatty acids shows that oleic acid and 2-hydroxyoleic acid (18-carbon acyl chain with a single cis double bond) causes the most significant disarray in lipid bilayer structures. Oleic acid reduces the order within the lipid bilayer. In Elaidic acid (the oleic acid trans-isomer), the kinked carbon chain's two parts are almost linear, resulting in a rod-shaped structure: Spatially, linear molecules pack in rigid, organized arrays, whereas bent molecules cannot do this. Membrane disorder resulting from the kinked oleic acid-lipid chain increases membrane fluidity and maintains bilayer hydration (60).

Oleic acid and 2-hydroxyoleic acid (a synthetic, hydroxylated analogue of oleic acid) modulate the liquid-ordered/liquid-disordered structure ratio and the microdomain lipid composition affecting lipid rafts. Oleic acid can be efficiently incorporated into phospholipids, forming the core of the lipid bilayer and regulating the activity of integral or peripheral membrane proteins. Oleic

acid embedded in the bilayer or its free form can alter targeted molecular functions in the cell by modulating membrane properties upon release from the sn-2 position of phospholipids via phospholipases. Oleic acid has a co-solvent effect that increases the solubility of lecithin in oil and suppresses phospholipid reverse micelles formation at low water content. OO produces spherical, dotty, cubic, or flower-like vesicles in the fatty acid chains.

Colloidal assemblies of phospholipids in oil are susceptible to changes in system composition, temperature, and water. Moderate amounts of oleic acid in the oil delay removing phospholipid reverse micelles upon adding water, and more water is needed to form lamellar structures. Adding more water stabilises oleic acid in the reverse micelles, and even more water added induces phase separation. Lecithin/water/oil systems are characteristically sensitive to water concentrations. Minor changes to the water content can alter micelle morphology or cause phase separation. Including an additive (e.g., oleic acid) that modifies or stabilizes the surfactant assembly can stabilize reverse micelles in Lecithin/water/oil systems. Oleic acid improves the stability of reverse micelles against precipitation due to the increased water concentration in oil by allowing the reverse micelle cores to expand and accommodate more water. The shape and size of the reverse micelles changed at high temperatures, and irreversible elongation was observed, especially in oleic acid (54).

2.9.4. Co-solvents

Co-solvents used in microemulsion preparation must dissolve large amounts of hydrophilic surfactants or hydrophobic drugs in the lipid base and increase solubilization, solvent capacities, and dispersion (48). However, aqueous dilution reduces solvent capacity, precipitating the solubilized drug inside the shell and evaporation from capsules (63). The organic halogenated solvent chloroform, traditionally used to prepare liposomes because of its high evaporation rate and low boiling point, has no therapeutic value and could accelerate the decomposition of encapsulated solvents, but cannot be removed entirely from liposome preparations due to chemical and physical barriers. Chloroform may induce chronic CNS, kidney and liver pathologies, dermatitis, and irritation of the skin, eyes, mucous membranes, and upper respiratory tract. Ethyl acetate, a non-halogenated solvent, is a suitable substitute for chloroform as it has similar properties to chloroform, including high polarity and vapour pressure and its

utility includes small and large-scale production (68). Ethyl acetate is a class III solvent partially miscible in water, suitable for spontaneous emulsification for safety reasons (Table 2.19) (69).

Table 2.20: Solvent Toxicity classes (69)

Class	Toxicity	Preferred action
Class I:	High	Avoid
Class II:	Medium	Limit
Class III:	Low	Minimal toxicity (preferred)

Table 2.21: Physicochemical properties of chloroform and nonhalogenated solvents **(68)**

Properties	Chloroform	Ethyl acetate	Methanol
Polarity index	4.10	4.40	5.10
Solubility in water (g/100 mL)	0.82	8.70	Miscible
Viscosity (cP)	0.57	0.45	0.55
Vapour pressure (kPa)	25.90	9.73	13.02
Lecithin solubility	S	S	S
Allowable concentration (g/kg)	Prohibited	0.05	0.05

Solvents miscible in water cannot form lipid bilayer for w/o/w emulsion and dispersal-like micelles. Individual non-halogenated solvents did not form stable inverted micelles when used alone. A ratio of ethyl acetate: n-hexane 4: 1(v/v) formed stable inverted micelles without phase separation. The study implies that combinations of nonhalogenated solvents could be promising substitutes for chloroform, which may harm human health (68).

2.9.5. Surfactants

Surfactants, ‘edge activators’, possess hydrocarbon chains that penetrate the phospholipid bilayer, resulting in steric stabilization, reducing vesicle fusion, and improving liposome stability (70). Surfactant molecules have hydrophilic and lipophilic groups that make them surface-active; they form an interfacial film and minimise the interfacial tension, which aids dispersion (33). Amphiphilic surfactants can solubilize large quantities of lipophilic drugs, preventing precipitation in the gastrointestinal lumen and prolonging drug molecules' lifespan. In addition, surfactants protect drugs against physicochemical and enzymatic degradation (42). Surfactants modify GIT

membrane permeability and increase the flexibility of liposomes, enabling them to pass through holes smaller than their size. Surfactants form micelles that reduce the energy needed for droplet distortion (70).

When stirring two liquids without a surfactant, more viscous liquids disperse into less viscous ones. Although surfactant combinations decrease droplet size and improve the stability of nanoemulsions, increased surfactant concentrations can increase droplet size at CMC because water penetrates the oil droplets, disrupting the interface and ejecting oil droplets into the aqueous phase (1) (15). Increased surfactant concentrations decrease drop size by inhibiting coalescence below the critical micelle concentration (82) (3).

Table 2.22: HLB values vs. uses (71)

HLB	USE
4-6	w/o emulsifiers
7-9	Wetting agents*
8-18	o/w emulsifiers
13-15	Detergents
10-18	Solubilizer

Surfactant selection depends on the charge, molecular weight, chemical structure, and hydrophile-lipophile balance (HLB) for a particular lipid matrix. The relationship/balance between the size and strength of the surfactant's hydrophilic and lipophilic groups determines the emulsifier's HLB grading. All applications requiring a surfactant have an HLB requirement. When the HLB value compares to the HLB requirement in a formulation, the formulation performs well and is more stable.

Water-soluble surfactants obtained from the chemical hydrogenation of organic vegetable oils must solubilize the PNL easily to produce oil/water emulsions with aqueous characteristics. Water-insoluble surfactants, synthesized by mixing polyethylene glycol with hydrolysed VO, include lipid excipients with HLB values between 8 and 12. O/w emulsion needs an emulsifying agent that is more soluble in the aqueous phase. W/o emulsion needs an emulsifying agent more soluble in the oil phase (33).

Non-ionic surfactants are less toxic, less affected by pH and ions, possess a low CMC and are more compatible with biological systems than ionic surfactants (40). Non-ionic surfactants produce a negatively charged interface at neutral pH because the smaller OH- is more abundant near the interface than the hydrated proton (72). All non-ionic surfactants have an HLB value ranging from 0-20. SEDDS use surfactant HLB <12, while non-ionic surfactants with an HLB value >12 prepare SMEDDS and SNEDDS that require high emulsifying performance for their rapid formation and dispersion into tiny o/w droplets in aqueous media.

Spans and Tweens are mild non-ionic surfactants, stable in mild acids, alkalis, and electrolytes and nonreactive with ionic ingredients or actives. Spans and Tweens also increase formulation stability, flexibility, and compatibility. Different Spans-Tween ratio systems with wide HLB ranges emulsify most oils and waxes. Specific Spans and Tweens are highly effective solubilisers, dispersing agents and wetting aids, non-ionic emulsifiers and co-emulsifiers that are electrolyte tolerant and stable over a comprehensive pH range (73).

Spans are unsaturated or branched-chain fatty acids emulsifiers. Tweens are hydrophilic, ethoxylated Spans that solubilize or disperse in water and dilute electrolyte solutions. The Tween's aqueous solubility increases with the degree of ethoxylation and decreases with increasing numbers of ester groupings for specific degrees of ethoxylation. Aqueous solubility decreases with increasing molecular weights of the fatty acid, provided that the degree of ethoxylation and esterification remains fixed (73). Span 80 is excellent for water in the oil emulsification of hydrocarbons.

Spans-Tween combinations yield a variety of o/w and w/o emulsions and make efficient co-emulsifiers for o/w systems, e.g., emulsifiers with an unsaturated alkyl chain, such as an oleyl chain, have an increased affinity for oils with unsaturated bonds, and a blend of Span 80 and Tween 80 can emulsify a VO. Combinations of high and low HLB emulsifiers are more effective than single emulsifiers. Emulsifier blends with saturated alkyl chains such as Span and Tween 60 can emulsify these saturated materials with stability depending on identifying the required HLB. The optimum concentration of the emulsifier blend, determined by experimentation, uses

10% of the level of the emulsified material as a starting point, i.e., making a 30% oil emulsion needs a 3% emulsifier blend as the optimum level (73).

2.9.6. Co-surfactants

Single surfactants rarely produce stable interfacial tensions. Cosurfactants are medium-chain length alcohols (C3–C8) that increase the interfacial film's flexibility and decrease its bending stress by reducing the interfacial tension to a negative value. Curvature type depends on nanoemulsion compositions (33). Emulsifiers typify the interfacial film's chemical reactivity, electric charge, hydrophobicity, and thickness and synergise lipid nanoparticle dispersions by preventing particle agglomeration (50).

Emulsifier choice depends on the route of drug administration. High concentrations of emulsifying surfactants needed to dissolve large quantities of hydrophobic drugs may irritate the GI mucosa and should be used sparingly in parenteral and oral formulations. The self-emulsification and dispersion of LBDDS in the aqueous physiological environment are affected by pH, ionic content, the ratio of oil to surfactant and temperature. pH ranges from 1.2 (stomach) to ≥7.4 (blood and intestine). Droplet size is inversely related to surfactant-stabilised oil droplets at the oil-water interface (1).

2.9.7. The sequential addition of ingredients

Ingredient order affects dispersion type. Drugs disrupt self-emulsification, changing the ideal oil: surfactant ratio (48). SEDDS are unaffected by mixing order; however, surfactants must be mixed with the oily phase first to generate SNEDDS. SMEDDS only form if the surfactant combines with water before introducing the oily phase (44).

2.10 Designing the SELF

The goal of LBDDS is efficient drug absorption by the intestinal mucosal cells. For optimised LBDDS, factors that affect emulsification, such as absorption, delivery targets, digestion, dispersion, formulation objectives and solubility, are considered pre-formulation. The drug must be lipid-soluble. Generally, formulations with more lipids (>60%), less surfactant (<30%), and cosolvent (<10%) solubilize drugs more efficiently on dilution (63).

When developing the ideal SELF, check that the drug has a low dose with log P ≥2 lipophilicity, is highly soluble in pharmaceutically accepted lipids, surfactants, and co-solvents, and evades extensive first-pass metabolism (47). Surfactant properties determine droplet characteristics. Adding one or more surfactants and hydrophilic co-solvents may improve the dispersion and prevent drug precipitates. The LBDDS must ensure drug solubilization after dispersion and digestion; therefore, the properties of dispersed colloids in gastric fluids are as crucial as those of the formulation for enhancing drug absorption. MCT imparts drug solubility and stability excellently in formulations, while LCT facilitates efficient bile salt-lipid colloid formation, increasing bioavailability. As intestinal lipases metabolize digestible lipids and fatty acids and emulsify any remaining oil in the GIT, large amounts of surfactants are not necessarily needed to generate tiny particles with large surface areas for drug release. Undigestible surfactants generally improve bioavailability (41) (50).

Determine the physicochemical properties and the target site of the prospective molecule. Decide on the type and quantity of phospholipids, oils and surfactants and calculate the correct HLB ratios for the formulation (Table 2.21). Select the administration route and determine the barriers to overcome. Barriers to bioavailability include the physicochemical drug properties like intrinsic solubility, permeability, and stability and biological barriers such as gastrointestinal tract transit time, absorption windows, transmembrane efflux of drugs, and pre-systemic metabolism.

Approximate limits used to design LBDDS specifications come from predictor systems describing factors influencing behaviour during and after formulation. These systems include Lipophilicity/hydrophobicity of the API (Table 2.22); Lipid System Classification (LSC) (Table 2.23); Biopharmaceutical Classification System (BCS) (Table 2.24); Biopharmaceutical Drug Disposition Classification System (BDDCS) (Figure 2.8); Hydrophilic/Lipophilic Balance (HLB) of oils, surfactants, co-surfactants, and co-solvents (Table 2.21).

2.10.1. SwissADME

An effective drug molecule must display high bioactivity and low toxicity, reach its target site in therapeutic quantities, and remain bioactive long enough to elicit a biological response in the body. SwissADME, a free web application, allows drug development and research experts and

nonexperts to forecast drug molecules' physicochemical, pharmacokinetic, drug-likeness, and medicinal chemistry. SwissADME assesses absorption, distribution, metabolism, and excretion (ADME) and predicts BBB permeation and passive HIA. SwissADME uses drug similarity to estimate oral drug molecule bioavailability in formulation development. Lipophilicity and water solubility are critical in parenteral formulations that require high solubility in small volumes and influence absorption in oral routes. Access to physical samples is often limited. Predictive ADME early in drug development reduces pharmacokinetics-related clinical failures and makes computer models effective alternatives to experiments (85).

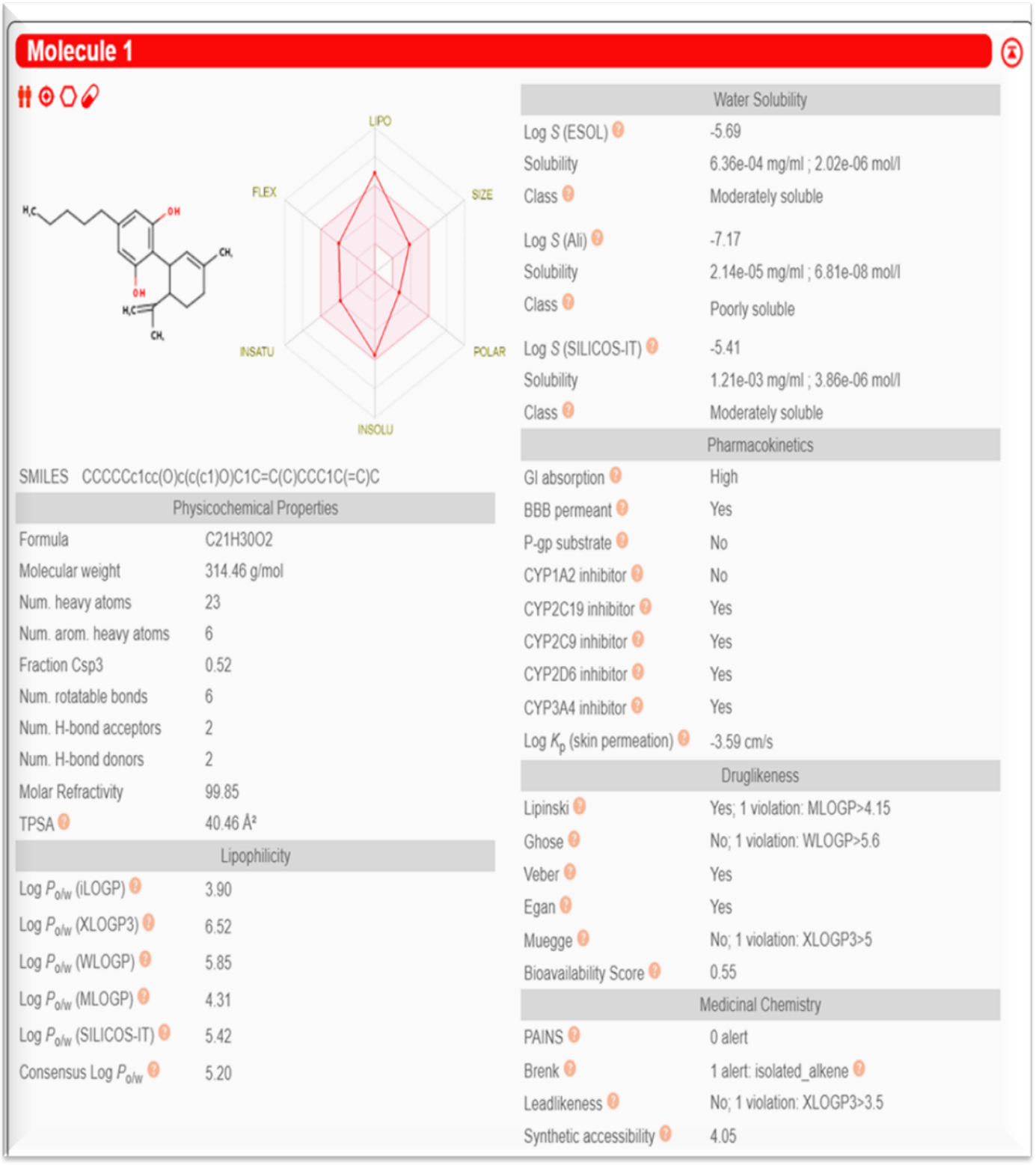

Figure 2.6: The canonical SMILE formula of CBD copied from PubChem was inserted into the user-friendly SwissADME program and run. The picture shows physicochemical and ADME predictions for the CBD Molecule (login-free website http://www.swissadme.ch).

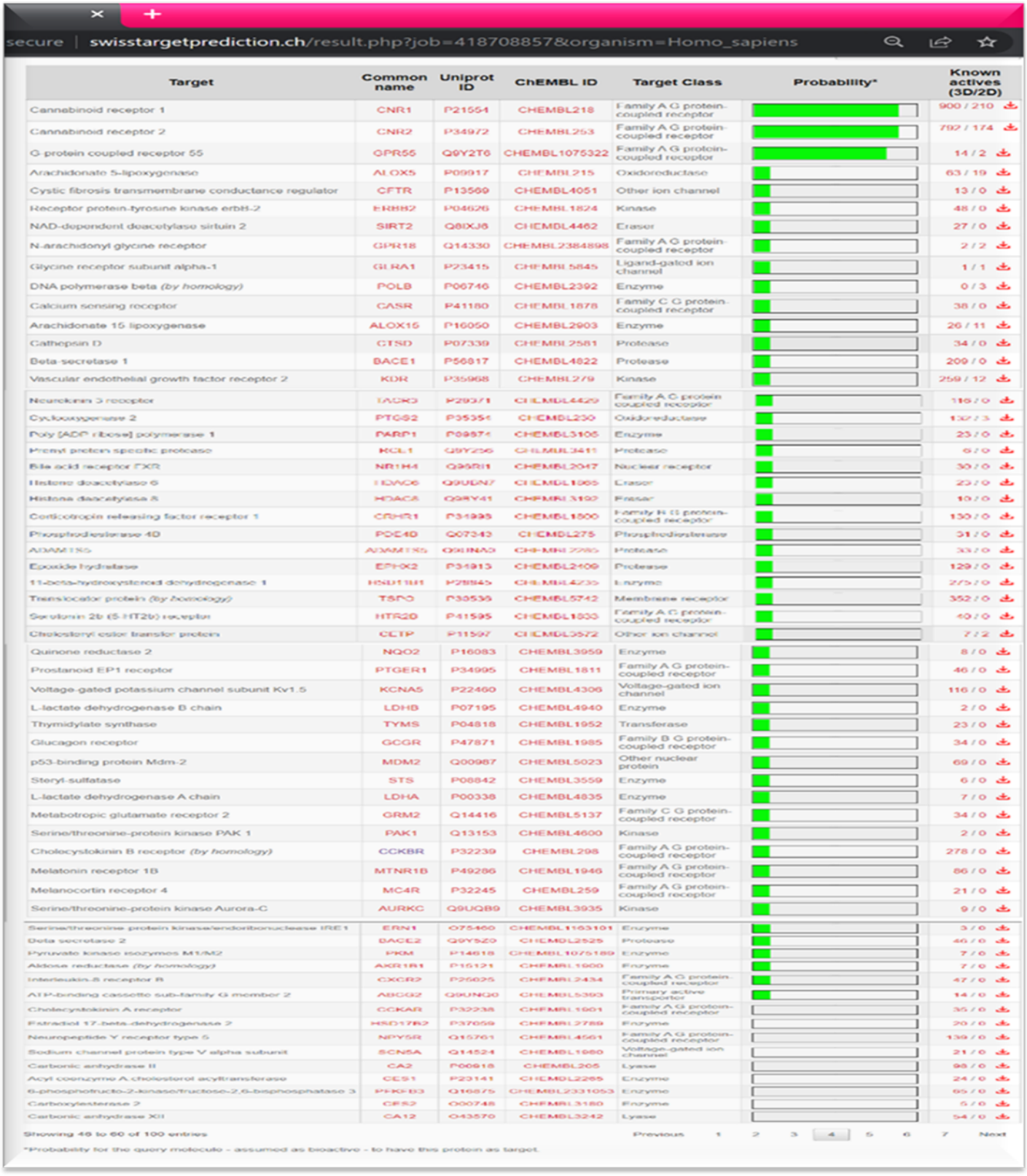

Target	Common name	Uniprot ID	ChEMBL ID	Target Class	Probability*	Known actives (3D/2D)
Cannabinoid receptor 1	CNR1	P21554	CHEMBL218	Family A G protein-coupled receptor		900 / 210
Cannabinoid receptor 2	CNR2	P34972	CHEMBL253	Family A G protein-coupled receptor		792 / 174
G-protein coupled receptor 55	GPR55	Q9Y2T6	CHEMBL1075322	Family A G protein-coupled receptor		14 / 2
Arachidonate 5-lipoxygenase	ALOX5	P09917	CHEMBL215	Oxidoreductase		63 / 19
Cystic fibrosis transmembrane conductance regulator	CFTR	P13569	CHEMBL4051	Other ion channel		13 / 0
Receptor protein-tyrosine kinase erbB-2	ERBB2	P04626	CHEMBL1824	Kinase		48 / 0
NAD-dependent deacetylase sirtuin 2	SIRT2	Q8IXJ6	CHEMBL4462	Eraser		27 / 0
N-arachidonyl glycine receptor	GPR18	Q14330	CHEMBL2384898	Family A G protein-coupled receptor		2 / 2
Glycine receptor subunit alpha-1	GLRA1	P23415	CHEMBL5845	Ligand-gated ion channel		1 / 1
DNA polymerase beta *(by homology)*	POLB	P06746	CHEMBL2392	Enzyme		0 / 3
Calcium sensing receptor	CASR	P41180	CHEMBL1878	Family C G protein-coupled receptor		38 / 0
Arachidonate 15-lipoxygenase	ALOX15	P16050	CHEMBL2903	Enzyme		26 / 11
Cathepsin D	CTSD	P07339	CHEMBL2581	Protease		34 / 0
Beta-secretase 1	BACE1	P56817	CHEMBL4822	Protease		209 / 0
Vascular endothelial growth factor receptor 2	KDR	P35968	CHEMBL279	Kinase		259 / 12
Neurokinin 3 receptor	TACR3	P29371	CHEMBL4429	Family A G protein-coupled receptor		116 / 0
Cyclooxygenase 2	PTGS2	P35354	CHEMBL230	Oxidoreductase		132 / 3
Poly [ADP-ribose] polymerase 1	PARP1	P09874	CHEMBL3105	Enzyme		23 / 0
Prenyl protein specific protease	RCE1	Q92554	CHEMBL3411	Protease		6 / 0
Bile acid receptor FXR	NR1H4	Q96RI1	CHEMBL2047	Nuclear receptor		30 / 0
Histone deacetylase 6	HDAC6	Q9UBN7	CHEMBL1865	Eraser		23 / 0
Histone deacetylase 8	HDAC8	Q9BY41	CHEMBL3192	Eraser		10 / 0
Corticotropin releasing factor receptor 1	CRHR1	P34998	CHEMBL1500	Family B G protein-coupled receptor		130 / 0
Phosphodiesterase 4D	PDE4D	Q08499	CHEMBL275	Phosphodiesterase		31 / 0
ADAM10	ADAM10	O14672	CHEMBL2385	Protease		33 / 0
Epoxide hydrolase	EPHX2	P34913	CHEMBL2409	Protease		129 / 0
11-beta-hydroxysteroid dehydrogenase 1	HSD11B1	P28845	CHEMBL4235	Enzyme		275 / 0
Translocator protein *(by homology)*	TSPO	P30536	CHEMBL5742	Membrane receptor		352 / 0
Serotonin 2b (5-HT2b) receptor	HTR2B	P41595	CHEMBL1833	Family A G protein-coupled receptor		60 / 0
Cholesteryl ester transfer protein	CETP	P11597	CHEMBL5572	Other ion channel		7 / 2
Quinone reductase 2	NQO2	P16083	CHEMBL3959	Enzyme		8 / 0
Prostanoid EP1 receptor	PTGER1	P34995	CHEMBL1811	Family A G protein-coupled receptor		46 / 0
Voltage-gated potassium channel subunit Kv1.5	KCNA5	P22460	CHEMBL4306	Voltage-gated ion channel		116 / 0
L-lactate dehydrogenase B chain	LDHB	P07195	CHEMBL4940	Enzyme		2 / 0
Thymidylate synthase	TYMS	P04818	CHEMBL1952	Transferase		23 / 0
Glucagon receptor	GCGR	P47871	CHEMBL1985	Family B G protein-coupled receptor		34 / 0
p53-binding protein Mdm-2	MDM2	Q00987	CHEMBL5023	Other nuclear protein		69 / 0
Steryl-sulfatase	STS	P08842	CHEMBL3559	Enzyme		6 / 0
L-lactate dehydrogenase A chain	LDHA	P00338	CHEMBL4835	Enzyme		7 / 0
Metabotropic glutamate receptor 2	GRM2	Q14416	CHEMBL5137	Family C G protein-coupled receptor		34 / 0
Serine/threonine-protein kinase PAK 1	PAK1	Q13153	CHEMBL4600	Kinase		2 / 0
Cholecystokinin B receptor *(by homology)*	CCKBR	P32239	CHEMBL298	Family A G protein-coupled receptor		278 / 0
Melatonin receptor 1B	MTNR1B	P49286	CHEMBL1946	Family A G protein-coupled receptor		86 / 0
Melanocortin receptor 4	MC4R	P32245	CHEMBL259	Family A G protein-coupled receptor		21 / 0
Serine/threonine-protein kinase Aurora-C	AURKC	Q9UQB9	CHEMBL3935	Kinase		9 / 0
Serine/threonine-protein kinase/endoribonuclease IRE1	ERN1	O75460	CHEMBL1163101	Enzyme		3 / 0
Beta-secretase 2	BACE2	Q9Y5Z0	CHEMBL2525	Protease		46 / 0
Pyruvate kinase isozymes M1/M2	PKM	P14618	CHEMBL1075189	Enzyme		7 / 0
Aldose reductase *(by homology)*	AKR1B1	P15121	CHEMBL1900	Enzyme		7 / 0
Interleukin-8 receptor B	CXCR2	P25025	CHEMBL2434	Family A G protein-coupled receptor		47 / 0
ATP-binding cassette sub-family G member 2	ABCG2	Q9UNQ0	CHEMBL5393	Primary active transporter		14 / 0
Cholecystokinin A receptor	CCKAR	P32238	CHEMBL1901	Family A G protein-coupled receptor		35 / 0
Estradiol 17-beta-dehydrogenase 2	HSD17B2	P37059	CHEMBL2789	Enzyme		20 / 0
Neuropeptide Y receptor type 5	NPY5R	Q15761	CHEMBL4561	Family A G protein-coupled receptor		139 / 0
Sodium channel protein type V alpha subunit	SCN5A	Q14524	CHEMBL1980	Voltage-gated ion channel		21 / 0
Carbonic anhydrase II	CA2	P00918	CHEMBL205	Lyase		98 / 0
Acyl coenzyme A:cholesterol acyltransferase	CES1	P23141	CHEMBL2285	Enzyme		24 / 0
6-phosphofructo-2-kinase/fructose-2,6-bisphosphatase 3	PFKFB3	Q16875	CHEMBL2331053	Enzyme		65 / 0
Carboxylesterase 2	CES2	O00748	CHEMBL3180	Enzyme		5 / 0
Carbonic anhydrase XII	CA12	O43570	CHEMBL3242	Lyase		54 / 0

Showing 49 to 60 of 100 entries Previous 1 2 3 4 5 6 7 Next

*Probability for the query molecule - assumed as bioactive - to have this protein as target.

Figure 2.7: Results of the SwissADME transcript showing target probability predictions for the CBD molecules

2.10.2. HLB Calculations

Calculate the HLB of the surfactants. Most formulations use a blend of surfactants for the best results. Add up the oil phase ingredients and determine the total % of oil in the formulation. Determine each oil's contribution ratio/percentage to the total oil phase. Multiply the percentage of each oil by its stated HLB value and add the resulting numbers together to give the estimated required HLB of the oil blend. The required HLB for the oil must equal the HLB value of the surfactant blend.

The HLB of the surfactant blend should be ±1 of the calculated HLB of the oil blend. HLB estimates the water solubility of surfactants. The lowest oil and water interfacial tension occurs when the required HLB for the oil and the surfactant are the same. The lowest interfacial tension equals the lowest amount of emulsifier/surfactant to achieve a stable emulsion. Two emulsifiers with the same HLB may exhibit very different solubility characteristics. Surfactants with HLB numbers below 9.0 are lipophilic and oil-soluble, while those above 11.0 are hydrophilic and water-soluble. The intermediate range falls between 9 and 11 (74,75).

2.10.3. Determination of lipophilicity/hydrophobicity

Determine the lipophilicity/hydrophobicity of the drug (Table 16). Bioavailability is a parameter highly dependent on clearance, permeability, and solubility, which depend on lipophilicity. Lipophilicity is critical to a drug's pharmacokinetic performance, i.e., absorption, distribution, metabolism, and excretion (ADME) and vital for permeation across membranes and biological barriers. Despite its in vitro potency, a drug cannot be effective if it cannot reach or maintain therapeutic concentrations. Lipophilic drugs cannot penetrate specific barriers in the body, and accumulation in fatty tissues makes excretion and elimination difficult, resulting in systemic toxicity.

The partition coefficient (LogP) estimates the distribution of chemical substances in the body by measuring their hydrophilicity or hydrophobicity. LogP describes the dissolution of a neutral, uncharged compound (solute) in an immiscible biphasic lipid system (octanol and water). LogP, a constant, indicates the proportion of compounds in an equilibrated mixture of two immiscible solvents and compares the solute's solubilities in these two liquids. LogP aids drug selection and analogue optimization by predicting drug transport, targets, ADME by living tissue, and

dissemination by water in physiological and ecological systems, among other possible limitations (76).

LogP = log10 (Partition Coefficient) Partition Coefficient, P = [organic]/[aqueous]

Where [ ] = the solute concentration in the organic and aqueous partition (76)

Table 2.23: LogP Values vs Compound Properties (76)

LogP Values	Compound properties
LogP = 1	There is a 10:1 partitioning in the organic-aqueous phases.
LogP= positive (+)	The drug is more attracted to the lipid phase (i.e., lipophilic).
LogP = 0	The drug partitions equally between the lipid and aqueous phases
LogP= negative (-)	The drug has a higher attraction to the aqueous phase (i.e., hydrophilic)
LogP= 0 to LogP= 3	The drug has good bioavailability.
LogP >5	The drug has high lipophilicity and metabolic turnover, low solubility and oral absorption, and an increased risk of indiscriminate binding to hydrophobic targets other than the specified target, increasing potential toxicity.
LogP <5	Oral administration (Lipinski Ro5)
LogP ~ 2	Drugs targeting the CNS
LogP >5	Sub-lingual absorption
LogP 1.35 to 1.8	Oral and intestinal absorption

2.10.4. Poulton's Lipid Classification system

Poulton's Lipid Classification system (LCS) identifies critical performance characteristics of lipid systems. Determine the lipid systems (SELF) suitable for the type of drug by applying Poulton's LCS (Table 2.23). The LCS classifies Type I, II, III and IV formulations by appearance, aqueous dilution, composition, cosolvents, digestibility of the formulation, emulsion type, oil ratio, particle size, physicochemical drug characteristics, preparation method and surfactants.

Surfactant-cosolvent blending improves solvent capacity on dilution by forming micelles, facilitating surfactant dispersion, and reducing gastric irritation caused by high surfactant concentrations compared to cosolvent alone. Type I formulations are oils; Type II are water-

insoluble SEDDS; Type IIIA is SMEDDS contains water-soluble surfactants and cosolvents; and Type IIIB has a more significant ratio of water-soluble components. Type IIIA/IIIB formulations form clear/transparent solutions that differ in hydrophilicity and lose solvent capacity on dispersion. Type IV formulations consist of surfactants and cosolvents and no oils. Type IV formulations are unsuitable for chronic use, highly hydrophilic and helpful for hydrophobic but not lipophilic drugs (77).

Table 2.24: Lipid Formulation Classification System (Poulton 2006) (32,77,78)

Formulation Emulsions	Type I Non-dispersing	Type II SEDDS	Type IIIA SMEDDS	Type IIIB SNEDDS	Type IV Micelles	Ref
Composition	Oil without surfactant	Oil, water-insoluble surfactant	Oil, water-soluble/ insoluble surfactants; cosolvents	Oil, water-soluble/ insoluble surfactants, cosolvents	Contains no oil Water-soluble surfactants and cosolvents	(32,77,78)
Hydrophilicity	drug solubilised in triglycerides and mixed glycerides.	Drug solubilised in triglycerides and mixed glycerides; blended with non-ionic surfactants	drug solubilised in triglycerides and mixed glycerides, blended with non-ionic surfactants and co-solvents.	forms colloidal solutions of drug and oil in aqueous micelles	Synthetic lipid formulations have the highest hydrophilicity	
Solubility of components	Water-insoluble components	Water-insoluble components	Water-soluble components	Water-soluble components	Water-soluble components	
% Triglycerides /mixed glycerides	100% oil content	40 to 80 High oil content	40 to 80 High oil content	<20 Low oil content	0% oil content	(32,34,77)
% Surfactants	-	20 to 60 (HLB <12)	20 to 40 (HLB >12)	20 to 50 (HLB >12)	0 to 20 (HLB <12) 20 to 80 (HLB >12)	(32,34)
% Hydrophilic cosolvents	-	-	0 to 40	20 to 50	0 to 80	(32,34,77)
Digestibility significance	Crucial requirement	Not crucial but is likely to occur Digestible	Not crucial but may be inhibited Digestion not necessary	Not required and not likely to occur	Digestion limited	(32,78)

Formulation Emulsions	Type I Non-dispersing	Type II SEDDS	Type IIIA SMEDDS	Type IIIB SNEDDS	Type IV Micelles	Ref
	Requires digestion			Digestion not necessary		
Aqueous dilution and significance	Importance limited; poor solvent capacity unless the drug is highly lipophilic	Solvent capacity unaffected	Loss of solvent capacity	Loss of solvent capacity/ significant phase changes High drug precipitation risk.	Significant phase changes and potential loss of solvent capacity	(32,34)

Determine the pKa value and state of the ionization state of the drug. Ionised drugs do not absorb as well as ionized drugs; absorption depends on the surrounding pH and pKa value. CBD has a charge of 0.

2.10.5. The Biopharmaceutical Classification System

The Biopharmaceutical Classification System (BCS) allows safe scale-up and post-approval adjustments to oral medicinal products at low cost. The BCS postulates that solubility, dissolution, and intestinal permeability determine the rate and extent of absorption from solid oral dose forms (Table 2.24). Drugs in solution or suspension dissolve and absorb faster than solid dose forms. BCS recommendations are from the USFDA, WHO, EMEA, and the International Council for Harmonisation (ICH) (31,91).

Table 2.25: The Biopharmaceutics Classification System (23,79)

Class I	High Solubility High Permeability	Compounds are adequately absorbed, with absorption rates higher than that of excretion.
Class II	Low Solubility High Permeability	The solvation rate limits bioavailability. In vitro solvation correlates with in vivo bioavailability.
Class III	High Solubility Low Permeability	The drug is rapidly solvated, but the permeation rate limits absorption. No formulation permeability or GI transit time change means a class I criteria apply.
Class IV	Low Solubility Low Permeability	The intestinal mucosa absorbs compounds poorly, with poor bioavailability and likely variability.

Equation 2.4: BCS principle **(23)**:

$J = PwCw$

J = flux across the gut wall

Pw = permeability of the gut wall to the drug

Cw= = concentration at the gut wall

In similar formulations, drug substance(s) tested against reference products are bioequivalent when two orally administered drug substances with identical concentration profiles have the same plasma report or if the drug falls under BCS Class 1. BCS-based

biowaivers (dissolution data) can replace in vivo bioequivalence (AUC and C_{max}) tests to evaluate the degree and rate of drug absorption in systemically acting oral immediate-release (IR) products.

Solubility is when the quantity of substance dissolved is at equilibrium with the excess (undissolved) substance at a specified temperature and pressure. An API is highly soluble when the formulation's highest dose or strength is soluble in ≤250 ml of an aqueous medium over the specific pH ranges of 1-7.5 (USFDA), 1.2-6.8 (WHO) and 1-6.8 (EMEA) at 37 ± 1°C (23). Drug concentration in selected buffers or pH conditions should be assessed with validated solubility indicators to distinguish drug substances from their degradation products (63). Do any minimum of three replicate solubility determinations in at least three pharmacopeial grade buffers (pH 1.2, 4.5, 6.8) and at the pKa. Confirm the pH of a solution before and after adding the drug to a buffer (23).

2.10.6. Permeability

In a stable gastrointestinal tract, a drug substance is highly permeable when the rate or extent of absorption is ≥90% (USFDA guidelines) or ≥85% (WHO, EMEA and ICH BCS guidance) of an administered dose in comparison with an intravenous reference dose or the mass balance determination. Drugs with linear and complete absorption are highly permeable (EMEA BCS guidance) (89).

Polar surface area (PSA) is a metric that optimizes a drug's ability to permeate cells. A molecule's topological polar surface area (TPSA) is the surface sum of all polar atoms or molecules, primarily oxygen and nitrogen, including their attached hydrogen atoms.

Table 2.26: Topological Polar Surface Area (TPSA)

TPSA	Permeability
PSA ≥40 angstroms squared	Molecules permeate cell membranes poorly.
PSA ≤90 angstroms squared	Molecules penetrate the BBB and bind to CNS receptors.

2.10.7. Dissolution determination

A Biowaiver is an application to the regulatory authorities requesting exemption from performing expensive, time-consuming bioavailability (BA) and bioequivalence BE studies to approve dossier applications for registration. The BCS provides biowaivers for Class I, II and III drugs for pre- and post-approval phases and only applies to immediate-release solid oral dosage formulations containing one or more API(s). The submitted pharmaceutical product vs. the comparator product should be similar, and the biowaiver must show proof of equivalence other than through in vivo equivalence testing. Multisource products can dissolve rapidly or very rapidly if ≥85% of the labelled amount of drug substance dissolves in a specified time as defined by the USFDA, WHO or EMEA dissolution guidelines (23).

2.10.7.1. Class I drugs

Class 1 drugs are immediate-release drugs eligible for biowaivers because they are highly soluble and permeable with rapid dissolution in the three recommended dissolution media, and two drug substances typically have similar dissolution profiles when using the similarity factor ($f2: 50$) (90). Class 1 drugs are highly soluble, highly permeable, and are not rate-limiting steps for drug absorption. Very rapid dissolution makes gastric emptying the rate-determining step; however, to mitigate this effect, Class 1 drug release can be modulated with controlled-release technology (23).

2.10.7.2. Class II drugs

Except at extremely high dosages, solubility determines class II drug absorption and bioavailability. Unionised class II pharmaceuticals are weakly soluble weak acids (pKa $f \leq 4.5$) with an inherent 0.01 mg/ml solubility. Class II drugs take longer to absorb orally than Class I drugs. The stomach continues to the small intestine, which has three parts: the duodenum, jejunum, and ileum. Class II drugs are poorly soluble in stomach pH and sport a residence time of 3 hours in the fasted state. Transit time in the small intestine is longer, allowing these drugs sufficient time to dissolve. Class II drug solubility in the jejunum, >1 mg ml, is quick and dependable in fasting. Eligible for a biowaiver provided the drugs rapidly dissolve at typical pH values of the small intestine (23).

2.10.7.3. Class III drugs

Class III drugs rapidly dissolve under all physiological pH conditions, making them behave like oral solutions in vivo. Despite rapid dissolution, absorption varies significantly because of membrane permeability and altered physiology instead of dosage form factors. In Class III drug absorption, gut wall permeability forms the rate-determining step, not drug solubility, and justifies the eligibility for a biowaiver (91). Class III drugs exhibit site-dependent absorption, making transit time through specific regions of the upper intestine critical for BE.

2.10.7.4. Class IV drugs

Class IV drugs seldom reach the market due to oral administration and absorption problems. Not eligible for biowaivers (23).

2.10.8. Lipinski's rule of 5 (Ro5)

Lipinski's rule of five (Ro5) helps determine a chemical's potential bioactivity and physicochemical suitability for oral bioavailability. Ro5 pertains to compounds, not active transporter substrates, even though all drugs are substrates for at least one transporter. Ro5 predicts the drug ability of prospective drug molecules based on pharmacokinetic parameters (absorption, distribution, metabolism, and excretion) but cannot discriminate non-drugs from therapeutically valuable drugs.

All Ro5 factors are multiples of 5. Ro5 predicts poor absorption or penetration in molecules with more than 5 H-bond donors, 10 H-bond acceptors, a molecular weight of 500 Da, and a computed LogP (CLogP) of 5.

New molecular entities (NMEs) are frequently large-molecular-weight, lipophilic, poorly water-soluble, BCS Class 2 drugs outside the Ro5 parameters. A breach of two or more conditions predicts a non-orally available drug molecule with poor solubility and permeability.

2.10.9. Biopharmaceutics Drug Disposition Classification System

The Biopharmaceutics Drug Disposition Classification System (BDDCS) cannot replace Lipinski's Ro5 but extends the BCS predictions of drug character and potential drug-drug interactions for enzymatic and transporter drug activity. BCS Class 1 and 2 drugs clear the body via metabolic processes, while most BCS Class 3 and 4 elimination occurs via bile and urine (17) (80).

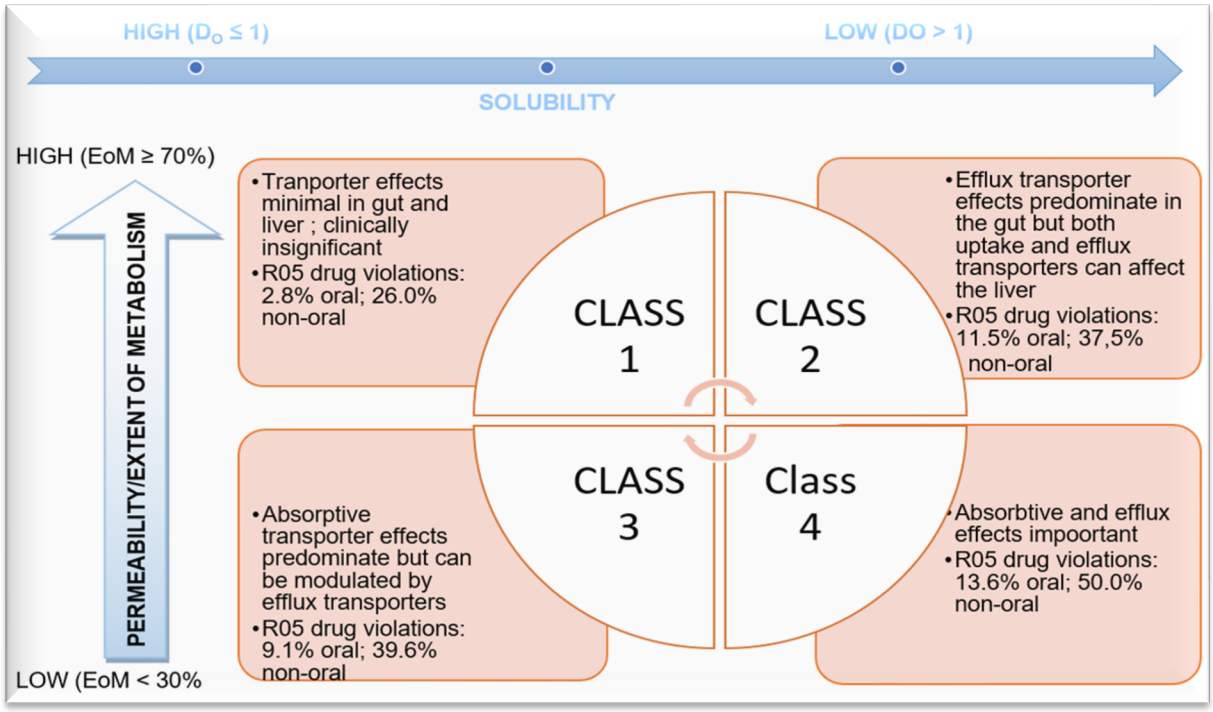

Figure 2.8: Biopharmaceutics Drug Disposition Classification System (BDDCS)

CHAPTER 3
THE DEVELOPMENT AND CHARACTERIZATION OF A CBD NANOFORMULATION FOR PAIN MANAGEMENT

3.1. Introduction

This experiment aims to formulate a stable LBDDS capable of carrying CBD to its target receptors, CB1 and CB2 of the CNS (brain and spinal cord) and the PNS (immune cells), to induce inflammatory and analgesic antinociception. The LBDDS should increase the bioavailability and therapeutic efficiency of the poorly soluble lipophilic CBD molecule by increasing absorption across the GIT enterocytes via the lymphatic system into the systemic circulation, evading renal and hepatic metabolism, RES, MPS and opsonin elimination, then diffuse through the BBB to its target receptors.

Solubility, dissolution, and permeability are criteria for the systemic absorption, bioavailability, and therapeutic efficacy of poorly soluble drugs. Drugs entrapped in ASD matrices are more soluble than their equivalent crystalline form at equilibrium and do not affect membrane permeability, unlike other formulation methods that cannot enhance solubility without reducing permeability (59).
Organic polymers like lecithin form ASDs; the amorphous polymer forms a chain network, and solute molecules plasticize the polymer, reducing its glass transition temperature.

The hot melt extrusion process is suitable for ASD preparations, providing a promising alternative for solvent processes, transforming the physical state of crystallized drugs into an amorphous form, and dispersing drugs in a matrix down to the molecular level (89). The Hot Melt Extrusion method synthesizes solid and semi-solid preparations for oral, parenteral and topical applications and sustained or controlled-release dosage forms like reservoir systems, using excipients of different particle sizes, amorphous solids, or other polymorphic forms of the same product. Extrusion technology can layer drugs in dosage delivery systems with precision down to the micrometre. The polymer's processing conditions determine device design and have a bearing on its crystallinity, morphology, microporous structure, and polymeric chain orientation. Temperature-sensitive drugs can be processed successfully, and exposure to oxygen is limited as the residence time is

short compared to processes like sterilization. Alternate preparation techniques include fusion, solvent, and supercritical fluidization (89).

X-ray diffraction and DSC reveal excipient matrix polymorphism. Polymorphic alterations in the excipient matrix may lengthen solidification time, affecting capsule filling and handling during production and causing non-uniformity of the solidified formulation matrix, which might vary the product release profile, especially with age. Before encapsulation, excipients should be heated at 20°C above their melting point and adequately combined to reduce matrix polymorphism. Heat breaks prefabricated crystalline structures and homogeneously disperses the many components of these excipients. Consistent alteration of the molten material will solidify to give a uniform, predictable drug release profile (33).

Ethyl acetate (cosolvent) dissolves significant amounts of hydrophilic and hydrophobic drugs, increasing solubilization, solvent capacity, dispersion, and surfactant removal. Co-solvent evaporation and aqueous dilution in liposomal formulations can precipitate CBD inside capsule shells during drying or filling (45)(1)(48).

Safe, stable, and efficient CBD-LBDDS formulations require homogenous, monodisperse, size-specific nanoparticles. Particle size affects the bio-distribution, cellular uptake, drug release, encapsulation efficiency, mucoadhesion, and stability of LBDDS. Therapeutic nanoliposomes (50–100 nm) avoid renal, hepatic, and MPS clearance, prolong blood circulation and facilitate passive BBB transport. Therefore, the LBDDS must be formulated as SMEDDS or SNEDDS with monodispersed particles less than 100 nm to facilitate passage through the BBB to interact at the brain and spinal cord CB1 and CB2 receptor sites.

In addition to the HLB, oil ratios, surfactant quantities and the percentage of CBD required for the formulation preparation (Tables 21-23), lecithin and coconut oil required mass calculation because these ingredients are semi-solid at room temperature.

As calculated by the HLB system, various formulations of LBDDS prepared confirmed the quantities of each surfactant/emulsifying agent required to produce emulsions with droplets in the range of nanospheres, i.e., ≤100 μm. The in-process controls monitored were temperature and time during formulation preparation. Zeta potential, particle size and polydispersity index assessed the formulation efficiency of the colloidal dispersion and stability of the o/w emulsions. The phase behaviour of the oil/water emulsions monitored over 30 minutes visually confirmed the stability of the mixtures - only the two optimal formulations selected were further characterized and compared.

The nature and ratios of the oils, surfactants and co-solvents used during their LBDDS preparation and size reduction techniques like extrusion, sonication, homogenization, and freeze-thawing can manipulate particle size and size distribution (31).

3.2. Materials and Method for Formulating the CBD-LBDDS

3.2.1. Materials for the CBD - LBDDS Preparation

Cannabidiol (CBD), Ethyl Acetate, Lecithin, Span 80, Tween 20 and BP grade Castor oil, Coconut oil, and Olive oil were manufactured by Sigma-Aldrich, St. Louis, MO, USA, and supplied by the University of the Witwatersrand. Consumables included disposable cuvettes, 0.22 μm filters, Petri dishes, polytops, spatula and syringes.

3.2.2. Method of CBD - LBDDS Preparation

Analytical characterization of M4 and M13 CQA established the suitability of these formulations for transporting the CBD molecule, boosting solubility and bioavailability, and targeting the CBD action site. A blank sample and three validation batches of M4 and M13 were prepared according to the formulations (Tables 3.1 and 3.2) by the hot melt emulsification method, where melting disperses, disrupts, and crystallizes particles in a continuous liquid phase (81). In a 40°C water bath, steps 1 and 2 were prepared separately in scintillation tubes and gently swirled with a magnetic stirrer at 4 rpm until homogenous solutions formed. Steps 1 and 2 were combined and stirred until homogenous. CBD powder (step 3) was added and stirred till homogenous. This pre-concentrate emulsified spontaneously into an o/w emulsion on gentle agitation in the

aqueous phase. Upon lyophilisation, the PNL was transformed into an amorphous solid organogel, then encapsulated for oral administration in a hard HPMC capsule.

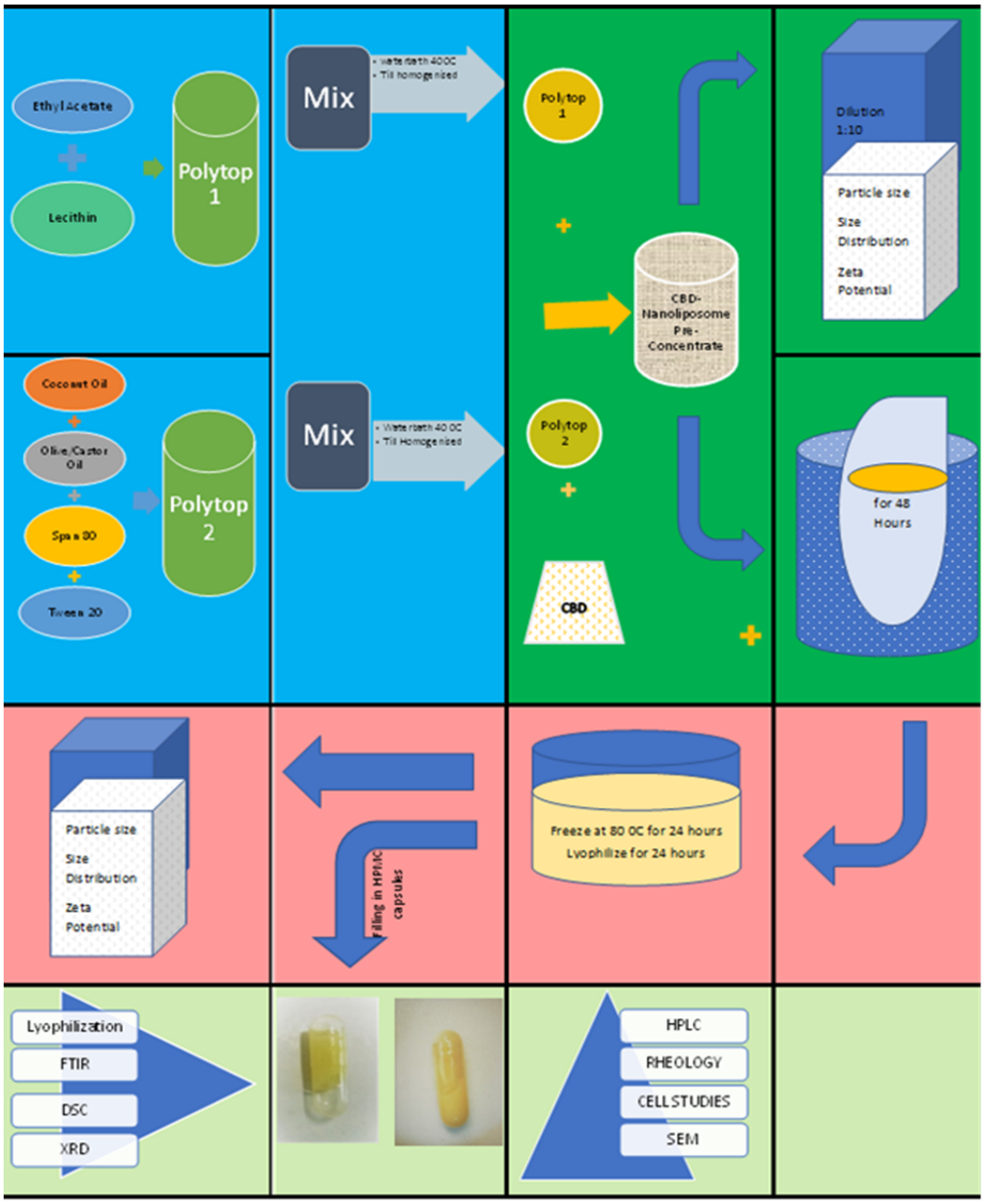

Figure 3.1: Schematic of the Preparation of the Oral Nanoliposome Dosage Form

3.2.3. FORMULATIONS

Table 3.1: Formulation 4

Method 4					Trial 1	Trial 2		Trial 3	Trial 4			
Step	CAS-No.	Ingredients	Ratio	Qty	Qty	Blank	Qty	Qty	Blank	V1	V2	V3
1	141-78-6	Ethyl Acetate	8	8,0 ml	8,0 ml	8,0 ml	8,0 ml	8,0 ml	8,0 ml	8,0 ml	8,0 ml	8,0 ml
	8002-43-5	Lecithin	1	1,03 g	1,0345 g	1,0330 g	1,0385 g	1,0353 g	1,0330 g	1,0305 g	1,0320 g	1,0335 g
2	621-71-6	Coconut oil	1	0,98 g	0,9849 g	0,9826 g	0,9877 g	0,9852 g	0,9853 g	0,9852 g	0,9809 g	0,9848 g
	8001-25-0	Olive oil	1	1,0 ml	1,0 ml	1,0 ml	1,0 ml	1,0 ml	1,0 ml	1,0 ml	1,0 ml	1,0 ml
	9005-64-5	Span 80	1	1,2 ml	1,2 ml	1,2 ml	1,2 ml	1,2 ml	1,2 ml	1,2 ml	1,2 ml	1,2 ml
	1338-43-8	Tween 20	1	0,8 ml	0,8 ml	0,8 ml	0,8 ml	0,8 ml	0,8 ml	0,8 ml	0,8 ml	0,8 ml
3	13956-29-1	CBD	0,37%	48,0 mg	48,6 mg	-	48,1 mg	48,4 mg	-	48,3 mg	48,6 mg	48,5 mg

Table 3.2: Formulation 13

Method 13:					Trial 1				
Step	CAS-No.	Ingredients	Ratio	Qty	Blank	V1	V2	V3	Function
1	141-78-6	Ethyl Acetate	8	8 ml	8,0 ml	8,0 ml	8,0 ml	8,0 ml	Solvent
	8002-43-5	Lecithin	1	1,03 g	1,0322 g	1,0377 g	1,0379 g	1,0369 g	Emulsifier
2	621-71-6	Coconut oil	1	0,98 g	0,9846 g	0,9848 g	0,9847 g	0,9815 g	Solubilizer
	8001-79-4	Castor oil	1	1,0 ml	1,0 ml	1,0 ml	1,0 ml	1,0 ml	Solubilizer
	9005-64-5	Span 80	1	0,5 ml	0,5 ml	0,5 ml	0,5 ml	0,5 ml	Liposoluble surfactant
	1338-43-8	Tween 20	1	1,5 ml	1,5 ml	1,5 ml	1,5 ml	1,5 ml	Liposoluble surfactant
3	13956-29-1	CBD	0,37%	48,0 mg	-	48,6 mg	48,1 mg	48,6 mg	Active Ingredient

Table 3.3: Calculation: HLB Formulation 4

No.	Method 4	Ratio	Fraction		% Oil	HLB Oil	HLB required: Surfactant blend	% Surfactant/ emulsifier	HLB Surfactant	HLB: Surfactant blend	Qty
1	Ethyl Acetate	8	8/13	61,5%							
	Lecithin	1	1/13	7,7%				33,33%	7	2,331	1ml
2	Coconut oil	1	1/13	7,7%	50%	8	4				
	Olive oil	1	1/13	7,7%	50%	7	3,5				
	Span 80	1	1/13	7,7%				40%	4	1,6	1,2 ml
	Tween 20	1	1/13	7,7%				26,67%	17	4,53	0,8 ml
3		13	13/13	100%	100%		7,5	100%		8,46	3 ml
Required HLB for surfactant blend Range:							6,5 – 8,5				

Table 3.4: Calculation: HLB Formulation 13

No	Method 13	Ratio	Fraction		% Oil	HLB Oil	HLB required: Surfactant blend	% Surfactant/ emulsifier	HLB Surfactant	HLB: Surfactant blend	Qty
	Ethyl Acetate	8	8/13	61,5%							
	Lecithin	1	1/13	7,7%				33,33%	7	2.331	1 ml
	Coconut oil	1	1/13	7,7%	50%	8	4				
	Castor oil	1	1/13	7,7%	50%	14	7				
	Span 80	1	1/13	7,7%				16,67%	4	0,667	0,5 ml
	Tween 20	1	1/13	7,7%				50%	17	8.5	1,5 ml
TOTALS		13	13/13	100%	100%		11	100%		11,5	3 ml
Required HLB for surfactant blend Range:							10 – 12				

Table 3.5: Miscellaneous Calculations

No.	Calculation	Formula	Calculation
1	Conversions	Mass = Volume x Density	Lecithin:1ml x 1.03 = 1.03 g Coconut oil: 1.0ml x 0.98 = 0.98 g
2	Concentration (CBD) 0.37% of the total volume(ml) of formula 1 and 2	3.7/100 x total volume	CBD: Mass=Volume from below (4) x Density (1.04)
3	The concentration of Mannitol (15%)		

3.2.4. Calculation of Encapsulation efficiency and drug loading capacity of the Lipid-Based Drug Delivery System

Encapsulation efficacy, an essential parameter in liposome analysis, reflects the concentration of the drug in the liposome. Encapsulation efficiency is the percentage of the drug successfully entrapped into the liposome.

Equation 5: Encapsulation efficiency (EE%)

$$EE\% = \frac{(Total\ drug\ added - \ free\ non - entrapped\ drug\ in\ supernatant)}{Total\ drug\ added}$$

Loading capacity is the amount of drug loaded per unit weight of the nanoparticle, indicating the percentage of the mass of the nanoparticle due to the encapsulated drug.

Equation 6: Loading capacity ($LC\%$)

$$LC\% = \frac{the\ amount\ of\ total\ entrapped\ drug}{total\ nanoparticle\ weight}$$

Yield, expressed as a percentage, reflects the quantity of free drug relative to the quantity encapsulated. A quick and accurate approach for determining drug concentrations in $EE\%$ is high-performance liquid chromatography (HPLC).

As per the formulation (Tables 3.1 and 3.2), 48 mg of CBD was loaded into 13 ml of excipients in the CBD Preconcentrate.

48 mg =0,048 g, therefore

0,048 g of CBD X 100

13 ml Excipient

= 0,37% of CBD

3.2.5. Characterisation of LBDDS

3.2.5.1 Particle Size, Polydispersity and Zeta Potential

1:10 dilutions of PNL pre-concentrate in distilled water (37°C) were vortexed for 3 minutes, then filtered three times using a 0.22µm filter to remove big colloid particles and contaminants. The sample dilutions of formulations M4 and M13 loaded in disposable cuvettes (DTS 1070) were analysed by Dynamic light scattering (DLS) experiments (Zeta-sizer (NanoZS, Malvern Panalytical, Malvern, UK), measured before and after lyophilization at 25°C for particle size, Pdi, and zeta potential.

The energy for particle size reduction and homogenisation supplied by a bar sonicator (Sonics Vibra Cell, Newtown, Newtown, CT, USA) was applied to the sample sizes for 10 minutes at 60 mV, pulsing for 50 seconds at 10-second intervals.

The primary stages of liposome preparation involve evaporating the organic solvent from the lipid mixture, then optimally diluting and dispersing the residue in aqueous media before purifying the resultant liposome and analyzing the final product. Liposome drug loading can be active or passive. Passive loading techniques include mechanical or solvent dispersion or detergent removal (removal of nonencapsulated material). Mechanical methods include sonication, French pressure cell extrusion and the freeze-thawing of liposomes, and lipid film hydration by hand or non-hand shaking or freeze drying: micro-emulsification, membrane extrusion, and dried reconstituted vesicles.

Sonicating MLVs with a bath or a probe sonicator under a passive atmosphere produces SUVs. Probe sonication immerses the sonicator's tip directly into the liposome dispersion; this high-energy input method imparts local heat at the tip, necessitating the immersion of the vessel in a water/ice bath. However, sonication yields a polydispersion of MLVs and SUVs, degrading phospholipids, encapsulated compounds, large molecules and de-esterifying lipids. Moreover, the method has very low encapsulation efficacy and introduces metal pollution from the probe tip as the titanium sloughs off. Alternatively, the temperature control of liposome dispersions placed into a bath sonicator is more manageable than probe sonication, and the sonicated material can be protected in a sterile vessel, dissimilar to probe units, or under an inert

atmosphere (41). Particle size, Pdi, and zeta potential of sample formulations M4 and M13 loaded in disposable cuvettes (DTS 1070) were determined before and after lyophilization at 25°C. Dynamic light scattering (DLS) tests (Zeta-sizer (NanoZS, Malvern Panalytical, Malvern, UK) evaluated average particle size, polydispersity index Pdi, and zeta potential.

3.2.5.2 Sterilization, Dialysis and Lyophilization of the Nano-emulsions

Validated M4 and M13 samples in a SnakeSkin™, 3500 MWCO dialysis membrane were submerged in 250 ml distilled water in glass beakers for 48 hours. Afterwards, samples transferred from the dialysis tubes to Petri dishes containing 5 ml of mannitol (15%) were gently agitated to facilitate mixing. The Petri dishes froze at -80°C for 24 hours in preparation for lyophilization before being placed in the lyophilization machine to freeze-dry for over 24 hours.

3.2.5.3 Fourier Transform Infrared Spectroscopy (FTIR)

FTIR spectroscopy (Nicolet Impact 400 D FT-IR Spectrometer, ThermoFisher Scientific, Germany) identified the molecular functional groups and chemical bonds (molecular fingerprint) present in formulations M4 and M13 at FTIR settings 500-4000 cm^{-1} at 20°C and 120 psi, in comparison with those of CBD, Lecithin and MM nanoformulations.

3.2.5.4 Differential Scanning Calorimetry Thermal Analysis (DSC)

Liposomal preparation's phase transformation processes can either be endothermic (energy required) or exothermic (energy produced). Differential scanning calorimetry (DSC), a thermal technique that assesses the transition of one lipid phase to another, determined LBDDS' thermal behaviour. Place approximately 10 mg of lyophilized PNL pre-concentrate in aluminium crucible pans, seal the lid and perforate it. Position the crucibles containing the samples in the sampling tray. Purge the samples with nitrogen. Switch on the nitrogen tank, set the barometer to 90-100 Kpa, and turn the valve setting on the tank to 200 to release the gas. Run the samples. Set the DSC temperature range to 0-300°C and scan the sample at an increasing heating rate of 10°C/min. The lipid transition temperature of soy lecithin is -20°C to -30°C.

3.2.5.5 X-Ray Diffraction (XRD)

X-ray diffraction (XRD RIGAKU MiniFlex, RIGAKU Inc., Tokyo, Japan) determined M4 and M13's crystalline fingerprints by assessing the lipid phase's structure. Analytical conditions settings were 2θ with a range of 5°–90°, scan rate 10 deg/min, current 15 mA, voltage 40 kV and temperature 20°C.

3.2.5.6 Scanning Electron Microscopy (SEM)

SEM (ZEISS Electron Microscopy, Carl Zeiss Microscopy Ltd., Cambridge, UK) examined M4 and M13 sample morphology from low (200 X) to high (80.00 KX) magnification. An aliquot was applied to the aluminium specimen stub and dried thoroughly in a laminar flow hood before adding a conductive double coating of gold to generate anodic positive charges, enabling electrons to flow across the sample's surface. The tungsten filament of the SEM provides the source of the electron beam.

3.2.5.7 Rheology

The yield stress and viscosity of formulations M4 and M13 and their corresponding blanks, analysed with a viscometer (Anton Paar Rheolab QC rotational viscometer), recorded rheograms showing the effects of shear stress versus shear rate. Shear rate settings ranged between 5 s^{-1} and 200 s^{-1} at 20°C.

3.3. Results and Discussions

The delivery system's chemical, physical, and mechanical robustness are analysed and assessed to determine whether the formulation falls within the acceptable parameters suggested by the predictor systems. The results include DLS (Particle Size Analysis, Particle Size Distribution, Zeta Potential), FTIR Spectroscopy, DSC, SEM, X-Ray Diffraction, and Rheological Analysis.

.

3.3.1. Sterilization and Purification of Liposomes

Sterilization and purification of liposomes are important in liposome production. M4 and M13 emulsions were sterilised through filtration and purified by dialysis.

3.3.1.1 Purification of liposomes

Most lipid excipients are ‘generally recognised as safe’ (GRAS) for human consumption and can be added to foods and beverages without further manipulation. Therefore, the excipients that formulate the CBD pre-concentrates can be loaded in a gel capsule and ingested without further manipulation. CBD, however, has non-GRAS status and must be handled as a controlled substance (82).

Drugs loaded into liposomes have distinct pharmacokinetic characteristics from non-encapsulated drugs. Although purification methods can destabilise emulsions due to the leaching out of essential excipients, purification is vital for the quality control of liposomal products, as it separates and removes organic solvents and surfactants/detergents from the pre-nanoliposome concentrate used during the preparation process in addition to nonencapsulated drugs. Well-defined liposome preparations should use well-characterized lipids and avoid using organic solvents and detergents, which are difficult to remove.

Methods for liposome purification include dialysis, column chromatographic separation, centrifugation, protamine aggregation, ion exchange, resin, and ultrafiltration. Suitable purification methods are chosen based on the characteristics of every liposome, and the separation condition should be optimised.

3.3.1.2 Sterilization of liposomes

Sterilization is a validated process of delivering a product free of viable microorganisms without altering its properties, and this is a mandatory step in liposomal formulations intended for parenteral administration. However, liposomes are susceptible to physicochemical degradations, which induce physicochemical alterations such as phospholipid oxidation and hydrolysis, vesicle aggregation, phase transition, degradation, leakage and change in encapsulated drug release. Unlike ethylene oxide, a flammable, explosive gas that leaves hazardous residues, super critical carbon dioxide ($ScCO_2$) offers an ecologically safe, non-flammable, non-toxic option for sterilising temperature-sensitive liposomes. $ScCO_2$, which is already a component of liposome manufacturing, may sterilize the liposome product in a single step, enabling the creation of liposomes with acceptable properties that meet the SAL

requirements for pharmaceuticals. Alternately, $ScCO_2$ can sterilize liposomes created by other traditional ways if the operating circumstances preserve the liposomes' properties and reach the SAL necessary for medicinal applications.

0.22 μm membrane filters sterilised M4 and M13 pre-nanoliposome (PNL) concentrates and nano-emulsions. Conventional sterilization techniques (except filtration) use chemicals, dry heat sterilization, ethylene oxide, final steam sterilization, gamma irradiation, heat, radiation and ultraviolet, none suitable for liposomes as it may affect their stability (Table 3.6) (40,83). Terminal sterilization in primary packaging is superior to aseptic methods; however, it chemically and physically degrades liposomes sensitive to heat, radiation, and chemicals. Filtration of thermolabile liposomes with high pressure (≥25 kg/cm^2) equipment is expensive and time-consuming. However, it does not expose liposomes to conditions that degrade or cause leakage of encapsulated materials. Polycarbonate membranes are less efficient than hydrophobic Fluoropore membranes and cellulose acetate/surfactant-free membrane filters (92).

Table 3.6: Sterilization of Lipid-Based Drug Delivery Systems (83)

Method	Advantage	Disadvantage	Convenience
Dry Heat	Cost-effective	Liposome degradation risk	High
Ethylene Oxide	Low temperature	Possible carcinogenic residues	Low
Filtration	Low temperature	For liposomes ≤ 200 nm Requires aseptic conditions	Low
Final steam sterilization	Cost-effective	Liposome degradation risk	High
Irradiation	Maximum microbial death; Medium temperature	Liposome degradation risk Large scale action	High
UV Sterilization	Cost-effective	Liposome degradation risk Weak penetration into the product	High

Aseptic manufacturing and filtration offer a viable but expensive alternative to conventional sterilization techniques; however, aseptic production cannot assess sterility assurance levels (SAL). Sterilizing liposomes through a 0.22 μm membrane filter is unsuitable for liposomes ≥0.2

μm as it does not purge bacteria and viruses smaller than 200 nm. An option is to filter the initial solutions through 0.45 μm regenerated cellulose and glass fibre filters before aseptic production (50).

3.3.2. Dialysis of Nano-emulsions

Size differentiates liposomes from the non-encapsulated material when purifying by dialysis. Purifying formulations M4 and M13 by dialysis removed residual solvents like ethyl acetate, surfactant, and impurities from the emulsions. Phospholipids combined with surfactants interact with the aqueous phase to produce mixed micelles. Dialysis extracts surfactant from the mixed micelles, spontaneously forming unilamellar liposomes. This technique is unsuitable for water-soluble drugs because the removal of small water-soluble molecules is unavoidable.

Surfactant solubilization enables manipulating liposome sizes through precision control of surfactant addition and removal to obtain highly homogenous liposomes. Hydrophobic drugs solubilize in the hydrophobic phospholipid bilayer. During liposome preparation, hydrophobic drugs like CBD and lecithin phospholipids solubilize in the organic solvent (ethyl acetate). Hydrophobic molecules poorly attract to the liposomes' inner or outer aqueous regions and prefer lodging in the liposome bilayer's hydrophobic region during hydration. After membrane formation, liposome encapsulation of lipid-soluble drugs can attain up to 90% efficiency (83).

Osmotic shrinkage of steroid-stabilised liposome (SSLs) surfaces occurs in two stages, i.e. the initial liposome size decreases with the outflow of water through the bilayer, decreasing the lipid area, followed by the spherical to lens-shaped deformation of liposomes. The polymer layer of SSLs seals areas susceptible to water permeation. Phospholipid bilayers containing saturated fatty acids are less permeable than unsaturated fatty acids. Cholesterol and PEG integrated into the lipid bilayer reduce water permeability and, thus, the osmotic shrinkage of liposomes (94). When molecules and impurities in aqueous media are impermeable across the membrane (e.g., sugar molecules or large ions), a net water transfer generates an osmotic pressure that cannot counterbalance the additional bending of the membrane. Thus, the internal vesicle volume will remain steady, with no osmotic pressure build-up (57). (72).

3.3.3. Lyophilization

Liposomes are prone to leakage due to physical and chemical instability during long-term storage because of phospholipid hydrolysis or oxidation, liposome aggregation and fusion, and increased bilayer permeability. Preserving the therapeutic functionality, biological activity, and long-term drug stability in encapsulated liposomes is achievable through freeze drying, which usually produces a dry liposome-laden powder with low residual water content (84).

Liposome morphology, examined by TEM, identifies possible fusion and aggregation of liposome particles. Membrane fusion aggregates and increases the size of liposome vesicles as the system attempts to maintain thermodynamic equilibrium, resulting in vesicular fusion, breakage and drug leakage during freeze-drying and reconstitution. Meticulous optimization of liposome composition and drug characteristics can minimise drug leakage. Freeze drying, however, negatively affects liposome structure and function because phospholipid membranes fuse during freezing, drying, rehydration or loss of the encapsulated drug. Adding cryo and lyoprotectants to the outer aqueous phase of liposomal dispersions destined to be freeze-dried improves liposomes' functional properties after freezing and product stability after drying by protecting the membranes' integrity.

Polyhydroxy compounds and carbohydrates, preferable saccharides like trehalose, lactose, glucose, mannitol, sucrose, and maltodextrins, are used as cryo/lyoprotectants during the dehydration/rehydration of liposomes, preserve the physical integrity of liposomes during the freeze-drying process (84).

Saccharides theoretically act via water replacement, vitrification or kosmotropic effects. The water replacement theory asserts that saccharide molecules replace the phospholipid bilayers' bound water molecules by interacting with polar lipid head groups at low hydrations, thus stabilizing the liposome. Hydrogen bonding occurs between the carbohydrates and the hydrophobic moiety's carbonyl, phosphate, and methyl group, replacing hydrogen bonding with water and stabilizing the vesicle structure. Multiple hydrogen bonding of sugars can bridge three phospholipids simultaneously. Sugars increase the distance between phospholipid polar heads, minimizing van der Waals interactions among hydrocarbon chains, preventing T_m increases during dehydration, and decreasing T_m in completely hydrated bilayers. The concomitant

encapsulation of a protectant in the aqueous core of the vesicles reduces the osmotic gradient caused by cryo-concentration, preserving the size (55,84).

According to the vitrification theory, the freezing of sugars results in a viscous, slow-moving, amorphous (vitrified) matrix. This glassy matrix creates distance between adjacent bilayers of entrapped liposomes, reducing liposome mobility, minimising liposome aggregation and fusion, and protecting the bilayer from damage by ice formation during freeze-drying. High quantities of sugars needed for reproducible protective effects affect viscosity and, therefore, the rehydration of the vesicles. Depending on vesicle type and protectant concentration, melting temperatures increase in dispersions with high solute and low water concentrations (55,84). Kosmotropic effects establish that cryoprotectant interaction with water disrupts its structure at the membrane interface, reducing water content and minimising damage during freeze-drying (55,84).

Mannitol, 15% mv, was added to the freeze-dried liposome formulations as a cryoprotectant to protect liposomal membranes from damage by the lyophilization process. Mannitol, crystalline sugar alcohol, localizes in the aqueous core without interacting with the lipid head groups and maintains the integrity of dry solids as scaffold structures, thus preventing micro-collapse. Mannitol forms a relatively high eutectic point with ice. Therefore, liposome formulations can endure a relatively high primary drying temperature and short drying cycle. Mannitol, as a cryoprotectant, crystallizes during freeze-drying. Formulations containing mannitol as a cryoprotectant have crystalline properties, and its crystal formation during drying can rupture the liposome membrane, causing drug retention failure (85). Crystal formation further weakens liposome's protective effects, causing leakage of the encapsulated drug (85,86).

Combining mannitol with another cryoprotectant, such as sucrose and glucose, may assist in this matter. Sucrose or trehalose make for effective lyoprotectants, as their very high viscosity and low molecular mobility create an amorphous, glassy matrix after drying. Sucrose, a polyhydroxy cryoprotectant, never crystallizes when freezing any solution because the interactions between the –OH groups of sugar and water molecules are similar in configuration and energy, leading to very low nucleation probabilities. The stabilization and protective effects of saccharides as cryo/lyoprotectants are concentration-dependent. Liposome size and Pdi in

compositions without saccharides significantly increase after freeze-drying, and insufficient sugar concentrations only partially coat the glassy matrix surrounding nanoparticles, promoting aggregation.

Freeze-dried liposomes containing an 8:1 sugar: lipids, mass ratio, used as a cryo/lyoprotectant form fewer fused or aggregated particles, minimise particle size increases and form stable homogenous populations in liposome formulations. Trehalose and sucrose produce smaller particle sizes at higher concentrations; however, only sucrose at an 8:1 (sugar: lipids) mass ratio allows for a homogeneous suspension, with Pdi around 0.1. Higher sucrose molar ratios produce highly monodispersed nanoparticles using the 8:1 mass ratio. Morphologically, this optimised sugar-lipid ratio has the potential to protect encapsulated drugs and provide controlled drug release as they have minimal contact with the aqueous environment, thus favouring an extended diffusion pathway (84).

The residual water content significantly affects the stability of freeze-dried liposomal formulations in terms of liposome formation and encapsulation efficiency. High levels of residual water can unpredictably dissolve samples immediately after freeze-drying or contribute to poor long-term storage stability of nanoparticles. After freeze-drying, the liposomal formulation must have a water content of <2%. TGA analysis will indicate the total quantity of residual water in liposomes after freeze-drying. A minimal water content proves the efficiency of primary drying, avoiding an additional secondary drying step (84).

Freeze-drying (lyophilization) frozen products must only remove water when drying thermolabile products. Water keeps liposomes round. Lyophilization removes water molecules, shrinking or collapsing the bilayer membrane. The lyoprotective activity of saccharides at below-freezing temperatures protects nanoparticles. Amorphous protectants are ideal because crystalline chemicals disrupt phospholipid bilayers during freezing. Thus, before freeze-drying, all liposomal suspensions must be held in a deep freezer for at least six hours at −80°C (95).

3.3.4. Particle Size; Polydispersity Index (Pdi); Zeta Potential

Dynamic light scattering (DLS) measures particle sizes and the uniformity of the dispersion's distribution. Before DLS analysis, sample dilution can alter the swollen micelles' size, possibly destroying them and invalidating the characterization (45).

The preconcentrates formed using formulation M4 (Table 3.1) produced a yellow oily fluid. The 1:10 dilutions of the pre-concentrate in double distilled water produced a grade B emulsion, which became clear upon homogenization. The particle size distribution ranges from polydisperse bimodal to separated bimodal with an average Pdi of 0.49, an average zeta potential of -18.20 and an average particle size of 86.55 μm, respectively, indicating multiple particle size populations. The average particle size range was less than 100 μm, but the higher values and the emulsion properties were characteristic of SMEDDS.

The preconcentrates formed with formulation M13 (Table 3.1) produced an oily yellow fluid. A grade B emulsion was created by diluting the pre-concentrate 1:10 in double-distilled water; this emulsion turned transparent when homogenized. Particle size distributions were monodisperse with an average Pdi of 0.21, an average zeta potential of -9.63 and an average particle size range of 51.48 μm, characteristic of SNEDDS. Aqueous dilutions of M4 and M13 produced turbid emulsions upon initial mixing, which cleared after shearing them with a probe sonicator, yielding a bluish, opaque grade B emulsion (Table 2.7). Emulsions, categorized by globule size, influence the emulsion's optical rheology and physical and chemical properties. Turbidity, a property linked to droplet size, decreases whether the drops enlarge or shrink (58). Maximum turbidity occurs when the drop size is 2-5 μm. Nanovesicles ≤80 nm barely scatter visible light and remain transparent at low concentrations and when the refractive index and the suspension medium are alike (80).

Emulsions are prepared by high or low-energy methods, depending on the equipment and power needed to produce an emulsion. Particle size influences the rheological, physical, and chemical properties of emulsions. Conventional or macroemulsions (SEDDS) with droplet sizes (100 nm to 100 μm) are thermodynamically unstable and opaque. SMEDDS droplets (5-50 μm) and SNEDDS droplets (20-100 nm) are kinetically stable but thermodynamically unstable (50).

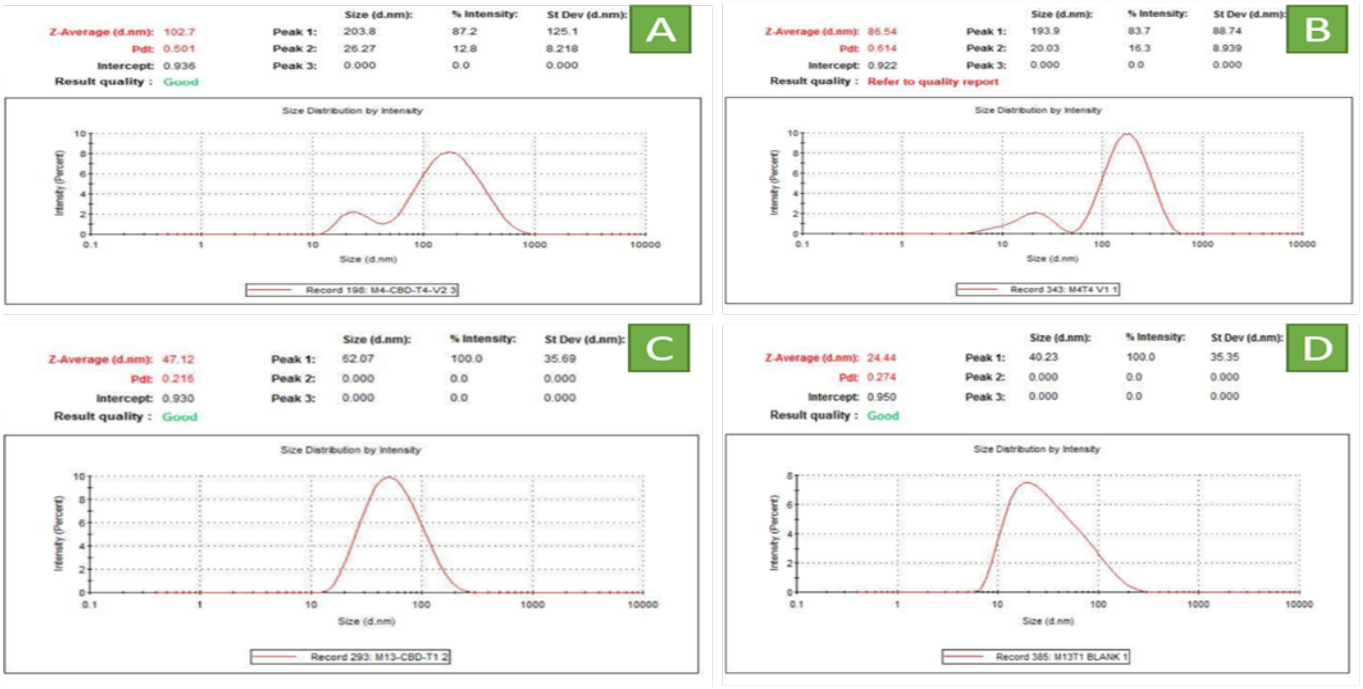

Figure 3.2: DLS results show the particle size and size distribution in 1:10 dilution of pre-concentrate in double-+ water. A) M4 after emulsification and sonication (B) M4 after dialysis and lyophilization (C) M13 after emulsification and sonication (D) M13 after dialysis and lyophilization

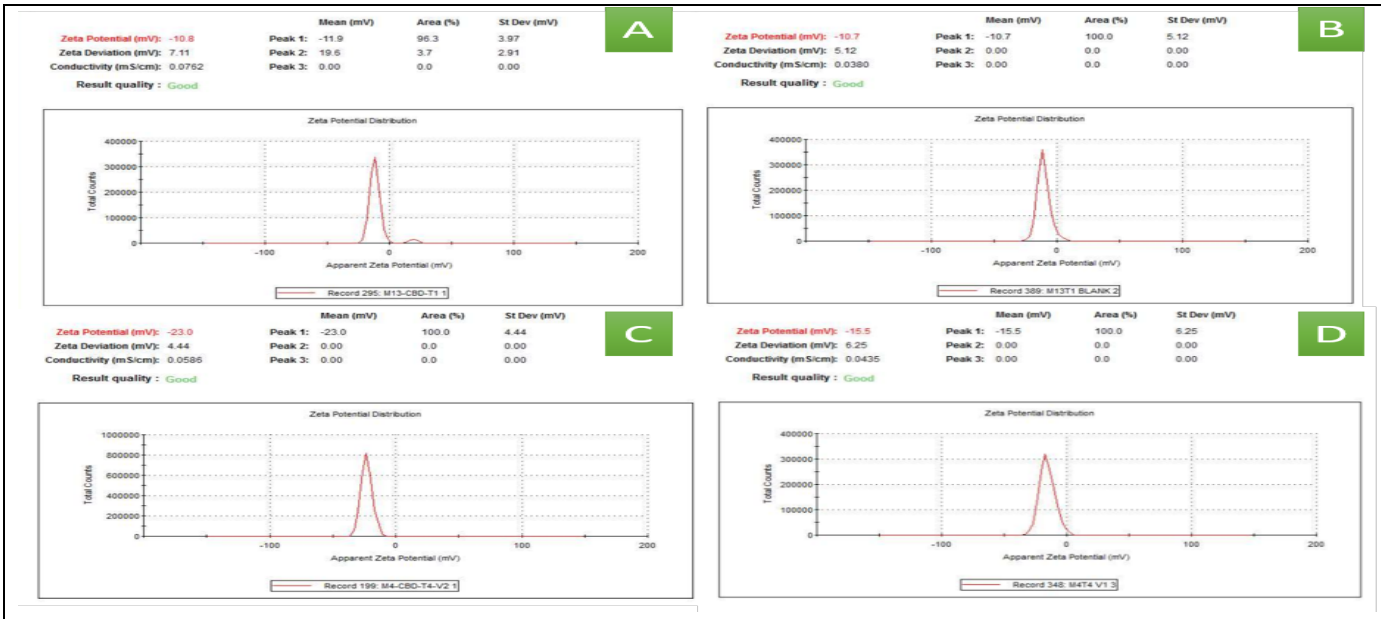

Figure 3.3: DLS results show the zeta potential of the 1:10 dilution of pre-concentrate in double-distilled water. A) M4 after emulsification and sonication (B) M4 after dialysis and lyophilization (C) M13 after emulsification and sonication (D) M13 after dialysis and lyophilization

Table 3.7: Measures of central tendency pre-lyophilization

Parameter	M4				M13			
Central Tendency	Min	Max	Average	Std Dev	Min	Max	Average	Std Dev
Particle Size	55,33	117,7	86,55125	18,04102	40,27	68,16	51,48	12,03585
Pdi	0,334	0,569	0,492083	0,056891	0,189	0,226	0,208667	0,011885
Zeta Potential	-15,3	-23	-18,19583	2,056855	-11,5	-7,03	-9,63444	1,472405

Table 3.8: Measures of central tendency post lyophilization

Formulation	M4				M13			
Central Tendency	Min	Max	Average	Std Dev	Min	Max	Average	Std Dev
Particle Size	55,98	101,7	84,75	16,42679	24,08	39,27	31,258	7,2296
Pdi	0,541	0,641	0,5818	0,0374	0,258	0,319	0,2848	0,02099
Zeta Potential	-11,7	-18,3	-15,83	1,9663	-6,23	-10,70	-8,92	1,4824

\

3.3.4.1 Particle size

The vesicles' size distribution and morphology are critical quality attributes of a liposome vesicle's physical stability during manufacture and storage (12) (28). Particle size variations can result in instabilities like coalescence, flocculation, gravitational separation, Ostwald ripening and phase separation. Nanoparticulate size influences the stability of lipid particulate systems, and Brownian motion prevents lipid nanoparticle sedimentation. Pdi values range from 0,05 (impeccably uniform particles) to 1,0 (diverse particle size populations). Polymer-based nanoparticles have Pdi ≤0.2. Phospholipid vesicles may tolerate Pdi ≥3.

The distribution shape provided data on emulsion formation, changes, and evolution. Particle size distribution, assessed using measures of central tendency, computed the mean as an average, median, or mode. The mode is the most frequently sized particle, whereas the median splits scattered particle sizes into 50% little and 50% big drops. Two modes point to two separate blending processes, while incomplete mixing gives an asymmetrical spread with an elongated tail on the more significant drop size in the log scale. The tapering off the smaller drop size (left part of the principal peak) indicates slow ripening. Increased frequency in the same area suggests impending stability problems (72).

Drugs disperse at the molecular level within the ASD carrier. Micronizing or nanosizing actives or excipients increase the drug's surface area, dissolution rate, and thermodynamic solubility, improving absorption and bioavailability. Nanocrystalline formulations reduce inconsistency and eliminate food effects for orally administered drugs (87).

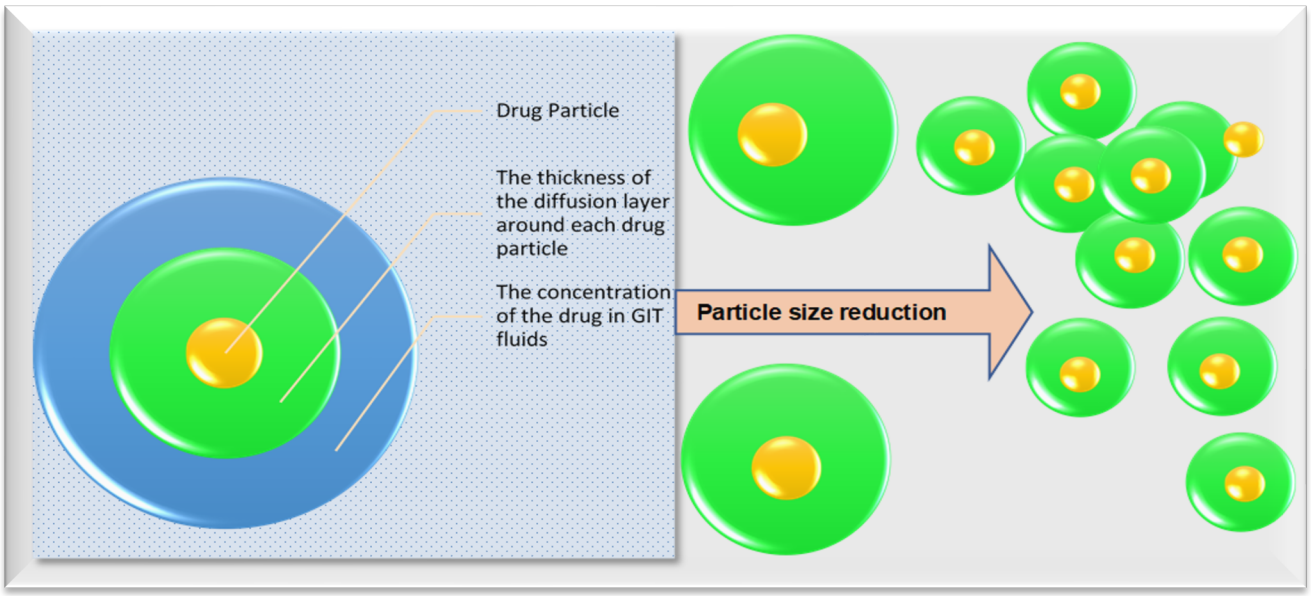

Figure 3.4: Particle size reduction **(88)**

Under sink conditions, the intrinsic dissolution rate is the mass transfer rate per dissolving surface area when the width of the boundary layer remains constant. Intrinsic and extrinsic factors affect the dissolution rate. Intrinsic factors include crystal habit, distribution particle size, and surface area, which are solid-state properties of a pure substance; extrinsic factors include hydrodynamics and test conditions.

The Noyes-Whitney equation describes how smaller particle sizes increase the total effective surface area and, therefore, the dissolution rate.

Equation 3.7: Noyes-Whitney equation **(87)**:

$$\frac{dC}{dt} = \frac{DA(CS - C)}{h}$$

Where:

dC/dt = dissolution rate of the drug particles

D = Diffusion coefficient of the drug in gastric fluid

A = Effective surface area of drug particles in gastric fluid

h = diffusion layer width around each drug particle

CS = Drug saturation solubility in the diffusion layer

C = Concentration of the drug in gastric fluid

The parameters in the equation are constants except for A and C because A increases by decreasing particle size. Reducing the particle size narrows the width of the diffusion layer around drug particles, increasing the concentration gradient and speeding up the dissolution rate (87,88).

3.3.4.2 Polydispersity Index (Pdi)/Uniformity of Particle Size

Polydispersity/heterogeneity index (Pdi) measures the polymer's molecular weight distribution (MWD) width and is a dimensionless number expressing the degree of nonuniformity of sample size distribution. Drop size distribution affects viscosity and stability (82). Moreover, Pdi parameters are described in ISO 13321:1996 E and ISO 22412:2008 but do not provide acceptance criteria for particle size and Pdi, which are critical for evaluating colloidal dosage forms' clinical and storage stability. Nanosystems have a sizeable surface area, so size stability is more crucial for nano than micro-drug delivery systems. Optimum clinical outcomes for nanocarrier formulations need a constant, narrow distribution (31).

Table 3.9: Polydispersity Index (Pdi) (31)

Pdi Values	Size Distribution
0,0	Perfectly uniform particles
<0,05	Highly monodisperse
>0,7	An extensive particle size distribution
1,0	Highly polydisperse, diverse particle sizes
≤ 0,2	Acceptable for polymer-based nanoparticles
≤ 0,3	Acceptable for polymer-based nanoparticles
	Indicates homogenous phospholipid vesicles

3.3.4.3 Zeta potential

SEM images corresponding to the zeta potential in the M4 matrix show less incipient instability than M13 with minimal particle aggregation. M4 has an average zeta potential of -18,19583 (range -15,3 to -23) and a standard deviation of 2,056855.

SEM images corresponding to the zeta potential in the M13 matrix show more incipient instability than M4, with zeta potentials of -9,63444 (range -11,5 to -7,03) and a standard deviation of 1,472405 implying possible coagulation and flocculation.

Zeta potential indexes the extent of repulsive or attractive interactions between neighbouring particles and indicates the stability of colloidal dispersion systems. Each particle in the dispersion acts as a single entity surrounded by an electrical double layer consisting of a stern inner layer with firmly bound ions and a diffuse outer layer (slipping plane). The zeta potential forms an electrical potential at the slipping plane when an increased concentration of oppositely charged ions (counter ions) is attracted to the particles' interfacial surface to create a nett electrical charge (89).

Two approaching interfaces of drops at the sub-micrometre range are subject to repulsive electrical, entropic, or steric forces and attractive static Archimedes or Van der Waals forces (Table 3.10) (97). Repulsive forces must dominate to maintain stability. Attractive forces overcome repulsive forces for small zeta potential values, offering little to no force to prevent the particles from approaching each other and creating dispersion instabilities like particle aggregation, coagulation, and flocculation.

In a colloidal system, dispersed particles can aggregate, increasing size and settling out due to gravity. Flocculation and deflocculation can reversibly form and unform aggregates (FLOC). Coagulation is irreversible and occurs when aggregates become dense. Changing the ion concentration in a system can stabilise or flocculate the system.

Polymer adsorption to the particle surface promotes repulsion by steric stabilization (80,98). Interfacial contact sparks steric and entropic forces that increase depending on the compressibility or elasticity between the particle's adsorbed layers. Conversely, large zeta potential values (negative or positive) stabilize small particles with stronger repulsive forces, creating stable dispersions. The isoelectric point has the least stable zeta potential in the colloidal system (60) (72).

Table 3.10: Zeta potential stability limits (89)

Zeta potential (mV)	Stability behaviour of particles
0 to ±5	Rapid flocculation or coagulation
±10 to ±30	Insipient Instability
±30 to ±40	Moderate stability
±40 to ±60	Good stability
> ±61	Excellent stability

The zeta potential at the o/w interface causes thermodynamic instability and degradation in nanoemulsions. Relative colloidal dispersion stability lies between +30 and -30mV. Particles with more significant negative or positive zeta potentials in the range of ±30mV are stable (90). Suitable emulsifiers that impart a minimum zeta potential of at least 8-9 mV and steric stabilization can prevent high ionic strength and low pH from destabilising nanoparticles through aggregation and precipitation in the gut. Cationic surfactants form positively charged surfaces. Anionic surfactants form negatively charged surfaces (80).

Particle surfaces in aqueous colloidal dispersions can adopt a negative or positive charge, resulting in a negative or positive zeta potential, the strength that is a function of pH. When coupled with its environment (pH, ionic strength, the concentration of additives), the zeta potential versus pH curve is negative at high and positive at low pH. A zero zeta potential, the isoelectric point, is the least stable as the probability of aggregation is very high (90,91).

The surface charge created by the solution's pH and the acid/base strength of the surface are quantified using electrolytic conductivity. The electrolytic conductivity in the oil is 100 to 1000 times smaller than in aqueous brine. Massive conductivity changes alter emulsion type. Variation is proportionate in o/w emulsions and zero in w/o. Deviation from the straight-line rule suggests multiple emulsions (83).

pH affects the extent of phospholipid hydrolysis during storage (81). The acid or alkaline strength of the solution affects the ionization (protonation and deprotonation) of functional surface groups or the differential loss of ions, which determines the dispersion's charge and stability. Protonation breaks down stabilized phospholipid structures by decreasing bond strength. The dissociation

of primary groups on particle surfaces yields positively charged surfaces, and the dissociation of acidic groups yields negatively charged surfaces. Particles acquire a more negative charge in alkali and a more positive charge in acidic suspensions.

3.3.5. Fourier Transform Infrared Spectroscopy (FTIR) of M4 and M13

FTIR provides information about lipid membrane structure and phase transition properties. In the liquid crystalline phase, lipids move in membrane planes, intermittently crossing the two monolayers of the phospholipid bilayer in a flip-flop motion. The liquid crystalline phase vibrates freely and produces broad spectral FTIR bands absorbed at the phospholipid's phosphate group, providing data on the lipids' hydration state and hydrogen bonding. Gel-phospholipid bilayers (Gel/solid) have less conformational freedom and cannot flip-flop; this loss of lateral mobility produces sharper FTIR bands, resulting in higher resolution of the hydrocarbon chain.

FTIR of lipids in the gel phase indicates the exudation of water from most lipid membranes when the polar/apolar interfaces cool. Temperature reduction also sharpens the headgroup peaks.
At the same time, the vibrational methylene group rocking of the hydrocarbon chain at 2850 cm^{-1} measures the changes to conformational disorder and freedom of the hydrocarbon chain, which is indicative of hydrocarbon chain melting and the lipid membranes' phase transition between the liquid and gel phase. The liquid and gel states differ in that all hydrocarbon chain methylene groups exist in the trans conformation in the gel phase, seen by the disappearance of the methylene rocking and signifying hydrocarbon chain melting (92).

Phospholipids have active infrared bands on the headgroup, interfacial, and hydrophobic regions. The FTIR spectrum of soy lecithin (Figure 3.5D) has intense absorption bands between 3010 cm^{-1} and 2500 cm^{-1}. The most intense bands correspond to 1) 3009 cm^{-1} asymmetric CH_2 stretching; 2) 2956 cm^{-1} asymmetric CH_3 stretching and scissoring; 3) 2854 cm^{-1} symmetric CH_2 stretching (alkane bands) and scissoring; 4) CH_2 scissoring at 2928 cm^{-1} and 1462 cm^{-1}; 5) 1736 cm^{-1}; carbonyl stretching; 6) the highly overlapped PO_2 – and P–O–C infrared vibrations between 1200 cm^{-1} and 970 cm^{-1}, centred around 1061 cm^{-}

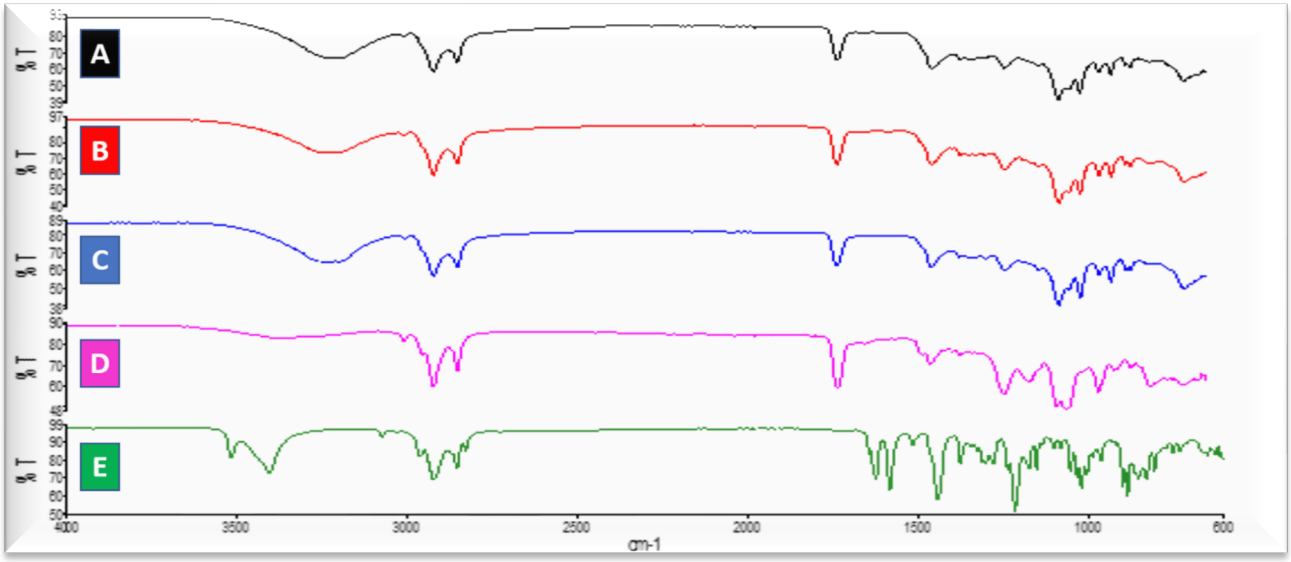

Figure 3.5: FTIR results for (A) M4; (B) Trial Run; (C) M13; (D) Soya Lecithin; (E) CBD

CBD's FTIR spectrogram (Figure 3.5E) exhibits two distinctive bands of intermolecularly bound O-H spanning between ~3500-3400 cm^{-1}. Alkenes (C=C), including cyclical and conjugated alkenes of the benzene skeleton, stretch around ~1600 cm^{-1} and ~1650 cm^{-1}. The weak (small) peak around 3070 cm^{-1} due to the benzene ring's alkene signifies a small number of C-H bonds stretching next to the alkene functional groups in the crystalline structure. CH2 and CH3 produce aliphatic C-H stretching between ~2850-2900 cm^{-1}.

In the fingerprint region of the spectrum, hydroxyl or methyl bending produces a medium-strength peak at ~1440 cm^{-1}, while ethers or hydroxyl functional groups produce a significant spectral peak from C-O stretching at ~1210 cm^{-1}. Sharp peaks from alkenes bend around ~1010 cm^{-1}, and those below 900 cm^{-1} typically result from C-H deformations, like twisting, bending, and rocking (93–95).

In M4 and M13 absorption spectra, CBD is encapsulated within soy lecithin liposomes, as shown by the elimination of the CBD fingerprint (Figure 3.5E) and the preservation of the lecithin fingerprint (Figure 3.5D) (Figures 3.5A and 3.5C). Adding CBD to its hydrophobic areas and hydrating lecithin phospholipids changes its fingerprint.

M4 and M13 contain edible vegetable oils distinguished from other oils based on cis and trans double bonds and impurities in their composition. Fats and oils have characteristic solid absorption bands resulting from the vibrations of the hydrocarbon chain and carbonyl groups in the NIR region. The asymmetric CO stretching of ester groups (CCO at 1300 cm^{-1} and OCC at 1000 cm^{-1}) tells the oils apart between 1600-1800 nm and 2100-2200 nm on NIR spectra patterns. The spectrum of M4 and M13 are similar because they contain similar ingredients. Variations in the two optimised formulations consisted of swapping olive oil for castor oil. Impurities detected in the fingerprint region are bands of cis double bonds of straight carbon chains. Vegetable oils differ in their cis double bond content and partially hydrogenated vegetable oils in their trans-CH bending absorbances.

M4 and M13 on the FTIR spectroscopy (Figure 3.5) indicate the presence of water near the lipid bilayer. Water typically vibrates in the broad, structureless spectrum of 3,000-3,800 cm^{-1}, providing information about the structure and orientation of water species. Water has a layered geometry around the polar interface. The H-bond network, dipolar water interactions, and lipid zwitterionic headgroups affect water and lipid structure. Gibbs free energy also affects structuring by minimising the system's energy to reach thermodynamic equilibrium (72).

Hydrogen-lipid bonds are stronger than hydrogen-hydrogen bonds; therefore, water located further from the bilayer has fewer hydrogen bonds than water near the bilayer. Hydrogen bond strength around lipid bilayers diminishes in the succession of water–phosphate group >water–O–CO (sn1) >water–O–CO (sn2) >water–water. The average number of strong H-bonds formed between water and lipids increases closer to the bilayer, from the second hydration layer with zero bonds to the carbonyl groups with about two water bonds. Multimer water forms fewer H-bonds than network water. Multimer water increases with increasing distance from the lipid headgroups, transforming the lipid phase from gel to liquid (96).

FTIR distinguishes low-density network water and high-density multimer water. The organised, highly connective network water absorbs discrete O–H vibrations in the hydrogen-bonded network around 3,250 cm^{-1}, whereas less structured and linked dense multimer water vibrates water in structures with shattered hydrogen bonds at approximately 3,600 cm^{-1}.

Network water, epitomised by strong H-bonds and more order, decreases with temperature and hydration. Around 3250 cm^{-1}, only the primary (first) hydration layer interacts strongly with the polar surface of the phospholipid via strong solvent: solute (water: substrate) interactions, with water molecules, firmly H-bonded to form a low density, well-structured "network water'' interphase. The maximum intensity of the water band, around 3400 cm^{-1}, is unaffected by isotopic dilution, reflecting the hydrogen bonds' strength in the network structure. Tiny water molecules fit between voids of the bilayer, creating pliable water clusters composed of hydrogen bonds, phosphate, and carbonyl groups. Water connects neighbouring zwitterionic lipid headgroups (phosphate and carbonyl groups) by chainlike water bridges. Absorbance around 3,600 cm^{-1} detects vibrations of disturbed hydrogens of ''multimer water'' due to phospholipid headgroups that ''perturb'' the order and dynamics of the water molecules. Like bulk water, water beyond the primary hydration layer has properties that change with changing temperature and increasing distance from the membrane (96).

Lipid hydration affects the phase behaviour of lipid/water systems and the repulsive hydration forces between lipid bilayers. Hydration changes the conformation of acyl chains, and hydrogen bonding with phosphate and carbonyl groups elongates functional groups, shifting the stretching frequencies of water molecules and decreasing the frequencies of the chemical bonds. As seen in M4 and M13, water molecules interact with the phosphate groups before the carbonyl groups during hydration (96).

The polar interphase changes the network and multimer water composition and orientation. Dehydration increases the network water fraction by 30-60%, like that in supercooled water at 25°C. Heat melts lipids, transferring large amounts of network water from the lipid headgroup to the multimer water in the lipid hydration shell and melting partially disorders lipids, reorientating water dipoles parallel to a perpendicular orientation relative to the membrane. The proportion of structured network water in the ordered gel phase exceeds that of the liquid crystal phase (96). It increases progressively as the gel transitions to the liquid crystalline phase, eventually increasing the absorption to around 3600 cm^{-1}, characteristic of weakly hydrogen-bonded water

aggregates (96). The lack of order in the water network occurs predominantly in the interfacial region of phospholipids.

Hydration pressure affects lipid phase transition by increasing RH and decreasing temperature and external hydrostatic pressure. Above RH 75%, lipids have a sufficient water content to pass into the liquid phase (79). The water band intensity increases with increasing RH, reflecting progressive, incremental water absorption and weakening of the water structure during the gel-liquid crystalline phase transition.

3.3.6. Differential Scanning Calorimetry

DSC measures lipid membranes' thermal behaviour and response to additives, lipid excipients, drug molecules and environmental stresses. Lipid excipients' thermal behaviour fluctuates throughout formulation due to their complicated chemical makeup and wide melting ranges. Heating and phospholipids' hydration states cause various phase transitions (80).

As temperature increases, amorphous and semi-crystalline polymers undergo a glass transition (T_g). T_g describes a temperature range over which the material's physical properties gradually change from a rigid, brittle, or amorphous solid ‘glass’ state into a viscous or rubbery state. In the glass phase, drugs have the molecular organization of high entropy fluid states, making them macroscopically like solids (67). Some materials have stable glass phases over long periods; others recrystallize over time because the API amorphous state has a low activation energy barrier. Molecular crystallization of glass-forming molecules is reduced by “quenching”, i.e., the rapid cooling of material from above its melting temperature (T_m) to below its T_g. Drug molecules cooled below their T_m without crystallizing become supercooled liquids in which molecular motion will cease at a temperature point called the glass transition (T_g) temperature. Drug molecules must liquify by falling below their melting temperature (T_m). After that, the liquid material must become a supercooled liquid at a temperature drop below its T_m and then drop further below the T_g before being immediately quenched to reach a hardened glass state of an ASD API (97,98).

The reverse process transitions the viscous liquid into a glass (vitrification). A glass transition is not a phase transition, and T_g is always lower than the T_m of crystalline materials. Amorphous polymers exhibit T_g phase transitions, while semicrystalline polymers have crystallization T_c and melting temperatures T_m.

DSC analysis of ASD glass transition temperatures of M4 and M13 indicates the extent of the drug and polymer's miscibility in the ASDs. The miscibility of an ASD binary mixture refers to the degree of homogeneity between an API and polymer upon mixing; inadequate mixing of the components leads to phase separation or API recrystallization. API and polymer miscibility have three levels:1) Immiscible: Densely packed API; 2) partly miscible: polymer saturation rises; 3) supersaturation: API and polymer are molecularly miscible.

Two compounds are utterly miscible in the liquid state but minimally so in the solid-state form of simple eutectic mixtures. Solid eutectic mixtures form upon rapid cooling of two co-melted compounds that produce a physical mixture of very fine crystals. A mixture of a slightly soluble drug and an inert, highly water-soluble carrier dissolve rapidly in an aqueous medium, releasing very fine crystals of the drug (106).

In formulations, M4 and M13, CBD and lecithin form a eutectic mixture, an assorted mixture of substances that solidify or melt below the melting point of any individual ingredients. Each constituent of non-eutectic mixtures has different melting temperatures because one component's lattice melts lower than another or solidifies and cools at different temperatures, forming a lattice until the entire mass solidifies.

M4 and M13 (Figure 3.6) show the favourable integration of CBD into the liposomes to form a homogenous lipid formulation, i.e., CBD and polymer are miscible in ASD. The CBD-LBDDS has a T_g value between CBD and Soy lecithin (polymer). CBD melting temperature is 66-67°C, depending on the polymorph, and lecithins are 236,1°C (8,99).

M4 and M13 show the formation of a single endothermic peak (T_g) between 160-170°C. A single T_g value indicates miscibility between the drug and the polymer in a homogeneous system (236,1°C minus 66-67°C gives a range of 170,1-169,1°C).

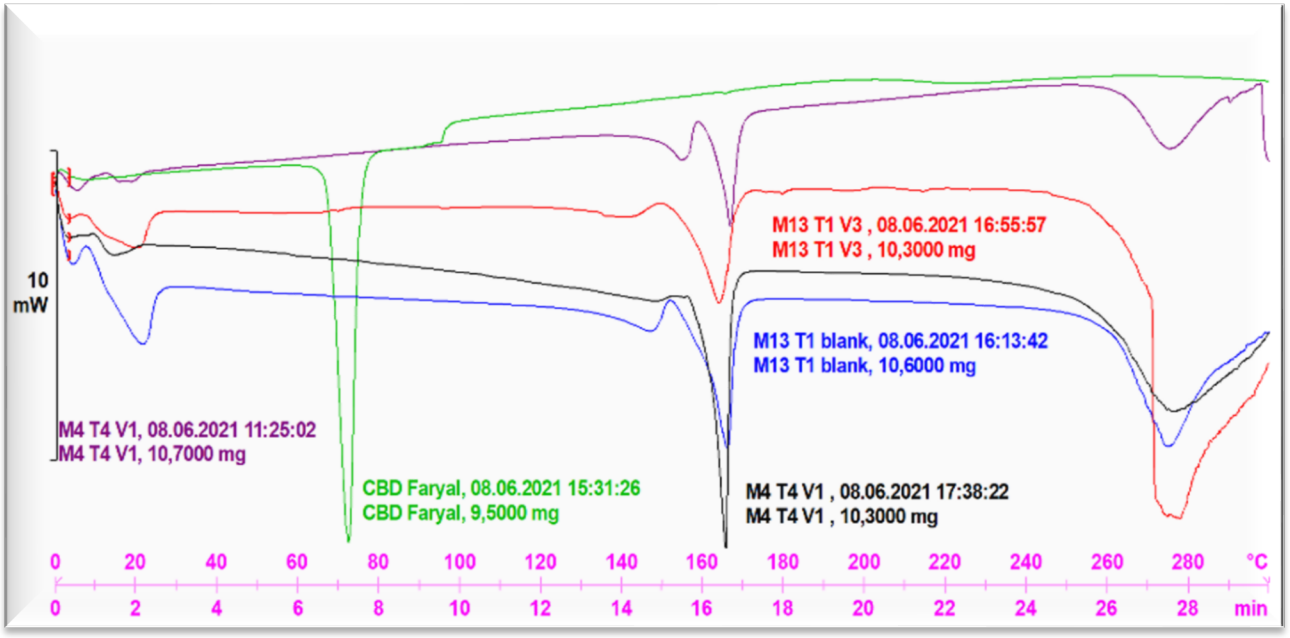

Figure 3.6: DSC Temperature analysis of components of the SELFs

The phase of a drug molecule and its physicochemical properties impact the bioavailability and efficacy of the drug. Crystalline materials, low energy state lattices of organised molecular arrays bonded by solid intermolecular forces, need large amounts of energy to disrupt their order during digestion, unlike the intermolecular forces of less orderly amorphous (glassy) materials, which are associated with a high entropy state that increases the drug's dissolution and bioavailability. Polymers have an anti-plasticizing effect that reduces molecular mobility and retard the crystallization process. An energy barrier lies between the phase changes of a drug molecule. Pure substances have small energy barriers that need little input to overcome the energy barrier phase change from amorphous to crystalline states. Polymers can increase glass phase stability by raising the energy barrier so that more significant energy input is required to induce phase transition into a crystalline state. Drugs with T_g below room temperature recrystallise, but adding polymers with a higher T_g raises the drugs' T_g above room temperature, stabilising the ASD (97).

3.3.7. X-Ray Diffraction

Preparations of amorphous solid dispersion (ASD) use the hot melt emulsification method. Globules formed in o/w emulsions vary from droplet to droplet, forming characteristic amorphous, crystalline, or liquid structures during crystallization, depending on the factors that influence nucleation. Decreasing temperatures increase crystallization (exothermic). Plummeting temperatures condense droplets into supercooled liquids and form amorphous particles, mono or multi-crystalline structures. Hotmelt emulsification and cooling processes and surfactant-induced heterogeneous nucleation at the interface influence particle configuration and the physical size, shape, configuration, and state of dispersions after crystallization, which influences the bioavailability, drug loading, and release behaviour in colloidal delivery systems. Nucleation rates increase with secondary heterogeneous nucleation caused by collisions, and shear stress forms shear-dependent crystalline structures that influence nucleation mechanisms (81). XRD and DSC analytical methods determine the crystallinity degree. However, thermo-optical analysis using polarising microscopes with an accurate heating/cooling stage can detect and characterise crystallization behaviour and events of single droplets and clusters (> 1 µm) in concentrated microemulsions. Furthermore, using a crystallization index (CI_N), the morphology, size and Pdi within droplet clusters and the distinction between liquid, amorphous, and crystalline structures can be calculated (81).

Equation 3.8: Calculation of the crystallization index $\boldsymbol{CI_N}$

$$CI_N = \frac{Ncp}{Np + Nd}$$

CI_N= Crystallization Index
Ncp = number of crystalline particles (mono and multi-crystalline structures)
Np = total number of particles
Nd = total number of droplets

The crystallization Index (CI_N) can be calculated as either the mass (CI_M) or the volume (CI_V) of the investigated material from the micrographs; it depends on the application (81).

M4 and M13, prepared by the hotmelt method, produced ASDs that XRD analysed to compare the proportion of crystallinity of powdered CBD to the LBDDS with or without CBD in the formulation. CBD shows several sharp peaks, indicating high crystallinity (Figure 19A). The comparative XRD Diffractogram shows the crystalline spikes of CBD powder against the broad halos of the ASD states of M4 without CBD, M4 containing CBD, M13 without CBD and M13 containing CBD (Figure 3.7B). Amorphous materials do not diffract X-rays coherently; therefore, diffractograms form broad halos with few distinctive peaks (67). Amorphous materials lack a crystalline structure. The crystallinity of a mixture is the proportion of crystalline material present.

Table 3.11: Crystallinity

The proportion of crystalline material	Degree of crystallinity
100%	Perfect crystals with zero entropy
0%	Non-crystalline/amorphous with high entropy

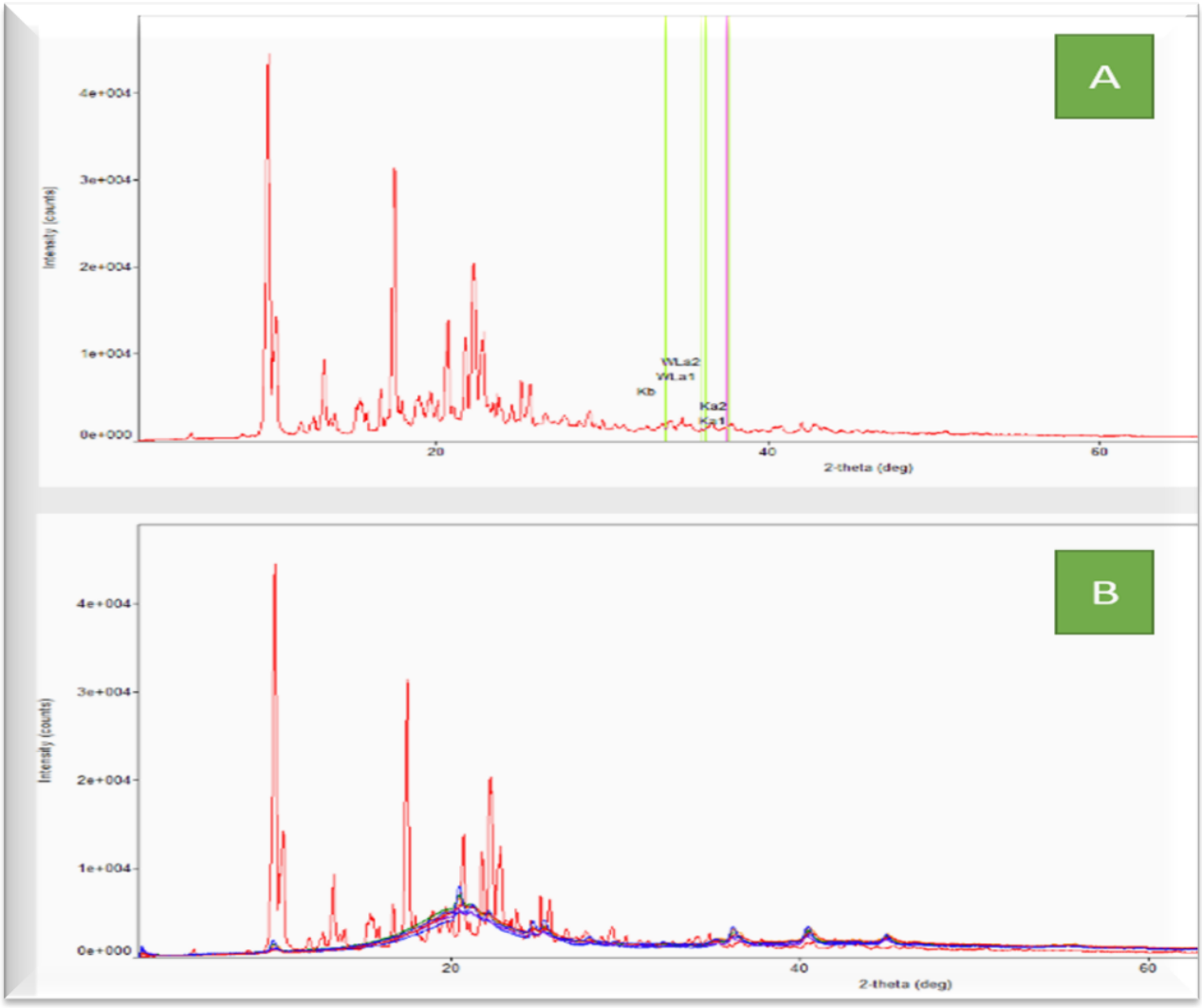

Figure 3.7: XRD Diffractogram of (A) Crystalline spikes of CBD Powder; (B) A comparative XRD Diffractogram showing the crystalline spikes of CBD Powder and the amorphous solid dispersion state of M4, blank, M4 containing CBD and M13 blank, M13 containing CBD

Solid substances like crystalline, amorphous, or partly solid drugs have varied physicochemical qualities and biological activities. Amorphous solids can co-exist with or become crystalline solids. Unlike their crystalline counterparts, amorphous substances lack the organization, orientational symmetry, and long-range three-dimensional structure of crystals. Unlike crystals, ASD molecules have high internal energy, mobility, and "free" volume. Liquids have chaotic short-range molecular organisation. Crystalline compounds are more stable than amorphous substances. Free volume, the space in a material not occupied by molecules, gives amorphous forms a lower density than crystalline materials. Amorphous areas have varied densities,

polymorphic states, and residual crystallinity. Thermodynamic, chemical, and physical instability in low-molecular-weight amorphous materials affects molecule mobility, orientation, oxidation, and hydrolysis.

Amorphous materials crystallize to form nuclei, which then grow into crystals. The mobility of amorphous solids changes structurally below and above the glass transition temperature (the frozen solid and the supercooled viscous liquid). Materials composing ASDs have large amounts of surplus energy. The ASD tries to lose this excess energy by re-crystallizing into a more thermodynamically stable form (106). The recrystallization of dispersed drugs negates the solubility advantage of ASDs and decreases bioavailability; however, storing ASDs below their T_g and avoiding exposure to substances that depress the T_g, like water, can reduce recrystallization (76).

ASDs are more hygroscopic and moisture-sensitive relative to their crystalline counterparts. Moisture and temperature promote molecular mobility, catalyses chemical and physical reactivity in ASDs, and accelerate nucleation. Moisture absorption by ASDs initiates hydrolysis by increasing the free volume and reducing the degree of molecular bonding in the solid, increasing molecular mobility, depressing T_g, and promoting spontaneous crystallization. Furthermore, moisture and solute molecules can plasticize the ASD, reducing its glass transition temperature. Mitigating the risk of ASDs reverting to the crystalline state involves increasing the barrier to nucleation, slowing the crystal growth rate (propagation), and ensuring the purity of crystalline materials.

ASDs are glasses that can crystallize or undergo primary relaxation in high-density areas or secondary structural relaxation in the low-density regions between high-density regions. The crystallisation rates of an ASD are highest between the T_g and the T_m. T_g depends on the heating rate and the moisture content. The DSC analysis of T_g and relaxation is measured by heating the material and observing any change in the heat capacity.

Differences in heating and cooling rates may cause ASD matrix relaxation. Mitigating the risk of ASDs reverting to the crystalline state involves increasing the barrier to nucleation, slowing the crystal growth rate (propagation), and ensuring the purity of crystalline materials.

ASD offers less solubilizing benefit for drugs that recrystallize slowly as these compounds exhibit liquid-liquid phase separation and coexist at high amorphous solubility. Process conditions affect the ASD product. Rapid freezing during lyophilization forms amorphous solutes; adding an annealing step may promote crystallization; crystalline materials are less soluble in aqueous media than their amorphous counterparts. Kinetically, slow crystallization rates turn the material into a "frozen liquid" or cause vitrification without crystallization. ASD preparation is effortless for suitable glass formers but difficult for poor glass formers. Poor glass formers can transform into amorphous materials if crystallization is deliberately prevented by adding antisolvents, molecular quenching of melts, rapid precipitation, freeze-drying, spray-drying, and impurities. Eventually, the solute in the supersaturated solution crystallizes to attain the equilibrium solubility of the crystalline phase.

Transient solubility increases of >10x significantly improves biopharmaceutical performance. Rapid cooling of eutectic mixtures consisting of a slightly soluble drug and an inert, highly water-soluble carrier dissolved in an aqueous medium; the carrier dissolves rapidly, releasing excellent drug crystals solid dispersions use fusion, hot-melt extrusion, solvent, and supercritical fluid as preparation methods. A simple eutectic mixture consists of two completely miscible compounds in the liquid state but only to a minimal extent in the solid state. Solid dispersions differentiate into amorphous, continuous, discontinuous, eutectic, interstitial, solid and substitutional solutions.

Hot Melt Extrusion, a possible alternative to solvent-dependent methods, changes the physical state of crystalline drugs into a molecularly dissolved amorphous state, enabling semi-solid and solid preparations for oral, parenteral and topical sustained-release applications (77). However, poor mixing of the components causes phase separation or drug recrystallization, resulting in liposome leakage or collapse and undermining the goal of the polymer in the ASD oral medicinal delivery system (73).

Polymers prevent nucleation and crystal formation and maintain ASD solubility by modifying solute adhesion onto the crystal, increasing activation energy, lowering molecular mobility and plasticization, and decreasing drug-polymer interactions through van der Waals forces and hydrogen bonding.

Less supersaturated polymers partition more into the organic phase in ASDs because they remain below the crucial nucleation threshold, limiting nucleation and growth. Alternatively, additives that stabilize the labile biomolecules (proteins and peptides) prevent crystallization of amorphous excipients, prevent chemical degradation and microbial growth (with anti-oxidant, pH buffer, and preservatives), and enable specification of acceptable storage temperatures (shelf life). Drugs introduced to liposomal systems impact phospholipid phase transition and bilayer fluidity depending on their placement in the bilayer (77).

3.3.8. Scanning Electron Microscopy (SEM) of M4 and M13

Water content is critical to liposome and lyotropic liquid crystal (LLC) formation and structure. Liposomes form vesicles spontaneously when phospholipids' phosphate and carbonyl groups interact with water molecules during hydration. Samples M4 and M13 are lecithin organogels that form amorphous solid dispersions with different degrees of hydration, which can affect the SEM imaging process. Samples placed directly into the SEM imaging chamber do not need special preparation. However, removing volatile components like water prevents rapid evaporation, alteration or damage to the specimen or its appearance. Liquids exchanged with a polymer in a drying process called “fixation” must be done before imaging under a vacuum. Sample surface topography shows bright sections representing edges and dark regions recesses. Electron bombardment charges non-conducting material; however, the electron beam cannot scan a charged object. Therefore, samples coated with a conducting layer (e.g., platinum/gold) using a sputter coater convert to non-conducting samples before SEM analyses.

3.3.8.1. SEM of Formulation M4

SEM images for M4 (Figure 3.8A) show a polydispersed mixture of separate, unilamellar, small (<100 nm), and large (>100nm) liposomes entrapped in a 3-dimensional amorphous gel matrix.

The viscous gel network embeds the liposomes within its voids, providing protection and increasing the liposome's stress tolerance. Liposomes incorporated into the gel matrix do not significantly alter in size post-lyophilization, as shown in the DLS results (Tables 3.7 and 3.8). Changes to vesicle size are a valuable gauge of the liposomes' physical stability. The liposomal vesicles' size depends on the phospholipid concentration. Over time, the liposomes' average size increases with aggregation and fusion and decreases with the loss of entrapped drugs due to leakage, physically destabilizing them.

M4 (Figure 3.8A) also shows the ruptured membranes of vesicles and leakage of encapsulated drugs attributable to liposome membranes' fluidic nature, mechanical properties, the composition of the phospholipid bilayers and the fatty acid acyl chains.

Vesicle shapes observed in M4 (Figure 3.8A) range from spherical and quasi-spherical to ellipsoid. The irreversible elongation of shapes is attributable to oleic acid. Olive oil contains oleic acid (~ 55% to 83%), the principal bioactive portion of olive oil, which modifies or stabilizes surfactant assembly and reverse micelles in Lecithin/water/oil systems.

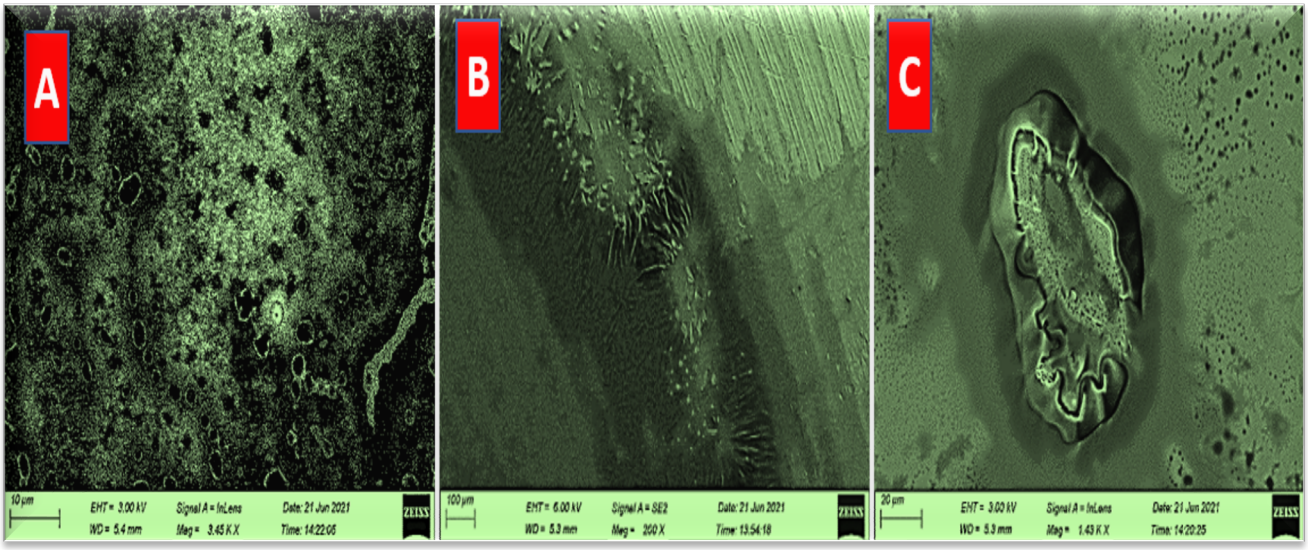

Figure 3.8: A) Spherical, quasi-spheroidal and ellipsoid shapes of unilamellar, polydispersed liposomes, intact, ruptured and fused; B) Streaking, rippling, and crystallization of the ASD; C) Hardening of the ASD due to oxidation at the air interface

Oleic acid ($18n^{-1}$) kinks at the cis-double bond at C9 from the methyl extremity. Even in small quantities, the boomerang-shaped Oleic acid induces a negative curvature strain into the lamellar sheets, forming HII non-lamellar membranes that impact membrane fluidity, incompressibility, and bending resistance. In addition, oleic acid expands reverse micelle cores in oil to hold more water, improving its resistance to precipitation (74).

In the SEM image, formulation M4 (Figure 3.8B) features lamellar structures with streaks and mosaic-like textures characteristic of anisotropy, a critical physical property of formulated materials. The anisotropic lamellar phase generates one-dimensional, planar lipid bilayer structures separated by water sheets, with polar head groups directly coupled to water and hydrophobic tails facing the interior of the bilayer.

Membrane systems consist of agglomerations of self-assembled nano-domains in which anisotropic nanodomains form stable lipid bilayer tubes. These tubes are not supported internally by microtubules, external pulling forces, optical tweezers, or motor proteins (kinesin and dynamin) (63,107,110,113).

Anisotropy, described by tensors, assumes different multi-directional properties, unlike isotropy, which is uniform from all angles. Tensors describe multilinear relationships between sets of algebraic objects in a vector space like vectors, scalars, dual vectors, multilinear maps between vector spaces, and the dot product. Different tensors at each object point measure a property's directional dependence along different axes and provide the mathematical framework for formulating and solving physical and mechanical problems like absorbance, refractive index, conductivity, tensile strength, stress, elasticity, and fluid mechanics (100).

Anisotropic monocrystalline material with symmetric crystals has fewer independent coefficients in tensor descriptions of a given property - directional dependence in polycrystalline material results from processing techniques, e.g. heat treatment.

Directional measurement impacts mechanical properties like creep rates, ductility, yield strength, and Young's modulus. Young's modulus describes the stress and strain impacting isotropic

materials deformed elastically, while tensors describe elasticity in anisotropic materials. Lamellar structures are less viscous than hexagonal structures.

Randomly oriented grains produce isotropic materials, whereas textured materials often result from processing techniques and are typically anisotropic. Fluid flow is isotropic if there is no directional preference, whereas a solid is isotropic when expanded equally in all directions on exposure to thermal energy. Like liquid crystals, anisotropic liquids flow with structural order along the molecular axis, unlike water or chloroform molecules, which contain no structural ordering (100,101). Crystals that exhibit optical anisotropy can have birefringent properties whereby isotropic light propagation in crystalline media breaks along the "axis (or multiple axes) of anisotropy".

Intrinsic lipid bilayer shape depends on the aggregation/segregation of membrane components, composition, lateral membrane distribution and average rotational degrees of freedom of lipid molecules in the curvature field of the membrane under various physiological or nonphysiological conditions. Even though lipid molecules, protein-lipid complexes, and proteins display anisotropy, the thermal rotation of lipids about their vertical axes may give the impression that they are naturally axisymmetric or isotropic in form.

Lipid headgroups are typically anisotropic. Models of anisotropic membrane components have short-lived, energetically stable, narrow necks connecting the fused vesicles to the target membrane. The coupling of the liposome with the cell membrane results in the orientational ordering and non-homogeneous lateral distribution of membrane components/constituents/nanodomains, influencing optimal membrane curvature/configuration until the intrinsic shape of the membrane forms.

Two isotropic components form tiny spherical beads connected by narrow channels. The cylindrical protrusions form when at least one component is anisotropic, even in tiny amounts. One or two anisotropic components form thin tubular protrusions, the length of which depends on the concentration of anisotropic components accumulating in the vesicle's tubular neck. Tubules have a minimal surface area to the rest of the vesicle. The local concentration and

distribution of macromolecules that influence bending rigidity, membrane shape and curvature favour the thin tubular structural formation.

Components on vesicle surfaces separate due to distinct elements' curvature gradients and inherent curvatures; the concentration of membrane components influences membrane shape, while membrane curvature determines component distribution. If component distribution were not shape-dependent, components would mix uniformly to maximize entropy. Increased concentrations of anisotropic components add stability to more extended, broader tubular structures. Small anisotropic concentrations form stable shapes with and without up-down symmetry. Smaller volumes with varied components form unstable cylindrical, pearl-like protrusions with up-down symmetry.

Tubular structures cannot form with one anisotropic component. The intrinsic curvature of anisotropic components is directly proportional to the tubule radius. In well-proportioned cylindrical protrusions, the tubule radius decreases linearly with increasing curvature. Smaller intrinsic curvature values indicate underdeveloped cylindrical tubules. Tubular width depends on the intrinsic curvatures of anisotropic components. Molecules with small intrinsic curvature radii form narrow tubular membrane protrusions, while membrane-bound anisotropic molecules have wide diameters. Bobrovsky et al. illustrate vesicle shapes of membranes composed of (aniso+aniso), (iso+aniso), and (iso+iso) components for different values of the reduced volume. The radius of the vesicle tube is a function of the anisotropic component's intrinsic curvature (102). Changing the properties of the isotropic component induces cylindrical protrusions. Increasing the intrinsic mean curvature of the isotropic component for fixed reduced volumes results in cylindrical protrusions whose length increases with the increasing intrinsic mean curvature of the anisotropic component. Membranes composed of isotropic components without any external force create stable protrusions by building a series of connected beads (110). An accumulation of anisotropic components creates stable tubular protrusions. In contrast, isotropic components only form cylindrical structures when exposed to external forces, like when growing microtubules push or molecular motors pull at the membrane. Dispersed droplets of lyophilised emulsions are assumed to be spherical (71) (103,104).

SEM images for M4 (Figure 3.8B) show symmetric and asymmetric rippling. The three basic transition phases when heating or cooling the phospholipid bilayer are:
COOL | ↔ L_β-phase (gel)↔ P_β-phase (ripple) ↔ L_α phase (sol) ↔ | HEAT

Ripple structures appear in the P_β-phase between phosphatidylcholines' pretransition and transition phase, with saturated acyl chains forming periodic bilayer undulations. Rippling occurs in multilamellar/multibilayer vesicles and giant unilamellar vesicles. In contrast, the high curvature of small unilamellar vesicles suppresses ripple formation.

Asymmetric ripples form in ASDs with multilamellar/multibilayer vesicles and giant unilamellar vesicles when a preparation warms from a lower temperature (L_α phase → P_β-phase) and, to a lesser extent, cools from a higher temperature L_α phase ← P_β-phase). Enlarged asymmetric ripples are visible only after cooling from the L_α phase.

Molecular packing constraints cause asymmetric rippling. The P_β-phase (ripple) directly precedes the fluid L_β-phase (sol) on heating. Increased rotational mobility from heating the phospholipids and oils expands each headgroup area, and hydration swelling displaces interacting headgroups vertically, affecting molecular packing in the bilayer. Moreover, the cross-sectional area of the hydrocarbon chains is slightly more prominent because of the presence of gauche conformers (105).

Asymmetric ripples, a continuation of symmetric ripples, maintain constant periodicity without a directional change. Asymmetric ripples consist of oppositely tilted broad and small segments or single tilted segments separated by small steps, forming breaks in the bilayer. Asymmetric surface undulations form from the periodic folding or splitting of the bilayer surface into a series of recurring, asymmetric quasi-lamellar bilayer segments with differing tilt directions. Altered periodicity or folding of the bilayers impart angularity to asymmetric ripples. Molecules tilt at about 30° from the normal phospholipid bilayer in two positions, giving asymmetric ripples a sawtooth-like profile. The hexagonal molecular chain packing arrangements of DPPC in the gel phase have a parallel and angular (60° and 120°) arrangement of chains with secondary tilting perpendicular to the primary tilting in the ripple formation (105).

Simple symmetric ripples have two equally broad, oppositely tilted single segments. Symmetric ripples have fluid- and gel phases co-existing between the L_α phase and P_β -phase, alternating in both monolayers of the bilayer or at periodic distances within the structure. Short "pre-ripples" approaching the L_α phase have periodic gel-like domains. The phase transition creates a pleated bilayer with symmetric ripples by repeatedly switching bilayer segment tilt directions. Triangular symmetric ripples without valley ridges emerge following warming from the L_β-phase. Symmetric ripples with ridges in the valleys, present after cooling from the Lα phase, have asymmetric steps of small unstable ripples (105).

The amphiphile's molecular geometry (e.g., short chains or bulky heads) facilitates the self-assembly into monolayers with no water in the interior, like spherical or cylindrical micelles. Vesicle shape transformations can occur in membranes that are amenable to shear. Budding transitions transform spherical vesicles into prolate ellipsoids mainly due to the area's thermal expansion with temperature increases and less due to its enclosed volume. Further temperature increases result in a pear shape, followed by neck closure to form two spherical compartments connected by a narrow constriction. Alternatively, spheres evolve into oblates, followed by stomatocytes with increasing temperature. Shapeshifting demonstrates fluidity as a vital attribute of the vesicular system. The robust bilayer structure does not form mesoscopic pores/holes, and the vesicle maintains its topology as the buds do not fission from the mother vesicles.

M4 (Figure 3.8C) shows fusion and irreversible hardening of the amorphous gel at the lipid-air interface, liposome rupture, and content leakage (dark areas). Liposomal stability is unaffected by compounds lodged in the liposome’s interior; lipid oxidation or the hydrolysis of the ester bonds holding lipid constituents together are responsible for liposome degradation and destabilization (42).

The oxidation rate of oxidation-prone lipid excipients is proportional to the degree of unsaturation in fatty acid molecules exposed to air. Impurities such as peroxides, metal ions and light interactive photochemical sensitizers catalyse oxygen to a highly reactive singlet or triplet oxygen species.

Lipids peroxidised to alcohols, furans, aldehydes, ketones, and acids produce rancid lipids, short-chain carboxylic acids and aldehydes, the amounts of which depend on polymer age and molecular weight. Older polymers have greater concentrations of peroxides, while high molecular weight polymers have lower concentrations (33).

Polyoxyethylene moieties oxidise to ethylene glycol at high temperatures in water, which further oxidizes to formaldehyde. The carboxylic acids formed during auto-oxidation lower the pH of aqueous polyethylene glycol solutions, depending on their handling and storage. The low pH degrades the compounds susceptible to hydrolytic degradation under acidic conditions. Reactive aldehydes can cross-link compounds containing amino groups in their structures through methylene groups (33).

3.3.8.2. SEM Formulation of M13

SEM images from M13 show monodispersed, small (<100 nm) individual liposomes spread throughout the ASD matrix (Figure 3.9A). These images confirm the DSC obtained (Tables 3.7 and 3.8). Vesicle shapes are uniform, cubic, and angular (Figure 3.9B). The lamellarity of the vesicles in M13 is not visible from the SEM images unless viewed with atomic force microscopy (AFM) or Transmission electron microscopy (TEM).

Lyotropic liquid crystals (LLCs) encapsulate hydrophilic, hydrophobic, and amphiphilic drugs, protecting them from hydrolysis and enzymolysis. Amphiphilic molecules have tightly packed polar heads that contact and associate with water, minimizing the system's free energy while shielding the non-polar hydrophobic tails from water. Typically, hydrophilic drugs anchor near the lipid polar head or in proximate water channels, while lipophilic drugs reside in the lipid layer and amphiphilic drugs at the lipid layer interface.

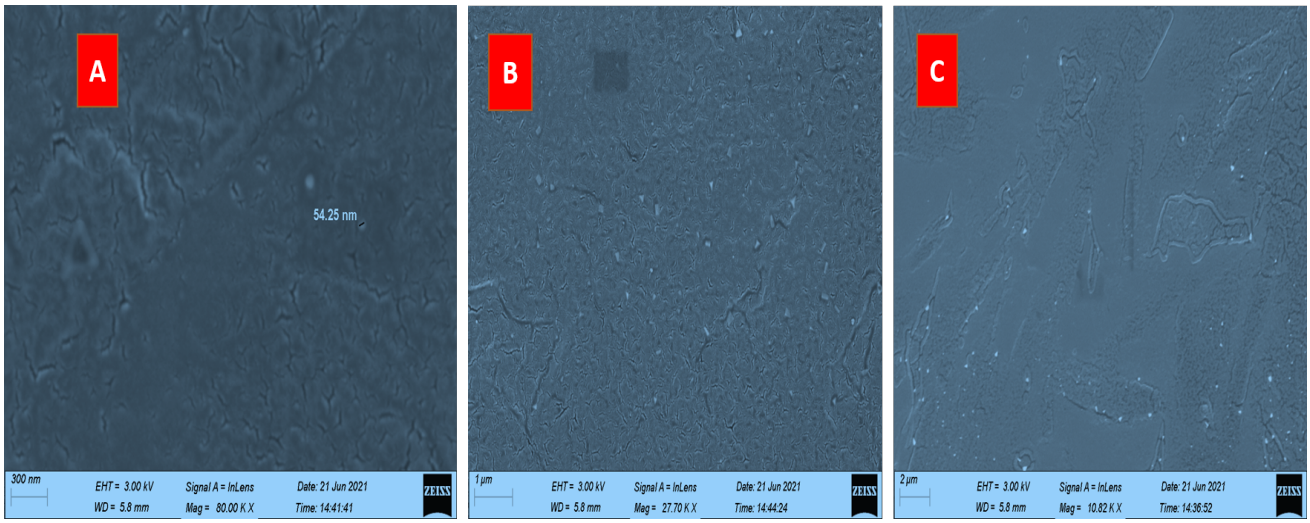

Figure 3.9: Measurement of nanoparticles in textured ASD gel matrix; B) Cubic and triangular, monodispersed liposomes; C) Spherical liposomes in a textured ASD gel matrix show undulating rippling, rolling, swelling, unevenness, crevices, cracks, ridges.

Temperature: Internally, LLC structures consist of the hydrophilic, lipophilic domain and a lipid layer. Self-assembling amphiphilic molecules like phospholipids form LLCs when added to a polar solvent, usually an excess of water.

A series of thermodynamically stable phase transitions and nothing in a single process liquefies the solid state. The intermediary phase (mesophase) consists of organic liquid crystals that aggregate to form structures between the liquid and solid states. Pure organic substances reach the mesomorphic domain through temperature variations and form thermotropic liquid crystals (TLC), while organic substances dispersed in aqueous solutions form LLCs by adjusting temperature and concentration. The “mesomorphic” domain lies between two temperature-specific limits. The lower temperature limit at the solid-state border is the melting point, while the isotropic liquid state begins at the higher clearing point. The multi-anisotropic mesophase has liquid flow and crystal order proprieties of a liquid, the texture of which can be observed microscopically together with its specific structural formations (106).

Metastable lamellar crystals (LC) form at low temperatures and must be stored at 20-25°C to avoid structural changes. LCC structures are sensitive to temperature, pH, light, magnetic fields, amphiphile type, water content and additives. LLC, prepared at 20°C and stored at 4°C, forms

lamellar crystals. Conversely, LLC prepared at 0°C and stored at 20°C changes lamellar crystals to the cubic phase. Lamellar and reversed bicontinuous cubic phases form at room temperature, and the cubic-to-reverse hexagonal phase transition occurs around +80°C. Increasing temperature increases CPP and volume by shortening the tail length while decreasing the hydration and area of the lipid's polar head (49).

Pressure increases produce phases with negative spontaneous curvature (49).
Concentration: Temperature influences certain thermotropic and lyotropic liquid crystal phases. However, lyotropics are solutions of at least two compounds where concentration and not temperature are determinant parameters. LLCs' formation depends on the amphiphile concentration and the water content in the formulation. The maximum capacity of hydrophilic groups to bind water determines water content. Minor changes to the water-to-phospholipid ratio (w/w) of ASDs and LLCs can drastically alter micelle morphology, control phospholipid aggregation and shape and cause phase separation.

At the CMC value, colloidal-sized aggregates of amphiphiles appear and spontaneously assemble into a network. If the solution does not show liquid crystal behaviour, it is an isotropic micellar solution. However, as amphiphile concentrations increase, the micellar solution forms a less viscous, anisotropic, liquid crystal solution with lyotropic-specific structures. Aggregates in isotropic micellar solutions are spherical (globular). Mesoforms exist as cylinders, rods, or discs. At the CMC, entropy favours the aggregation order of spheres over rods and rods over discs (106).

Above the CMC value, monomers aggregate at the water surface to form a film until saturation establishes a new equilibrium, and structures distribute into the bulk solution. Amphiphile concentrations exceeding the CMC in water assemble micelles into LLCs into lamellar, bicontinuous cubic, micellar cubic and hexagonal mesophases. Normal micelles form when the amphiphilic heads meet water, and the hydrocarbon tails occupy the micelles' interiors. Below a specific water content, amphiphile heads and tails interchange positions and micelles become reversed(106).

At minimal water content, LLC phases form hexagonal or cubic mesoforms. High amphiphile and low water concentrations form normal o/w micelles, the regular cubic and hexagonal phase, the lamellar phase, the reversed cubic (w/o) and the hexagonal phase. The lamellar, the reversed cubic and the reversed hexagonal phase have highly ordered internal structures, imparting great potential as drug delivery systems (50).

Below the CMC value, physical parameters such as boiling temperature, density, electrical conductibility, and osmotic pressure increase with concentration: low amphiphile and high water content tile amphiphilic molecules at the water interface (106).
LLC shapes with specific hydrocarbon chain lengths, geometrical constraints, and molecular packing patterns depend on the cross-sectional polar head area's size and packing parameters.

The lamellar phase and hydrocarbon chain conformation
The lamellar phase is planar, consisting of mono and bi-layer units with specific textured and optical characteristics. This phase is not viscous; the bilayers can slip easily over each other (58).

Orderly bilayers stack parallel under each other at a constant repetitive vertical distance, periodically alternating with water layers, as the gravitational effect does not unsettle the bilayer ordering. Hydrocarbon chains become structured at moderate temperatures, only rotations around the molecule's axis occur. In the stable phase, phospholipids have swollen bilayers, with a fluid lamellar phase at high temperatures (L_α -phase), 2D gel (L_β' -phase) bilayers at low temperatures, and an intermediate textured ripple phase (P_β -phase) (Figure 3.9C). The L_α (liquid phase) only accommodates limited quantities of water. Only a minimal amount of lipid swells with water, and the excess water co-exists with the L_α -phase vesicles (50).

The amphiphilic bilayer in the lamellar phase has L_β (stiff, parallel chains), L_β' (tilted extended chains) and δ (coiled into helices), and $P_{\beta'}$ (ripple phase) type conformational ordering. The difference in hydration intensity and the number, lengths, and degree of unsaturation of alkyl chains influence the phase behaviour of different amphiphilic molecules (106).

Cubeosomes

Nano particulates in M13 (Figures 3.9B and 3.9C) show monodispersed cuboidal structures. The viscous isotropic cubic structure has three different packing forms: cubic, cubic face-centred, and cubic body-centred and aggregated shapes can be normal or reversed spheres or rods. Optically, cubic phases have no texture because they are isotropic, differentiated from isotropic micellar solutions only by their high viscosity. The cubic phases I and V can correctly identify by location during certain phases. As the surfactant concentration increases, the I-phase lies between the isotropic micellar and the hexagonal solution, and the V-phase between the hexagonal and lamellar phase (106).

The bicontinuous cubic "honeycomb" structure stacks amphiphilic molecules in a three-dimensional space. The reversed bicontinuous cubic and the reversed micellar cubic phases are subdivisions of the reversed cubic phase. The two water channels separated by a lipid bilayer face back-to-back without intersecting and are structurally robust enough to sustain drug release.

The reversed bicontinuous cubic phase is a periodic, 3D lipid bilayer with zero mean curvature at each point. Three reversed bicontinuous cubic phases exist: the primitive, double-diamond, and gyroid lattice. Structurally, the reversed bicontinuous cubic phase has two continuous, nonintersecting water channels separated by a curved bicontinuous lipid bilayer. The bulk phase forms a viscous, transparent gel without optical textures (49).

The reversed micellar cubic (discontinuous cubic) phase organises micelles into two primary cubic lattice phases: Fd3m and Fm3m. The closed, compact structure of Fd3m contains two sizes of monodisperse reverse micelles that form face-centred cubic (fcc) lattices organized in a double-diamond network capable of increased drug loading. Fm3m, stable in excess water at equilibrium, can disperse into particles for a delivery system (49).

The reverse hexagonal phase comprises numerous densely packed, water-filled cylindrical micelles approximately 1–2 nm in diameter, containing 30–60% water (w/w), following a long-range order in a 2D lattice. The hexagonally packed micelles enclosed by a cylindrical micelle

do not directly contact the outside water. The reversed bicontinuous cubic phase is more viscous than the “fan-like” textured reversed hexagonal (49).

Additives structurally transform LLC phases, e.g., hydrophobic compounds and fatty acids like Vitamin E Acetate transform LLCs into reversed micelle or hexagonal phases. Hydrophilic compounds form lamellar phases, and incorporating hydrophilic additives and drug molecules into LLCs results in phase changes from cubic to lamellar mesoforms, unlike hydrophobic drugs. Additives with the HLB values 1.5, 3, 4, and 5 form reversed hexagonal phases, while HLB values 7, 10, and 11 form lamellar phases. Short-chain TAG (e.g., triacetin) does not affect phase behaviour in the Q2 and L2 phase.

Middle chain TAG (e.g., tricaprylin), a very stable and effective additive, directly transforms the L2 phase to the H2 phase by incorporating hydrophobic chains, filling void volumes, and increasing CPP values. Solvents like ethanol added to LLCs form low-viscosity isotropic solutions (49).

Light can control LLCs' phase transition by promoting structural transformation. Gold nanorods absorb and convert light energy into heat, binding photochromic molecules (e.g., spiropyran (SP), spiroxazine (SOX), and spiropyran laurate (SPL)) to lipid molecules and exposure to UV irradiation disrupts lipid packing changing the system's lattice parameters (49).

Magnetic nanoparticles, like Fe_3O_4, improve solute mobility by creating a straight line during mesophase transport. Drug diffusion depends on water flow size, symmetry, and direction (60).

3.3.9. Rheology of M4 and M13

M4 and M13 CBD preconcentrates form o/w emulsions at specific aqueous dilutions; however, dialysis and lyophilization of the same o/w emulsion produce an amorphous solid dispersion (ASD) in the form of a liposomal organogel. Therefore, the rheological behaviour and parameters of the formulation system is a critical quality attribute that correlates with the system's composition, consistency, bioavailability, stability and compliance at the therapeutic level and influences drug entrapment at the technological level (107). Factors influencing the viscoelastic

rheological behaviour of o/w emulsions containing liposomes include particle fraction/concentration in the dispersed phase, shape, size, distribution, and surface charge. Emulsion composition, process conditions, environment and the linear relationships between shear rate and shear stress are also CQP that can cause Newtonian or non-Newtonian (pseudoplastic) behaviour in simple and complex fluids.

Thus, liposomal gels' more robust flow properties improve the handling and application of formulation and dosage forms, ensure prolonged residence time at the administration site, and provide a reservoir for sustained drug release. Viscoelastic properties and the flow behaviour of liposomal gels can predict gel formulations' deformability, spreadability and stability. Liposomes increase the viscoelasticity of gel matrices, imparting higher critical strain values and yield stresses for the liposomal gel than plain gels, making it more resistant to deformation. Coated liposomes within gels exhibit even higher elastic modulus, critical strain, yield stress, and cohesive energy, indicating the strengthening of the internal forces of the polymers (72). Incorporating liposomes into gel overcomes the liquid nature of liposomal dispersion and preserves the liposome's original structure (74).

SEM images of M13 show spherical liposomes. Spheres display shear-thinning behaviour at high shear rates. A particle can have non-spherical shapes (elongation), and particle surfaces can be irregular and unevenly convex, resulting in increased viscosity as solvent flow lines deflect around granular particles compared to symmetrical spheres of the same size. Large particle surface areas increase particle-particle interactions and inter-particle friction, significantly impacting concentration and shear rate. Spherical particle-particle interactions become less pronounced at high shear rates and show shear thinning behaviour.

Intrinsic viscosity [η] describes the particle shape. M4 shows a mixture of irregular spheres and elongated particles. Spheres and ellipsoids display shear thinning; however, ellipsoid suspensions have high viscosities at low shear rates, and spherical suspensions have high viscosities at high shear rates. Elongated/non-spherical particles have a larger surface and higher viscosity than spheres and are in disarray at rest. However, when shear is applied, these

ellipsoids align in the flow direction, reducing viscosity as opposed to spheres at higher shear rates.

Table 3.12: Yield Stress and Viscosity Results M4 and M13

Method	Yield Stress	Viscosity
M4 BLANK	42,22 Pa	6,402 ^{e05}
M4-CBD	36,59 Pa	4,629 ^{e05}
M13 BLANK	51,85 Pa	7,158 ^{e05}
M13 CBD	0.0 Pa	9,01 ^{e05}

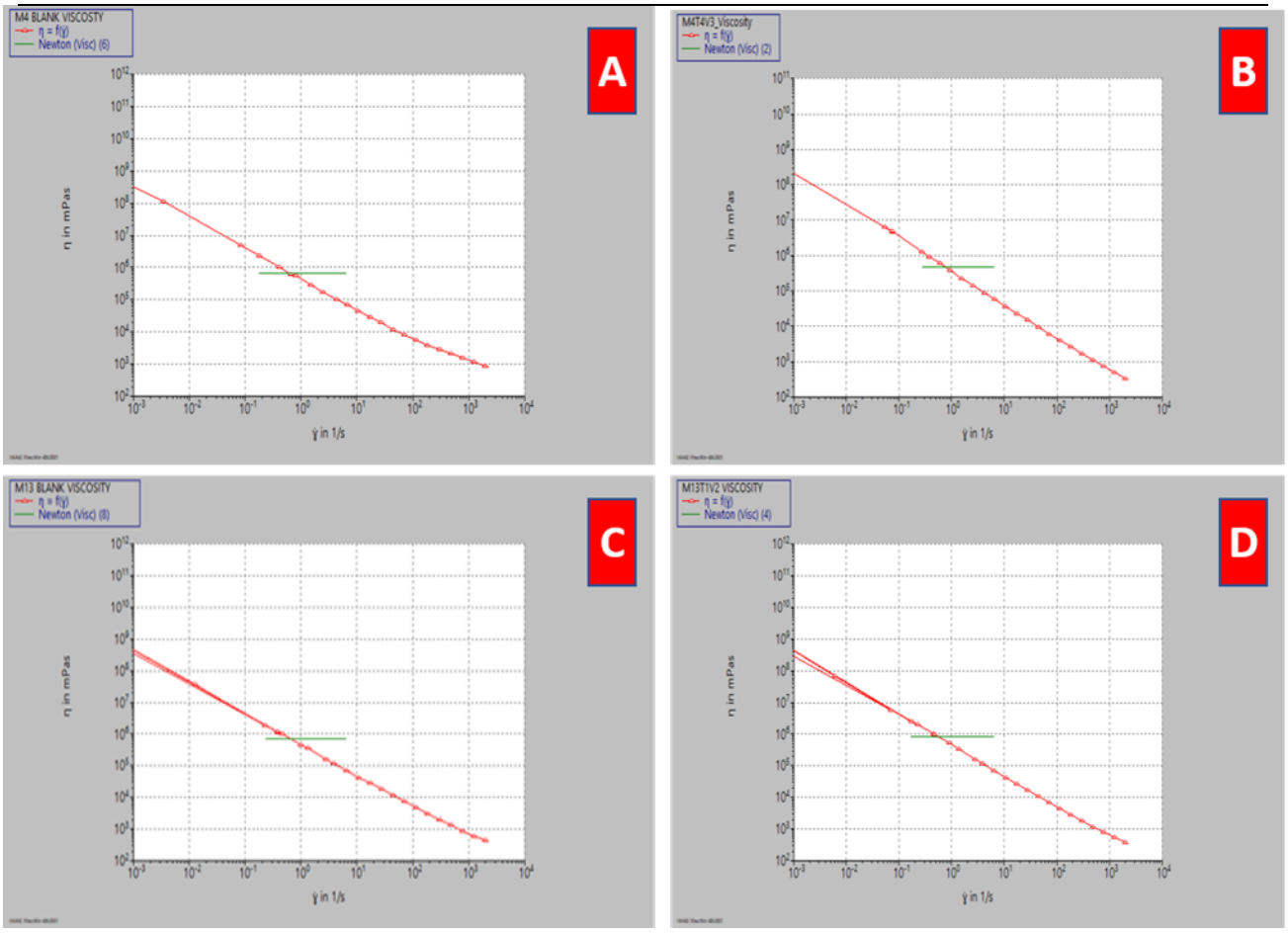

Figure 3.10: Yield stress deformations of ASD A); B) polydispersed liposomes containing CBD;(C); D) M13: monodispersed liposomes containing CBD

The rheogram for M13 reports viscosity as a function of shear rate, showing non-Newtonian, shear-thinning pseudoplastic, and thixotropic behaviour at ambient temperatures (23-37ºC). M13 has an average particle size of 51,48, Pdi of 0,208667, and a standard deviation of 0,011885 (Table 3.8). M13 has smaller, more uniform, spherical particles that deviate very little from each other and tend toward monodispersity. Small monodispersed articles have greater viscosity for a specified shear rate and a solid fraction, evident in the viscosity reading of 9,01 ^{e05} and visual observation of the preparation, i.e., the formulation looks like a paste. Flow behaviour: The corresponding yield stress values obtained were 0,0 Pa. Low or no stresses produce plastic deformation attributable to dislocations (Figure 3.10 D).

The Rheogram of M4 and M13 and their corresponding blanks (Figure 3.10 A, B, C, and D) illustrate the viscosity vs. shear rate function, where the viscosity declines with inclining shear rate and demonstrates non-Newtonian shear thinning behaviour (107,108).

Plastic deformation of materials results from dislocations, abrupt changes or movements in the atomic arrangement of a crystal lattice structure due to linear (one-dimensional) crystallographic defects or irregularities that cause atoms/particles to slide (glide or slip) over each other when a force or stress is applied. Slip describes arrays of directionally dependent, symmetrically identical slip planes and their corresponding axes (crystallographic planes) along which dislocation causes plastic deformation. Slip displaces large portions of one crystal lattice relative to another by moving dislocations on compact slip or glide planes. Dislocations can be sessile (immobile) or glissile (mobile). Mobile dislocations can be edge or screw dislocations. Atoms/particles that terminate in the middle of the crystal form an edge dislocation. Planes surrounding dislocation edges bend into orderly crystal structures on either side. (109,110).

A defect's geometry or dimensionality classifies crystallographic defects in amorphous solids. Defects include linear (one-dimensional) and non-linear (two-dimensional) surfaces, interfaces, boundaries, and volume defects like inclusions, cracks, voids, and pores. Crystalline imperfections include point defects (single/few atoms) at or around individual lattice points involving missing or additional atoms of empty/densely packed local atomic areas, regular

vacancies, crystal interstitials, and impurities. Significant defects in ordered structures form dislocation loops (109,110).

A critical resolved shear stress (CRSS), an external force applied in the direction of the slip, triggers the slip, which causes the gliding of sections of the crystal lattice, changing the material's geometry. Under load, a “weaker” grain will yield before a “stronger” grain; as it deforms, a stress concentration will build up in the more robust grain boundary between them. This concentrated stress will activate dislocation movement in the available glide plains (111).

Zeta potential changes, generated by particle repulsion, increasing hydrodynamic volume and viscosity at low shear rates, create particle-particle distances and facilitate an ordered particle arrangement. M13 has a low average Zeta Potential of -9,63444, indicating flocculation, coagulation, and possible incipient instability. The weak repulsion minimises the energy required when particles have a low to near-zero surface charge. Fine particle dispersions (<1 μm), sensitive to zeta potential changes, maintain a zero-shear viscosity because gravitational forces subordinate small and light particles, while Brownian motion dominates at low solid fractions.
The rheogram for M4 shows viscosity as a function of shear rate with results of non-Newtonian, shear-thinning pseudoplastic, and thixotropic behaviour at ambient temperatures (23-37ºC). The corresponding yield stress values obtained were 36,59 Pa. M4 has an average of 86,55125 nm, a particle size distribution of 0,492083, and a standard deviation of 18,04102 (Table 3.8). These results show that M4 has larger, less uniform particles that deviate from each other and tend toward polydispersity. Polydispersed nanoparticles have lower viscosity at specific solid fractions and shear rates, as seen in the viscosity reading of 4,629 ^{e05} and visual observation of the preparation.

Newtonian materials have constant viscosity despite changes in shear stress, but temperature affects it. The shear rate in Newtonian fluids is directly proportional to shear stress, and the function produces a straight-line graph. Newtonian liquids show an exemplary flow. According to the power-law model, if a liquid's flow index (n) equals 1, it is Newtonian, and if the flow index value deviates from 1, then it is non-Newtonian behaviour. The Power Law evaluates the behaviour of oils (Equation 5).

Oil types greatly influence the rheological behaviour of emulsions. Olive and coconut oil have a flow index that deviates from 1, i.e., 0.84 and 0.90, respectively, approaching non-Newtonian behaviour. However, other oils have flow indices very close to 1 and are Newtonian. The oils' viscosity depends on chain length, saturation, unsaturation, and the fatty acids' hydroxyl group (OH) location. Oils with long chains are very viscous. Castor oil has long carbon chains and thus a high viscosity because its main component, Ricinoleic acid, an 18-carbon fatty acid, has an OH-group at C12, a unique feature that makes it unusually polar with properties that deviate from other oils (59).

Solid complex fluids (e.g., polymer networks and emulsions) affected by yield stress have a structural skeleton that spans the entire volume of the system. The stress at which the structural skeleton breaks down is the yield stress and indicates the degree of deformation of a structured fluid. The related strain is the yield strain, which coincides with a peak value equal to the yield stress before plateauing to its equilibrium value. Below the yield stress, the fluid stretches like a spring and flows like a liquid above. A complex fluid only flows when applied pressure surpasses the critical yield stress value. Low shear rates applied to solid-like complex fluids below its critical strain cause strain hardening of the system as elastic elements stretch in the shear field. The structure collapses as the elastic elements approach their critical strain, causing shear thinning (strain softening) and consequent flow (82,83). The elastic modulus (G') represents the elastic behaviour of deformed material. The viscous modulus (G") indicates the flow of deformed material. After exceeding the critical strain (γ_c), G’ for all the gels decreases with increased applied strain until it reaches the breakpoint (γ_b), where the gel begins to flow (G’’ >G’) (112).

3.3.9.1 The Power Law

Equation 3.9: The Power Law Model describes Fluid Behaviour (2):

$\sigma = K \times n$

σ = Shear stress (Pa)

K = The consistency coefficient (Pa sn)

g = The shear rate(s-1)

n = The flow behaviour index (a dimensionless number)

where the emulsion displays:

$n = 1$: Newtonian behaviour

$n < 1$: shear-thinning behaviour

$n > 1$: shear-thickening behaviour

$n > 1$: shear-thickening behaviour

The flow index (n)) references the extent of shear-thinning due to pseudo-elasticity. Shear-thinning behaviour represents non-Newtonian flow because the viscosity is non-constant at a constant temperature and composition (Newton's law of viscous flow). Shear-thinning behaviour arises from the deformation of the polymer chains and their alignment in the flow direction. Liposomal gel matrices are more viscoelastic due to the rigidity of liposomes and have higher G' because the liposomes store the applied stress in their elastic components under applied shear and are more resistant to deformation.

Table 3.13: Power-law analysis of castor, coconut and olive oil (59)

Oil	Consistency index	Flow index	Confidence in fit (%)
Castor oil	705,6	0,98	99,4
Coconut oil	96,4	0,90	98,9
Olive oil	124,7	0,84	99,0

Coated liposomes increase gel matrices' viscoelasticity because they store applied stress more effectively in their elastic component than the noncoated liposomes, increasing the G' of liposomal gels. Liposomal gels containing coated liposomes are more resistant to breakdown caused by stress during transportation or handling. Pseudoplastic flow may result from the progressive rupture of the gels' internal structure by intensifying shear and subsequent reconstruction through the Brownian movement. According to the power law, n values smaller than (1) indicate non-Newtonian shear-thinning pseudoplastic flow behaviour. The lower n, the more shear-thinning.

Polymeric gel systems are typically non-Newtonian and exhibit shear thinning behaviour. Hybrid systems (emulsions, suspensions, and liposomal gels) exhibit non-Newtonian, thixotropic, pseudoplastic behaviour at ambient temperatures (23-37ºC) and have polydisperse character (73). Gels' thixotropic and pseudo-elastic behaviour favours specific semisolid systems because high shear rates enable the effortless flow of material on an application. Conversely, the material thickens at lower shear rates, regaining its original rheological properties and favourably gelling during storage. In liposomal gels with high shear viscosity, the yield stress is attributed to the liposomes, increasing the formulation's rigidity and making the gel more resistant to flow. Unmodified liposomes are prone to vesicle aggregation that leaks the encapsulated material. The liquidity of liposomal preparations limits administration routes and incorporation into various dosage forms. Semisolid liposomal formulations overcome these issues.

3.3.9.2 Particle size:

Dispersed phase concentration/volume fraction enhances viscosity. Fluids are Newtonian below particular dispersed phase concentrations and non-Newtonian above them.

Particles in a liquid are obstacles that increase viscosity and, hence, resistance to its flow. Increasing solid fractions increases particle collisions, creating friction requiring additional shear force.

Particles change liquids' physical and optical characteristics (e.g., viscoelasticity, density, and colour). A low particle volume fraction (“solid fraction”) induces shear-thinning, whereas a high particle volume fraction causes shear thickening. The extensive surface areas of microscopic particles increase viscosity and exhibit Brownian motion under shear pressures: surface charge, absorption, and hydration impact tiny particles. High shear rates rearrange particles for flow regardless of particle size, rendering viscosity irrelevant.

3.3.9.3 Polydispersity Index (Pdi)

Emulsions have a polydisperse character (113). Polydisperse suspensions have higher maximum packing densities and lower viscosities than monodisperse suspensions. The packing of binary mixtures of spheres is a function of diameter ratio and composition (Equation 2.2). The highest maximum packing fraction occurs with the random arrangement of large particles and the packing of small particles to fill the voids of an extensive particle system to minimise the gaps

in the whole system. The smaller particles lubricate bimodal particle size distributions. M4 has a significant standard deviation for particle sizes and a broad particle size distribution (Table 3.8). A more substantial and positive effect on the packing density occurs with a broader particle size distribution. Despite the low viscosity, polydisperse colloidal suspensions with bimodal distributions can have high yield stress values, as observed in the viscosity and yield stress results of M4.

3.3.9.4 Electrical charge

Large particles and agglomerates sediment under gravitational forces. Zeta potential controls agglomeration behaviour. Particles with low zeta potential stick together, favouring flocculation, whereas high zeta potential induces particulate repulsion. Particulate repulsion overshadows van-der-Waals forces of attraction by creating an energy barrier with a high surface charge that prevents particle proximity. The weak repulsion and minimum energy needed to maintain specific particle-particle distances in orderly particle arrangements come from near-zero surface charges.

The zero-shear viscosity plateau of spheres increases with increasing zeta potential in fluids with constant solid fractions. Low zeta potentials agglomerate large particles or high solid fractions and introduce yield points. If the solid fraction of the particles forms a three-dimensional network, yield stresses will apply. In contrast, high shear rates cause shear-thickening and high viscosities due to inter-particle repulsion by high zeta potential, affecting solvent interaction and inter-particle behaviour.

Lecithin–water dispersions and lecithin–oil emulsions exhibit pseudoplastic non-Newtonian behaviour. Lecithin–water dispersions have more pronounced pseudoplastic behaviour than the corresponding lecithin–oil emulsions because they only exhibit yield stress. Lecithin–oil, however, has a higher apparent viscosity than lecithin–water. In concentrated emulsions, the particles are close, resulting in strong interparticle interactions, making such systems highly viscous with viscoelastic behaviour and high yield stress resulting from noncontinuous phase crowding (1).

CHAPTER 4
DRUG RELEASE AND CELLULAR TOXICITY OF CANNABIDIOL NANOFORMULATIONS CONTAINING OLIVE OIL AND CASTOR OIL

4.1 Introduction

Drug release kinetics hinge on the matrix materials, the release medium and drug characteristics. A suitable LBDDS should protect the drug en route to the target site and only release it on arrival (38). Drugs like CBD with poor water-solubility and a short half-life display concentration-dependent toxicity, minimised with sustained-release formulations to reduce administration frequency. However, sustained-release ASD formulations can recrystallize within the dosage form and have trouble releasing the drug from the capsule mass or reaching the desired supersaturated state.

According to the Noyes- Whitney equation (Equation 3.1), micronization and drug dispersion within the ASD carrier increase the molecular levels' surface area and dissolution rate. Polymers assist by maintaining a high-supersaturation state, maximising drug absorption, and inhibiting phase separation, nucleation, and crystal growth. Reducing the supersaturation rate reduces recrystallization and optimizes the dissolution profile by modifying the release rate.

4.2 Drug Release

4.2.1. Drug Transfer Kinetics

Drug release occurs when drugs or solutes travel from their initial location to the polymer matrix's exterior rim, interacting with the aqueous release medium. Drug release patterns depend on the interplay between the solutes' physicochemical qualities, the material system's structural features, and the release environment—degradation, diffusion, and erosion move solutes principally inside a polymeric matrix (53).

Loew et al. described a kinetic transfer model for transferring poorly soluble drug molecules and small, mobile pharmaceutical nanocarriers (colloids, micelles, and nanoparticles) between liposomal carrier systems. Donor liposomes harbour several drug

molecules that pass directly to proximate acceptor liposomes on collision, with negligible exposure to the aqueous phase until equilibrium (Figure 4.1A). Drug diffusion occurs from one liposome to another through the aqueous phase (Figure 4.1B). The two mechanisms act simultaneously in drug transfer between donor and acceptor liposomes.

Due to proportionate rate constants and drug concentrations, low drug loading, and negligible drug aggregation within liposomes, both transfer methods exhibit simple exponential behaviour with first-order kinetics. The kinetics of intraliposomal flip-flops do not overlap (39).

Liposomal carrier efficiency improves by loading additional drug molecules into the liposome, increasing the attractive interactions and the rate constant for diffusion. Liposomes with high drug loads slow down the initial release of drug molecules when interacting with other highly loaded donor liposomes; then, as load decreases, the release accelerates, leading to sigmoidal behaviour. The direct transfer of drug molecules from one liposome to another requires the drug molecule to switch from the inner to the outer monolayer. Flip-flop time varies depending on whether the drug is amphiphilic, extremely lipophilic, or surface active. In symmetrical lipid bilayers, the rate constants for a drug molecule's movement from the outer to the inner layers and vice versa are identical (51).

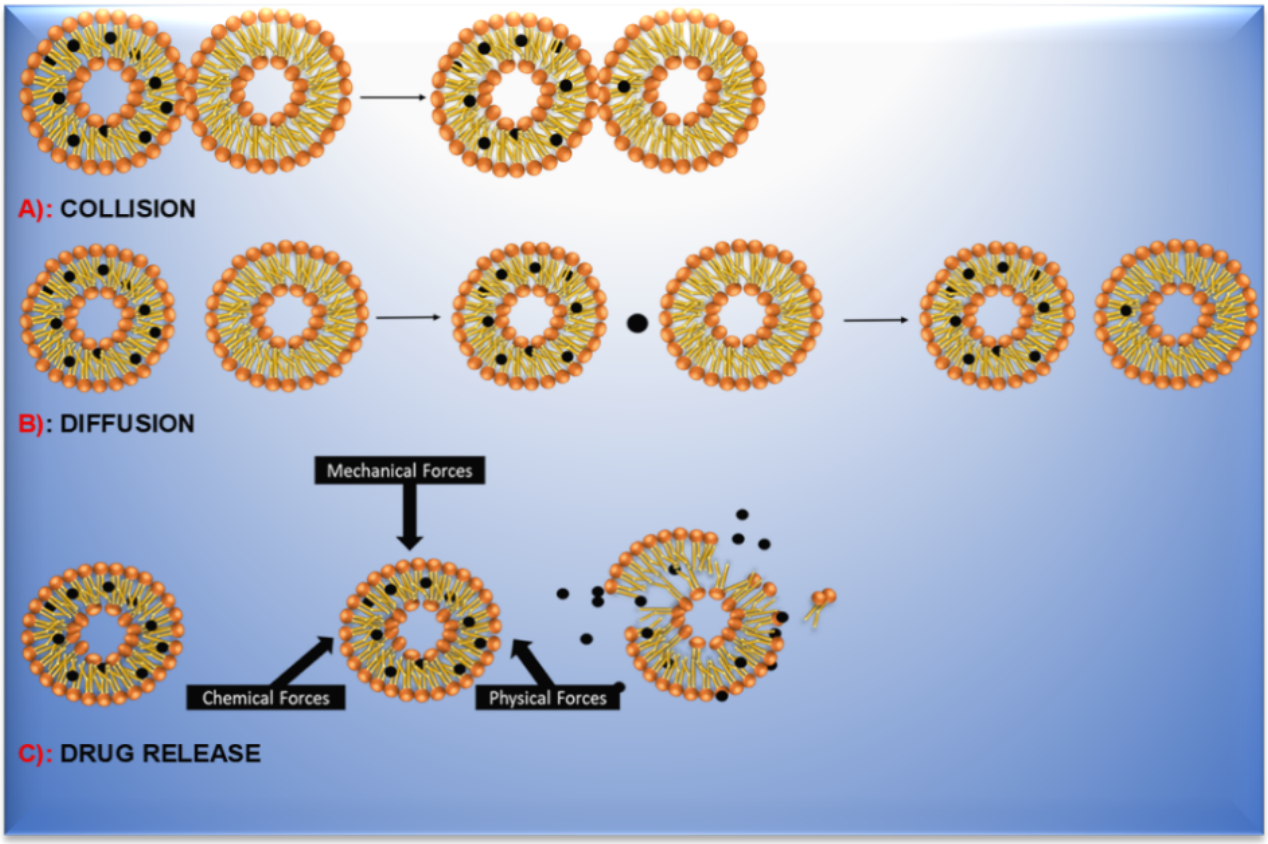

Figure 4.1: Release kinetics of drug molecules from liposomes **(38)**

4.2.2. Types of drug release

4.2.2.1. Diffusion

Polymeric matrices and ASDs facilitate sustained drug release and solute transport by diffusion (swelling and dissolution), degradation and erosion (114). ASD drug release mechanism is dissolution-controlled as the ASD carrier solubilizes in the dissolution medium, hydrating and dissolving the drug and inducing supersaturation in the drug-polymer system. The dissolved drug diffuses through hydrophilic and hydrophobic matrices or gelatinous networks according to their solubility in the dissolution medium.

Polymer properties influence swelling and dissolution, increasing or decreasing the release rate. The drug must diffuse through the gel layer to be released; therefore, polymer hydration, gelling, clumping, and agglomeration promote recrystallization that hinders or slows drug release and prevents the complete dissolution of non-ionic,

amorphous APIs. Polymer swelling increases drug and polymer mobility due to polymer relaxation, increasing release rates, and lengthening the diffusion pathway, decreasing concentration gradient-driven diffusion and drug release rates. The dominant mechanism will accelerate or decelerate drug release (67).

4.2.2.2. Dissolution

Polysaccharides like HPMC hydrolyze and dissolve in aqueous media due to solvent penetration, swelling, polymer chain disentanglement, and relaxation at extreme pH and temperature. Polymer breakdown causes mass loss without disrupting polymer chains. Polysaccharide matrices can diffuse or dissolve solutes (124).

4.2.2.3. Degradation

Degradable polymer chains scission into oligomers and monomers, while non-degradable polymers form "reservoir-" or "matrix-" type contrivances. Matrices rely on the concentration gradient, diffusion distance, and degree of swelling for Fickian diffusion-driven drug release. Reservoirs possess an inert membrane that controls the diffusion rate independent of the concentration gradient but relies on the polymeric membrane's width and permeability (124).

Biodegradable polymers in biological systems offer extended dosing and specific targeting, which improves patient compliance by reducing side effects. Biodegradable polymers contain labile ester-, amide-, and anhydride bonds predisposed to hydrolysis or enzymatic degradation in controlled delivery systems that offer extended dosing, and specific targeting improves patient compliance by reducing side effects. Degradation quantification determines the change in the mean molecular weight of the polymer over time. Surface-degrading polymers degrade at the outer surface of the device. Water ingress into the device, essential during hydrolysis, significantly affects degradation and release kinetics. Bulk polymer degradation occurs homogeneously throughout the material. In contrast, semicrystalline polymers degrade as water infuses into the amorphous regions, inducing degradation by the random hydrolytic scission of labile bonds, followed by the scission of the polymer chain in the second stage (114).

4.2.2.4. Erosion

Bioerosion is the loss of surface or bulk material from a polymeric dosage form, facilitating complete drug release upon contact with a biological system. By avoiding recrystallization in thermodynamically unstable ASDs, drug release by erosion improves solubility. Additionally, it does not require water absorption. However, erosion cannot release lipophilic, weakly water-soluble drugs from the dosage form.

4.2.3. The Solubility Advantage of ASDs

Solubility and permeability primarily govern drug absorption. ASDs promote solubility without decreasing membrane permeability, conferring a solubility advantage over poorly soluble drugs with a short half-life. ASDs methods of manufacture include spray-drying, solvent evaporation, or thermal processing, such as hot-melt extrusion. Sustained-release ASDs increase bioavailability by minimizing the administration frequency, preventing high toxic concentrations, and decreasing the medium's reprecipitation rate. Sustained-release ASDs are challenging to formulate because of Intramatrix recrystallization, low supersaturation states due to slow dissolution rates, and inefficient drug release due to drug-polymer gelling.

Equation 4.1: Solubility Advantage of ASDs **(67)**
Equation 4.2: Solubility Advantage of ASDs **(67)**

$$S = \int (crystal\ packing\ energy + cavitation\ energy + solvation\ energy)$$

$Crystal\ packing\ energy$ = energy needed to disrupt the lattice and remove the isolated molecules (endothermic).
$Cavitation\ energy$ = energy needed to perturb water and create voids that accommodate the drug molecule (endothermic)
$Solvation\ energy$ = energy resulting from solvent-solute interactions (exothermic)

Solvation and crystallization reactions can either absorb or release energy. Crystals form when atoms or molecules precipitate from a solution into a highly organised solid structure

via a two-step process. As molecules integrate into the crystal lattice, energy is absorbed (endothermic), reducing the system's free energy. Crystal formation releases energy (exothermic) during crystallization (125). Heat (enthalpy) of crystallization is the change in heat (heat absorbed or released) when one mole of substance crystallizes.

Nucleation begins with the materialisation of particulate matter that crystallises when particles lodge into open anomalies such as cracks and pores, forming layers on the crystal surface that increase particle size.
ASD formulations can overcome poor drug solubility. Crystal packing energy has the highest enthalpy. This crystal packing energy disrupts the drugs' crystalline lattices and isolates molecules from the bulk crystal, releasing exothermic energy that promotes solvent and solute interaction and solubilization. Solvation energy thus enhances ASD solubility in thermodynamically unstable formulations.

Drug-ASD dispersions in aqueous media release stored potential energy, introducing excess energy into the system, creating a supersaturated state where solubility exceeds equilibrium, and the solute separates from the solution. Conversely, drug recrystallization reduces the system's free energy, overcoming activation energy during dissolution and restoring equilibrium. In ASDs, drug dispersion within the carrier increases surface area and dissolution rate at the molecular level. The Noyes Whitney equation (Equation 3.1) describes surface area expansion and dissolution rate increase on molecular drug dispersion in ASDs.

When solute diffuses from the bulk solution to the crystal interface, integrating into the crystal lattice, nuclei expand into crystals. The activation energy required for nucleation is proportional to the degree of supersaturation and interfacial tension. Nucleation and crystal formation (stage II) only occur when the activation energy exceeds the critical supersaturation threshold (C_{min}). Below C_{min}, the system stays metastable, and concentrations of nucleation and crystal formation diminish.

Due to the high free energy level relative to crystalline drugs, amorphous drugs recrystallize into more thermodynamically stable crystalline forms that negate any solubility advantage an ASD provides, decreasing bioavailability (stage III). ASDs have a solubility advantage, provided absorption occurs more rapidly than nucleation and growth. A dissolution rate below the critical supersaturation level (C_{min}) will maximize absorption by preventing nucleation and growth.

4.2.4. Sustained drug release in ASDs

Mechanisms in sustained-release ASD preparations depend on drug and polymer properties during dissolution. Drug release categories include diffusion (associated with swelling and dissolution), degradation or erosion. Hydrophilic and hydrophobic matrices release drugs by diffusion. Drug release in polymeric systems can decrease or increase depending on their solubility in the dissolution medium.

Swelling increases drug release by increasing the drug's and polymer's mobility. When a polymer swells, the length of the diffusion pathways increases, decreasing the concentration gradient that drives the diffusion process.

Drug release creates a porous network that improves drug solubility and dissolution in hydrophobic polymers that do not degrade or dissolve in aqueous media via aqueous pores or diffusion through the polymer carrier after the drug contacts the dissolution medium.

Drug release by carrier erosion and degradation does not require water uptake, eliminating recrystallization issues. Depending on the polymer, erosion can occur on the surface or inside the dosage form. Erosion refers to the partial loss of the polymer bulk, while degradation cleaves or scissions chains into oligomers and monomers.

Intramatrix recrystallization negates the solubility advantage provided by the controlled-release ASDs. Amorphous drugs are more hygroscopic than their crystalline counterparts, and ASDs are moisture-sensitive. Sustained-release ASDs exposed to

aqueous dissolution media for prolonged periods absorb water. Water ingress plasticises ASDs, causing a glass-to-rubber transition by decreasing the T_g and increasing molecular mobility within the dosage form, which results in recrystallization inside and on the outer surface of the dosage form. Temperature favours nucleation by promoting molecular mobility.

Polymer innovations, hydrophobic excipients, and sustained-release formulations reduce recrystallization in ASDs by anti-plasticization and provide a parachute effect. Viscous polymer gels impede molecular rearrangements and interactions and sustain high supersaturation conditions by limiting phase separation, nucleation, and crystal formation, optimising drug absorption. Furthermore, increased gel viscosity enhances activation energy, van der Waals contacts, and hydrogen bonding. On the other hand, hydrated polymers promote recrystallization and restrict drug release. As the drug and polymer gelate at a specific moisture level and time interval, formulations that prevent the attainment of this critical moisture level enhance drug delivery by reducing recrystallization.

Hydrophobic excipients or eroding systems that lower the dosage form's hydration reduce drug recrystallization in their device. Drugs sensitive to recrystallization and acidic or enzymatic chemical instability in sustained-release ASDs benefit from hydrophobic and water-insoluble polymers as these have a static contact angle greater than 90 degrees, thus preventing interaction with water and release through erosion or diffusion (56) (68).

Sustained release by ASDs is a diffusion-controlled mechanism. Sustained-release ASDs have a lower maximum serum concentration (C_{max}) and longer T_{max} than immediate-release LBDDS, reducing reprecipitation and improving bioavailability (70). The slow dissolution rate and the gradual increase in supersaturation sustain drug release over time. As a result of their slower dissolution rate, sustained-release formulations exhibit less supersaturation (i.e., a lower maximum kinetic solubility) than immediate-release formulations. Faster supersaturation maximises kinetic solubility and sharpens de-supersaturation by recrystallization. The degree of supersaturation does not decline drug

concentration due to diminished nucleation and crystallization rates because of the slower rate of supersaturation. Moreover, low supersaturation depends on the degree of polymer solubility in the dissolution medium. HPMC sustains drug release when incorporated into the ASD as a matrix-forming agent.

4.2.5. The mathematical drug release model for polymeric systems

Solute transports out of polymeric matrices by diffusion, degradation, and erosion if matrices maintain constant proportions and physical properties during drug release (i.e., degradation or mass loss of bulk materials). Diffusion matrix devices are simple, controlled drug delivery systems that homogeneously disperse drugs and are preferred over reservoir devices when manufactured on a large scale. Drug-related factors influencing release kinetics include dose/drug content, drug solubility, particle size and shape, molecular weight and size, physical state, and diffusion in the polymer and medium. Polymers can be water-soluble or water-insoluble. Polar polymers interact with aqueous media and generate sufficient energy to disperse polymer chains from the glassy state. Drug diffusion through the polymer increases with a high polymer content, dimension proportionally, and the interaction between the polymer and solute. Different degrees of polymer substitution create different hydration rates, reducing viscosity grades. Different proportions of polymers in matrices can vary the release profile from a matrix device, e.g. an increase in polymer proportion or content increases gel viscosity and the diffusional path length, decreasing the drug's and drug's effective diffusion coefficient release rate. The polymer particle properties influence particle contact points, porosity, viscosity, and tortuosity of matrices. There is an increased resistance to the infiltration of the aqueous medium when the bulk density increases as the porosity decreases (115).

Fick's laws of diffusion apply to crystalline drugs solubilised, dispersed, and released from polymeric matrices by diffusion-controlled mechanisms. The mathematical model of Fick’s law proposes solute transports from polymeric matrices in which the polymer relaxation time (*tr*) is more significant than the solvent diffusion time (*td*). When *tr* approximates td, the macroscopic drug release becomes non-Fickian. Solute diffusion,

polymeric matrix swelling, and material degradation drive solute transport from drug-containing polymeric matrices. The challenge, however, is preventing recrystallisation and releasing the drug efficiently (114).

Fick's first law says that diffusion rate is proportional to the difference in concentration and surface area and inversely proportional to membrane width for fluids and gases. Fick's first law predicts particle dispersion across a concentration gradient from high to low concentration only for steady-state systems when flux entry equals flux exit. Only the concentration gradient drives composition, which does not vary over time. Fick's first cannot estimate diffusion coefficients from composition profile changes over time without a time parameter.

Fick's first law defines particle dispersion across a concentration gradient from high to low concentration only for systems in a steady-state condition, i.e., flux entering must equal flux exit. The concentration gradient is the only driving factor, and the composition does not vary over time. Fick's first cannot estimate diffusion coefficients from composition profile changes over time because it lacks a time parameter (120).

Fick's second law explains the non-steady-state diffusion process, i.e. the change in concentration at a particular position with increasing annealing time (110). Fick's second law predicts how diffusion alters concentration over time in systems with unstable or unequal conditions and describes the substance's diffusion rate across the unit area of the surface/membrane as proportional to the concentration gradient (53). Fick's second law provides a mathematical model of diffusion for drug release for slab-like devices, described by:

Equation 4.3: Fick's second law of diffusion for drug release from slab-like devices (early-time approximation) **(114)**

$$\frac{M_t}{M_0} = 4\left(\frac{Dt}{\pi h^2}\right)^2$$

Where:

M_t = quantity of drug released at time t

M_0 = the total mass of drug-loaded into the device

D = the drug diffusion coefficient in the polymer matrix

π = 3.14

h = device-width

The equation is a derivative of Fick's second law of diffusion for an early-time estimate for the first 60% cumulative release in slab-like devices, i.e., 0 ≤Mt /M0 ≤ 0.6.

Equation 4.4: Fick's second law of diffusion for drug release from slab-like devices (late-time approximation) **(114)**

$$\frac{M_t}{M_0} = 1 - \left(\frac{8}{\pi^2}\right) \exp\left[(-\pi^2 Dt)/h^2\right]$$

The equation is a derivative of Fick's second law of diffusion for the late-time estimate for the remainder of the drug release, i.e., 0.4 ≤Mt/M0 ≤1.0.

Table 4.1: Kinetic drug release models and their application in vitro release studies (115,116)

Drug release models	Application in vitro
Baker and Lonsdale	Drug release from spherical matrices
Cooney model	Spheres and cylinders undergoing surface erosion
Gallagher and Corrigan model	Percentage of drugs released from the biodegradable polymeric systems
Gompertz model	The in-vitro dissolution profile
Higuchi model	Drug release from matrices
Hixson -Crowell cube root law	drug release from systems with altered surface areas and particle diameters
Hopfenberg model	Drug release from surface-eroding polymers
Korsmeyer and Peppas	Analyze Fickian and non-Fickian drug release from nonswelling and swelling polymeric delivery systems.
Weib model	drug dissolution and release from dosage forms express the accumulated fraction of drug 'm' in solution at the time 't'.

The Higuchi and zero-order models define transport and drug release constraints in an oral controlled drug delivery system and aid device optimization and drug release mechanism comprehension.

Zero-order release kinetics models the behaviour of drug delivery devices (dosage forms) that release drugs consistently regardless of concentration, minimising fluctuations in drug plasma levels. The cumulative drug release vs. time plot yields a linear slope (115). Equation 4.5: Zero-order release kinetics

$Q = Q_0 + K_0t$

Where

Q = the amount of drug released or dissolved

Q_0 = the initial amount of drug in solution (usually zero)

K_0t = the zero-order release constant.

First-order release kinetics explains a concentration-dependent system release (125)

Equation 4.6: First-order release kinetics: concentration-dependent release

$dC / dt = - Kt$

K = first-order rate constant expressed in units of $time^{-1}$

Alternate expression of the equation:

Equation 4.7: First-order release kinetics: log cumulative of % drug remaining vs. time

$Log\ C_t = Log\ C_0 – kt / 2.303$

Where

C_0 = the initial concentration of the drug

C_t = the concentration of drug in solution at time t

The equation predicts a first-order dependence on the concentration gradient ($C_0 - C_t$) across the bulk liquid and the static liquid layer next to the solid surface. The log cumulative of % drug remaining vs. time yields a straight line with a slope of –K/2.303.

Higuchi Model explains the release of water-soluble and poorly soluble drugs incorporated in semisolid and solid matrices by the equation (115):

Equation 4.8: Higuchi Model

$Q = A\,[D\,(2C - Cs)\,Cs\,t]^{1/2}$

Q = quantity of drug released in time t per unit area A

C = the initial drug concentration

Cs = drug solubility in the media

D = diffusivity of the drug molecules (diffusion coefficient) in the matrix

Based on the Fickian diffusion Equation $Q = KHt^{1/2}$, the Higuchi model calculates the cumulative percentage of drug release from the insoluble matrix as a square root of time, where the cumulative drug released is directly proportional to the square root of time.

4.2.6. Burst Release

A controlled-release formulation in a release medium releases an initial drug surge before reaching a stable profile. Burst release accelerates initial drug delivery, shortening the device's lifespan and half-life by increasing metabolism, excretion, and rapid activity loss before reaching therapeutic concentrations, increasing the dosing frequency and the possibility of local/systemic toxicity. Favourable burst release triggers rapid or high initial delivery rates needed for targeted delivery, pulsatile or burst release, followed by tapering off the drug in long-term controlled release devices. However, burst release is unpredictable, inadequately controlled in short-term controlled-release devices, and therapeutically and economically wasteful.

Reservoir drug delivery devices envelop the drug molecule with an inert membrane. During the storage of these reservoir systems, the diffusion of drug molecules to the membrane surface saturates the enveloping membrane. The drug molecules on the membrane's surface are immediately released on contact with the release medium, causing a burst effect. After that, the drug diffuses through the membrane at a steady, controllable rate, achieving zero-order or continuous drug delivery. Capsule coating flaws and the reservoir systems' storage effect can cause a significant burst release. Polymers

and copolymers take time to set, leaving some drug molecules unencapsulated and enabling the " free drug " to burst release" (117).

Swellable and non-swellable matrix systems burst release from the matrix or monolithic formulations like reservoir-type devices due to heterogeneous polymer matrices manufacturing processes, drug properties, and percolation-limited diffusion. Drugs that migrate to the polymer matrix surface during drying and storage become trapped in a heterogeneous distribution and burst release on contact with the release medium. Burst release proportions and properties from matrices depend on solute size, the extent of drug loading and the type of polymeric system.

Drug dissolution in matrices precedes diffusion through the swollen, porous gel network toward the release medium. The diffusion and migration of drugs occur during drying and storage or by water convection, resulting in higher concentrations at the surface and uneven distributions across the gel. Uneven drug distribution can provide consistent release by loading higher drug concentrations toward the centre of the device. Despite uniform dissolution and drug dispersion in matrices, release rates dwindle with time because increased diffusion distance from the centre of the device hinders drug diffusion. Increasing the concentration gradient in multilaminate devices could overcome diminishing release rates to achieve zero-order release.

Cracks, pores, and fissures formed during the synthesis of polymeric matrices contribute to burst release from matrices, especially in solvent evaporation, where removal of the organic solvent increases matrix porosity. The drug molecule's chemical and physical structure affects the burst release in controlled release systems and systems with low molecular weight solutes and large molecules like proteins and peptides. Highly soluble LMW solutes travel easily through the porous matrix before swelling occurs. The burst release of protein and peptides occurs through surface adhesion and desorption. LMW drug molecules burst release via percolated limited diffusion where solute molecules connected to pores freely diffuse faster than isolated solute immobilised by the matrix.

The immobilised solute can only diffuse if hydrolytic degradation of the matrix increases the pore size upon hydration (117).

The ideal controlled release system should carry high drug loads without burst release. Triggered burst release occurs by changing the device's chemical environment or rapid shrinkage of gels at high temperatures. Burst release avoidance includes extracting the drug from the surface before in vivo application, using double-walled microspheres composed of inert erodible polymers and surface modification by coating the drug-loaded matrix with an external layer of polymer (117).

CBD has biological effects in conditions of pain and inflammation. Pain suppresses the vagus nerve responsible for gastrointestinal secretion and motility, reducing disintegration and dissolution and impairing the absorption and bioavailability of standard, orally administered medications. Dissolution and disintegration, however, are independent of gastrointestinal secretion and motility. The crucial rate-limiting step for drug absorption and bioavailability is drug solubility. CBD, a BCS Class II drug with limited solubility, undergoes slow dissolution and absorption over a lengthier period than BCS Class I drugs. It presents more formulation problems than highly water-soluble drugs, affecting its stability in gastric fluids and bioavailability.

4.3 Materials and Methods

4.3.1. Materials:

Consumables procured from Sigma-Aldrich St. Louis, MO, USA, included cell culture assays, PBS tablets, DMEM, RPMI, FBS, DMSO and penicillin-streptomycin antibiotics. The solvents (methanol and ethanol) used were of analytical grade.

4.3.2. Methods:

The drug release profiles of formulations M4 and M13 were evaluated over 48 hours at 37°C in PBS drug release buffer at pH 1.2 and 7.4. Weighed lyophilized pre-concentrate media (0,5 g) loaded into HPMC size 00 vegan capsules were submerged in the pH-adjusted PBS (5 ml) and agitated in an orbital shaking incubator (YIHDER LM-530,

YIHDER Co., Ltd., Taipei, Taiwan) to simulate gastrointestinal tract motility. Aliquots (1 ml) of dissolution media were extracted at t = 0, 0.5, 1, 2, 3, 4, 6, 7, 24, and 48 h and replaced with equivalent volumes of dissolution media to keep sink conditions constant.

4.3.2.1. HPLC analysis of CBD nanoliposomes in simulated gastric fluid

0.5 g of CBD loaded into an HPMC capsule, placed in 0.5 ml of dissolution media and diluted with 2 ml of mobile phase (85:15 HPLC grade methanol/distilled water) were analysed using HPLC. Sample quantities retrieved were too small for UV Spectrometer or nanophotometer analysis; therefore, HPLC quantified CBD, with the mobile phase flowing through a C18 column (settings: rate 1,0 ml/min; detection 220 nm). Lipid or capsule residue in samples was removed by filtering twice with 0,22 µm filters, producing a clear fluid free of particulate matter.

Standard solutions preparation for HPLC analysis of released CBD

External calibration standards use known amounts of CBD (pure analyte) to create dilutions to calibrate the instrument's sensitivity to the analyte (Table 4.2). These calibrated results serve as a reference standard for comparing unknown sample values. Comparing peak area height or spot intensity to a reference standard of the analyte of interest allows for quantification of the sample.

An internal standard compensates for changes in the sample or analysis that affect the reproducibility of the injected sample. These changes can result from changes in extraction efficiency, detector response due to sample loss, fluctuations in the sample, or detector response due to different flow rates. The internal standard is a substance like the analyte (paracetamol) introduced consistently to the blank, standards and samples, ensuring the standard-to-analyte ratio remains constant (118).

External Standards: Prepare a CBD stock solution (1 mg/ml) by dissolving 40 mg of CBD in 40 ml methanol

Internal Standard: Prepare a paracetamol stock solution (1 mg/ml) by dissolving 40 mg of paracetamol in 40 ml methanol

Using the equation $C_1V_1=C_2V_2$, calculate the different concentrations of CBD solutions as an external standard for the HPLC analysis. The total volume of each aliquot is 5 ml.

Table 4.2: External standard dilutions

Concentration	CBD stock solution (1 mg/ml)	Methanol ad	Total volume
1,0	5 ml	0 ml	5 ml
0.8	4 ml	1 ml	5 ml
0,6	3 ml	2 ml	5 ml
0,4	2 ml	3 ml	5 ml
0,2	1 ml	4 ml	5 ml
0,1	0 ml	5 ml	5 ml

4.3.2.2. Cell Culture Proliferation Studies

Rationale for the choice of cell cultures used in the cell study

Human Embryonic Kidney cells transfected with sheared adenovirus 5 (Ad5) DNA mutated into the highly efficient, adaptable human cell line, HEK293, the second most used human cell line in research, the first being HeLa. HEK293 cells are a robust, low-maintenance cell type that divides fast, doubling every 36 hours on average. HEK293 cells are valuable in interaction investigations, cancer research, vaccine development, recombinant protein production, protein expression, signal transduction and transfection. Experimental results obtained from HEK293 are highly reproducible; however, when cultured over an extended period (more than 13-20 passages), their growth rate and translation efficiency deteriorate, making experimental results unreliable; it is advisable to restart with freshly thawed stock for quality results.

The semi-adherent HEK293 cells, cultivated in suspension or as a monolayer, need a 37°C humidified incubator with 5% CO_2 and a diet of high-glucose media such as Dulbecco's Modified Eagle's Medium (DMEM), supplemented with Fetal Bovine Serum (FBS) and a broad-spectrum antibiotic like Penicillin-Streptomycin-Glutamine to prevent common bacterial infections. Any human cell line risks contamination with human-specific viruses, a disadvantage mitigated by meticulous aseptic techniques (119,120).

NIH3T3 cells are mouse embryonic fibroblasts (MEFs) immortalized from a Swiss mouse embryo. They are easy to culture and maintain, making them suitable for various cell and molecular research applications. Fibroblasts are mesenchymal cells that produce extracellular matrix components, primarily collagens type 1. Universal fibroblast cells differentiate into lineage-specific and specialized cells that support the topography of their residence organ. Fibroblasts are heterogeneous, with universal and specialized subtypes and activated fibroblasts in diseased states in the same tissue—Fibroblast morphology consists of predominately elongated ‘spindle-shaped and more giant ‘cube-shaped cells. Fibroblasts are crucial to the inflammatory, proliferative, and regenerative phases of wound healing. Proto-myofibroblasts are reversible fibroblasts that may either undergo apoptosis or return to the normal phenotype without α-SMA expression. Myofibroblasts, a highly contractile cell type, express alpha-smooth-muscle-actin (α-SMA) upregulate fibronectin and collagen. Primary cilia in cells are microtubule-based organelles anchored to the cell membrane that transmit mechanical and chemical signals, activating fibroblast transformation into proto-myofibroblasts and myofibroblasts via the TGF-β signalling pathway. Primary cilia determine cell migration, wound closure, cell proliferation, differentiation, tissue development, and homeostasis, leading to severe diseases when disrupted. The long-term propagation of commercially available NIH3T3 may have homogenized the cell population, as more proliferative ones may have outcompeted slower proliferating fibroblasts(121).

Fibroblasts are the most abundant cell type in connective tissues, including the mammalian heart, where they maintain electrical, chemical, and biomechanical responsiveness. Fibroblasts respond to external stimuli and play a crucial role in wound healing, angiogenesis, and tissue regeneration, making them attractive for biological studies.

3T3 embryonic mouse fibroblasts are the most often utilized cell line for toxicity testing due to their well-defined, steady growth rate and universal acceptance of the neutral red uptake (NRU) assay, a standard approach for acute/routine toxicity testing, which estimates starting dosages for oral systemic toxicity studies in rodents, and the in vitro

cell transformation assay (CTA), which investigates the carcinogenic potential of substances. In biological and toxicological research, the 3T3 cell line examines bacterial toxins, antioxidants, medication toxicity, e-waste leachate, nanomaterials, and electromagnetic radiation.

It can also evaluate mitochondrial toxicity. Mitochondrial shape, distribution, function, and susceptibility to toxicants vary considerably between species, which may be relevant for assessing mitochondrial toxicity. According to a study, 3T3 fibroblasts from mice are more susceptible to substances rich in polyphenols than human epithelial and endothelial cells, suggesting caution in choosing research participants. Their remarkable sensitivity in biological and biomedical applications results from their excellent response to external stimuli, principally attributable to the cardiac fibroblasts scattered throughout connective tissue (122).

Cell viability and toxicity of nano-formulations M4 and M13 used NIH3T3 fibroblasts cultured in RPMI and HEK293 kidney cells cultured in DMEM, and penicillin/streptomycin (1%) and FBS (10%) served as a growth medium for the cell lines (Cellonex, Johannesburg, South Africa).

The single Pipetted, spun, and pelleted cells were centrifuged (1500 rpm; 5 minutes). After discarding the supernatant, the pellets were re-suspended in 1 ml of their growth fluid and separated by automated pipetting. cell NIH3T3 and HEK293 suspensions, incubated in T25 culture flasks (37°C, 5% CO_2, humid conditions), were harvested on reaching ≥90% confluence under microscopic visualization. Harvested cells were flushed with trypsin for 5 minutes to dislodge them from the surface of the T25 culture flasks. Trypsin action was halted by adding PBS to prevent cell damage.

The suspension was diluted based on the pellet size. This pelleted cell suspension, mixed with 0,4% trypan blue stain/PBS in a 1:1 ratio, was left standing for 3-5 minutes at room temperature. Exceeding the time range would have reduced viability counts by inducing cell death. The trypan blue-cell suspension mixture was dropped onto a haemocytometer

and counted separately under a microscope for viable (unstained) and nonviable (stained) cells. Multiplying the total number of viable cells by the trypan blue dilution factor (x2) gave the total number of viable cells/ml of the aliquot. Adding the non-viable to the viable cells and multiplying it by 2 gave the aliquot total number of cells/ml (122).
The formula used to calculate viable cell percentage:

Equation 4.9: Percentage of Viable cells

$$\frac{Total\ number\ of\ viable\ cells/ml\ \ of\ aliquot}{Total\ number\ of\ cells/ml\ of\ aliquot} \times 100$$

HEK 293 kidney cell culture and NIH3T3 each used a separate 96-well plate containing a final 100 µl/well volume. Triplicate treatment of the experimental cells with 10 µl of the experimental formulations M4 and M13 produced treatment concentrations over a range of serial dilutions (1; 0.5; 0.25; 0.125; 0.0625; 0.03125; 0.015625; 0.0078125 µg/mL) in PBS (0.2% DMSO) and the pure CBD dissolved in methanol used as a comparator. The harvested cells density was 3.0 × 104, as calculated; 102 µL of HEK 293 kidney cell culture and 133 µL of NIH 3T3 fibroblast cell culture seeded for incubation (37°C, 5% CO_2, humid conditions) over 24 hours allowed the cells to stick to the well plates. Blank wells contained only solubilizing agents and a growth medium. MTT solution (10 µL; 5 mg/mL) pipetted into each well and incubated for 4 hours (37°C, 5% CO2, humid) formed formazan crystals. After 24 and 48 hours of incubation, the "MTT Cell Proliferation Kit I (Roche, Basel, Switzerland)" was used to assess mitochondrial metabolic activity and cell growth to detect toxicity (128). PBS was a positive control, and 5FU was the negative control.

Afterwards, the formazan crystals were dissolved in 100 µL of solubilizing agent (acid-isopropanol; 0.04 N HCl in isopropanol), followed by overnight incubation (37°C, 5% CO_2, humid conditions) and microscopic confirmation of solubilization of the purple formazan crystals. An “ELISA multimodal microplate reader (Victor X3, PerkinElmer, Waltham, MA, USA)” set to a wavelength of 570A (limits: between 550-600 nm and a reference

wavelength at 690A (limits: ≥650 nm) measured the spectrophotometric absorbance of the samples.

4.4 Results and Discussion of *In Vitro* Release Studies

4.4.1. Dosage Form

A clear two-piece Hydroxypropyl methylcellulose/Hypromellose (HPMC) capsule made a suitable dosage form for the oral delivery of the SELFs M4 and M13. The filled capsules had no pinholes, leakage, distortion or discolouration (123). The phospholipid organogel formulation M4 and M13 formed an amorphous solid dispersion (ASD), a semi-solid filling that can liquify under temperature changes, causing content leakage due to distortions and softening of the capsule shell. Therefore, the two-piece capsule must have a self-locking feature with a positive closure to prevent the involuntary separation of capsules. The capsule must have rim grooves, indentations, and tapered rims to lock capsule ends together and prevent premature opening, splitting, and denting after filling. Drug bioavailability from filled capsules is better than that of compressed tablets because altering drug formulation properties during capsule manufacture is rarely necessary. Also, capsules have relatively large surface areas, which enables quicker drug dissolution and absorption on exposure to gastrointestinal fluids. Moreover, formulation filling, tightly enclosed by the capsule's shell, protects the drug from light, oxidation, moisture, and physiological fluids, improving drug stability (124).

Once filled, the ASD will solidify on cooling or return to its resting state in the capsule, forming a solid plug. Sealing the intersection between the cap and the body with a sealing liquid (“banding”) is crucial to avoid the leakage of filling material. Air vents included in rugged capsule design prevent pressure build-up during production and filling, enabling air to escape, thereby mitigating the risk of capsules bursting or re-opening after closure. Liquid capsules, however, exclude air vents to prevent leakage before sealing. Liquids and semi-solids can accurately and uniformly fill hard capsules if formulation rheology is compatible with the liquid pumping capacity of the filling machines. Liquid filling of capsules improves the uniformity of fill weight and content, although careful handling of low-viscosity liquids is required to prevent spillage of filled capsule bodies (124).

HPMC, a naturally occurring viscolizing polymer produced by chemically modifying purified cotton linter or wood pulp cellulose, is safe for human consumption (98). HPMC is a versatile rate-determining polymer ideal for producing sustained-release drug carrier systems and coating, emulsifying, thickening, and stabilizing various pharmaceutical formulations. HPMC capsules are inert hydrophilic polymers with no ionic charge and a physical and mechanical strength capable of tolerating various environmental conditions. HPMC, an alternative to animal-derived gelatin capsules, excludes challenges like drug incompatibility, transmissible spongiform encephalopathy (TSE), and bovine spongiform encephalopathy (BSE) and gelatin crosslinking and has broad acceptance among populations with dietary preferences/religious restrictions (125).

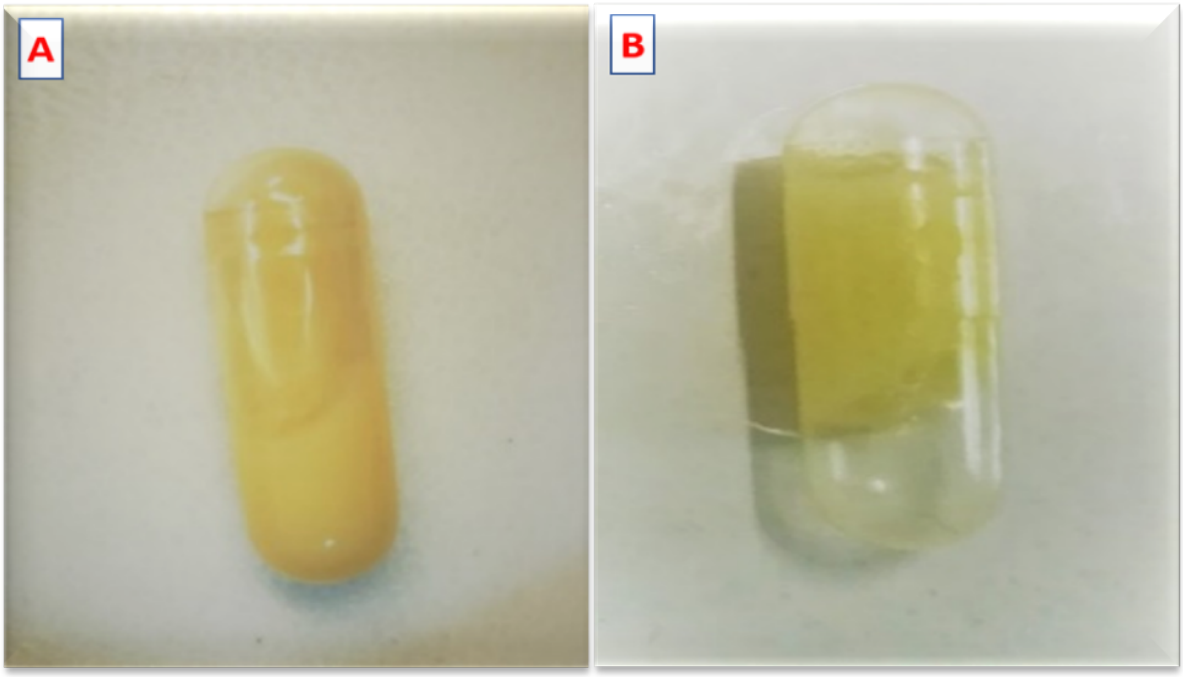

Figure 4.2: HPMC-filled capsules with (A) M4 Olive Oil; (B) M13 Castor Oil

Liposomes can be encapsulated either in hard HPMC capsules or soft gelatin capsules. Hard capsules are odourless, tasteless, easy to swallow, hydrating in the mouth, mask odours, and come in various colours. Capsules, preferable for formulations with a bitter taste, low compressibility, and slow dissolution, must be robust enough to hold and deliver

the required drug dose and provide a reproducible release and bioavailability. Hard HPMC capsules are convenient for the direct fill of actives with no or few excipients or for actives that cannot granulate for tabletting (33).

Depending on the grade, HPMC is insoluble in acetone, chloroform, 95% ethanol, ether and hot water, but cold water solubilizes HPMC into a viscous colloidal solution capable of reversible thermal gelation. HPMC is soluble in mixtures of dichloromethane with ethanol or methanol, propan-2-ol, water and alcohol, aqueous acetone solutions, and organic solvents. HPMC browns between 190-200°C, chars between 225-230°C, and has a T_g between 170-180°C. Non-ionic HPMC does not complex with metallic salts or organic material to form insoluble precipitates; however, it is incompatible with specific oxidizing agents (124,125).

The mechanical strength of the shell and its components can deteriorate. The choice of the container and its closure for storage and transportation (shipping) should be compatible with the dosage form, protecting the capsules from moisture and preventing sorption and leaching of construction materials with the dosage form.

HPMC shell walls are weaker than gelatin shells. At ambient temperatures and low moisture content, gelatin capsules are more robust, stiffer, and rigid but less elastic and more flexible than HPMC capsules. A strongly hygroscopic drug will attract moisture from the filled capsule shell, affecting drug release rate and shelf life. Capsule shells absorb moisture during prolonged humid storage conditions. As determined by disintegration, dissolution, mechanical and visual testing, HPMC shells exhibit superior short-term stability at high temperatures and retain their mechanical qualities at low and high relative humidity.

Humidity and moisture soften hard capsule HPMC and gelatin shells and affect their physical characteristics. Unlike HPMC, high moisture content causes gelatin capsules to lose plasticity and become distorted, soft, and sticky, and filling stuck to the capsules' inner surfaces does not leave the device. HPMC and gelatin capsules differ mainly in

moisture content, affecting the brittleness and breakage of capsules. As brittleness is a function of relative humidity, the storage of HPMC capsules (moisture content of 2-7%) must occur at a relative humidity of 10-60%, while storage of gelatine capsules (moisture content of 13-16%) and should be at a relative humidity of 35-65%. Less than 10% moisture/water in gelatin hard capsules and storage below 40% relative humidity causes brittleness (125).

Mechanically robust HPMC capsule shells remain flexible at a 30-50% moisture level, with no brittleness or breakage even at a minimum of 1-2% water content. In contrast, gelatin capsules have a critical brittleness value of <4% w/w (119). Dried HPMC capsule shells contain less moisture and are more hygroscopic than gelatin capsules, with an increased affinity for moisture above 75%, facilitating compatibility with poorly soluble, hygroscopic drugs and excipients (78)(80); CBD is non-hygroscopic (125).

Due to a loose shell wall structure, HPMC capsules are permeable to gases (oxygen and water vapour). Therefore, oxygen-sensitive formulations filled into HPMC capsules should contain an anti-oxidant or the filled capsule packaged in an aluminium foil blister. Banding of filled hard capsules prevents gaseous diffusion through the cap and body space to fill the overlap region. The capsule fill and shell must be compatible. Inert HPMC capsules contain no chemically reactive groups, and solubility is impartial to pH and properties of the dissolution medium. Except for some oxidizing agents, HPMC capsules are compatible with a broad range of products and reduce crosslinking.

Crosslinking, particularly in gelatin capsules, negatively affects capsule solubility and drug bioavailability because the shell becomes tough, rubbery, and swollen due to ageing and exposure to stressful physical conditions and chemical interactions. Physical stresses include rapid drying, high temperatures, humidity, UV and gamma-radiation, and chemical interactions with aldehydes, ketones, imines, and carbodiimides that affect product dissolution, disintegration, and rupture of the soft gel shell. At the time of encapsulation, the high initial water content of the capsule shell formulation (30%) causes water migration from the capsule shell into the lipid filling or vice versa, which can affect drug

solubility in LBDDS. HPMC capsules are better resistant to water migration; however, capsule softening by formulation filling is inevitable. Excess moisture renders the capsule shell prone to microbial decomposition; however, HPMC capsules respond to ionizing radiation sterilization (34).

Bio-adhesive HPMC capsules have a rough, matt surface that sticks to the oesophagus, a grave concern, especially for corrosive drugs. Hard capsules are retained longer in the oesophagus compared to enteric-coated tablets. Two concerning aspects of HPMC capsules are capsules lodging in the oesophagus and the initial disintegration time. Capsules sticking in the oesophagus increase their oesophageal residence time before reaching the stomach. The volume of water swallowed and posture determines the capsules' oesophageal transit time. To avoid/minimize oesophagus entrapment of solid dosage forms, take capsules with enough water (150–200 ml) in an upright position for several minutes. Delayed oesophageal transit of the dosage form may delay drug absorption, and oesophageal disorders may develop. Viscosity grades of HPMC do not affect the GI tract transit times of the capsules (125,124).

Table 4.3: HPLC Results

Time	**M4 (µ/L)**		**M13 (µ/L)**	
	pH 1.2	**pH 7.4**	**pH 1,2**	**pH 7,4**
0 min	0	0	0	0
15 min	5,8091	9,8062	37,84173	10,51127
30 min	41,1779	49,9303	41,7711	59,05007
1 hour	83,0426	104,0675	45,8729	63,89287
2 hours	105,4915	167,0642	67,0529	88,50077
3 hours	139,4895	212,5055	84,4017	115,0219
6 hours	167,1706	251,0075	88,1396	118,3387
12 hours	192,3041	282,5702	92,0058	122,2061
24 hours	203,1327	293,8345	95,5888	136,092
48 hours	216,8702	299,4367	99,9384	144,6009

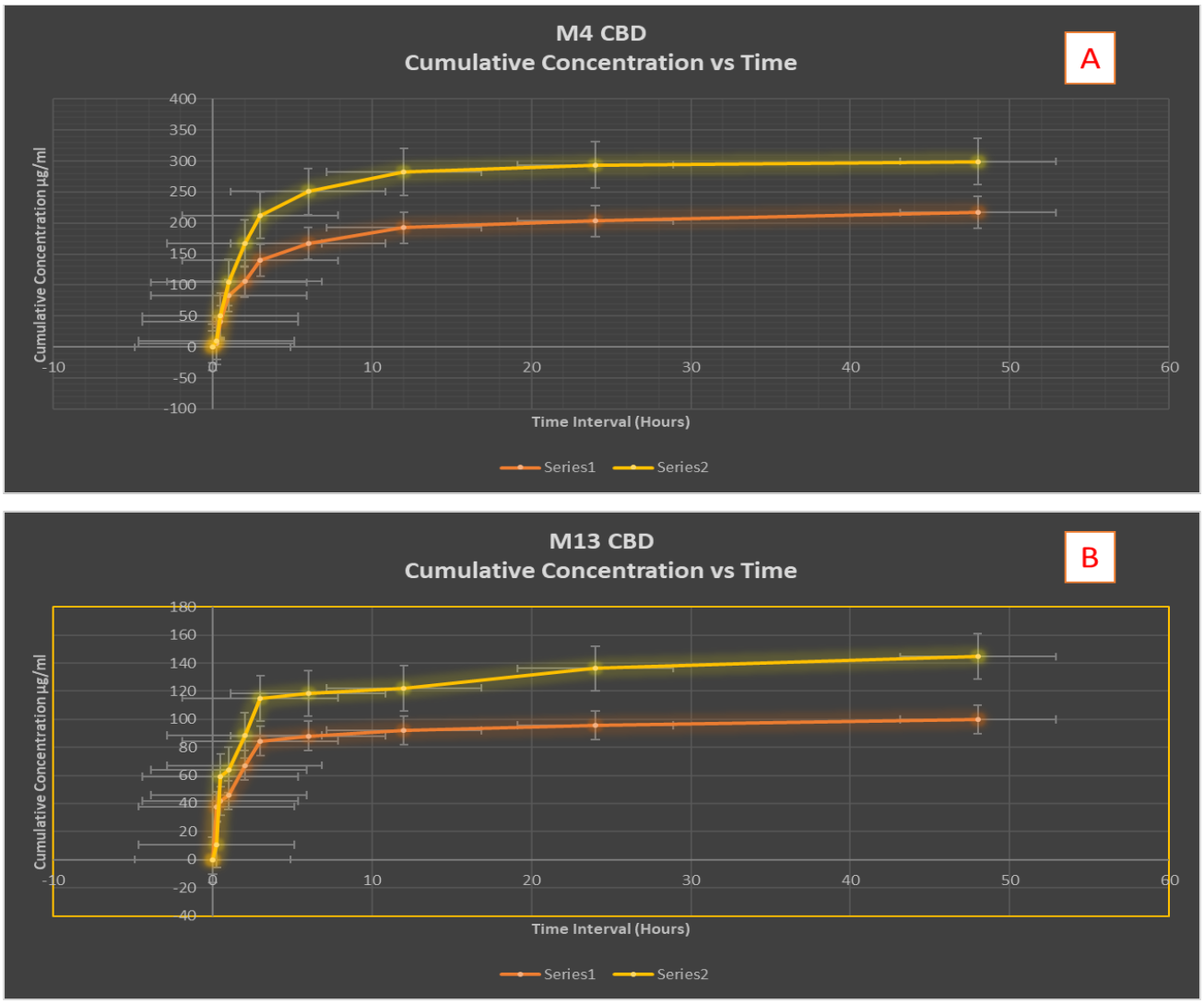

Figure 4.3: HPLC release of CBD under pH 1,2 (orange) and pH 7,4 (yellow) (A) M4; (B) M13

As HPMC capsule shells are more fragile than hard gelatin capsules, adding gelling systems such as carrageenan or gellan gum polysaccharides can increase their durability. Although gelling agents slow HPMC capsule dissolution/disintegration rates without lowering bioavailability, their absence decreases dissolution/disintegration problems.

HPMC capsules containing M4 and M13 immersed in PBS dissolution medium were agitated in an Orbital Shaker (37°C) to simulate gastrointestinal tract motility. M4 and M13 HPMC capsules ruptured, disintegrated and dissolved. Hydrated HPMC capsules

disintegrated at the shoulders where the wall is thinnest (0-15 minutes), then split and dissolved uniformly and instantly across the shell (15-30 minutes), quickly releasing their contents (30 minutes to 1 hour).

HPMC capsule rupture depends on the dissolution medium's composition, grade, and ionic strength but is unaffected by capsule size. HPMC shell dissolution is independent of temperature between 10-55°C at a pH ≤5.8. HPMC capsules are soluble at temperatures ≥10°C; however, dissolution and disintegration decrease as temperature increases above 30°C (solubility range 10-30°C); therefore, swallowing HPMC capsules with cold water, although carbonated drinks do not affect drug release. Hypromellose capsules take a long time to dissolve because moisture passes slowly through HPMC capsule walls.

HPMC capsules dissociate in aqueous dissolution media when cations diffuse out of the network, disrupting the film and the drug. The pKa value indicates the strength of an acid; lower pKa values indicate more potent acids that dissociate more entirely in water. M4 and M13 capsule dissolution in PBS solutions of pH 1,2, and 7,4 had a lag time of approximately 4 to 5 minutes before the drug was released. Simulated gastric fluid (pH 1,2) protracts rupture time more than simulated intestinal fluid (pH 7,2).

M4 and M13 preconcentrates formed lecithin organogel ASDs after emulsification, purification, and lyophilization. M4 and M13 ASD lipid nanocarriers exhibited burst release (1-3 hours) followed by favourable sustained release profiles (3-48 hours) under pH 1,2 and pH 7,4 of PBS buffer under sink conditions. ASD lipid nanocarrier's release behaviour is biphasic, where the drug entrapped near the surface detonates an initial burst release preceded by a sustained release from the drug diffusion from the nanoliposome core, improving bioavailability relative to the drug suspension (44)(51).

CBD was released faster at pH 7,4 (yellow) than at pH 1,2 (orange) in M4 and M13 (Figures 4.3 A and B). In M4, more CBD was released compared to M13 (Cumulative

percentages of CBD 299,4367 vs 144,6009 for pH 7,4 at 48 hours and 216,8702 vs 99,9384 for pH 1,2 at 48 hours) upon dissolution in PBS (Table 4.3).

M4 (SMEDDS) and M13 (SNEDDS) increase solubility, prolong retention time in the GIT, and facilitate the lymphatic absorption of CBD, enhancing its bioavailability (34). Controlling ASD parameters reduces instability and improves the LBDDS dissolution rate and bioavailability.

4.4.2. Encapsulation

Amorphous solid dispersion (ASD) produced using dialysis and lyophilization was filled into a capsule containing 0.5 g of ASD and immersed in 5 ml of pH-adjusted PBS, where it disintegrated and dissolved to generate a supernatant. 1 ml aliquots of the supernatant were taken under sink conditions at specified intervals for HPLC analysis.1 ml aliquots of the supernatant were taken under sink conditions at specified intervals for HPLC analysis. Proportionally, the cumulative yield of 0.1 g/ml CBD aliquot at physiological pH 7,4 as analysed by HPLC.

X = 0,1 g or 100 mg

Formulation M4 = 299,4 µg/L = 299,4 µg/1000ml = 0,2994 µg/ml

Formulation M13 = 144,6 µg/L= 144,6 µg/1000ml = 0,1446 µg/ml

Table 4.3: Encapsulation Efficiency and Drug Loading Capacity of M4 and M13

Formulation	**Maximum**	**M4**	**M13**
Encapsulation efficiency (EE%)	100%	37,60%	69,88%
Drug loading Capacity	100%	0,18%	0,34%

The more a liposome can encapsulate, the greater the drug concentration transported to its target (56). Considering the original formulation containing 0.37% CBD, M13 appears

to have superior encapsulation efficiency and drug loading capacity compared to M4. However, M13 released less CBD than M4 during 48 hours.

Liposome encapsulation efficiency and drug release kinetics depend on the drug and liposome characteristics. While the characteristics of the liposome, such as aqueous volume, membrane stiffness, surface area, particle size, lamellarity, and manufacturing procedures, substantially impact encapsulation efficiency, the hydrophilicity or lipophilicity of the drug affects encapsulation efficiency.

Examination of the SEM results for M4 (Figure 3.4:A) shows a polydispersed mixture of separate, unilamellar, small (<100 nm), and large (>100nm) liposomes entrapped in a 3-dimensional amorphous gel matrix. The spherical, quasi-spheroidal and ellipsoid liposomes are in intact, ruptured, and fused states. The release of CBD from ruptured liposomes into the matrix and supernatant reduces the liposomes' encapsulation efficiency and drug-loading capacity, resulting in low encapsulation effectiveness and drug-loading capabilities (Table 43).

The particle size of liposomes increases with lamellarity, or the number of concentric lipid bilayers in a vesicle. Particle sizes ≤120 nm mostly form unilamellar liposomes, whereas liposomes are predominantly multilamellar when the particle size exceeds 120 nm. The multiple lipid bilayers of oligolamellar liposomes boost barrier efficiency, improve drug retention, and limit drug release more than single-membrane liposomes, making them more effective. Liposome fragility, as seen in the unilamellar liposomes of M4, can be strengthened by incorporating cholesterol into the bilayer, enhancing membrane stability and, consequently, encapsulation efficiency. The release rate hinges on drug precipitation in the liposome interior (19,20).

SEM images from M13 (Figure 3.9A) show cubic and angular uniform monodispersed, small (<100 nm) individual liposomes spread throughout the ASD matrix. The lamellarity of the vesicles in M13 is not visible from the SEM images unless viewed with atomic force microscopy (AFM) or Transmission electron microscopy (TEM). However, small liposome

vesicles have a larger surface area, greater curvature and looser packing between membrane lipids than giant liposomes, releasing drugs more readily (126).

4.4.3. Release of Lyotropic Liquid Crystals (LLC)

Geometry and structure correlate to drug diffusion release kinetics. Internal structures, drug polarities and the molecular weight of solubilized drugs influence release rates. Hexagonal LLCs have parallel, one-dimensional water cylinders; cubic LLCs have continuous but nonintersecting water channels; and lamellar LLCs have hydrophobic bilayers that divide the water layer. Lyotropic liquid crystals (LLC) control drug release rates by solubilising drugs with hydrophilic, hydrophobic, or amphiphilic polarities anchored in the liposome. Hydrophilic drugs settle in water channels or close to the polar head; amphiphilic drugs settle at the fringe (interface), while hydrophobic drugs penetrate the lipid layer.

The drug release rate of hydrophilic drugs residing in the polar core of inverse micellar cubes is as follows: Dlamellar phase > Dcubic phase > Dhexagonal phase > Dmicellar cubic. Hydrophilic drug release in the inverse hexagonal (H2), reversed bicontinuous cubic (V2), inverse micellar (L2), and micellar cubic (I2) phases obey first-order diffusion kinetics. Hydrophobic drug release and drug release from LLC obey Higuchi diffusion kinetics, where the cumulative percentage release of drugs is a function of the square root of the time (2).

Molecular weight affects drug release, with low molecular weight molecules releasing faster than macromolecules (e.g. protein-based drugs) via Higuchi diffusion kinetics (49).

4.5 Cell Culture Analysis

Cell proliferation occurs when cell division exceeds cell death or differentiation. Cell viability assays, typically used to determine cellular toxicity, estimate the number of healthy cells to screen the cellular response against drugs or chemical agents or to correlate cell behaviour to cell numbers (122). CBD inhibits the proliferation of

hyperproliferative keratinocytes, has good antibacterial activity and selectively inhibits cancer cells while sparing normal cells (12,14).

The colourimetric MTT assay spectrophotometrically analyses the cells' metabolic activity, proliferation/viability, and survival. Mitochondria and dehydrogenase enzymes reduce the tetrazolium salt at 37°C to an insoluble purple formazan dye in viable living cells with an active metabolism. Dead cells cannot reduce tetrazolium salts into coloured formazan products. The solubilised formazan salt produces a purple product quantified with a spectroscopic multi-plate reader at an absorbance maximum near 570nm. Viable cell quantities present in the culture are directly proportional to the intensity of the coloured product (122).

Neither MTT nor formazan absorbs at 690 nm; therefore, the wavelength of 570nm forms the reference absorbance. As CBD is a component of many products, small doses consumed simultaneously from different sources can act synergistically to exceed toxicity limits, impeding cell proliferation without consequent cell death. Therefore, evaluating CBD concentrations in human tissues is rational. CBD inhibits cell viability subject to dose and time (80). Low CBD concentrations increase mitochondrial Ca^{2+}, boosting mitochondrial metabolism and cell growth, while elevated concentrations cause mitochondrial dysfunction and cell death. Low doses of CBD do not stimulate apoptosis, while high doses significantly stimulate apoptosis.

Proliferation studies on 3T3 mouse cells used the cumulative values obtained from the HPLC drug release studies of 144,6009 µ/ml for M13 and 299,4367 µ/ml for M4 (Table 4.3). This study showed no cell growth in blank wells and cell death in the 3T3 and HEK 293 cell lines exposed to the negative control containing 5FU. The untreated cells and the positive control displayed cell growth, suggesting that CBD at specific concentrations can induce mitochondrial stress and changes in cell morphology. Treatment with high CBD concentrations (10 µM) resulted in cellular detachment, rounding and wrinkling, and morphological changes characteristic of dead cells (83). Higher CBD concentrations' loss

of mitochondrial activity correlated with cell death and longer incubation times (i.e., 48 hours). Compared to the control group, treatment did not change cell viability (Table 4.3). Cell proliferation increases with CBD dilution (Figures 4.8 and 4.9). HEK 293 proliferates more than 3T3 cells. In the histograms of HEK 293 (Figure 4.9 A and B), M13 cell viability decreases in dilutions above 0,0625 µg/ml. M4 cell viability decreases at concentrations above 0,125 µ/ml at 24 and 48 hours. In the histograms of 3T3 (Figure 4.8 A and B), M13 cell viability decreases in dilutions above 0.25 µg/ml. There is little change in cell viability over the first 24 hours in dilutions of M4. After 48 hours, cell viability decreases at concentrations above 0.5 µg/ml. M4 cell viability is better than M13 over the whole dilution range.

CBD is safe when administered via various routes at low doses (<100mg) (21). M4 and M13 showed CBD to have negligible effects at low doses but significantly reduced cell viability at higher concentrations, causing cell damage. Therefore, therapeutic use of CBD should be limited to lower doses. (78).

Table 4.4: Summary of results

Dilution 0.03125 um	3T3 24 Hours	3T3 48 Hours	HEK 293 24 Hours	HEK 293 48 Hours
Blank	Absence of growth	Absence of growth	Absence of growth	Absence of growth
Negative control (5FU)	morphological changes; cell death	morphological changes; cell death	morphological changes; cell death	morphological changes; cell death
Positive control (PBS)	Viable cells	Viable cells	Viable cells	Viable cells
Untreated	Viable cells	Viable cells	Viable cells	Viable cells
CBD Plain	Cell viability: 89.45%	Cell viability: 90%	Cell viability: 111.91%	Cell viability: 186,2%
M4	Cell viability: 102.91%	Cell viability: 106.27%	Cell viability: 115.86%	Cell viability: 185,52%
M13	Cell viability: 99.91%	Cell viability: 90.43%	Cell viability: 112.24%	Cell viability: 180,05%

Observation:	M4 and M13: slightly higher cell viability than plain CBD	CBD and M13: similar viability at 90.43 and 90%, respectively	M4 and M13: slightly higher cell viability than plain CBD	M13: slightly lower cell viability than plain CBD and M4

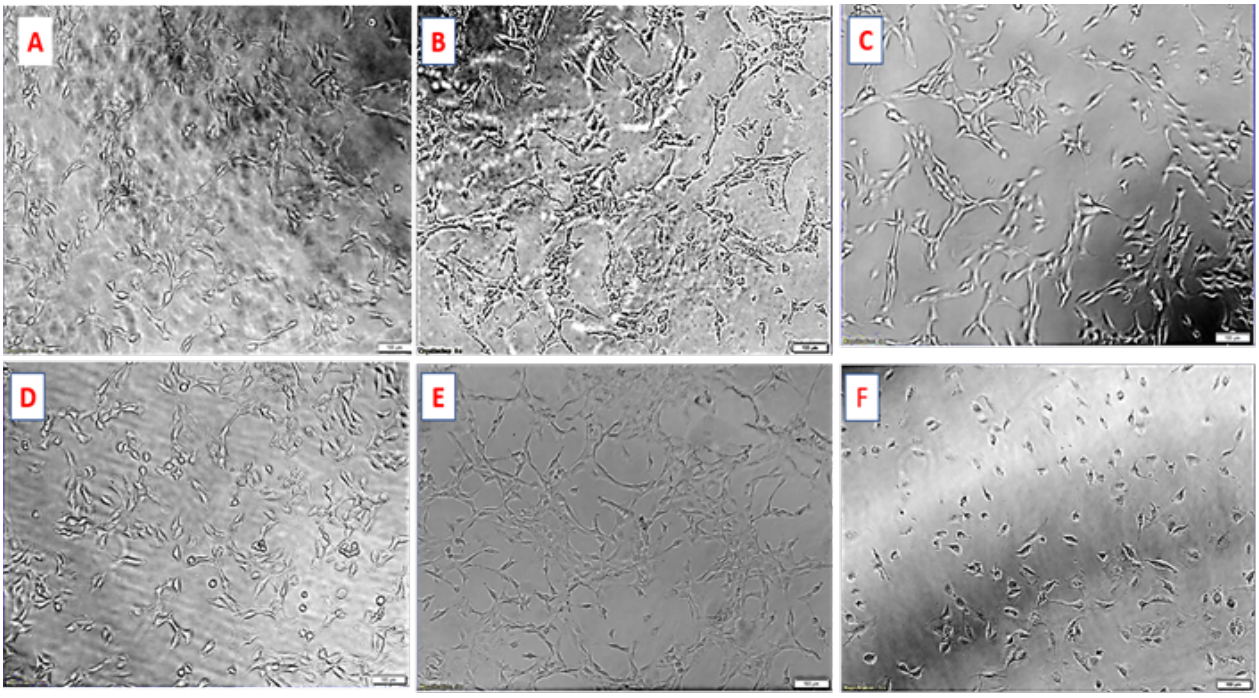

Figure 4.5: Electron on Microscope Images for 3T3 Cell Culture. Images of 3T3 cell proliferation at 24 Hours (A) M4 CBD/1; (B) M13 CBD/1; (C) CBD Plain/2; (D) Untreated; (E) Positive control (PBS/1); (F) Negative Control (5-FU/2).

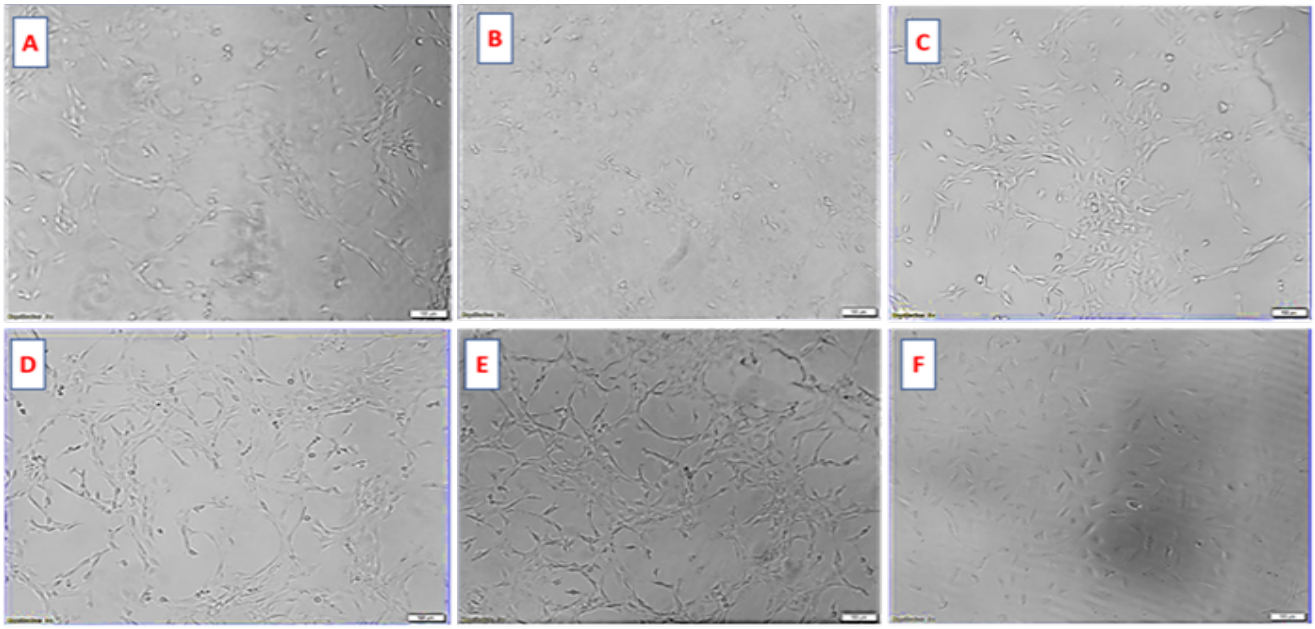

Figure 4.6: Images of 3T3 cell proliferation at 48 Hours (A) M4 CBD/1; (B) M13 CBD/1; (C) CBD Plain/2; (D) Untreated; (E) Positive control (PBS/1); (F) Negative Control (5-FU/2)

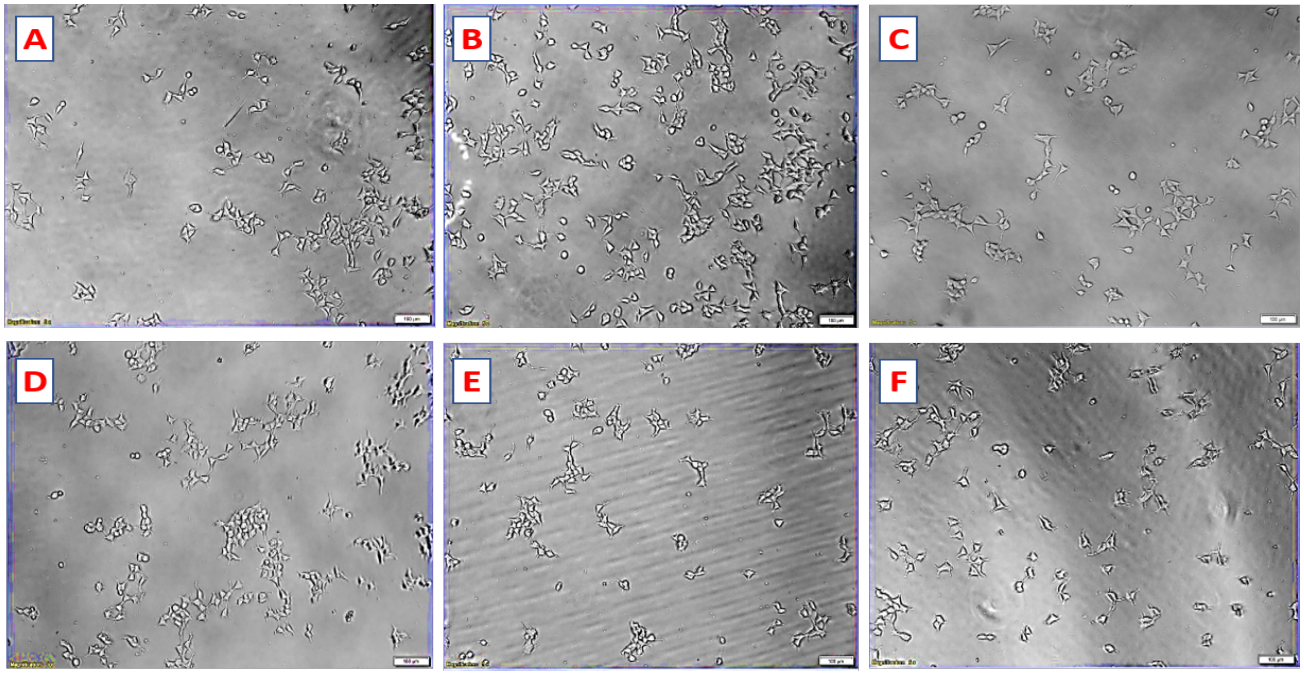

Figure 4.7: Electron Microscope Images for HEK 393 Culture.
Images of HEK 393 cell proliferation at 24 Hours (A) M4 CBD/1; (B) M13 CBD/1; (C) CBD Plain/2; (D) Untreated; (E) Positive control (PBS/1); (F) Negative Control (5-FU/2)

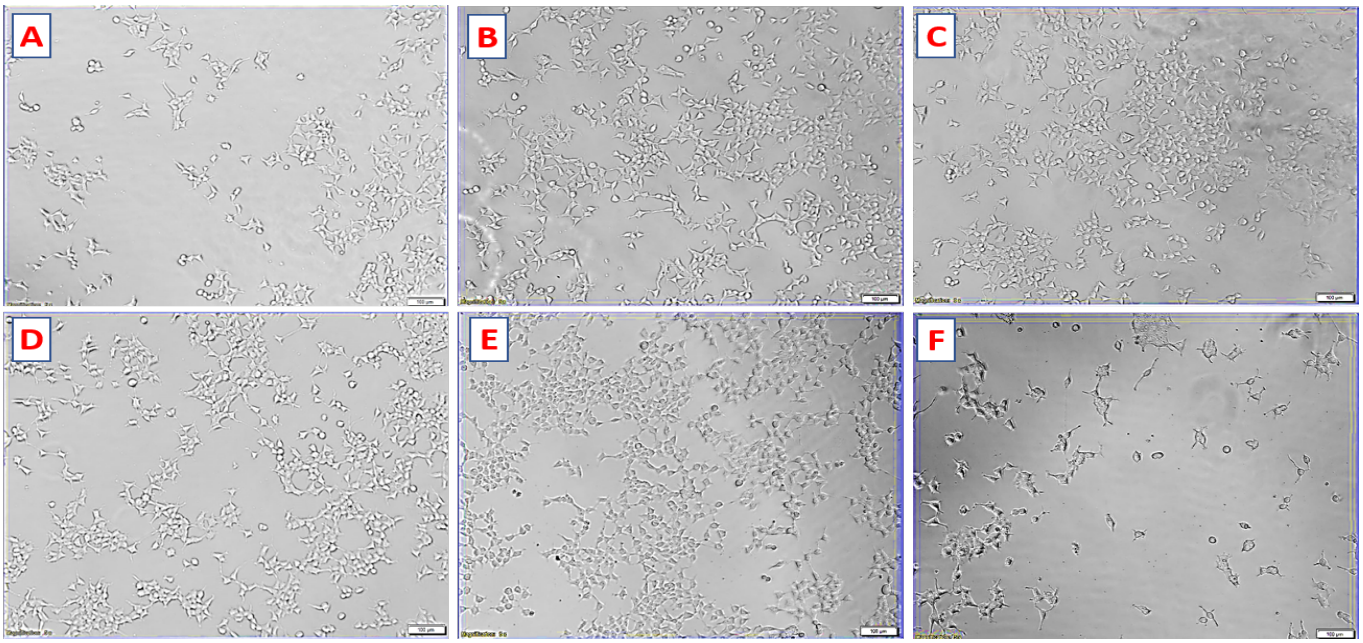

Figure 4.8: Images of HEK 393 cell proliferation at 48 Hours (A) M4 CBD/1; (B) M13 CBD/1; (C) CBD Plain/2; (D) Untreated; (E) Positive control (PBS/1); (F) Negative Control (5-FU/2).

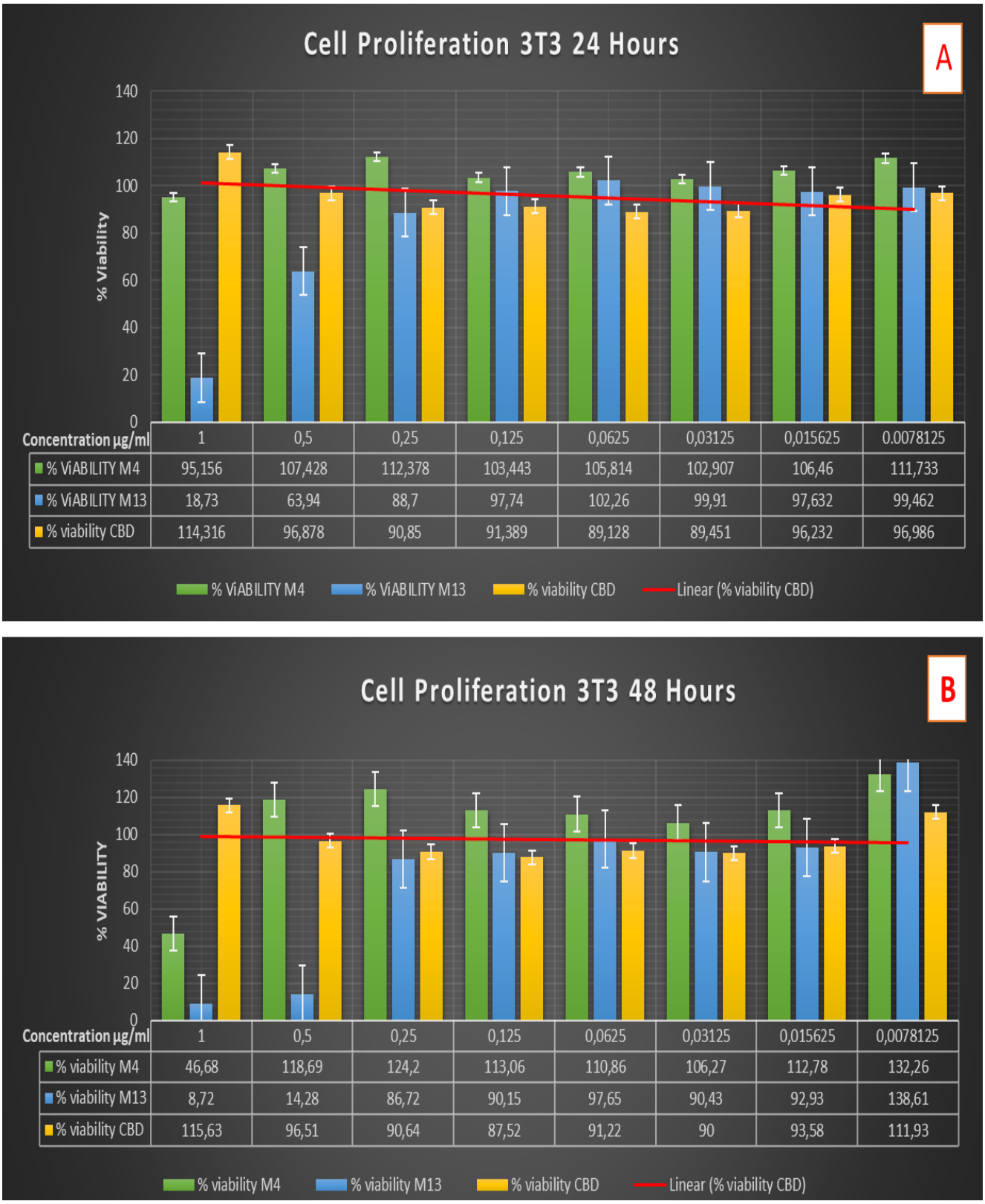

Figure 4.9: Cell proliferation of 3T3 over A) 24 Hours and B) 48 Hours; comparing the cell viability of formulation M4 and M13 against unformulated CBD concentrate.

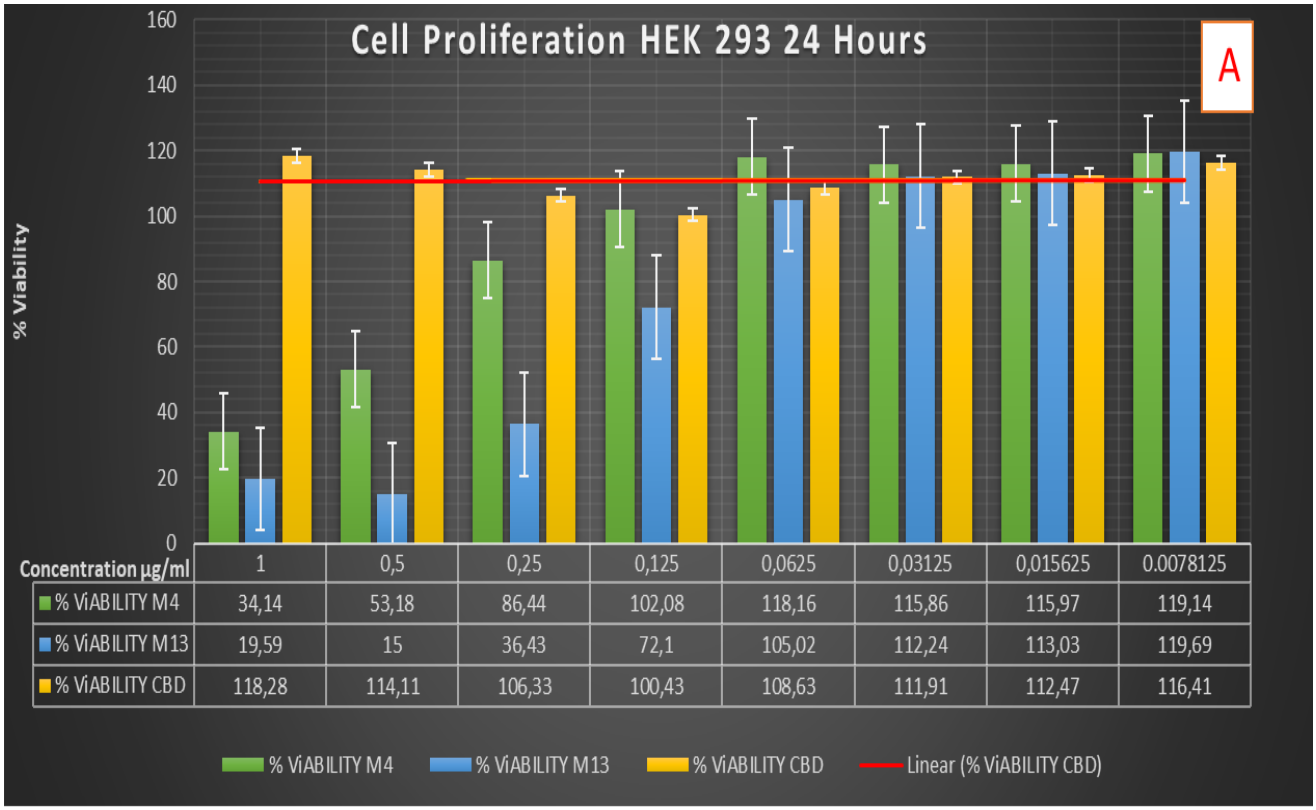

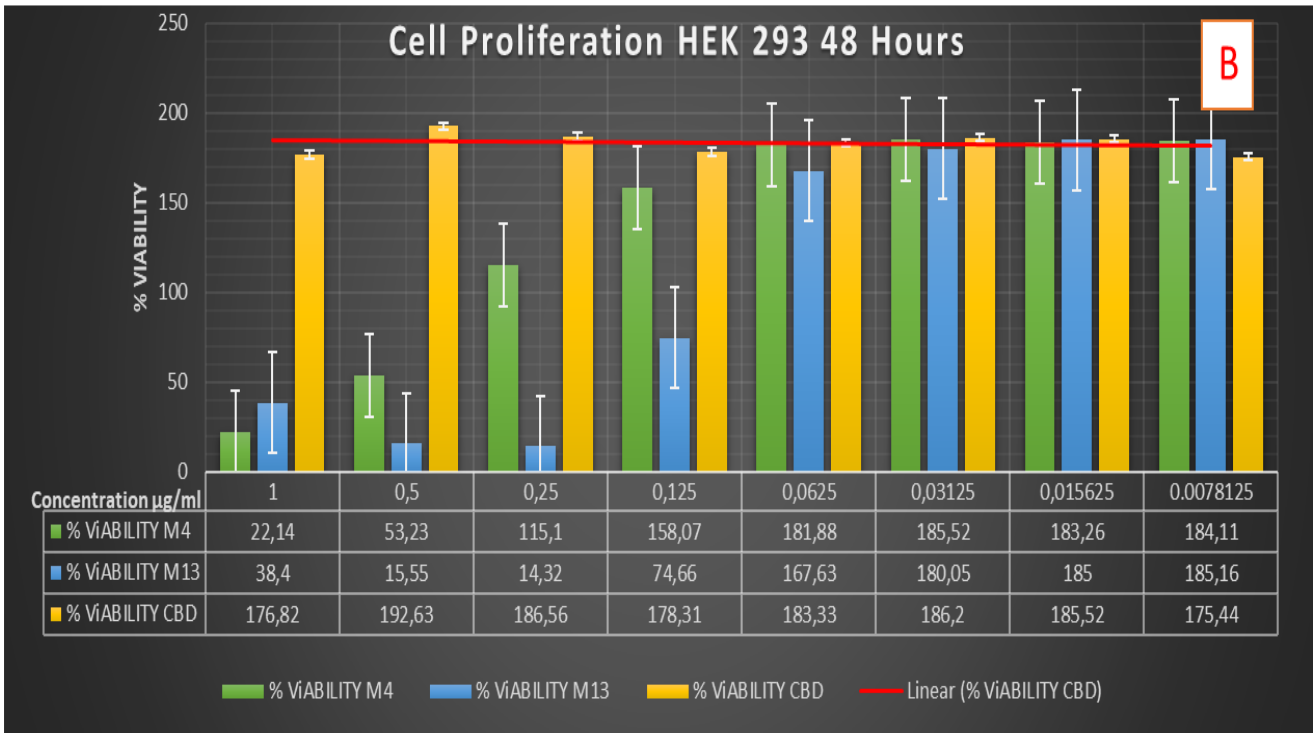

Figure 4.10: Cell proliferation of HEK 293 over A) 24 Hours and B) 48 Hours; comparing the cell viability of formulation M4 and M13 against unformulated CBD concentrate

5.1. Conclusion

CBD interacts with CB1 and CB2 receptors, providing a complementary approach to pain management in the human body. Targeting these cannabinoid receptors activates cytokines via the endocannabinoid pathway, resulting in antinociceptive analgesic and anti-inflammatory effects, modulation of the immune system, and pain management in humans. CBD must traverse biological barriers such as the GIT lumen and the BBB to reach central and peripheral nervous system receptors at therapeutic levels to induce pain responses. Therefore, the optimised formulation, M13, must undergo permeation studies to establish whether CBD release occurred in the GIT (stomach or intestine) and whether permeation across the GIT lumen occurred. In addition, blood plasma concentration measurements should determine the effect of obstacles in the circulatory system. Then, permeation experiments must be simulated across the BBB to establish CBD entrance into the brain and interaction with pain receptors.

CBD, a crystalline solid, was introduced successfully into ASD. CBD, solubilized in unmodified plant oils (coconut, olive/castor oil), stabilised with surfactants (Span 80 and Tween 20) and mixed into soy lecithin polymer, generated liposomes of the desired size. In the hot melt/solvent process, ingredient proportions were maintained and optimised.

Surfactant quantities were calculated according to the HLB for each formulation to ensure emulsion stability. Variations in the two optimised formulations consisted of swapping olive oil for castor oil. Both formulations produced favourable results in their capacities. Aqueous dilution of the olive oil preparation (M4) produced SMEDDS consisting of polydisperse unilamellar liposomes, while the castor oil preparation (M13) produced SNEDDS monodisperse lyotropic liquid crystals. Analytical results suggest that M13 is a more suitable carrier for circumventing barriers to CBD bioavailability, especially crossing the BBB.

DSC thermal analysis of CBD-SNEDDS showed single endothermic peaks, demonstrating that CBD is miscible with ASD in that CBD homogenously integrates into liposomes, forming eutectic mixtures. FTIR data confirms the incorporation of CBD into

phospholipid liposomes and water in the lyophilized products. The olive and castor oil preparations differed in SEM, particle size and rheology. XRD verified amorphousness. Unilamellar vesicles of various diameters burst in olive oil composition.

The ASD's composition, formulation and process variables interact, affecting liposome shape, fluidity, and the dosage form's surface area to volume ratios. The importance of water in preparations M4 and M13 is evident throughout the analysis of the formulations regarding the liposome's size, shape, distribution, lipid hydration and organogel formation with phospholipids. Organogels are ASDs whose appearance, structure, chemistry, and rheology depend on water content. Drug solubility, hydrophobicity, supersaturation, and the propensity of drugs to recrystallize depend on the degree of hydration. Gel-to-sol transitions affected by temperature and moisture levels influence the medium's solubility, polymer chemistry, dosage form dimensions, and the mechanism by which the ASD releases the drug.

5.2. Recommendations and Future Outlook

A risk management-based quality-by-design strategy that defines and profiles the product's development can modify the formulations M4 and M13 to generate more robust nanoparticles for CBD drug delivery. A risk assessment technique for establishing a repeatable experimental design space should evaluate the influence of CPPs and CQAs at each manufacturing phase and adopt a control mechanism to assure continuous improvement (66).

Although analytical results of formulations M4 (olive oil) and M13 (castor oil) indicated that the formulations could function within the current design space, further experimentation can optimise formulation design and enhance robustness for efficient, targeted drug delivery of nanoparticles containing CBD.

Hydrogenated castor oil (HCO) improves the taste, odour, and oxidative and thermal stability of LBDDS. Hydrogenated oils are preferable to vegetable oils because the partial hydrolysis of vegetable oil produces mixed mono- and diglycerides, whereas

hydrogenated oils are amphiphilic molecules well known for their emulsifying properties. Unmodified castor and olive oil replaced with their hydrogenated versions should improve SNEDD characteristics.

A SNEDDS formulation with a particle size <100 nm capable of carrying CBD across the BBB should base formulation ratios on using a surfactant/surfactant blend with an HLB value >12, a surfactant concentration of 40-80% and an oil concentration >20%. The HLB value of the surfactant blend and the formulation must be similar to create a stable formulation. M4 and M13 used Span 80 (HLB = 4) and Tween 20 (HLB = 17) as the surfactant blend; however, o/w emulsions should contain surfactant blends with HLB values between 8-18. Replacing Span 80 with an equivalent Span surfactant with an HLB value closer to 8-18 is suggested.

Liposome formation requires high energy input to form particles of the required size. Probe sonication used in methods M4 produced a highly polydisperse emulsion. Probe sonication is inefficient and can damage the sensitive drug molecule and nanocarrier. A sonic bath controls micronizing sonication better. Alternatively, microfluidic technology that only involves a single step for clinical and industrial applications can improve liposome formation instead of conventional methods. A high-pressure homogenization or microfluidization technique increases the chances of obtaining monodispersed nano particulates. It also allows for controlled mixing and precise control of particle size, charge, and surface modification. Modern technology and equipment can give more reproducible results depending on availability and cost.

Formulations M4 and M13 were lyophilised, a standard method of preserving the integrity of the drug encapsulated in nanoparticles. Marine, vegetable, and essential oils, chemically unstable and susceptible to degradation, can use microencapsulation to prepare high-quality oil-based products that improve these oils' chemical, oxidative, and thermal stability and, therefore, their shelf-life. Moreover, biological, physicochemical, and functional activity improves, and the controlled drug release is manageable. The microencapsulation of oils frequently uses spray drying and coacervation techniques for

encapsulation. Alternate techniques for freeze drying include coaxial electrospray systems, coacervation, extrusion-coating, fluidized-bed-coating, in situ polymerization and supercritical fluid technology. Unlike spray drying, supercritical fluid technology does not expose the oils and drugs to high temperatures; solvent removal is straightforward, and the treatment of various particles can produce controlled particle sizes. Moreover, the method is non-toxic and environmentally friendly.

Water concentration, temperature, and free fatty acid optimization are essential as they affect the shape and structure of the phospholipid bilayer membrane and the stability of freeze-dried liposomal formulations in terms of liposome formation and encapsulation efficiency. A minimal water content improves primary drying efficiency, avoiding the need for an additional secondary drying step (95). As assessed with TGA, lyophilized liposome formulations must contain <2% residual water. Water content plays a significant role in formulation stability. Lyophilization cycle optimization in primary and secondary drying cycles and water content should be monitored closely with TGA analysis.

Mannitol, a cryoprotectant, forms crystals during freeze-drying that can rupture the liposome's membrane, weakening the liposome's protective effects and causing drug retention failure and leakage of the encapsulated drug (85,86). Replacing mannitol or combining it in optimal ratios with other cryoprotectants, such as sucrose or glucose, shields the liposome membrane with their very high viscosity and low molecular mobility, creating an amorphous, glassy matrix after drying. Sucrose does not crystallize when freezing in any solution.

Encapsulation efficiency (EE), a CQA, estimates the nanocarrier's drug delivery and release capacity as the percentage of nanoparticles that successfully encapsulate drugs. Conventional liposomes have 50-72% EE limitations, and stealth liposomes have 65-81%. Encapsulation efficiency is affected by synthesis methods, drug, carrier and dissolution medium properties. Drug retention in liposomes improves with additives like cholesterol, silicone, and cryoprotectants and optimal lyophilization conditions that improve membrane stability.

To avoid oxidative hardening, additives like saturated medium-chain triglycerides (C6-C12), anti-oxidants and metal chelators (e.g., ethylenediaminetetraacetate/EDTA) can prevent oxidative hardening of the ASDs. Antioxidants include ascorbic acid, b-carotene, vitamin E (α-tocopherol), propyl gallate, butylated hydroxyanisole (BHA), and butylated hydroxytoluene (BHT) (33,63). "Hydroxypropyl methylcellulose (HPMC) employed for various pharmaceutical and food preparations is used as a viscolizing agent (thickening agent), coating polymer, bioadhesive, solid dispersion to enhance solubility, and binder in granulation and modified release formulations. HPMC also replaces animal-derived gelatin in two-piece capsule shells. This review aims to systemically survey published literature on the HPMC use in capsule shells and resolve questions regarding their suitability as a replacement for hard gelatin capsules. Future refinements in producing and filling HPMC capsule shells and improving their in vivo/in vitro dissolution would ensure their superiority over hard gelatin capsules. Lipid-soluble antioxidants in the formulation or the HPMC shell can reduce oxidation by reducing permeability to oxygen. Further improvement against oxidation includes capsule sealing and banding and filling the capsule headspace with nitrogen. Manipulating the HPMC capsule with coating materials of different pH enables targeted enteric delivery (solubility ≥5.5) and colonic delivery (solubility ≥7), effectively protecting the drug from capsule release in acidic environments (42) (125).

REFERENCES

1. Bruni N, Della Pepa C, Oliaro-Bosso S, Pessione E, Gastaldi D, Dosio F. Cannabinoid Delivery Systems for Pain and Inflammation Treatment. Molecules [Internet]. 2018 Sep 27 [cited 2021 Sep 1];23(10):2478. Available from: http://www.mdpi.com/1420-3049/23/10/2478
2. Knaub K, Sartorius T, Dharsono T, Wacker R, Wilhelm M, Schön C. A Novel Self-Emulsifying Drug Delivery System (SEDDS) Based on VESIsorb® Formulation Technology Improving the Oral Bioavailability of Cannabidiol in Healthy Subjects. Molecules [Internet]. 2019 Jan [cited 2021 Sep 28];24(16):2967. Available from: https://www.mdpi.com/1420-3049/24/16/2967
3. Elikottil, MBBS J, Gupta, MD P, Gupta, PhD K. The analgesic potential of cannabinoids. J of Opioid Management [Internet]. 2018 Jan 29 [cited 2021 Sep 1];5(6):341–57. Available from: https://www.wmpllc.org/ojs/index.php/jom/article/view/952
4. World Health Organization. WHO guidelines for the pharmacological and radiotherapeutic management of cancer pain in adults and adolescents [Internet]. Geneva: World Health Organization; 2018 [cited 2021 Sep 7]. 138 p. Available from: https://apps.who.int/iris/handle/10665/279700
5. Nahler G, Grotenhermen F, Zuardi AW, Crippa JAS. A Conversion of Oral Cannabidiol to Delta9-Tetrahydrocannabinol Seems Not to Occur in Humans. Cannabis Cannabinoid Res [Internet]. 2017 May 1 [cited 2021 Oct 4];2(1):81–6. Available from: https://www.ncbi.nlm.nih.gov/pmc/articles/PMC5510776/i]=-bb cxvcv
6. Manzanares J, Julian M, Carrascosa A. Role of the Cannabinoid System in Pain Control and Therapeutic Implications for the Management of Acute and Chronic Pain Episodes. Curr Neuropharmacol [Internet]. 2006 Jul [cited 2021 Sep 24];4(3):239–57. Available from: https://www.ncbi.nlm.nih.gov/pmc/articles/PMC2430692/

7. Singh B, Bandopadhyay S, Kapil R, Singh R, Katare OP. Self-Emulsifying Drug Delivery Systems (SEDDS): Formulation Development, Characterization, and Applications. :96.
8. Nelson KM, Bisson J, Singh G, Graham JG, Chen SN, Friesen JB, et al. The Essential Medicinal Chemistry of Cannabidiol (CBD). J Med Chem. 2020;19.
9. Marchand S. The Physiology of Pain Mechanisms: From the Periphery to the Brain. Rheumatic Disease Clinics of North America [Internet]. 2008 May [cited 2022 Jan 26];34(2):285–309. Available from: https://linkinghub.elsevier.com/retrieve/pii/S0889857X08000288
10. Świeboda P, Filip R, Prystupa A, Drozd M. Assessment of pain: types, mechanism and treatment. Ann Agric Environ Med. (1):7.
11. Lu HC, Mackie K. An introduction to the endogenous cannabinoid system. Biol Psychiatry [Internet]. 2016 Apr 1 [cited 2022 Jan 28];79(7):516–25. Available from: https://www.ncbi.nlm.nih.gov/pmc/articles/PMC4789136/
12. Nelson KM, Bisson J, Singh G, Graham JG, Chen SN, Friesen JB, et al. The Essential Medicinal Chemistry of Cannabidiol (CBD). J Med Chem [Internet]. 2020 Nov 12 [cited 2021 Sep 25];63(21):12137–55. Available from: https://pubs.acs.org/doi/10.1021/acs.jmedchem.0c00724
13. Branca JV, Carrino D, Pacini A. Targeting cannabidiol to specific areas of the brain: an ultrasound-based strategy. Neural Regen Res [Internet]. 2020 [cited 2021 Oct 7];15(12):2247. Available from: http://www.nrronline.org/text.asp?2020/15/12/2247/284992
14. Calapai F, Cardia L, Sorbara EE, Navarra M, Gangemi S, Calapai G, et al. Cannabinoids, Blood–Brain Barrier, and Brain Disposition. Pharmaceutics [Internet]. 2020 Mar 15 [cited 2021 Oct 7];12(3):265. Available from: https://www.ncbi.nlm.nih.gov/pmc/articles/PMC7150944/
15. Anthony AT, Rahmat S, Sangle P, Sandhu O, Khan S. Cannabinoid Receptors and Their Relationship With Chronic Pain: A Narrative Review. Cureus [Internet]. 2020 Sep 14 [cited 2021 Oct 9];12(9). Available from: https://www.cureus.com/articles/39887-cannabinoid-receptors-and-their-relationship-with-chronic-pain-a-narrative-review

16. Lowin T, Straub RH. Cannabinoid-based drugs targeting CB1 and TRPV1, the sympathetic nervous system, and arthritis. Arthritis Research & Therapy [Internet]. 2015 Sep 6 [cited 2021 Oct 14];17(1):226. Available from: https://doi.org/10.1186/s13075-015-0743-x
17. Manzanares J, Julian M, Carrascosa A. Role of the Cannabinoid System in Pain Control and Therapeutic Implications for the Management of Acute and Chronic Pain Episodes. Curr Neuropharmacol [Internet]. 2006 Jul [cited 2021 Sep 7];4(3):239–57. Available from: https://www.ncbi.nlm.nih.gov/pmc/articles/PMC2430692/
18. Mackie K. Cannabinoid Receptors: Where They are and What They do. Journal of Neuroendocrinology [Internet]. 2008 [cited 2021 Oct 5];20(s1):10–4. Available from: https://onlinelibrary.wiley.com/doi/abs/10.1111/j.1365-2826.2008.01671.x
19. Milligan AL, Szabo-Pardi TA, Burton MD. Cannabinoid Receptor Type 1 and Its Role as an Analgesic: An Opioid Alternative? Journal of Dual Diagnosis [Internet]. 2020 Jan 2 [cited 2021 Oct 9];16(1):106–19. Available from: https://doi.org/10.1080/15504263.2019.1668100
20. Aparicio Blanco J, Romero I, Male D, Slowing K, Garcia-Garcia L, Torres-Suarez A. Cannabidiol Enhances the Passage of Lipid Nanocapsules across the Blood-Brain Barrier Both in Vitro and in Vivo. Molecular pharmaceutics. 2019 May 6;16:1999–2010.
21. admin. LIPID-BASED DELIVERY - Are Lipid-Based Drug Delivery Systems in Your Formulation Toolbox? [Internet]. Drug Development and Delivery. 2017 [cited 2023 Aug 15]. Available from: https://drug-dev.com/lipid-based-delivery-are-lipid-based-drug-delivery-systems-in-your-formulation-toolbox/
22. He H, Lu Y, Qi J, Zhu Q, Chen Z, Wu W. Adapting liposomes for oral drug delivery. Acta Pharm Sin B. 2019 Jan;9(1):36–48.
23. Chavda H, Patel C, Anand I. Biopharmaceutics classification system. Syst Rev Pharm [Internet]. 2010 [cited 2021 Sep 16];1(1):62. Available from: http://www.sysrevpharm.org/text.asp?2010/1/1/62/59514
24. admin. LIPID-BASED DELIVERY - Are Lipid-Based Drug Delivery Systems in Your Formulation Toolbox? [Internet]. Drug Development and Delivery. 2017 [cited 2023

Aug 15]. Available from: https://drug-dev.com/lipid-based-delivery-are-lipid-based-drug-delivery-systems-in-your-formulation-toolbox/

25. Atalay S, Jarocka-Karpowicz I, Skrzydlewska E. Antioxidative and Anti-Inflammatory Properties of Cannabidiol. Antioxidants (Basel) [Internet]. 2019 Dec 25 [cited 2021 Oct 19];9(1):21. Available from: https://www.ncbi.nlm.nih.gov/pmc/articles/PMC7023045/
26. PubChem. 1,3-Benzenediol, 2-[3-methyl-6-(1-methylethenyl)-2-cyclohexen-1-yl]-5-pentyl-, (1R-trans)- [Internet]. [cited 2022 Jun 7]. Available from: https://pubchem.ncbi.nlm.nih.gov/compound/36688143
27. Millar SA, Maguire RF, Yates AS, O'Sullivan SE. Towards Better Delivery of Cannabidiol (CBD). Pharmaceuticals [Internet]. 2020 Aug 28 [cited 2021 Sep 24];13(9):219. Available from: https://www.mdpi.com/1424-8247/13/9/219
28. CannabidiolCriticalReview.pdf [Internet]. [cited 2021 Oct 4]. Available from: https://www.who.int/medicines/access/controlled-substances/CannabidiolCriticalReview.pdf
29. Fasinu PS, Phillips S, ElSohly MA, Walker LA. Current Status and Prospects for Cannabidiol Preparations as New Therapeutic Agents. Pharmacotherapy: The Journal of Human Pharmacology and Drug Therapy [Internet]. 2016 [cited 2021 Sep 4];36(7):781–96. Available from: https://accpjournals.onlinelibrary.wiley.com/doi/abs/10.1002/phar.1780
30. Millar SA, Stone NL, Yates AS, O'Sullivan SE. A Systematic Review on the Pharmacokinetics of Cannabidiol in Humans. Frontiers in Pharmacology [Internet]. 2018 [cited 2021 Sep 10];9:1365. Available from: https://www.frontiersin.org/article/10.3389/fphar.2018.01365
31. Danaei M, Dehghankhold M, Ataei S, Davarani FH, Javanmard R, Dokhani A, et al. Impact of Particle Size and Polydispersity Index on the Clinical Applications of Lipidic Nanocarrier Systems. Pharmaceutics. 2018;
32. Shrestha H, Bala R, Arora S. Lipid-Based Drug Delivery Systems. Journal of Pharmaceutics. :11.
33. Dokania S, Joshi AK. Self-microemulsifying drug delivery system (SMEDDS) – challenges and road ahead. Drug Delivery [Internet]. 2015 Aug 18 [cited 2021 Sep

12];22(6):675–90. Available from: http://www.tandfonline.com/doi/full/10.3109/10717544.2014.896058

34. Hasan NMY. Role of medium-chain fatty acids in the emulsification mechanistics of self-micro-emulsifying lipid formulations. Saudi Pharmaceutical Journal [Internet]. 2014 Dec [cited 2021 Nov 17];22(6):580–90. Available from: https://linkinghub.elsevier.com/retrieve/pii/S1319016414000061
35. Kumar A, Sharma S, Kamble R. SELF EMULSIFYING DRUG DELIVERY SYSTEM (SEDDS): FUTURE ASPECTS. 2:7.
36. Alberts B, Johnson A, Lewis J, Raff M, Roberts K, Walter P. The Lipid Bilayer. Molecular Biology of the Cell 4th edition [Internet]. 2002 [cited 2022 Mar 2]; Available from: https://www.ncbi.nlm.nih.gov/books/NBK26871/
37. A. A, A. M, F. P. Lipid Nanoparticulate Drug Delivery Systems: A Revolution in Dosage Form Design and Development. In: Sezer AD, editor. Recent Advances in Novel Drug Carrier Systems [Internet]. InTech; 2012 [cited 2021 Sep 1]. Available from: http://www.intechopen.com/books/recent-advances-in-novel-drug-carrier-systems/lipid-nanoparticulate-drug-delivery-systems-a-revolution-in-dosage-form-design-and-development
38. Loew S, Fahr A, May S. Modeling the Release Kinetics of Poorly Water-Soluble Drug Molecules from Liposomal Nanocarriers. Journal of Drug Delivery [Internet]. 2011 Jun 7 [cited 2021 Oct 26];2011:1–10. Available from: https://www.hindawi.com/journals/jdd/2011/376548/
39. Koog L van der, Gandek TB, Nagelkerke A. Liposomes and Extracellular Vesicles as Drug Delivery Systems: A Comparison of Composition, Pharmacokinetics, and Functionalization. Advanced Healthcare Materials [Internet]. [cited 2021 Sep 7];n/a(n/a):2100639. Available from: https://onlinelibrary.wiley.com/doi/abs/10.1002/adhm.202100639
40. Yadav D, Sandeep K, Pandey D, Dutta RK. Liposomes for Drug Delivery. J Biotechnol Biomater [Internet]. 2017 [cited 2021 Sep 1];07(04). Available from: https://www.omicsonline.org/open-access/liposomes-for-drug-delivery-2155-952X276-97370.html

41. Akbarzadeh A, Rezaei-Sadabady R, Davaran S, Joo SW, Zarghami N, Hanifehpour Y, et al. Liposome: classification, preparation, and applications. Nanoscale Res Lett [Internet]. 2013 Feb 22 [cited 2021 Sep 23];8(1):102. Available from: https://www.ncbi.nlm.nih.gov/pmc/articles/PMC3599573/
42. Anderson M, Omri A. The Effect of Different Lipid Components on the In Vitro Stability and Release Kinetics of Liposome Formulations. Drug Delivery [Internet]. 2004 Jan [cited 2021 Oct 26];11(1):33–9. Available from: http://www.tandfonline.com/doi/full/10.1080/10717540490265243
43. Hoogevest P, Wendel A. The use of natural and synthetic phospholipids as pharmaceutical excipients. European Journal of Lipid Science and Technology. 2014 Sep 1;116.
44. Mouritsen OG. Lipids, curvature, and nano-medicine. Eur J Lipid Sci Technol [Internet]. 2011 Oct [cited 2022 Mar 19];113(10):1174–87. Available from: https://www.ncbi.nlm.nih.gov/pmc/articles/PMC3229985/
45. Nagarajan R. Molecular Packing Parameter and Surfactant Self-Assembly: The Neglected Role of the Surfactant Tail. Langmuir [Internet]. 2002 Jan 1 [cited 2022 Jun 7];18(1):31–8. Available from: https://pubs.acs.org/doi/10.1021/la010831y
46. Burducea G. LYOTROPIC LIQUID CRYSTALS I. SPECIFIC STRUCTURES. :22.
47. 2.03_Membrane_Curvature.pdf [Internet]. [cited 2021 Nov 6]. Available from: https://batch.libretexts.org/print/url=https://phys.libretexts.org/Courses/University_of_California_Davis/UCD%3A_Biophysics_241_-_Membrane_Biology/02%3A_Membranes_-_Aggregated_Lipids/2.03%3A_Membrane_Curvature.pdf
48. Marsh D. Intrinsic curvature in normal and inverted lipid structures and in membranes. Biophys J [Internet]. 1996 May [cited 2021 Nov 6];70(5):2248–55. Available from: https://www.ncbi.nlm.nih.gov/pmc/articles/PMC1225199/
49. Huang Y, Gui S. Factors affecting the structure of lyotropic liquid crystals and the correlation between structure and drug diffusion. RSC Adv [Internet]. 2018 Feb 9 [cited 2022 Apr 29];8(13):6978–87. Available from: https://pubs.rsc.org/en/content/articlelanding/2018/ra/c7ra12008g

50. Barrales-Cureño HJ, López-Valdez LG, Reyes C, Cetina-Alcalá VM, Vasquez-García I, Diaz-Lira OF, et al. Chemical Characteristics, Therapeutic Uses, and Legal Aspects of the Cannabinoids of Cannabis sativa: A Review. Braz arch biol technol [Internet]. 2020 [cited 2021 Oct 6];63:e20190222. Available from: http://www.scielo.br/scielo.php?script=sci_arttext&pid=S1516-89132020000100902&tlng=en
51. Faizi HA, Frey SL, Steinkühler J, Dimova R, Vlahovska PM. Bending rigidity of charged lipid bilayer membranes. Soft Matter [Internet]. 2019 Jul 24 [cited 2022 Jun 6];15(29):6006–13. Available from: https://pubs.rsc.org/en/content/articlelanding/2019/sm/c9sm00772e
52. Deserno M. Fluid lipid membranes – a primer. :29.
53. Pichot R, Watson RL, Norton IT. Phospholipids at the Interface: Current Trends and Challenges. International Journal of Molecular Sciences [Internet]. 2013 Jun [cited 2021 Dec 7];14(6):11767–94. Available from: https://www.mdpi.com/1422-0067/14/6/11767
54. Lehtinen OP. Colloidal structures of phospholipids in vegetable oil and their potential usage in surface treatment of nanocellulose for food applications. :55.
55. Franzé S, Selmin F, Samaritani E, Minghetti P, Cilurzo F. Lyophilization of Liposomal Formulations: Still Necessary, Still Challenging. Pharmaceutics [Internet]. 2018 Aug 28 [cited 2021 Sep 24];10(3):139. Available from: https://www.ncbi.nlm.nih.gov/pmc/articles/PMC6161153/
56. Douglas JF. Weak and Strong Gels and the Emergence of the Amorphous Solid State. Gels [Internet]. 2018 Feb 23 [cited 2021 Dec 13];4(1):19. Available from: https://www.ncbi.nlm.nih.gov/pmc/articles/PMC6318627/
57. Yeligar V. ORGANOGEL: FACTORS AND ITS IMPORTANCE. International Journal of Biological and Chemical Sciences. 2014 Apr 1;4:758–73.
58. Yara-Varón E, Li Y, Balcells M, Canela-Garayoa R, Fabiano-Tixier AS, Chemat F. Vegetable Oils as Alternative Solvents for Green Oleo-Extraction, Purification and Formulation of Food and Natural Products. Molecules [Internet]. 2017 Sep 5 [cited 2021 Sep 1];22(9):1474. Available from: http://www.mdpi.com/1420-3049/22/9/1474

59. Naveed A, Adnan Q, Ahmad M, Mumtaz AM, Farzana K. Rheological Studies and Characterization of Different Oils. Journal- Chemical Society of Pakistan. 2009 Apr 1;31.
60. Lopez S, Bermudez B, Montserrat-de la Paz S, Jaramillo S, Varela LM, Ortega-Gomez A, et al. Membrane composition and dynamics: A target of bioactive virgin olive oil constituents. Biochimica et Biophysica Acta (BBA) - Biomembranes [Internet]. 2014 Jun 1 [cited 2022 Mar 6];1838(6):1638–56. Available from: https://www.sciencedirect.com/science/article/pii/S0005273614000091
61. Stanciu I. Rheological Behavior of Castor Oil: Shear Stress Dependence Shear Rate. 2020 Aug 15;3:37–42.
62. Baah Mensah M, Awudza JA, O'Brien P. Castor oil: A suitable green source of capping agent for nanoparticle syntheses and facile surface functionalization. Royal Society Open Science. 2018 Aug 1;5:180824.
63. Aryal S, Gyawali R, Regmi Y, Baby B. Lipid Based Drug Delivery System: An Approach to Enhance Bioavailability ofPoorly Water Soluble Drugs. Human Journals [Internet]. 2020 Sep 30 [cited 2021 Sep 1];19(2):693–714. Available from: http://ijppr.humanjournals.com/wp-content/uploads/2020/10/45.Sachin-Aryal-Roshan-Gyawali-Yuvraj-Regmi-Beny-Baby.pdf
64. Khor Y, Koh S, Long K, Long S, Ahmad S, Tan C. A Comparative Study of the Physicochemical Properties of a Virgin Coconut Oil Emulsion and Commercial Food Supplement Emulsions. Molecules [Internet]. 2014 Jul 1 [cited 2021 Sep 1];19(7):9187–202. Available from: http://www.mdpi.com/1420-3049/19/7/9187
65. Mubofu EB. Castor oil as a potential renewable resource for the production of functional materials. Sustainable Chemical Processes [Internet]. 2016 Jul 15 [cited 2022 Mar 2];4(1):11. Available from: https://doi.org/10.1186/s40508-016-0055-8
66. castor bean chemistry.pdf [Internet]. [cited 2022 Mar 2]. Available from: https://www.chem.uwec.edu/chem491_w01/%20Pharmacognosy%20491/castor%20bean%20chemistry.pdf
67. Maincent J, Williams RO. Sustained-release amorphous solid dispersions. Drug Deliv and Transl Res [Internet]. 2018 Dec [cited 2021 Nov 1];8(6):1714–25. Available from: http://link.springer.com/10.1007/s13346-018-0494-8

68. Yang E, Yu H, Park JY, Park KM, Chang PS. Microfluidic Preparation of Liposomes Using Ethyl Acetate/ *n* -Hexane Solvents as an Alternative to Chloroform. Journal of Chemistry [Internet]. 2018 Dec 18 [cited 2022 Mar 7];2018:1–6. Available from: https://www.hindawi.com/journals/jchem/2018/7575201/
69. Bouchemal20200420Int20J20Pharm.pdf.
70. Sopyan I. A Review: A Novel of Efforts to Enhance Liposome Stability as Drug Delivery Approach. 2020;11(6):8.
71. The HLB Book ICI.pdf [Internet]. [cited 2022 May 11]. Available from: http://www.scientificspectator.com/documents/personal%20care%20spectator/The%20HLB%20Book%20ICI.pdf
72. Salager JL. Emulsion Properties and Related Know-how to Attain Them. In: Pharmaceutical Emulsions and Suspensions [Internet]. CRC Press; 2000 [cited 2021 Oct 9]. p. 73–125. (Drugs and the Pharmaceutical Sciences; vol. 20000573). Available from: http://www.crcnetbase.com/doi/abs/10.1201/b14005-4
73. DI005-Span-and-Tween.pdf [Internet]. [cited 2022 Jul 4]. Available from: https://media.knowde.com/image/upload/v1616232658/production/Collateral/241523/DI005-Span-and-Tween.pdf
74. The HLB Book ICI.pdf [Internet]. ICI Americas Inc.; 1980. Available from: http://www.scientificspectator.com/documents/personal%20care%20spectator/The%20HLB%20Book%20ICI.pdf
75. The HLB system Croda's time-saving guide to surfactant selection. CRODA Oil and Gas; 2014.
76. Bhal S. LogP—Making Sense of the Value. :4.
77. R. Jadhav K, S. Pacharane S, P. Pednekar P, V. Koshy P, J. Kadam V. Approaches to Stabilize Amorphous Form - A Review. Current Drug Therapy [Internet]. 2012 Dec 1 [cited 2021 Nov 2];7(4):255–62. Available from: http://openurl.ingenta.com/content/xref?genre=article&issn=1574-8855&volume=7&issue=4&spage=255
78. Kalepu S, Manthina M, Padavala V. Oral lipid-based drug delivery systems - An overview. Acta Pharmaceutica Sinica B. 2013 Dec 1;3.

79. M9_Guideline_Step4_2019_1116.pdf [Internet]. [cited 2022 May 11]. Available from: https://database.ich.org/sites/default/files/M9_Guideline_Step4_2019_1116.pdf
80. Benet LZ, Hosey CM, Ursu O, Oprea TI. BDDCS, the Rule of 5 and Drugability. Adv Drug Deliv Rev [Internet]. 2016 Jun 1 [cited 2021 Nov 14];101:89–98. Available from: https://www.ncbi.nlm.nih.gov/pmc/articles/PMC4910824/
81. Abramov S, Ruppik P, Karbstein H. Crystallization in Emulsions: A Thermo-Optical Method to Determine Single Crystallization Events in Droplet Clusters. Processes. 2016 Aug 11;4:25.
82. Purification Method of Drug-Loaded Liposome _ SpringerLink.html.
83. Çağdaş M, Sezer AD, Bucak S. Liposomes as Potential Drug Carrier Systems for Drug Delivery. In: Sezer AD, editor. Application of Nanotechnology in Drug Delivery [Internet]. InTech; 2014 [cited 2021 Sep 24]. Available from: http://www.intechopen.com/books/application-of-nanotechnology-in-drug-delivery/liposomes-as-potential-drug-carrier-systems-for-drug-delivery
84. Guimarães D, Noro J, Silva C, Cavaco-Paulo A, Nogueira E. Protective Effect of Saccharides on Freeze-Dried Liposomes Encapsulating Drugs. Frontiers in Bioengineering and Biotechnology [Internet]. 2019 [cited 2021 Nov 1];7:424. Available from: https://www.frontiersin.org/article/10.3389/fbioe.2019.00424
85. Nugraheni RW, Mulyadi NA, Yusuf H. Freeze-Dried Liposome Formulation for Small Molecules, Nucleic Acid, and Protein Delivery. Systematic Reviews in Pharmacy. 2020;11(7):9.
86. Jiang ZM, Zhang SY, Wang XR, Yang NF, Zhu Y, Wilmore D. A comparison of medium-chain and long-chain triglycerides in surgical patients. Ann Surg [Internet]. 1993 Feb [cited 2022 Mar 14];217(2):175–84. Available from: https://www.ncbi.nlm.nih.gov/pmc/articles/PMC1242757/
87. Sigfridsson K, Lundqvist AJ, Strimfors M. Particle size reduction and pharmacokinetic evaluation of a poorly soluble acid and a poorly soluble base during early development. Drug Development and Industrial Pharmacy [Internet]. 2011 Mar [cited 2022 Jun 23];37(3):243–51. Available from: http://www.tandfonline.com/doi/full/10.3109/03639045.2010.505927

88. Dizaj SM, Vazifehasl Zh, Salatin S, Adibkia Kh, Javadzadeh Y. Nanosizing of drugs: Effect on dissolution rate. Res Pharm Sci [Internet]. 2015 [cited 2021 Nov 7];10(2):95–108. Available from: https://www.ncbi.nlm.nih.gov/pmc/articles/PMC4584458/
89. Zeta potential. In: Wikipedia [Internet]. 2021 [cited 2021 Sep 21]. Available from: https://en.wikipedia.org/w/index.php?title=Zeta_potential&oldid=1025574529
90. ZetaPotential-Introduction-in-30min-Malvern.pdf [Internet]. [cited 2021 Sep 21]. Available from: https://www.research.colostate.edu/wp-content/uploads/2018/11/ZetaPotential-Introduction-in-30min-Malvern.pdf
91. Olsen Eric. zeta_pot__colloid_chemistry.pdf [Internet]. [cited 2021 Sep 21]. Available from: https://www.particletechlabs.com/images/articles/zeta_pot__colloid_chemistry.pdf
92. 5.08_FTIR_on_Membranes.pdf [Internet]. [cited 2021 Nov 14]. Available from: https://batch.libretexts.org/print/url=https://phys.libretexts.org/Courses/University_of_California_Davis/UCD%3A_Biophysics_241_-_Membrane_Biology/05%3A_Experimental_Characterization_-_Spectroscopy_and_Microscopy/5.08%3A_FTIR_on_Membranes.pdf
93. Vlad RA, Sovány T, Kristó K, Ibrahim Y, Ciurba A, Aigner Z, et al. STRUCTURAL AND THERMAL ANALYSIS OF CANNABIDIOL ORODISPERSIBLE FORMULATIONS. FARMACIA. 2021 Jun 28;69:426–33.
94. Wang C, Wang J, Sun Y, Freeman K, Mchenry MA, Wang C, et al. Enhanced Stability and Oral Bioavailability of Cannabidiol in Zein and Whey Protein Composite Nanoparticles by a Modified Anti-Solvent Approach. Foods [Internet]. 2022 Jan [cited 2022 May 21];11(3):376. Available from: https://www.mdpi.com/2304-8158/11/3/376
95. Abraham OR. CHARACTERIZATION AND IDENTIFICATION OF CRYSTALLINE STRUCTURES IN CANNABIS SOLVENT EXTRACTS. :209.
96. Binder H. Water near lipid membranes as seen by infrared spectroscopy. Eur Biophys J [Internet]. 2007 Apr 10 [cited 2021 Nov 15];36(4–5):265–79. Available from: http://link.springer.com/10.1007/s00249-006-0110-6
97. Blass B. The Characterization of Cannabidiol Amorphous Solid Dispersions. :44.

98. Baird JA, Taylor LS. Evaluation of amorphous solid dispersion properties using thermal analysis techniques. Advanced Drug Delivery Reviews [Internet]. 2012 Apr 1 [cited 2021 Nov 7];64(5):396–421. Available from: https://www.sciencedirect.com/science/article/pii/S0169409X11002031
99. msds.pdf [Internet]. [cited 2022 Apr 28]. Available from: https://www.fishersci.com/store/msds?partNumber=O3376250&productDescription=LECITHIN+PURIFIED+250G&vendorId=VN00033897&countryCode=US&language=en
100. Tensor. In: Wikipedia [Internet]. 2022 [cited 2022 Jun 5]. Available from: https://en.wikipedia.org/w/index.php?title=Tensor&oldid=1082315155
101. Anisotropy. In: Wikipedia [Internet]. 2022 [cited 2022 Jun 4]. Available from: https://en.wikipedia.org/w/index.php?title=Anisotropy&oldid=1090105850
102. Bobrovska et al. - 2013 - On the Role of Anisotropy of Membrane Components i.pdf [Internet]. [cited 2022 Jul 4]. Available from: https://journals.plos.org/plosone/article/file?id=10.1371/journal.pone.0073941&type=printable
103. Bobrovska N, Góźdź W, Kralj-Iglič V, Iglič A. On the Role of Anisotropy of Membrane Components in Formation and Stabilization of Tubular Structures in Multicomponent Membranes. PLOS ONE [Internet]. 2013 Sep 16 [cited 2022 Jun 5];8(9):e73941. Available from: https://journals.plos.org/plosone/article?id=10.1371/journal.pone.0073941
104. Seifert U. Configurations of fluid membranes and vesicles. Advances in Physics [Internet]. 1997 Feb [cited 2022 Mar 20];46(1):13–137. Available from: http://www.tandfonline.com/doi/abs/10.1080/00018739700101488
105. Meyer HW. Pretransition-ripples in bilayers of dipalmitoylphosphatidylcholine: undulation or periodic segments? A freeze-fracture study. Biochimica et Biophysica Acta (BBA) - Lipids and Lipid Metabolism [Internet]. 1996 Jul [cited 2022 Oct 31];1302(2):138–44. Available from: https://linkinghub.elsevier.com/retrieve/pii/0005276096000549

106. Burducea - LYOTROPIC LIQUID CRYSTALS I. SPECIFIC STRUCTURES.pdf [Internet]. [cited 2022 Jun 7]. Available from: http://rrp.infim.ro/2004_56_1/Burducea1.pdf
107. Ortan A, Parvu CD, Ghica MV, Popescu LM, Ionita L. Rheological Study of a Liposomal Hydrogel Based On Carbopol. Romanian Biotechnological Letters. 2011;16(1):8.
108. Inc R. RheoSense Webinars | Viscosity Applications [Internet]. [cited 2021 Dec 7]. Available from: https://www.rheosense.com/en/viscosity-webinars
109. Dislocation. In: Wikipedia [Internet]. 2021 [cited 2021 Dec 12]. Available from: https://en.wikipedia.org/w/index.php?title=Dislocation&oldid=1047159183
110. Paul A, Laurila T, Vuorinen V, Divinski S. Fick's Laws of Diffusion. In 2014. p. 115–39.
111. Crystallographic defect. In: Wikipedia [Internet]. 2021 [cited 2021 Dec 12]. Available from: https://en.wikipedia.org/w/index.php?title=Crystallographic_defect&oldid=1057197380
112. © Applied Rheology. Appl Rheol. 2018;6.
113. Ochowiak M, Broniarz-Press L, Rozanski J. Rheology and Structure of Emulsions and Suspensions. Journal of Dispersion Science and Technology [Internet]. 2012 Feb [cited 2021 Sep 1];33(2):177–84. Available from: http://www.tandfonline.com/doi/abs/10.1080/01932691.2010.548694
114. Fu Y, Kao WJ. Drug Release Kinetics and Transport Mechanisms of Non-degradable and Degradable Polymeric Delivery Systems. Expert Opin Drug Deliv [Internet]. 2010 Apr [cited 2022 May 9];7(4):429–44. Available from: https://www.ncbi.nlm.nih.gov/pmc/articles/PMC2846103/
115. Paarakh MP, Jose PA, Setty C, Peter GV. RELEASE KINETICS – CONCEPTS AND APPLICATIONS. :9.
116. Pereira Camelo SR, Franceschi-Messant S, Perez E, Girod Fullana S, Ré MI. Factors influencing the erosion rate and the drug release kinetics from organogels designed as matrices for oral controlled release of a hydrophobic drug. Drug

Development and Industrial Pharmacy [Internet]. 2016 [cited 2022 May 30];42(n°6):985–97. Available from: https://hal.archives-ouvertes.fr/hal-01451927

117. Huang X, Brazel CS. On the importance and mechanisms of burst release in matrix-controlled drug delivery systems. Journal of Controlled Release [Internet]. 2001 Jun [cited 2021 Nov 14];73(2–3):121–36. Available from: https://linkinghub.elsevier.com/retrieve/pii/S0168365901002486
118. Chemistry LibreTexts [Internet]. 2020 [cited 2023 Aug 27]. Calibration Methods (Gray). Available from: https://chem.libretexts.org/Ancillary_Materials/Worksheets/Worksheets%3A_Analytical_Chemistry_II/Calibration_Methods_(Gray)
119. HEK293 Cells - A Guide to This Incredibly Useful Cell Line [Internet]. 2021 [cited 2022 Feb 3]. Available from: https://bitesizebio.com/45489/guide-to-hek293-cells/
120. HEK293 Cells: Background, Applications, Protocols, and More [Internet]. [cited 2023 Jun 13]. Available from: https://www.synthego.com/hek293
121. Heterogeneity of the NIH3T3 Fibroblast Cell Line - PMC [Internet]. [cited 2023 Aug 18]. Available from: https://www.ncbi.nlm.nih.gov/pmc/articles/PMC9455036/
122. Kamiloglu S, Sari G, Ozdal T, Capanoglu E. Guidelines for cell viability assays. Food Frontiers [Internet]. 2020 [cited 2022 Feb 3];1(3):332–49. Available from: https://onlinelibrary.wiley.com/doi/abs/10.1002/fft2.44
123. Pol A, Patel P, Hegde D. Peppermint oil based drug delivery system of aceclofenac with improved anti-inflammatory activity and reduced Ulcerogenecity. Int J Pharm Biosci Technol. 2013 Jul 1;1:2321–969.
124. Solaiman A. Properties of Capsule Shells made from Hydroxypropyl Methylcellulose (Hypromellose). [cited 2021 Nov 9]; Available from: https://core.ac.uk/reader/9994771
125. Al-Tabakha MM. HPMC Capsules: Current Status and Future Prospects. Journal of Pharmacy & Pharmaceutical Sciences [Internet]. 2010 Oct 14 [cited 2021 Nov 9];13(3):428–42. Available from: https://journals.library.ualberta.ca/jpps/index.php/JPPS/article/view/8870
126. Yamauchi M, Tsutsumi K, Abe M, Uosaki Y, Nakakura M, Aoki N. Release of Drugs from Liposomes Varies with Particle Size. Biological & Pharmaceutical Bulletin

[Internet]. 2007 [cited 2022 Apr 7];30(5):963–6. Available from: http://www.jstage.jst.go.jp/article/bpb/30/5/30_5_963/_article

APPENDIX

1. Turnitin Report

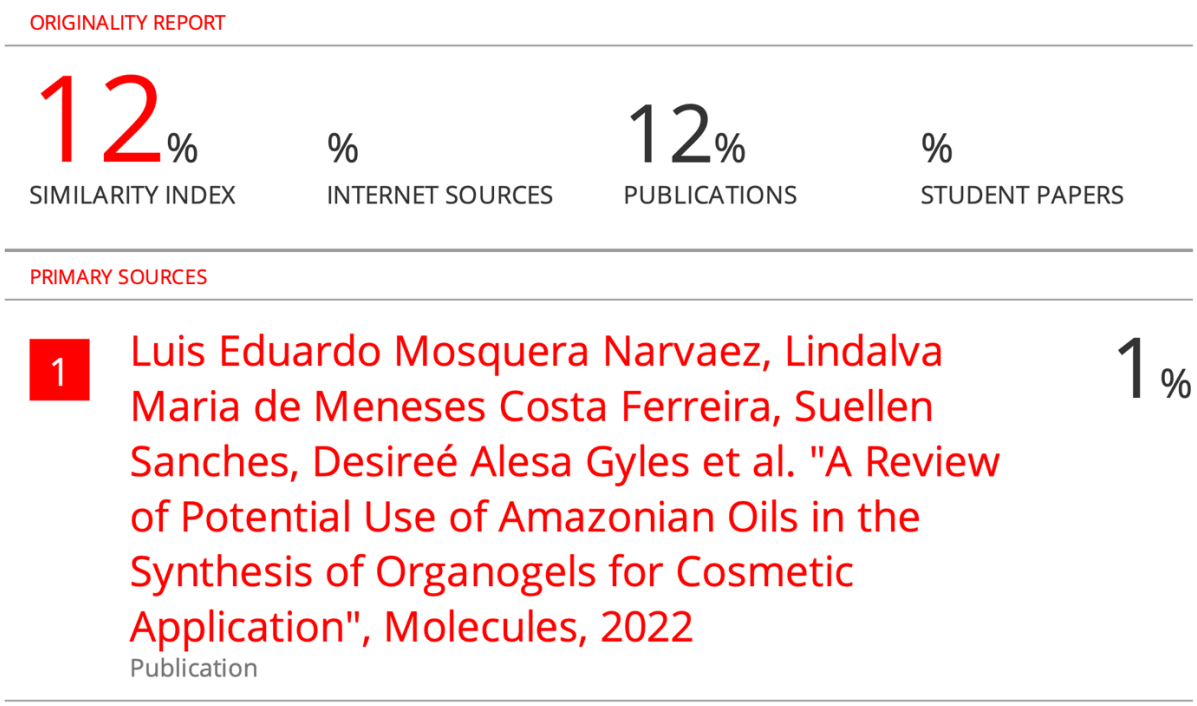

ORIGINALITY REPORT

12%	%	12%	%
SIMILARITY INDEX	INTERNET SOURCES	PUBLICATIONS	STUDENT PAPERS

PRIMARY SOURCES

1	Luis Eduardo Mosquera Narvaez, Lindalva Maria de Meneses Costa Ferreira, Suellen Sanches, Desireé Alesa Gyles et al. "A Review of Potential Use of Amazonian Oils in the Synthesis of Organogels for Cosmetic Application", Molecules, 2022 Publication	1%